EFFECTS OF GRAIN SIZE DISTRIBUTION ON DYNAMIC
PROPERTIES AND LIQUEFACTION POTENTIAL OF
GRANULAR SOILS

prepared by

Nien-Yin Chang and Hon-Yim Ko

for

NATIONAL SCIENCE FOUNDATION

under

Grant No. PFR 78-23094

Geotechnical Engineering Division
Department of Civil and Urban Engineering
University fo Colorado at Denver

Research Report R82-103
Geotechnical Publication 111

March 1982

50272-101

REPORT DOCUMENTATION PAGE	1. REPORT NO. NSF/CEE-82021	2.	3. Recipient's Accession No.
4. Title and Subtitle Effects of Grain Size Distribution on Dynamic Properties and Liquefaction Potential of Granular Soils			5. Report Date March 1982
			6.
7. Author(s) N.Y. Chang, H.Y Ko			8. Performing Organization Rept. No.
9. Performing Organization Name and Address University of Colorado at Denver Department of Civil and Urban Engineering Denver, CO 80202			10. Project/Task/Work Unit No.
			11. Contract(C) or Grant(G) No. (C) (G) PFR7823094
12. Sponsoring Organization Name and Address Directorate for Engineering (ENG) National Science Foundation 1800 G Street, N.W. Washington, DC 20550			13. Type of Report & Period Covered
			14.

15. Supplementary Notes

Submitted by: Communications Program (OPRM)
National Science Foundation
Washington, DC 20550

16. Abstract (Limit: 200 words)

Research was undertaken to investigate the effects of grain-size distribution grada-
tion on dynamic properties and on liquefaction potential of granular soils. Resonant
column tests were performed to determine the dynamic shear moduli and damping ratios
of granular soil samples prepared from a Denver sand. Cyclic triaxial test cells and
an MTS closed-loop servo control material testing machine were used to determine
liquefaction potential. Results indicate that the shear modulus of soils at small
strains is strongly dependent on the uniformity coefficient. The liquefaction poten-
tial was found to be strongly affected by the mean diameter.

17. Document Analysis a. Descriptors

Liquefaction
Sand
Grain size
Shear modulus

Dynamic properties
Damping
Granular soils
Statistical methods

b. Identifiers/Open-Ended Terms

Denver (Colorado)

N.Y. Chang, /PI

c. COSATI Field/Group

18. Availability Statement NTIS	19. Security Class (This Report)	21. No. of Pages
	20. Security Class (This Page)	22. Price

(See ANSI-Z39.18)　　　　　See Instructions on Reverse　　　　　OPTIONAL FORM 272 (4-77)
(Formerly NTIS-35)
Department of Commerce

ABSTRACT

The objective of this study is to investigate the effects of the grain-size distribution (gradation) characteristics on the following two properties:

- Dynamic properties (shear moduli and damping ratios) and

- Liquefaction potential of granular soils

A granular soil, Denver sand, with constituents ranging from fine silts to gravels was adopted as the test sand. Samples of the Denver Sand with different gradation characteristics: Mean diameters (D_{50}: 0.149 mm to 1.68 mm) and uniformity coefficients (C_u: 2 to 16) etc. were tested.

Resonant column test apparatus was used to evaluate the dynamic property of six-inch diameter samples. Cyclic triaxial test cells and MTS closed-loop servo control material testing machine were used to determine the liquefaction potential of two-inch diameter samples.

The result of this investigation showed that the shear modulus of the sand at small strains was strongly dependent on the uniformity coefficient. The liquefaction potential of the sand was found to be strongly affected, instead, by the mean diameter. Thus, statistical analyses were performed to express the shear modulus and the liquefaction potential of the sand as the functions of its uniformity coefficient and mean diameter, respectively.

ACKNOWLEDGEMENT

from the Eastern United States.

The successful conclusion of this research is the result of a synchronized and cooperative effort of multiple parties. This effort is gratefully acknowledged.

The opinions expressed in this report are those of the authors and not necessarily of the National Science Foundation.

TABLE OF CONTENTS

Chapter   Page

LIST OF TABLES

LIST OF FIGURES

Figure

Figure   Page

Figure   Page

Figure   Page

Figure   Page

Part I

GENERAL INFORMATION

CHAPTER 1

INTRODUCTION

During the past few decades, the dynamic behavior of soils
has received considerable attention, mainly because of the signi-
ficant growth in sizes and importance of engineering projects,
such as nuclear power plants, earth embankment dams, pipelines,
machine foundations and off-shore structures. Some of the
projects are located near or in areas which are heavily populated
and seismically active. These projects are very costly and
their failures could endanger the public safety or cause signi-
ficant environmental damages and/or property loss. Hence,
there exists some great concern about their safe designs which
involve the rigorous consideration of the static and dynamic
behaviors of soils.

For a sound dynamic design of a structure, it is essential
to know the dynamic properties and behaviors of soils which support
the structure or of which it is constructed. Research on earthquakes
and the resulting catastrophic events has focused much attention on
the behavior of granular soils under dynamic loads. In order to
evaluate the behavior of soil deposits subjected to earthquakes,
ocean waves and other nonstatic loads, it is necessary to evaluate
the dynamic properties, behaviors and strengths of underlying
soils.

Knowledge of the strain-dependent dynamic properties (shear modulus and damping ratio) is essential for predicting the performance of an earth structure, a soil deposit, and the soil-structure interaction during earthquakes, etc. Dynamic properties at small strains (less than 10^{-4} radian) are also important in assessing the behavior of large machine foundations under vibration-induced motions.

Catastrophic ground failures due to earthquakes may result in either partial or total destruction of earth-embankment dams, mine-tailings dams, slopes and other super structures. Very often these ground failures are the direct result of the lique-faction of saturated granular soils. To achieve safe designs of earth structures, etc. constructed of or supported by saturated granular soils, one must have sound knowledge of their liquefaction potential under various conditions.

The Alaska and Niigata earthquakes of 1964 which caused considerable damage to earth structures and other super structures have accelerated the research in the field of the dynamic properties and the liquefaction potential of granular soils on factors, such as the relative density, void ratio, mean effective stress and cyclic strain and/or deviatoric stress amplitudes, etc. However, the effects of grain-size distribution characteristics on the dynamic properties and the liquefaction, while known to be significant, have not been systematically studied over a wide range of grain sizes. This study is to investigate such effects.

Most data on the dynamic properties and the liquefaction potential are for uniform clean sands. However, natural granular

soil deposits are neither uniform nor clean. They usually contain particles over a broad spectrum of grain size. Therefore, samples prepared from Denver Sand were tested. The samples have the following grain shape and grain-size distribution characteristics:

Grain shape: Subrounded

Specific gravity: 2.6

Grain size: 0.038 mm to 9.5 mm

Mean grain size (D_{50}): 0.149 mm to 1.68 mm

Uniformity coefficient (C_u): 2 to 15

The free-free resonant column apparatus designed by Professor Vincent P. Drnevich at the University of Kentucky was used to determine the dynamic properties of 6-inch diameter dry sand samples. Dynamic shear moduli and damping ratios at strains smaller than 5×10^{-4} radian were determined. The closed-loop servo control universal dynamic material testing system and the triaxial cells manufactured by MTS and Geotest, Inc. were used to assess the liquefaction potential of saturated sand samples of 2-inch diameters through cyclic triaxial tests.

The shear modulus of the dry Denver Sand was found to be strongly dependent on its uniformity. The shear modulus of sand increases with the increasing uniformity coefficient. Thus a well graded sand is stiffer than the uniformly graded one.

The liquefaction potential of sand was found to be strongly affected by its mean grain size, D_{50}. It increases with the decreasing mean grain size. In other words, the fine sand is easier to liquefy than the coarse one.

Finally, regression analyses were performed to formulate the

functional relationships between the shear modulus and the uniformity coefficient and between the liquefaction potential and the mean diameter, D_{50}.

CHAPTER 2

TEST SANDS AND TEST PROGRAMS

2.1 Denver Sand

The primary material used in this study was a well-graded river sand purchased locally from the Denver Sand and Gravel Company in Denver, Colorado. Both coarse and fine particles of Denver Sand are subangular in shape. For comparison, Figs. 2.1, 2.2 and 2.3 show the grain size and shape of Denver Sand, a sample (DM-d_2) prepared from Denver Sand and Monterey No. 0 Sand. It is generally known that Monterey No. 0 Sand is a uniform sand with subrounded grain shape (Lee and Fitton, 1967 and Silver, et al., 1976). Denver Sand is a well-graded sand with subangular grain shape.

Denver Sand was oven dried first and then sixteen standard U.S. sieves with openings ranging from 38 microns (U.S. standard sieve No. 400) to 3/8 inch were used to segregate different size particles. As shown in the design gradation curves in Fig. 2.4, six different mean grain sizes (D_{50}) and uniformity coefficients (C_u) were adopted in sample preparation. The characteristics of samples for the determination of the dynamic property and the liquefaction potential are shown in Tables 7.1 and 14.1 respectively.

Minimum and maximum dry density of each sample were determined prior to testing. The procedures given in Appendix E-12

FIG. 2.1 GRAIN SHAPE AND SIZE OF
ORIGINAL DENVER SAND
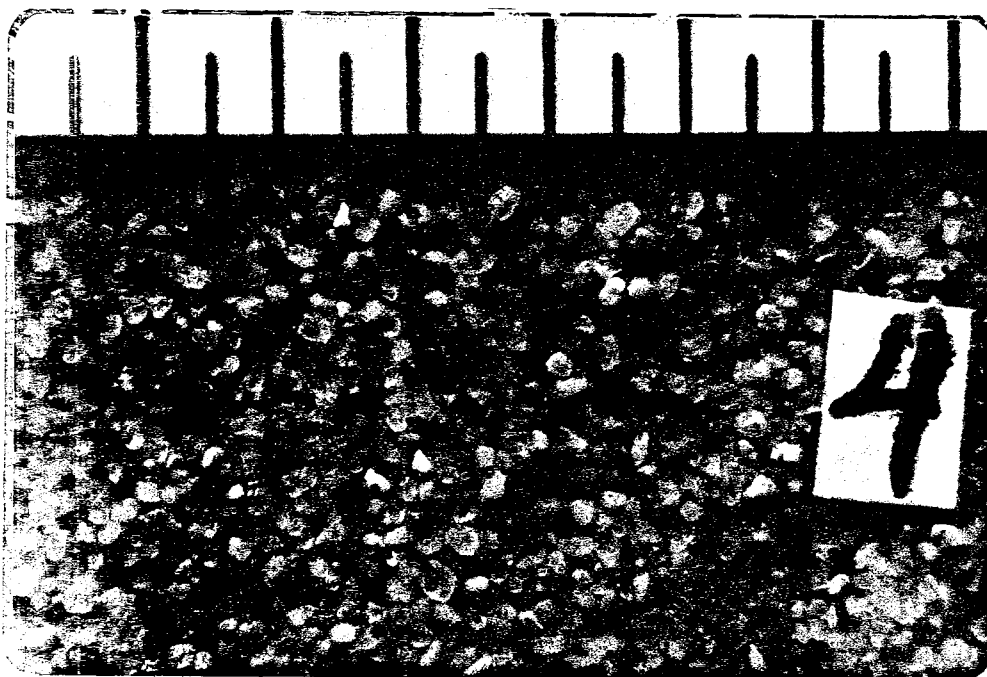
FIG. 2.2 GRAIN SHAPE AND SIZE OF SAMPLE
DM-d_2 RETAINED IN SIEVE NO. 40
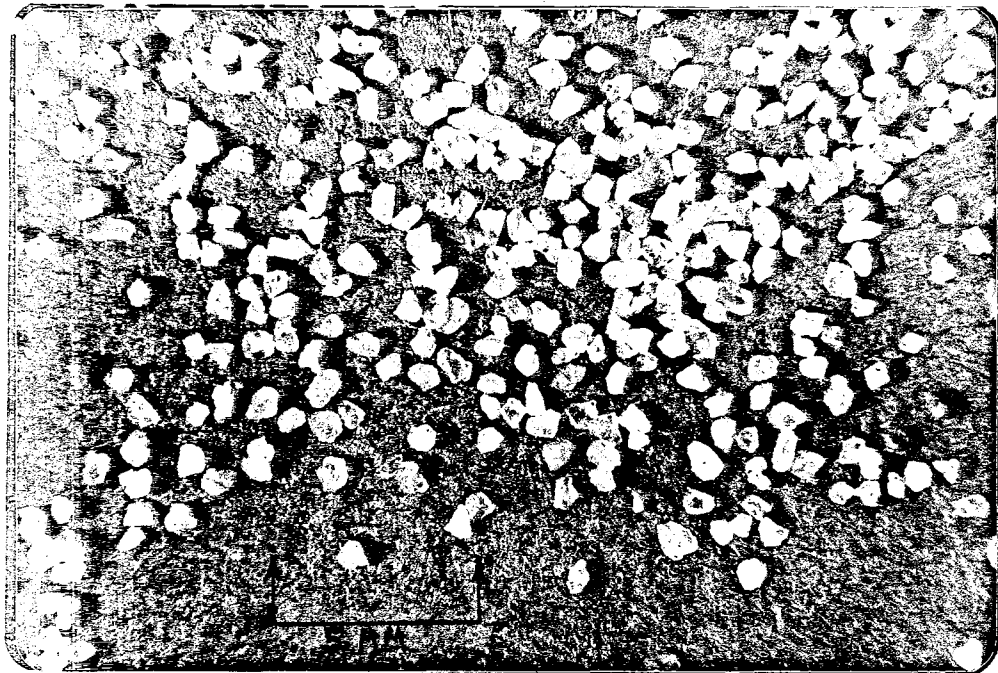
FIG. 2.3   GRAIN SHAPE AND SIZE OF
MONTEREY NO. 0 SAND
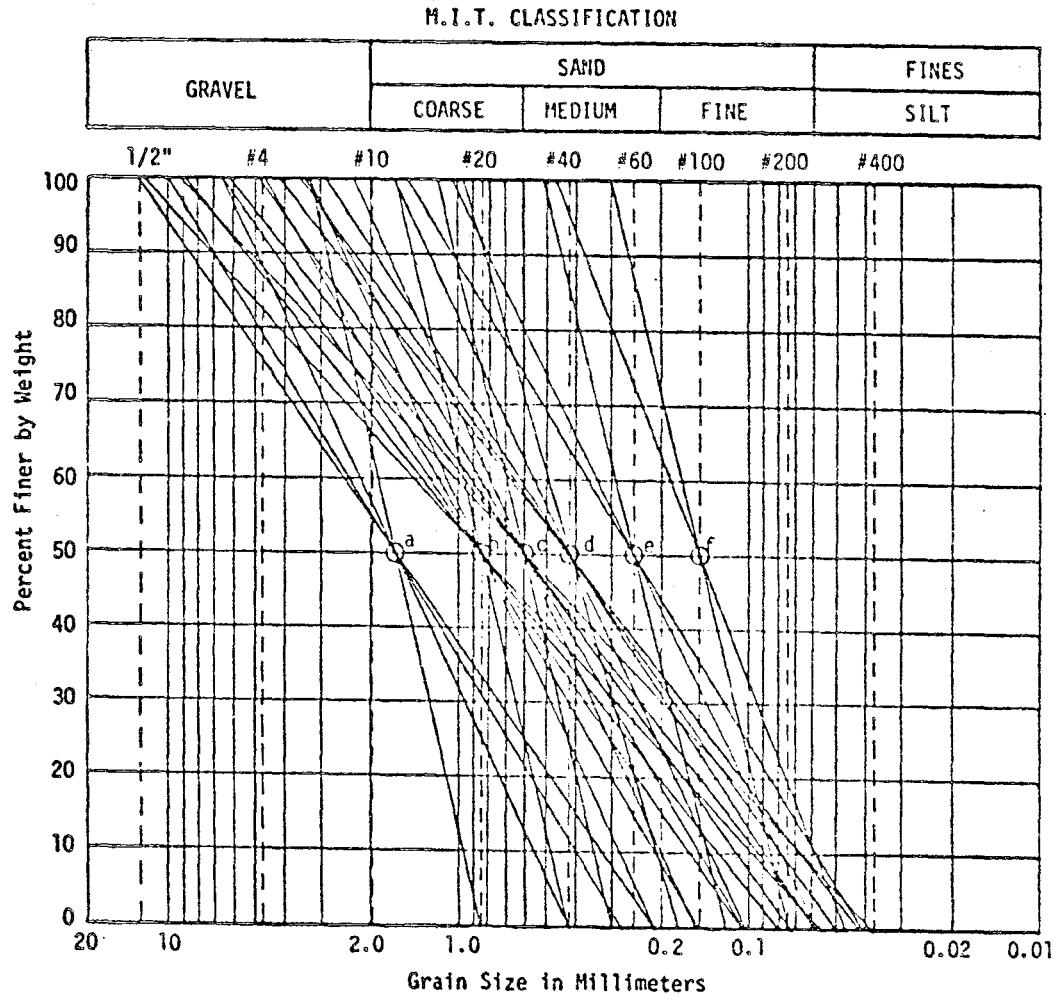
FIG. 2.4   GRADATION OF DENVER SAND SAMPLES

on "Relative Density of Cohesionless Soils" of the Earth Manual (2nd Edition, 1974) published by the U.S. Bureau of Reclamation were used in evaluating them. The resulting minimum and maximum densities are included in Tables 7.1 and 14.1.

2.2 Monterey No. 0 Sand

In addition, Monterey No. 0 Sand was also used in the resonant column tests for the purpose of comparing the dynamic shear modulus and damping ratio with the published data. The sand is a uniform medium beach sand from Monterey, California with the following index properties:

- Mean grain size (D_{50}): 0.4 mm
- Uniformity coefficient (C_u): 1.5
- Specific gravity: 2.655
- Maximum density: 105.92 lbs/ft^3
- Minimum density: 91.96 lbs/ft^3
- Grain shape: subrounded
- Mineral composition: mostly quartz and some feldspar

Fig. 2.3 shows that its grain shape is subrounded and somewhat elongated. Fig. 2.5 gives the gradation curve of Monterey No. 0 Sand.

2.3 Test Programs

Detailed test programs are presented in Part II on "Dynamic Properties at Small Strains" and Part III on "Liquefaction Potential." Only a brief summary is given here.

M.I.T. CLASSIFICATION

GRAVEL	SAND			FINES
	COARSE	MEDIUM	FINE	SILT
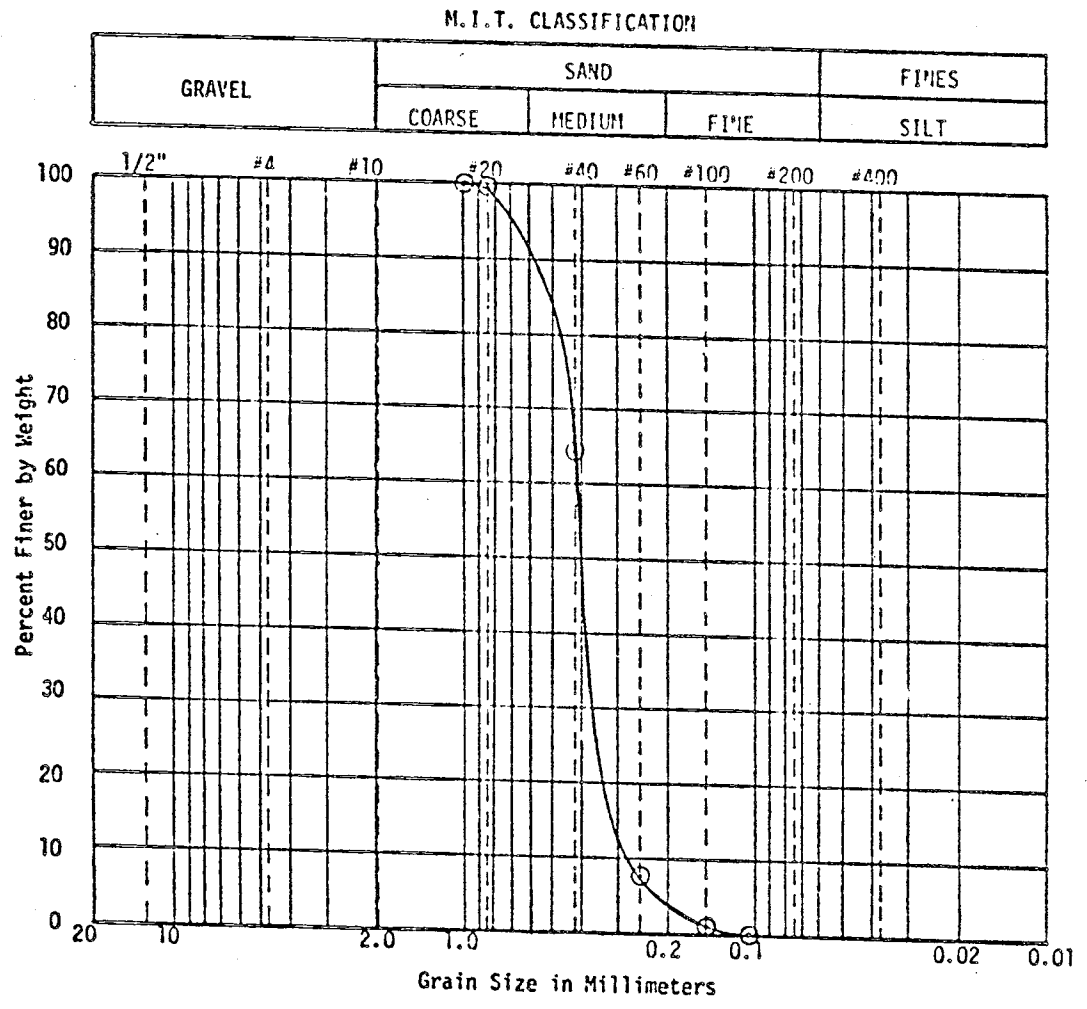
FIG. 2.5   GRADATION OF MONTEREY NO. O SAND

2.3.1 Dynamic Properties at Small Strains

To determine the dynamic properties (shear modulus and damping ratio) of six-inch diameter dry Denver Sand samples, the free-free resonant column apparatus manufactured by Professor Vincent P. Drnevich at the University of Kentucky was used. Twenty-four samples prepared from Denver Sand were tested. To fill the goal of assessing the effect of gradation characteristics on the dynamic properties, all parameters other than those describing the gradation characteristics were kept constant. All samples were prepared at the relative density of about 30% and tested under 30 psi confining pressure.

Three dry Monterey No. 0 Sand samples were also tested. The resulting properties were to be compared with the published data.

2.3.2 Liquefaction Potential

Undrained cyclic triaxial tests were conducted to determine the liquefaction potential of samples prepared from Denver Sand. Four samples were prepared from each of the twenty-four samples of different gradation characteristics. All samples were prepared to achieve the relative density of approximately 50% and subjected to the effective confining pressure of 30 psi and the back pressure and the Skempton porewater pressure parameter B of no less than 60 psi and 0.95 respectively before tests. Cyclic stress ratios, R_s, ranging from 0.1 to 0.45 were used, where the cyclic stress ratio is defined as:

$$R_s = \frac{\sigma_{dc}}{2\sigma_3}$$

where σ_{dc} = cyclic deviatoric stress

$\quad\quad = (\sigma_1 - \sigma_3)$ cyclic

$\quad\sigma_3$ = effective confining pressure

A total of 123 cyclic triaxial tests were conducted.

CHAPTER 3

STATISTICAL ANALYSES

3.1 Introduction

Statistical analyses were performed to assess the strength
of correlation between the dependent and independent variables.
Regression analyses (bivariate or multivariate) were then con-
ducted to formulate, for variables with strong correlation, their
functional relation. In this study, the dependent and independent
variables are listed as follows:

Dependent Variables	Independent Variables
- Maximum shear modulus G_{max} ($\gamma < 10^{-5}$ radian)	- Shear strain, γ
	- Mean grain size, D_{50}
- Shear modulus, G	- Effective diameter, D_{10}
- Cyclic stress ratio, R_s	- Uniformity coefficient, C_u
- Cyclic stress ratios required to cause liquefaction in 10 and 30 cycles, etc.	- Void ratio, e
	- Number of stress cycles, N

For the variables with nonlinear relationship, the variable(s)
was transformed before it entered the regression analysis. By
doing so, nonlinear functions, such as power, logarithmic, and
exponential functions, can be easily formulated through the
linear regression analysis.

The above statistical analyses can be performed by using the Statistical Package for the Social Sciences (SPSS) computer programs described by Nie, et al. (1975). These programs were available on the CDC 6400 computer system at the University of Colorado. Pertinent details regarding revisions to these programs have been presented by Hohlen (1978 a, 1978 b).

3.2 General Statistics

General statistics including the mean, standard deviation, coefficient of variation, range of values, and the 95-percent confidence interval about the mean can be computed by using SPSS programs. These statistics are defined in the following paragraphs.

3.2.1 Sample Mean

The arithmetic sample mean is the most representative parameter for the magnitude of a random physical quantity. The mean is defined as follows:

$$\bar{x} = \frac{\sum_{i=1}^{n} x_i}{n}$$

where $\bar{x}$ = the mean of the sample,

x_i = the ith value of a random variable X, and

n = the sample size, i.e., number of observations.

3.2.2 Sample Standard Deviation

The standard deviations serve as an absolute measure of the dispersion, or variation of the data. A large standard deviation

implies large dispersion and vice versa. The sample standard deviation is defined in the following equations:

$$s = \sqrt{\frac{\sum\limits_{i=1}^{n} (x_i - \bar{x})^2}{n - 1}}$$

where variables were defined in the previous section.

3.2.3 Coefficient of Variation

The coefficient of variation, V, is defined as the sample standard deviation divided by the sample mean:

$$V = \frac{s}{\bar{x}}$$

This coefficient provides a relative measure of the dispersion of the data which enables one to compare the variation in several sets of data.

3.2.4 Confidence Interval

The sample mean and sample standard deviation, an interval which contains the true mean μ can be calculated with an associated probability. The 95-percent confidence interval (C.I.) for the true mean, for a normal population with unknown population standard deviation σ, is computed by using the following equation (Miller and Freund, 1965, p. 149):

$$0.95 \text{ C.I.} = \bar{x} \pm t \left(\frac{s}{\sqrt{n}} \right)$$

where $t = 0.025$ t-statistic for $(n-1)$ degrees of freedom and other variables are as previously defined.

3.3 Scatter Diagrams

Scatter diagrams show the dispersion of the experimental data points. The diagram provides a visual aid for the assessment of the strength of correlation and for the observation of the possible functional relationships (linear or nonlinear) between a pair of parameters. It also enables one to look for piecewise relationships. If such a relationship exists for any variable pair, then a separate, piecewise analysis must be performed for each of the various regions of the diagram.

3.4 Analysis of Correlation Coefficients

The correlation coefficient measures the strength of correlation between two variables. Bivariate correlation coefficients are computed by using the following equation:

$$R = \frac{\sum\limits_{i=1}^{n} (x_i - \bar{x})(y_i - \bar{y})}{\left| \sum\limits_{i=1}^{n} (x_i - \bar{x})^2 \right| \left| \sum\limits_{i=1}^{n} (y_i - \bar{y})^2 \right|^{1/2}}$$

where R = estimate of the true correlation coefficient

between X and Y,

x_i = ith value of the random variable X,

y_i = ith value of the random variable Y,

n = number of pairs of observations,

$\bar{x}$ = sample mean of variable X, and

$\bar{y}$ = sample mean of variable Y.

When a straight line is a perfect fit to the data, the correlation coefficient R is equal to -1.0 or 1.0. A negative value of R implies that the regression line has a negative slope, which

indicates an inverse relationship. When a straight line is a poor fit to the data, the absolute value of R is close to zero and the variables are said to be uncorrelated. It is generally considered that if the absolute value of the correlation coefficient is equal to or greater than 0.7, then one variable can be predicted from the other by using a linear bivariate regression equation. A small correlation coefficient implies only that no linear relationship exists between two variables and the equation will not give a reliable prediction of the dependent variable. It does not imply that the variables are totally unassociated and have no relationship whatsoever. Indeed, a very strong nonlinear relationship between two variables can yield a correlation coefficient close to zero.

3.5 Regress Analyses

3.5.1 Bivariate Regression Analysis

In a bivariate regression analysis, a regression line is formulated by using a set of data involving two variables. An equation of the form $y = b_0 + b_1 x$ is developed, where y is the dependent variable, x is the independent variable, and the regression coefficients b_0 and b_1 are estimates of the y-intercept and slope, respectively, of the true regression line. The bivariate regression coefficients are computed from the data by using the following equations:

$$b_1 = \frac{n \sum\limits_{i=1}^{n} x_i y_i - \left(\sum\limits_{i=1}^{n} x_i \right)\left(\sum\limits_{i=1}^{n} y_i \right)}{n \sum\limits_{i=1}^{n} x_i^2 - \left(\sum\limits_{i=1}^{n} x_i \right)^2}$$

$$b_0 = \bar{y} - b_1 \bar{x}$$

where all variables are as previously defined.

The techniques of bivariate regression analysis have been described by Draper and Smith (1966), Walpole and Myers (1972), and in numerous other books.

3.5.2 Nonlinear Equations

In any regression analysis, the quality and usefulness of the developed prediction equation is limited by the form of the equation which was assumed. Therefore, in order to investigate many different models, nonlinear as well as linear relationships are often studied, and these nonlinear relationships can involve numerous transformed variables.

Furthermore, a nonlinear equation (nonlinear in the parameters to be estimated), which can be expressed by a suitable transformation of the variables in the standard linear form, is said to be intrinsically linear. For example, $y = \exp(b_0 + b_1 x_1)$ can be expressed in the standard linear form $\ln y = b_0 + b_1 x_1$, and therefore is an intrinsically linear equation.

It is generally considered that a linear bivariate regression equation can be used for engineering predictions if the absolute value of the correlation coefficient between the two variables is equal to or greater than 0.7. Furthermore, this correlation

coefficient should be significant, and thus based on a reasonable number of data pairs (cases). Finally, it must be noted that computed correlation coefficients are often based on data exhibiting a limited range of values. Furthermore, any prediction equation is valid only for the range of values of the independent variable used in its development.

3.6 Multiple Regression Analysis

In multiple regression analysis, an equation which involves more than one independent variable is formulated by using a set of data comprised of multivariate observations. An equation of the form $y = b_0 + b_1 x_1 + b_2 x_2 + \ldots + b_k x_k$ is developed, where y is the dependent variable, $x_1, \ldots, x_k$ are independent variables and $b_0, \ldots, b_k$ are regression coefficients computed from the data. In multiple regression, a multiple correlation coefficient R can be computed, which is similar to the bivariate correlation coefficient. The coefficient of multiple determination (R) measures the amount of variation of the dependent variable accounted for by the regression equation. The methods and techniques of multiple regression analysis have been described by Draper and Smith (1966), Walpole and Myers (1972), and in numerous other books.

As in bivariate regression analysis, the quality and usefulness of a developed multiple regression equation is limited by the form of the equation which was assumed. Therefore, in order to investigate many different models, transformed variables are often included in the analysis.

It is generally considered that a multiple regression equation

can be used for engineering predictions if the multiple correlation coefficient R is equal to or greater than 0.7. Furthermore, the equation should be developed by using a reasonable number of data sets and it is valid only for the ranges of values of the independent variables used in its development.

Part II

DYNAMIC PROPERTIES AT SMALL STRAINS

ABSTRACT

Knowledge of strain-dependent dynamic properties, such as shear modulus and shear damping ratio of soils is essential for predicting the performance of earth structures, the behavior of soil deposits, and the soil-structure interaction during earthquakes. These dynamic properties at low strains are also important in predicting the behavior of machine foundations under vibration-induced motions. Previous researchers have studied and demonstrated the strong dependence of dynamic properties of granular soils on several factors, such as the void ratio, relative density, shear strain amplitude and mean effective stress. However, the effects of grain size distribution on dynamic properties, while known to be significant, have not been systematically studied.

The purpose of this study is to investigate such effects and to formulate the functional relationships between the dynamic properties at low strain levels and the grain size distribution characteristics: Uniformity coefficient (C_u), mean diameter (D_{50}), effective diameter (D_{10}), etc. To study such effects, sand samples of various gradations were prepared. The uniformity coefficients and the mean diameters of these samples range from 2 to 15 and from 0.149 to 1.68 mm, respectively.

Resonant column tests were performed to determine their

dynamic shear moduli and damping ratios. Analysis of statistical correlation was performed on all dependent variables (shear modulus) and independent variables (the indices specifying the grain size distribution) to evaluate the strength of their correlation. Functional relations were then formulated among variables which show strong correlation through regression analyses. The functional relationship so obtained can then be used to determine the shear modulus of granular soils of known gradations at small strains.

CHAPTER 4

INTRODUCTION

Large engineering projects, such as large earth embankment dams, nuclear power plants and off-shore structures located near or in earthquake prone zones require some extensive dynamic analyses. The analysis would need the dynamic properties of soils over a wide range of strains. There has been a substantial increase in the number of such important engineering projects in the last two to three decades. This leads to an increasing importance of the subject of soil dynamics. The failure of these large, costly structures could endanger the safety of the general public, cause significant environmental damage and incur great property loss. Hence, there is great concern over the safe design of these engineering projects which require rigorous consideration of both static and dynamic loading conditions. To evaluate the behavior of structures under seismic loads, it is necessary to evaluate the dynamic property and strength of soils which support the structure or of which they are constructed.

Knowledge of the strain-dependent dynamic properties (shear modulus and damping ratio) is essential for predicting the performance of an earth structure, the behavior of a soil deposit, and the soil-structure interaction during earthquakes. The

dynamic properties of soils at small strains are also important
in assessing the behavior of machine-foundations under vibration-
induced motions.

Many factors affect the dynamic property of granular
soils. Previous researchers have demonstrated the strong
dependence of the dynamic property of granular soils on factors
such as the relative density, void ratio, mean effective stress
and shear strain amplitude, etc. These factors and their
effects on shear modulus and damping ratio are discussed in
Chapter 5. However, the effects of grain size distribution on
dynamic properties, while known to be significant, have not been
systematically studied over a wide range of grain sizes. This
study aims at providing this information and the functional
relationships between grain size distribution characteristics
and dynamic properties at low strain levels.

Most available data on dynamic properties of granular
soils are for uniform clean sands. Natural granular soil
deposits are neither clean nor uniform, they usually contain
particles over a broad spectrum of grain size. Therefore,
samples ranging from uniform to well-graded were tested. The
uniformity coefficients, C_u, and mean grain sizes, D_{50}, of
the samples range from 2 to 15 and 0.149 to 1.68 mm, respectively.

Resonant column tests were conducted to determine the
dynamic properties of soils at low strain levels (below 10^{-4}).
The Drnevich Free-Free resonant column device was used to
evaluate the shear modulus and dampoing ratio of granular soils
at shear strain amplitudes below 10^{-4}.

This study concluded that the shear modulus of granular soils is strongly affected by shear strain amplitude, void ratio and uniformity coefficient. Maximum shear modulus, G_{max}, is also affected by mean grain size, D_{50}, and effective grain size, D_{10}. In general, the shear modulus of granular soils increases with the increasing uniformity coefficient. No relationship was obtained for damping ratios because their values were found to be unusually large and their relationships with respect to the confining pressure and density are contrary to some expected trends.

CHAPTER 5

DYNAMIC PROPERTIES OF SOILS

5.1 Introduction

In order to analyze the dynamic behavior of soils and soil-supported structures under dynamic loadings, the shear stress versus strain relationship of the soil must be established. A general dynamic stress-strain relation of soils is very complex because of its dependence on a large number of parameters. However, by studying special cases and understanding them, one might be able to link them together to establish a generalized constitutive relation. In this study the dynamic shear modulus G and damping ratio D at shear strains less than 10^{-4} were determined for twenty-four samples of various gradations. The properties were determined by using Drnevich free-free resonant column test device.

Because of the stress versus strain behavior of soils being, in general, nonlinear and nonelastic, a loading-unloading cycle generally produces a hysteresis loop which represents the energy consumed during the process. A hysteresis loop shown in Fig. 5.1 gives the stress versus strain relationship of a soil for a complete cycle of loading and unloading. The slope of the secant B'B defines the shear modulus G. The shear damping ratio D is proportional to the ratio between the adsorbed energy (the area

SHEAR STRESS τ

SHEAR STRAIN γ

SHEAR MODULUS

$$G = \frac{\tau}{\gamma}$$

DAMPING

$$D = \frac{1}{2\pi} \frac{\text{AREA (LOOP)}}{\text{AREA (OAB + OA'B')}}$$
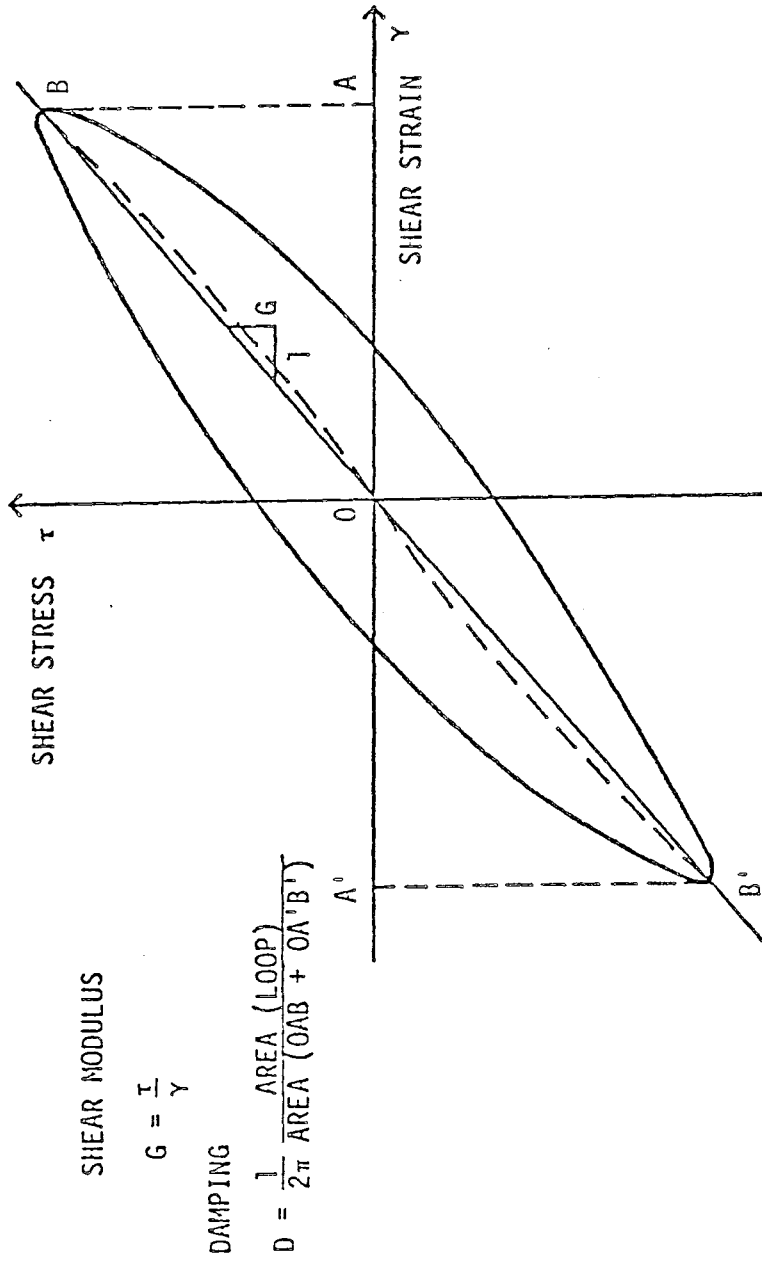
FIG. 5.1 HYSTERETIC STRESS-STRAIN RELATIONSHIP

of the loop) and the applied strain energy (the area OAB + OA'B')
and is defined as follows:

$$D = \frac{1}{2\pi} \frac{\text{Area of loop}}{\text{Area (OAB + OA'B')}} \qquad (5.1)$$

It should be noted, however, in defining G and D as above,
the nonlinear behavior of the soil is represented by an equiva-
lent linear viscoelastic model.

5.2 Measurement of Dynamic Properties

To obtain the representative shear modulus and damping
ratio for analyzing the performance of a soil-structure system
or an earth structure under a dynamic load, a dynamic test must
cover the expected strain spectrum. Three common types of labora-
tory tests used in obtaining such dynamic properties are: Cyclic
triaxial tests, cyclic simple shear tests, and resonant column
tests. The in-situ geophysical test is often used in evaluating
G_{max}, the shear modulus at a very low strain level. These tests
are discussed in the following sections.

5.2.1 Geophysical Tests

This test is used for the in-situ determination of the
maximum shear modulus, G_{max}, at strain levels below or at 10^{-7}.
Damping ratio cannot be easily measured in-situ due to the fact
that there is geometric damping besides the in-situ material
damping. Shear wave velocity of a soil layer is measured in
this test. The shear modulus of the soil layer, G, is then
related to the shear wave velocity as follows:

$$G = \rho \, v_s^2 \qquad (5.2)$$

where ρ is the mass density and v_s is the in-situ shear wave velocity measured in the field.

There are several methods for the measurement of the in-situ shear wave velocity such as: Refraction method, down-hole method, cross-hole method, and up-hole method (Richart, et al., 1970).

5.2.2 Cyclic Triaxial Tests

The cyclic triaxial test is the most popular laboratory dynamic test. This test can be used for determination of shear modulus and damping ratio at high strain levels (γ larger than 10^{-4}). After consolidation, isotropic or anisotropic, a cylindrical specimen is subjected to a series of repetitive axial compression and extension loads. The load can be either strain-controlled or stress-controlled. Although several different wave forms can be used, the most popular one is the sine wave with the frequency of half a Hertz (cycle per second). Vertical deformation is monitored during a test. Hysteresis loop of the tenth cycle is used in calculating the shear modulus G and the damping ratio D. The Poisson's ratio can also be determined if the diametrical deformation is also monitored.

Cyclic triaxial tests can also be used for liquefaction potential or cyclic strength investigation. In conducting a liquefaction test, in addition to the deformation measurement, the excess pore pressure should also be monitored. The purpose of conducting cyclic triaxial tests for dynamic properties is to observe the changes in hysteresis loop; namely, the changes in shear modulus and damping ratio. However, the purpose of conducting a cyclic

test for dynamic strength is two-fold: (1) to determine the number of cycles required to achieve a certain percent strain (sands and clays) and (2) to determine the number of cycles required to reach initial liquefaction.

5.2.3 Cyclic Simple Shear Tests

The loading conditions and the resulting strain of cyclic simple shear tests are believed to closely simulate the stress and strain in a soil mass subjected to a strong motion earthquake (Ishibashi, et al., 1974). In 1968, Peacock and Seed introduced a box-type simple shear device which more closely duplicated the in-situ stress-strain conditions in the laboratory and was capable of applying cyclic loads to a soil sample. In 1971, Finn reported an improved simple shear instrument. In 1974, Ishibashi and Sherif developed a torsional simple shear device, which eliminated the effects of wall friction. All stress components during a test are always known.

The test can be either stress-controlled or strain-controlled. A sinusoidal stress wave of 0.5 Hz is frequently used. Shear deformation and stress are monitored during a test. The hysteresis loop of the tenth cycle is used in calculating the shear modulus G and shear damping D. Similar to a cyclic triaxial test, a cyclic simple shear test can be used in determing both dynamic properties at strains larger than 10^{-4} and liquefaction potential.

5.2.4 Resonant Column Tests

According to Richart (1970) the resonant column test is the most convenient laboratory method for determination of dynamic

properties at a low strain level. There are various types of resonant column apparatus. The test is based on the principle of wave propagation in a soil column. In this test after consolidation, isotropic or anisotropic, a specimen is forced to vibrate either longitudinally and/or torsionally in one of its normal modes by the use of a vertical and/or torsional oscillator. The shear modulus is determined from the resonant frequency and the dimensions of a specimen. The damping ratio of a specimen can be determined from steady-state vibration and/or free vibration as discussed in Chapter 7.

Various types of resonant column apparatus give similar results. They differ mainly in the specimen boundary conditions. A torsional wave is applied either from the specimen top with its base fixed such as Hardin oscillator or from the specimen base with its top free to vibrate, such as Drnevich free-free resonant column apparatus. Specimen geometry (i.e., solid or hollow) and dimensions may also vary from one apparatus to the other. A group of researchers (Skoglund, et al., 1976) made the comparison of test results from six different types of resonant column test devices. Three of the devices had the capability of exciting a specimen in either the longitudinal mode or the torsional mode and were driven from their bases. The other three were for the torsional mode only, had fixed bases, and were driven from the specimen top cap. Solid samples were used. Their diameters ranged from 1.40 inches to 4.09 inches. The result of this investigation showed that no systematic or consistent differences could be associated with the different apparatus used.

Wave velocity in a soil column is measured at the top of
a specimen with a velocity transducer. In some resonant column
devices instead of the velocity transducer, an accelerometer is
used to measure the acceleration at the top of a specimen.
Almost all resonant column devices are designed to operate at
small strain amplitudes (less than 10^{-5} or sometimes up to 10^{-4}).
Due to its low strain level, the test is commonly known as being
nondestructive. However, studies of dynamic soil behavior at
relatively high strain levels (greater than 10^{-4}) were also con-
ducted by Drnevich (1967) using a torsional resonant column
apparatus developed at the University of Michigan. This device
was also capable of monitoring the change in length of a soil
specimen during a test.

Drnevich free-free resonant column apparatus, as described
in Chapter 6, was used in this study. Torsional vibration is fed
from the base. Two velocity transducers are located at the top
of a specimen.

5.3 Factors Affecting the Dynamic Properties of Granular Soils

In general shear modulus G and damping ratio D are affected
by many factors. Some of these factors have very strong effects
on dynamic properties, some have minor or insignificant effects,
and the effects of others are not known very well, mainly due to
the fact that they have not been studied systematically. In the
follwoing sections the very important factors (primary factors)
and less important factors (secondary factors) are discussed.
This classification is based on the results of studies of previous

researchers. However, it is important to note that this is not a general classification, because some factors might have very strong effects on shear modulus while they are insignificant with respect to damping ratio or vice-versa. Also all investigators do not agree with the importance or insignificance of some factors.

5.3.1 Primary Factors

Almost all researchers agree that strain amplitude γ, void ratio e, relative density D_r, and effective mean principal stress $\bar{\sigma}_0$ are the most important factors affecting the shear modulus G of all soils. However, according to some researchers $\bar{\sigma}_0$ does not have a strong effect on damping ratio D.

Shear modulus decreases very rapidly with shear strain γ. At very small strains ($\gamma < 10^{-7}$) shear modulus G has a maximum value, G_{max}, and it will remain relatively constant until strain amplitudes reach about 10^{-5}. At shear strains greater than 10^{-5} the rate of decrease of shear modulus with increasing strain depends primarily on the value of G_{max} and on the shear strength of the soil. Shear modulus seems to reach a steady magnitude at strains of about 10^{-2} to 5×10^{-2} depending on soil types (Richart, et al., 1970). Fig. 5.2 shows a typical variation of shear modulus with shear strain.

Damping ratio D increases very rapidly with strain amplitude γ and is equal to zero at zero strain. At a large strain damping ratio appears to approach a maximum value, D_{max}, asymptotically (Hardin, et al., 1972). Fig. 5.3 shows a typical variation of
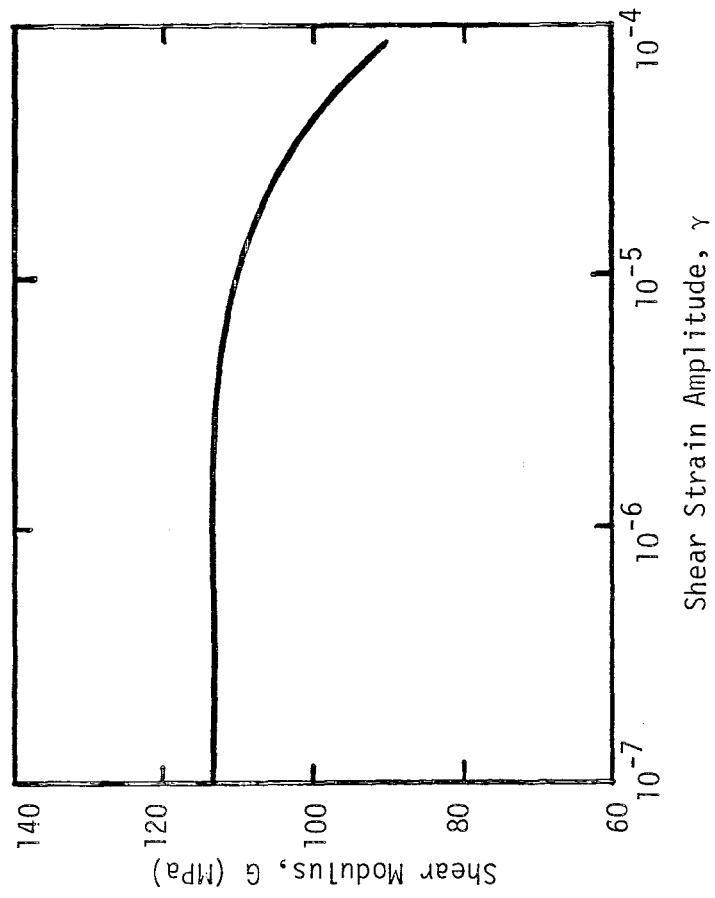
FIG. 5.2 SHEAR MODULUS VERSUS SHEAR STRAIN
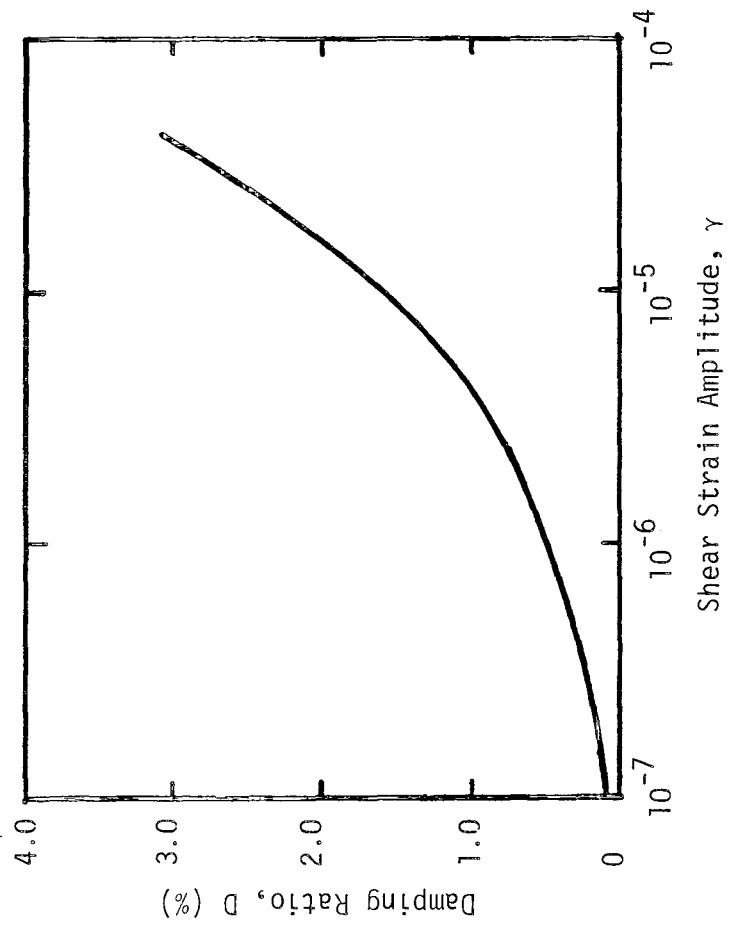
FIG. 5.3 DAMPING RATIO VERSUS SHEAR STRAIN

damping ratio with shear strain.

Shear modulus decreases with increasing void ratio, e, in undisturbed cohesive soils. Hardin, et al. (1969) suggested an empirical function for this effect as given by:

$$F(e) = \frac{(2.973-e)^2}{(1+e)} \qquad (5.3a)$$

where e is void ratio. Drnevich (1976) suggested the following continuous function F(e) for a quartz sand:

$$F(e) = 8.839 \exp(-1.51e) \qquad (5.3b)$$

Richart (1970) used equation (5.3a) for angular-grained materials and suggested another function for round-grained sands (with void ratios less than 0.80) as follows:

$$F(e) = \frac{(2.17-e)^2}{(1+e)} \qquad (5.3c)$$

According to Hardin and Drnevich (1972) and Edil and Luh (1978), void ratio is a very important factor affecting damping ratio. Damping ratio increases with increasing void ratio in undisturbed cohesive soils. However, according to Sherif, et al. (1977) and Seed, et al. (1970) void ratio has a very insignificant influence on damping ratio for void ratios in the range of 0.50 to 1.185.

Since relative density, D_r is a function of void ratio, e usually the effect of either D_r or e is considered. Relative density is known to have important influence on the densification and hysteresis of sands. When subjected to cyclic shear, sands exhibit dilatancy or densification and a highly nonlinear stress-strain relationship. The extent of these phenomena depends on

the relative density of sand, the amplitude of the shear strain,
and the state of stress. Sands with a low relative density
decrease in volume with the application of cyclic shear, whereas
the opposite is true for sands with a high relative density. If
the induced strains are very small, little relative movement
will take place between individual sand grains and the resulting
volume change will be small. In addition, the stress-strain
response of sands will be largely linear and elastic with rela-
tively little damping. However, at higher strain levels the
stress-strain behavior becomes distinctly nonlinear and inelastic
with significant hysteretic damping. As a consequence of grain
rearrangements that occur during successive cycles of shear,
shear modulus increases as the number of cycles increases and
decreases as strain amplitude increases. A group of researchers
(Cuellar, et al., 1977) conducted some strain-controlled cyclic
simple shear tests on a crystal silica No. 20 sand and concluded
that the densification of sands subjected to cyclic shear and the
shape of the hysteresis loop are strongly dependent on shear
strain, number of cycles, confining stress, and relative density
over a broad range of these parameters. The densification rate
increases with the shear strain amplitude and decreases with the
number of cycles and the relative density.

Shear modulus is strongly affected by effective mean prin-
cipal stress, $\bar{\sigma}_0$, and increases with increasing $\bar{\sigma}_0$. At very
small strains shear modulus varies with the square root of $\bar{\sigma}_0$,
but at large strains the modulus depends primarily on the strength
of soil and varies linearly with $\bar{\sigma}_0$ (Hardin and Drnevich, 1972).

Damping ratio at a given strain decreases with $\bar{\sigma}_0$. Hardin and Drnevich (1972) suggested that damping ratio decreases approximately with the square root of $\bar{\sigma}_0$. Sherif and Ishibashi (1977) indicated that damping is significantly affected by the confining pressure and it decreases with increasing confining pressure.

5.3.2 Secondary Factors

Hardin and Drnevich (1972) presented a list of less important or secondary factors which includes: Number of cycles of loading N_c, overconsolidation ratio O.C.R., effective strength parameters $\bar{c}$ and $\bar{\phi}$, octahedral shear stress τ_0, grain characteristics, time effect, frequency of loading f, soil structures, temperature, degree of saturation S, and stress history. The effects of some of these factors are discussed in this section.

A history of initial shear stress causes the modulus to be lower for the first few cycles of loading than it would be for the same soil without such a history of loading. However, Hardin and Drnevich (1972) conducted cyclic simple shear tests on clean sands and found that the effect of history of initial shear stress is removed by the tenth cycle, and the tenth and the 100th cycle data are similar. According to Wu (1975), for granular soils the effect of stress history is negligible on shear modulus. However, shear modulus is higher for overconsolidated soils than for normally consolidated soils.

Damping ratio is increased by the initial shear stress. The increase is more significant at a small strain. However, the deviatoric component, τ_0, (octahedral shear stress) of the initial

state of stress is much less important to the modulus and damping in soils than the isotropic component, $\bar{\sigma}_o$, effective mean principal stress (Hardin and Drnevich, 1972).

Hardin and Black (1969) reported that the number of loading cycles, N_c, has very little effect on maximum shear modulus, G_{max}. However, for a sand, shear modulus increases slightly with the number of cycles and for cohesive soils the modulus decreases somewhat with the number of cycles (Hardin and Drnevich, 1972). This behavior is dependent on stress ratio and test conditions and might not be valid in all tests. Edil and Luh (1978) suggested that the number of cycles of loading is relatively unimportant with respect to the shear modulus. However, it exerts a significant influence on the damping ratio. Sherif and Ishibashi (1976) reported that shear modulus increases with an increasing number of shear cycles, N_c, with the increase equal to approximately 28% for $2 < N_c < 25$ and remains nearly constant thereafter. However, they could not draw any definite conclusions with regard to the effects of number of loading cycles on the damping ratio. Hardin and Drnevich (1972) found that the damping ratio for both cohesive and cohesionless soils decreases approximately with the logarithm of the number of loading cycles. However, there is evidence that damping begins to increase with $N_c > 50,000$, which is due to some fatigue mechanism (Hardin, et al., 1972). Silver and Seed (1971) have also reported the tendency of damping to decrease with increasing number of cycles. From the above information one can conclude that the number of cycles, N_c is a secondary or less important factor for modulus and a primary or more important

factor with respect to the damping ratio.

The degree of saturation, S has a negligible effect on the modulus and damping for non-plastic soils but a strong effect for plastic soils. According to Hardin and Drnevich (1972), the effect of degree of saturation on shear modulus in cohesionless soils is small, but the modulus of cohesive soils increases rapidly with decreasing degree of saturation. The effect on damping in cohesionless soils is small.

Hardin and Black (1969) reported that frequencies up to 300 Hz have very little effect on maximum shear modulus for dry cohesionless soils. For undisturbed cohesive soils, damping ratio D only increases slightly with frequency within the range of 25 to 38 Hz. Although frequencies above 0.1 Hz have a relatively minor effect on G and D in cohesive soils, the behavior should be expected to change drastically for much lower frequencies where creep phenomena are involved (Hardin and Drnevich, 1972).

The effect of overconsolidation ratio, O.C.R. on maximum shear modulus, G_{max} has been reviewed by many researchers. The effect of preconsolidation is to increase G_{max} over its normally consolidated value, depending on the plasticity index, PI, of a soil. Overconsolidation ratio almost has no effect on G_{max} for soils with PI = 0 (Hardin, et al., 1972). Hardin and Black (1969) and Seed and Idriss (1970) have developed relationships for G_{max} considering the effect of O.C.R. These relationships are discussed in Section 5.4.

Beniwal (1977) reported that the modulus, G of most

particulate materials (coarse silty soil to gravelly boulders) increases with time (at least, at low strain amplitude). This behavior may be due to progressive increase in junction growth with or without oscillations. Final results may be more bonding (adhesion) between the particles, and the specimen will be more rigid. In the case of fine grained (uncemented) soils, inter-particle bond strength increases more rapidly than that of coarse grained soils. This could be a reason for higher gain in shear modulus of fine grained soil. But in coarse grained soil, the initial value of shear modulus is much higher than that in fine grained soil.

5.3.3 Grain Characteristics and Gradation

Grain characteristics and grain size distribution of soils can be characterized by many parameters such as: Grain size and shape, mineral types, and indices such as the uniformity coefficient C_u, the effective grain size D_{10}, the percent finer than 74 microns, the mean grain size D_{50}, and the coefficient of gradation C_g. A number of researchers have studied the effects of some of the above parameters on dynamic properties and the results of their findings are presented herein.

Seed and Idriss (1970) reported that at small strain levels, shear moduli for gravelly soils are between 1.25 and 2.5 times greater than those for dense sands. Afifi and Richart (1973) showed that the increase in G_{max} varied with grain size of the soil. Hardin and Drnevich (1972) explained that the grain charac-teristics will affect both the void ratio, a very important

parameter, and effective strength envelope, a less important parameter. But if the void ratio and the effective strength envelope of the soil are accounted for, then these two parameters will also account for most of the effects of grain characteristics, making it relatively unimportant in this context. Hardin (1973) (experimental data) found that shear modulus for coarse material (gravel size) is about 2.5 times of that for fine material (sand size). Krizek, et al. (1974) and Kuribayashi, et al. (1975) mentioned that for practical purposes, the particle size and distribution exert no influence on the wave propagation velocity (and hence the shear modulus). Based on the range of particle sizes and distribution used in their studies, results were inconclusive (Beniwal, 1977). Sherif, et al. (1977) observed that the damping is influenced by the coefficient of gradation, C_g (defined in Section 5.4). Iwasaki and Tatsuoka (1977) conducted a series of resonant column tests on clean sands (with $C_u < 1.8$ and no grains finer than 0.074 mm in diameter), natural sands which are well-graded and contain fine soils, and artificially graded sands which are not clean. The results of their tests show that, in general, shear moduli of sands decrease with the increase in uniformity coefficient, C_u and also decrease with the increase in the content of fine soils for the same values of mean principal stress, void ratio, and shear strain amplitude. They concluded that shear moduli of normally consolidated disturbed sands are greatly affected by grain size distribution characteristics. However, the effects of grain size distribution on damping properties of the sands tested are not so great as the effects on

shear moduli. Beniwal (1977) reported that the maximum shear modulus of a granular soil increases with increasing D_5 (grain diameter at 5% finer), whereas gradation, particle shape and particle size range do not show any effect on the shear modulus at strain amplitude, below 10^{-6}. However at higher strain amplitude the value of shear modulus is greatly influenced by the gradation of soils. Particle shape and particle orientation seems to have some influence on shear modulus at higher strain amplitudes. The mineral to mineral friction between grains also has some (minor) influence on the shear modulus of a granular soil. He used a resonant column device for his tests and most of his tests were conducted on gravelly soils. Yet other researchers (Edil and Luh, 1978) suggested that "reference shear modulus," G_0 (value of G at 0.25×10^{-4} shear strain amplitude) decreases with increasing mean roundness or decreasing angularity and is virtually independent of mean grain size within the range of $0.1 < D_{50} < 0.7$ mm and uniformity coefficient within the range of $1.2 < C_u < 3.4$. The sands used in their tests consist, mineralogically, of 80% or more quartz grains. Their final conclusion was that the effect of mean grain size, D_{50} and uniformity coefficient, C_u on dynamic modulus and damping is relatively unimportant.

5.4 Functional Relationships for Shear Modulus and Damping Ratio

Many researchers have studied the dynamic properties of soils, and in the past twenty years numerous relationships have been developed for shear modulus and damping ratio. In this

section some of these relationships are discussed.

Hardin and Richart (1963) suggested an empirical equation for maximum shear modulus which can be written as:

$$G_{max} = A \ F(e) \ \bar{\sigma}_0^{\ n} \qquad (5.4)$$

where G_{max} is the shear modulus at low strains less than 10^{-7}, $F(e)$ is the void ratio effect and was explained in Section 5.3.1 (equations 5.3a, b, c), $\bar{\sigma}_0$ is the effective mean stress and n varies from 0.5 to 0.6. The value of A for crushed quartz sand is 1230 $(psi)^{1/2}$, $\bar{\sigma}_0$ and G_{max} are both expressed in psi. For round-grained sands (e < 0.80), n = 0.5, A = 2630 $(psi)^{1/2}$, and $F(e)$ is from equation (5.3c).

Hardin and Black (1969) used the equation (5.4) for cohesive soils and modified it for stress history by including a factor for O.C.R. in the form of,

$$G_{max} = A \ F(e)(O.C.R.)^k \ \bar{\sigma}_0^{\ n} \qquad (5.5)$$

where k varies from 0 to 1/2 depending on the plasticity index and O.C.R. is the overconsolidation ratio.

Hardin and Drnevich (1970, 1972) presented a comprehensive study of nonlinear response and defined modulus and daming in terms of hyperbolic strain, γ_h. The modulus G, at a strain level γ is given by:

$$G = \frac{G_{max}}{(1 + \gamma_h)} \qquad (5.6)$$

where G_{max} is the maximum shear modulus and γ_h is defined by:

$$\gamma_h = \frac{\gamma}{\gamma_r} \left[1 + a \ exp \ \left(-b[\frac{\gamma}{\gamma_r}]^c \right) \right] \qquad (5.7)$$

where $\gamma_r = \tau_{max}/G_{max}$ and γ is the shear strain amplitude

$$\tau_{max} = \left[\left(\frac{(1 + K_0)}{2} \bar{\sigma}_v \sin \bar{\phi} + \bar{c} \cos \bar{\phi} \right)^2 - \left(\frac{(1 - K_0)}{2} \bar{\sigma}_v \right)^2 \right]^{1/2} \quad (5.8)$$

where K_0 = coefficient of lateral earth pressure at rest, $\bar{\sigma}_v$ = vertical effective stress, $\bar{c}$ and $\bar{\phi}$ are strength parameters, and the values of a, b, and c depend on· loading types and soil types. For clean sands in the case of complete stress reversal, a = -0.5, b = 0.16 and c = 1.0.

The damping ratio D, at a strain level γ is given by:

$$D = \frac{\gamma_h \, D_{max}}{1 + \gamma_h} \quad (5.9)$$

where γ_h is the hyperbolic strain defined as above and

$$D_{max} = 33 - 1.5(\log N_c) \quad (5.10)$$

for clean dry sands (N_c is the number of cycles), and in the case of complete stress reversal, a = $0.6(N_c^{-1/6}) - 1$, b = $1 - N_c^{-1/12}$ and c = 1.0.

Beniwal (1977) suggested a modified and generalized form of the following empirical expression for shear modulus of granular soils that includes the effect of grain size distribution:

$$G = \frac{G_{max}}{1 + \frac{\gamma}{\gamma_r} \left[1 + (1.75 \pm 0.5) \, C_u^{0.35} \exp(-[\frac{\gamma}{\gamma_r}]^{0.4}) \right]} \quad (5.11)$$

where $\gamma_r = \tau_{max}/G_{max}$, γ is the shear strain amplitude, τ_{max} is defined by equation (5.8) and C_u is the uniformity coefficient. (+) sign is for feldspar (clean) gravels and (-) sign is for natural gravels. As it was stated earlier most of the tests in his study were conducted on gravelly soils.

Sherif, et al. (1976, 1977) proposed relationships for modulus and damping for dry sands. In their studies the equivalent shear modulus, G_{eq} is defined as the slope of the line that connects the two ends of a nonsymmetric hysteresis loop. G_{eq} at a strain level γ is given by:

$$G_{eq} = [2.8 \, \phi \, (\bar{\sigma}_c)^{0.85}] \, \gamma^{-0.6} \quad \text{for } \gamma > 0.0003 \quad (5.12a)$$

$$G_{eq} = [2.8 \, \phi \, (\bar{\sigma}_c)^{11.67 \, \gamma + 0.5}] \, 40 \, (0.205)^{\gamma/0.03} \quad \text{for } \gamma < 0.0003$$
$$(5.12b)$$

where $\bar{\sigma}_c$ is the effective confining pressure and ϕ is the angle of internal friction. Equations (5.12a) and (5.12b) are valid for the second cycle only, in order to obtain G_{eq} for other cycles, one should use the correlation factors given by:

$$F_n(N_c) = 0.253 \, \log N_c + 0.924 \quad \text{for } 2 < N_c < 25 \quad (5.13a)$$

$$F_n(N_c) = 1.28 \quad \text{for } 25 < N_c \quad (5.13b)$$

where N_c is the number of cycles of loading and $F_n(N_c)$ is the correlation factor, when multiplied by the G_{eq} values for the second cycle (Eq. 5.12a and 5.12b), will yield the corresponding G_{eq} value for a specific number of cycles.

They also proposed a similar equation for damping ratio, D as:

$$D = \frac{50 - 0.6 \, \bar{\sigma}_c}{38} (73.3F - 53.3) \, \gamma^{0.3} \, R(N_c) \quad (5.14)$$

where $\bar{\sigma}_c$ is the effective confining pressure (psi), F is the soil gradation and sphericity factor given by:

$$F = \frac{1}{\psi^2 \, C_g} \quad (5.15)$$

where ψ = soil sphericity and C_g = coefficient of gradation =

$\dfrac{D_{30}^{2}}{D_{10} \times D_{60}}$, D_{10}, D_{30}, and D_{60} denote soil grain diameters corre-

sponding to 10, 30 and 60 percent finer by weight on the

gradation curve, γ is the shear strain in the range of 5×10^{-5}

to 10^{-2} and $R(N_c)$ is the correlation factor given by:

$$R(N_c) = 1.01 - 0.046 \log N_c \qquad (5.16)$$

where N_c is the number of cycles of loading. Equation (5.16) is

based on the results reported by Hardin, et al. (1972).

Iwasaki and Tatsuoka (1977) from Japan suggested an empirical

expression for shear moduli G of various clean sands given by:

$$G = A(\gamma) \cdot B \cdot \frac{(2.17 - e)^{2}}{(1+e)} p^{m(\gamma)} \qquad (5.17)$$

where $A(\gamma)$ is a function of shear strain γ and A (at $\gamma = 10^{-6}$) =

900, A (at $\gamma = 10^{-5}$) = 850 and A (at $\gamma = 10^{-4}$) = 700; $m(\gamma)$ is also

a function of γ: m (at $\gamma = 10^{-6}$) = 0.40, m (at $\gamma = 10^{-5}$) = 0.44 and

m (at $\gamma = 10^{-4}$) = 0.5, B is a parameter dependent on the variety

of a normally consolidated sand and for uniform clean sands

without fine soils is equal to 1.0, e is void ratio and p is mean

principal stress.

Edil and Luh (1978) proposed relationships for shear modulus

and damping ratio of sands for a certain range of strains given

by:

$$G = G_0 (1.004 - 345.4 \gamma) \qquad (5.18)$$

where G_0 is the reference shear modulus (G at 0.25×10^{-4} strain)

and is given by:

$$G_0 = [0.769 + \ln (\frac{\bar{\sigma}_0}{98.07} + 1)(2.793 - 2.195\ e) - 0.801\ R] \times 10^{-5}$$

(5.19)

G, G_0, $\bar{\sigma}_0$ (effective mean principal stress) all in (KN/m^2),
R is mean roundness and e is void ratio.

The relationship for damping D is expressed as:

$$D = D_0\ (1.131 - 0.0453\ \log N_c)$$ (5.20)

where D_0 is reference damping ratio (D at N_c = 1000 cycles) and
is given by:

$$D_0 = 0.88 + 6592\ \gamma\ e^{1/2} - 0.28\ \gamma^{1/3}\ (\frac{\bar{\sigma}_0}{98.07})^3 - 73.55\ \gamma\ \bar{\sigma}_0^{1/2}$$

(5.21)

D and D_0 are in %, $\bar{\sigma}_0$ in (KN/m^2), N_c is the number of cycles
and e is void ratio.

All equations suggested by Edil and Luh are only valid for
strains less than 2×10^{-3} and the sands used contain 80% or more
of quartz grains.

CHAPTER 6

TEST EQUIPMENTS

6.1 Drnevich Free-Free Torsional Resonant Column Apparatus

In using a torsional resonant column device to measure
dynamic properties of soils, a torsional excitation is applied
to one end of a specimen. The other end of the specimen can
either be free or fixed.

Usually a sinusoidal wave is used to excite a specimen.
However, theoretically any wave forms are acceptable. During
a test the wave frequency is continuously varied, usually de-
creased, in an attempt to obtain a resonant frequency. The
resonance is evidenced by a straight line Lissajous figure.
A shear modulus can then be determined from the corresponding
resonant frequency.

A damping ratio can be determined from the steady state
vibration or free vibration as shown in Step 15 of the section
on data reduction in Chapter 7. One of these methods utilizes
the curve of the logarithmic decay of torsional vibration
amplitude. A typical logarithmic decay curve is shown in
Fig. 7.12.

The schematic diagram of the free-free torsional resonant
column device is shown in Fig. 6.1. The excitation torsional

MASS RIGIDLY CONNECTED TO PLATEN

PASSIVE END PLATEN

SOIL SPECIMEN

ACTIVE END PLATEN
WEIGHTLESS TORSIONAL SPRING

WEIGHTLESS TORSIONAL
DASHPOT

{ PORTION OF VIBRATION EXCITATION
  DEVICE RIGIDLY CONNECTED TO PLATEN
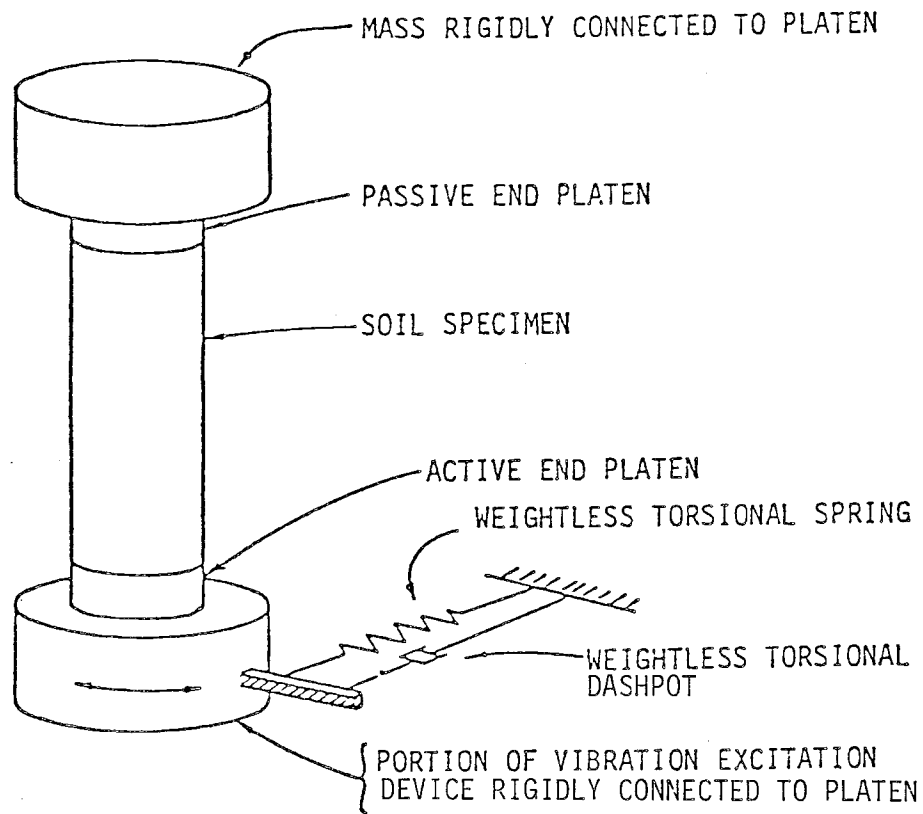
FIG. 6.1   FREE-FREE TORSIONAL RESONANT
           COLUMN SCHEMATIC

wave is applied from the lower end of a specimen and the other
end is free to vibrate. The excitation is applied by means of
two electric coils and magnets as shown in Fig. 6.2. The
device is capable of testing 2.8-, 4- and 6-inch diameter speci-
mens. Either vacuum or confining pressure can be used to
supply effective stresses to a specimen. Vacuum can be applied
from a quick connecter which leads to the inside of a specimen.
The connecter is located on the base of the apparatus. Confining
pressure can be applied from the top of the pressure chamber.
Specimens can be either dry or saturated. In testing saturated
specimens pore pressure can be measured by means of a transducer
located at the base of the apparatus. Confining medium can be
either air or water. Water can be filled into the chamber from
a quick connecter located at the base.

Two velocity transducers (active) located under the base
of the chamber are used to determine the resonant frequency of
the apparatus which includes the base, an active (or bottom)
platen, 8 rods and nuts, chamber and top lid. During a test
the resonant frequency can be determined for the system which
includes the apparatus including a passive (or top) platen and
a specimen. Hence, there are two resonant frequencies, one
for the "apparatus" (f_{oT}) and the other for the "system" (f_T).
Procedures for determining these frequencies are outlined in
Chapter 7.

6.2 Pressure and Vacuum System

The pressure and vacuum system which provides an access
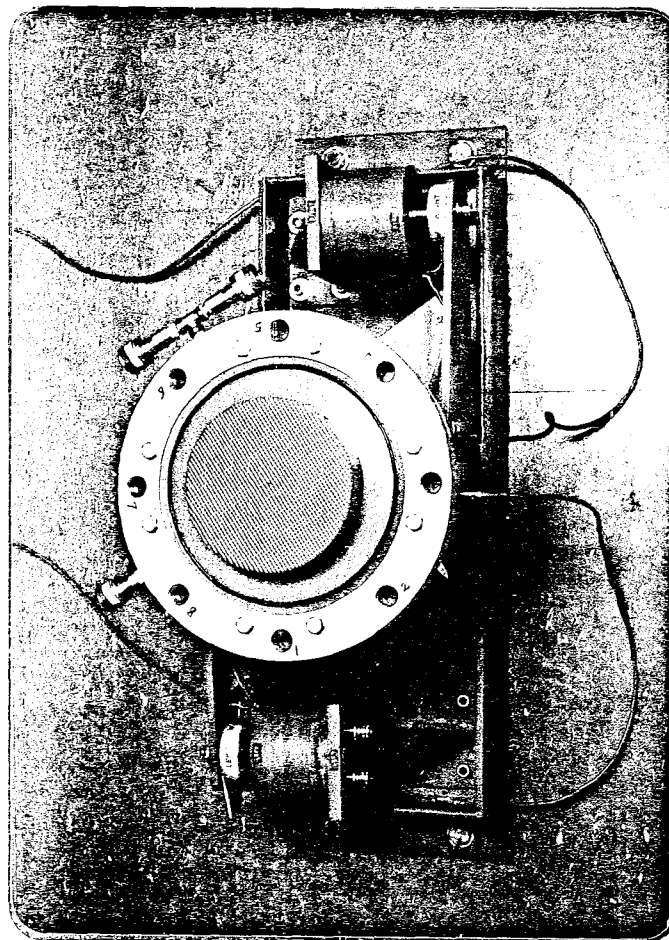
FIG. 6.2 DRNEVICH FREE-FREE RESONANT COLUMN APPARATUS

to vacuum, chamber pressure and back pressure is shown in Fig. 6.3. It consists of one vacuum gauge and regulator connected to a vacuum pump; two pressure gauges and regulators (one pair each for confining and back pressures respectively) connected to a house pressure line. A burette for monitoring the volume change of a saturated specimen during a test is also provided. A pair of quick connecters and shut-off valve is provided for each vacuum and pressure line.

6.3 Electronic Monitoring System

The electronic devices used in the test and the wiring diagram are shown in Figs. 6.4 and 6.5 respectively. The electronics include a function generator, a frequency counter, a power amplifier, a digital voltmeter and two storage oscilloscopes.

The sine wave generated by the function generator is amplified by the power amplifier and then fed into the driving coils which are located on the resonant column device. The frequency of the input wave can be adjusted by a frequency dial and read by a digital counter. The input wave induces vibration in the coils and the resulting torsional wave is fed into a soil sample. The wave travels upward in the sample and the output is picked up by the two velocity transducers at the top of the specimen (passive transducers). The voltage of the input and output waves is read through the digital voltmeter. If the switch is on the "Power" position the voltmeter reads the input voltage (torque) and if it is on the "Passive"
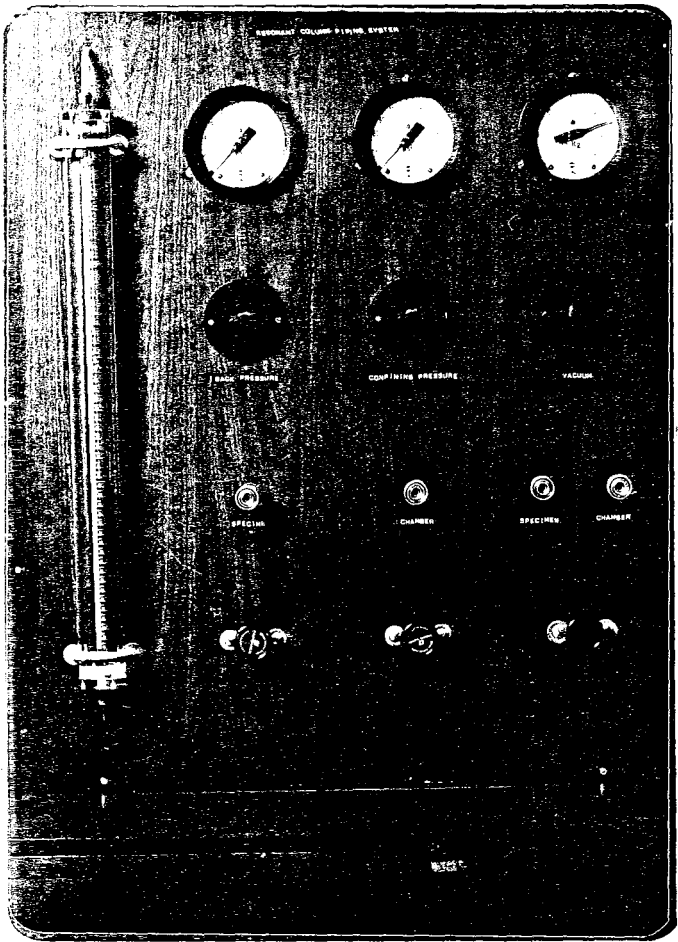
FIG. 6.3 PRESSURE AND VACUUM SYSTEM
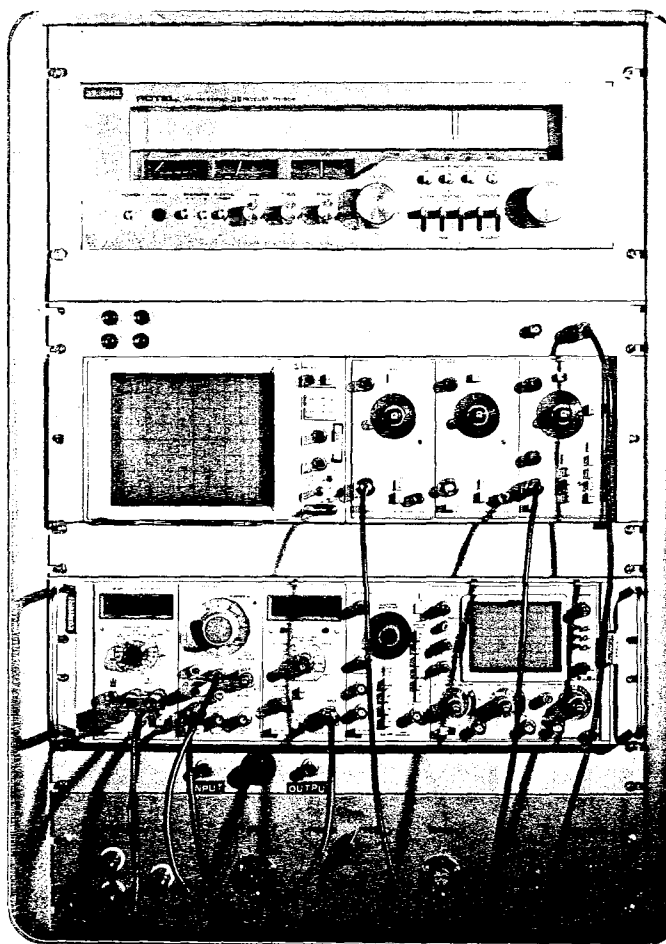
FIG. 6.4 ELECTRONIC MONITORING DEVICES
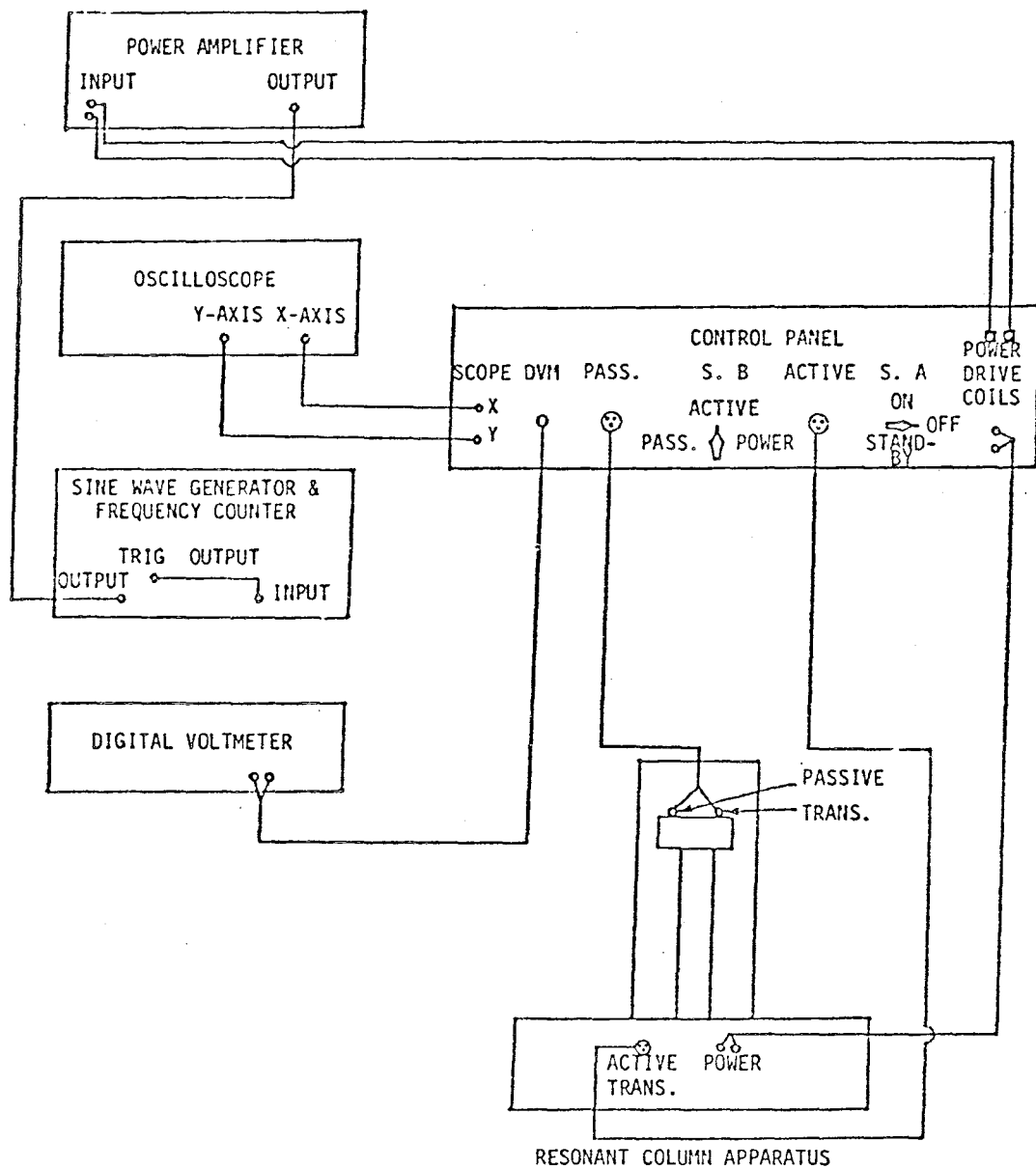
FIG. 6.5 WIRING DIAGRAM

position the voltmeter reads the output (passive) voltage.
The Lissajous figure can be observed on the oscilloscope.
The "Active" transducers located at the base of the chamber are
for measuring the resonant frequency of the apparatus without
a sample. The procedures for this measurement are described
in Chapter 7.

6.4 Additional Supporting Equipment

To improve the quality of artificially prepared specimens,
three additional devices were designed and manufactured. A
"zero-raining" device, shown in Fig. 6.6, was designed to
improve the repeatibility and uniformity of artificially prepared
specimens. It is a hollow cylinder with a screen attached to
its end. Procedures for its use are outlined in Chapter 7. End
screens with different openings can be used. The selection of
screens is guided by the particle size of a specimen.

A leveling device shown in Fig. 6.7 was designed to level
the top of a specimen in a mold. The device has a plate with
two holes for mounting the device on two supporting rods, a
circular rod with a leveling blade and a handle attached to its
ends. To level a specimen, set the blade on its top and rotate
the handle. Detailed procedures are given in Chapter 7.

Finally a temporary supporting device shown in Fig. 6.8
is used to support the passive (or top) platen. After a speci-
men is prepared and leveled, the passive platen is placed on
its top. This heavy platen needs to be supported by a fixed
temporary support to prevent sample disturbance. Therefore, the
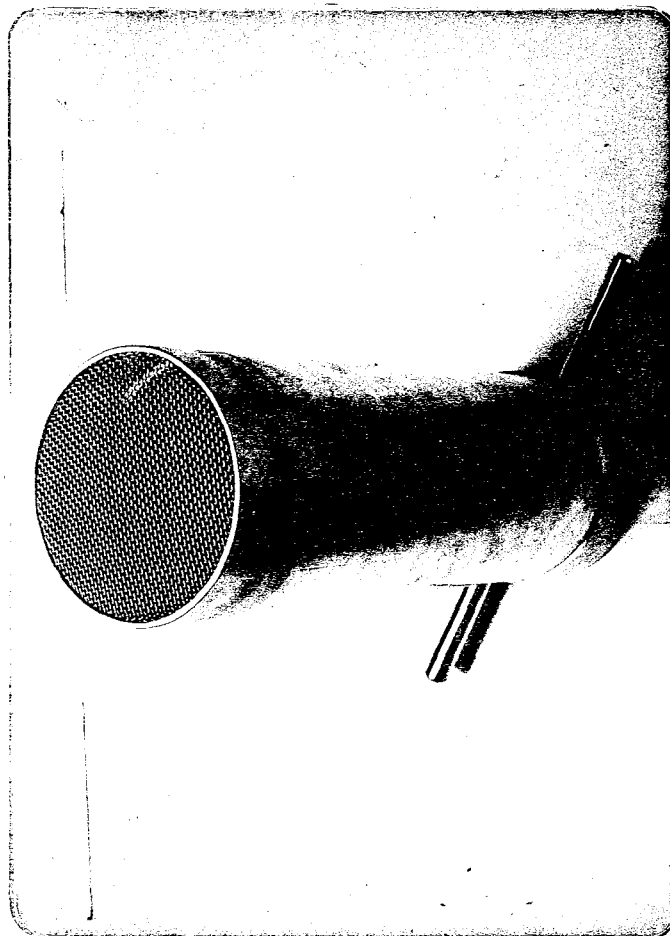
FIG. 6.6 ZERO HEIGHT RAINING DEVICE
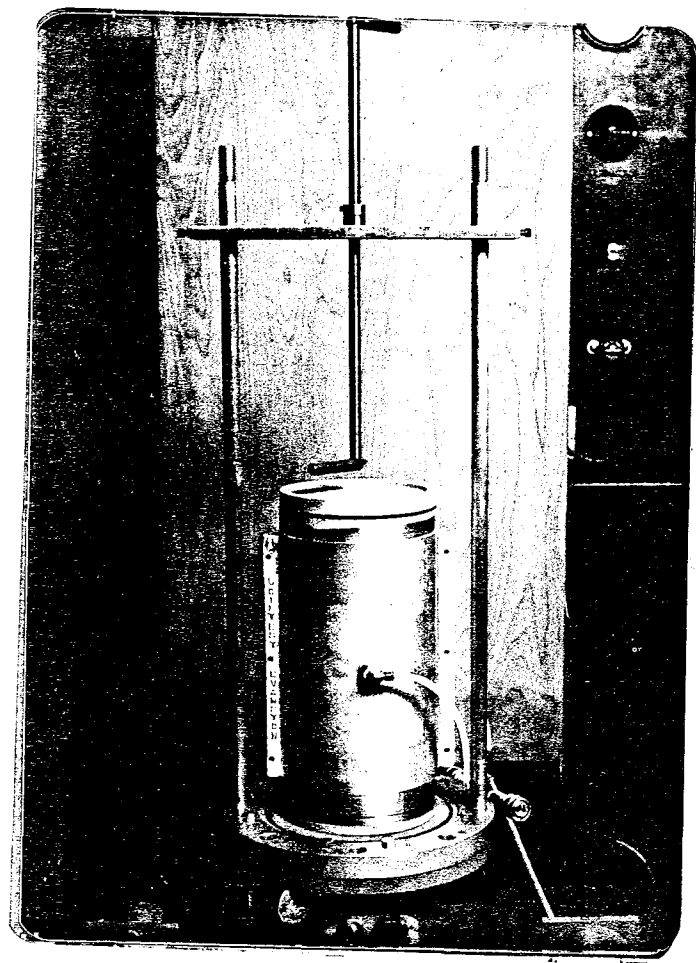
FIG. 6.7 LEVELING DEVICE
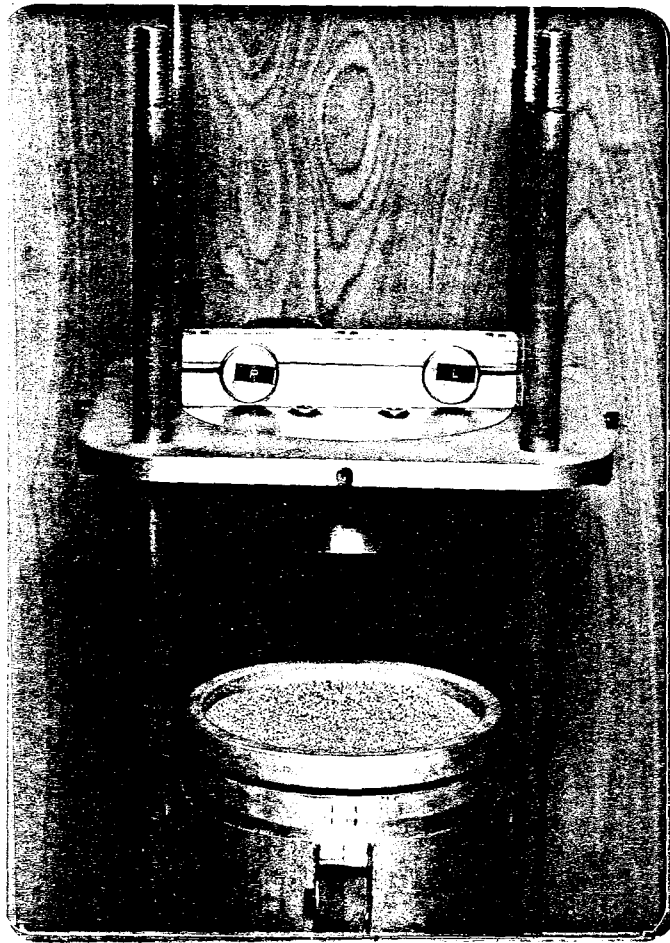
FIG. 6.8 TEMPORARY SUPPORTING DEVICE

temporary supporting device is used to support the platen during the placement of the membrane and O-ring. The support can be removed after the membrane and O-ring are in place as described in Chapter 7. Fig. 6.9 shows a complete resonant column test facility.

6.5 Improvements to the Testing Equipment

In order to achieve better accuracy and conduct more consistent tests, several modifications were adopted. After performing numerous tests it was found that the flexibility of the floor and the friction between the base of the equipment and the floor have important effects on the test results. Therefore, the apparatus was bolted to a 10 inch concrete floor by means of four anchor bolts and a concrete pad (2 inches thick) was constructed around the base of the apparatus in order to prevent any movements (Fig. 6.10). It was also observed that the tightness of the nuts at the top of the chamber influences the test results. Hence, the round aluminum nuts were replaced with hexagon steel nuts and each nut was tightened to 600 (lb-in) with a torque wrench. Eight more nuts were attached to the bottom of the rods to prevent their rotation.

Originally the apparatus was equipped with two boxes called the "Control" box and the "Switch" box, which were used to connect the equipment to the electronic devices. These boxes were replaced by a panel that accommodated all of the components of the boxes and was mounted on an instrument rack (Fig. 6.4). Therefore, the number of long wires were reduced and, as a
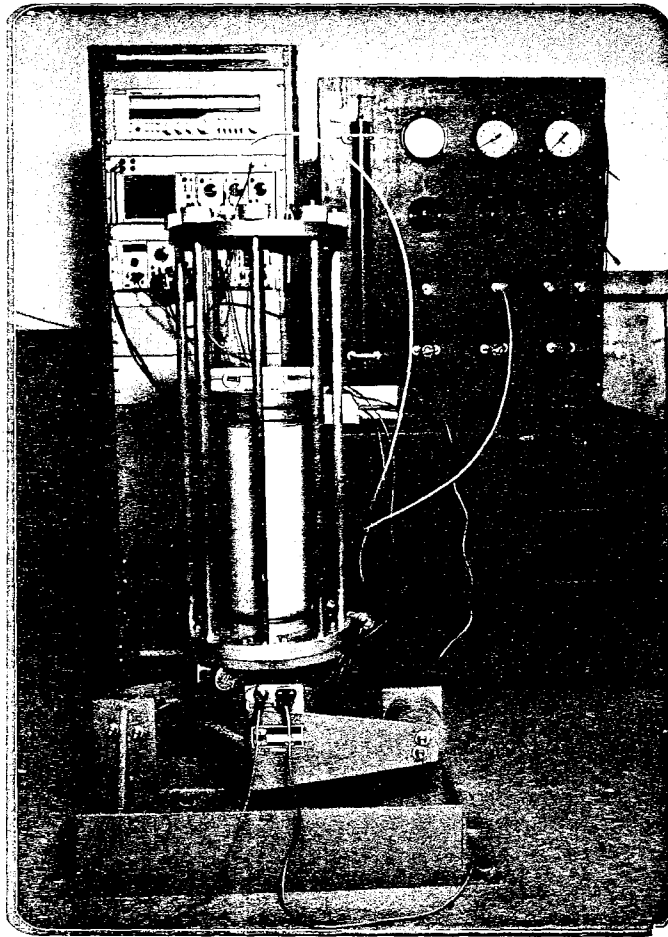
FIG. 6.9 COMPLETE RESONANT COLUMN TEST SYSTEM

FIG. 6.10 CONCRETE PAD AROUND THE BASE OF THE APPARATUS

result, the noise level in the circuit was lowered.

In order to provide faster and easier pressure and vacuum connections all of the valves and fittings were replaced by quick connecters.

CHAPTER 7

SPECIMEN PREPARATION, TEST PROCEDURES AND DATA REDUCTION

7.1 Material and Sample Preparation

The primary material used in this study was a well-graded river sand obtained locally in Denver, Colorado. Figs. 2.1 and 2.2 show the grain size and shape of the Denver sand, and one of the samples, respectively. Some of the samples were prepared by adding gravels to the above sand. Gravel sizes ranged from 3/8 inch to No. 10 sieve. After the sand was oven-dried, it was sieved by sieves ranging from No. 10 to No. 400. Six different mean grain sizes (D_{50}) were chosen as shown on the grain size distribution chart (Fig. 2.4). At each mean diameter grain size distribution curves with uniformity coefficients (C_u) ranging from 2 to 15 were plotted as shown in Fig. 2.4. Then a sample was mixed according to each grain size distribution curve. A total of twenty-four samples were obtained in this manner. Each sample was labeled according to its mean grain size and uniformity coefficient. Samples $DC-a_2$, $DC-a_4$, $DC-a_6$, and $DC-a_8$ have the same mean grain size, a $(D_{50} = 1.68$ mm) with uniformity coefficients of 2, 4, 6, and 8 respectively. Symbol DC stands for Denver Coarse sand. Similarly samples $DC-b_4$, $DC-b_6$, $DC-b_8$, $DC-b_{10}$, and $DC-b_{15}$ have the same mean grain size b $(D_{50} = 0.84$ mm) and different uniformity coefficients. The other samples

were prepared in the same manner with mean grain sizes: c

(D_{50} = 0.59 mm), d (D_{50} = 0.42 mm), e (D_{50} = 0.25 mm) and f

(D_{50} = 0.149 mm) and different uniformity coefficients. Symbols

DM and DF represent Denver Medium and Fine sands respectively.

In addition to the above samples, Monterey No. 0 sand was

also used in some tests. It is a uniform (C_u = 1.5), medium

grain size beach sand from California, composed mostly of quartz

and some feldspar. The grains are subrounded and somewhat

elongated (Fig. 2.3). Fig. 2.5 shows the grain size distribution

of Monterey No. 0 sand.

Minimum and maximum densities of each sample were measured

prior to testing. The procedures in the Earth Manual were used

to obtain these densities. The procedures are given in the

Appendix E-12 on "Relative Density of Cohesionless Soils" in the

Manual (2nd Edition, 1974), a publication of the Water and Power

Resources Service (formerly the Bureau of Reclamation). The

values of minimum and maximum densities and other material proper-

ties are given in Table 7.1.

7.2 Specimen Preparation

The preparation of a specimen is the most important and

critical part of the resonant column test. Extreme caution must

be exercised in order to prepare a desired specimen without any

grain segregation. Detailed procedures for preparing specimens

of granular soils are as follows:

1. Measure the inside diameter and height of the specimen

   mold.

TABLE 7.1

SAMPLE SPECIFICATIONS AND INDEX PROPERTIES

Sample*	γ_{max} lb/(ft)^3	γ_{min} lb/(ft)^3	D_r (%)	e	G_s	C_u	D_{50} (mm)	D_{10} (mm)
DC-a$_2$	104.89	87.03	29.9	0.811	2.66	2	1.68	0.97
DC-a$_4$	114.80	94.46	29.5	0.667	2.66	4	1.68	0.55
DC-a$_6$	121.24	98.91	29.8	0.587	2.66	6	1.68	0.40
DC-a$_8$	125.03	101.88	27.9	0.549	2.66	8	1.68	0.32
DC-b$_4$	116.00	95.45	27.4	0.656	2.66	4	0.84	0.28
DC-b$_6$	121.33	99.41	29.5	0.582	2.66	6	0.84	0.20
DC-b$_8$	123.96	102.38	29.8	0.537	2.66	8	0.84	0.16
DC-b$_{10}$	126.23	103.86	29.9	0.514	2.66	10	0.84	0.135
DC-b$_{15}$	129.58	106.83	29.2	0.475	2.66	15	0.84	0.10
DM-c$_2$	105.74	87.03	29.5	0.808	2.66	2	0.59	0.34
DM-c$_4$	118.36	93.96	28.8	0.663	2.66	4	0.59	0.195
DM-c$_8$	125.64	101.39	28.8	0.547	2.66	8	0.59	0.11
DM-c$_{10}$	127.41	103.47	30.9	0.511	2.66	10	0.59	0.09
DM-c$_{15}$	129.21	105.35	30.0	0.489	2.66	15	0.59	0.07

* DC = Denver Coarse Sand; DM = Denver Medium Sand; DF = Denver
  Fine Sand; M = Monterey No. 0 Sand

TABLE 7.1 (Continued)

SAMPLE SPECIFICATIONS AND INDEX PROPERTIES

Sample*	γ_{max} lb/(ft)^3	γ_{min} lb/(ft)^3	D_r (%)	e	G_s	C_u	D_{50} (mm)	D_{10} (mm)
DM-d$_2$	106.08	85.05	31.0	0.832	2.66	2	0.42	0.24
DM-d$_4$	115.75	91.98	30.5	0.692	2.66	4	0.42	0.14
DM-d$_6$	121.78	96.93	28.6	0.613	2.66	6	0.42	0.10
DM-d$_8$	123.35	98.91	31.2	0.575	2.66	8	0.42	0.08
DM-d$_{10}$	125.94	101.88	30.5	0.535	2.66	10	0.42	0.07
DM-e$_2$	106.38	82.67	34.3	0.854	2.66	2	0.25	0.145
DM-e$_4$	116.92	90.495	26.7	0.725	2.66	4	0.25	0.08
DM-e$_6$	119.67	94.55	30.5	0.644	2.66	6	0.25	0.06
DF-f$_2$	102.95	79.60	29.6	0.946	2.66	2	0.149	0.09
DF-f$_3$	108.86	84.06	30.2	0.839	2.66	3	0.149	0.06
M-1-1	105.92	91.96	11.8	0.774	2.655	1.5	0.40	0.27
M-2-1	105.92	91.96	45.1	0.696	2.655	1.5	0.40	0.27
M-3-1	105.92	91.96	73.0	0.629	2.655	1.5	0.40	0.27

* DC = Denver Coarse Sand; DM = Denver Medium Sand; DF = Denver
Fine Sand; M = Monterey No. 0 Sand

2. Measure the height of the lower platen. The difference between the height of the mold and platen is termed "effective height."

3. Measure the thickness of the membrane. The difference between the inside diameter of the mold and two times the thickness of the membrane is "effective diameter."

4. Calculate the "effective volume" of the mold. This volume indicates the maximum volume of soil that can be placed in the mold.

$$V_e = \frac{\pi (d_e)^2}{4} \times (H_e - h)$$

where V_e = effective volume,

   d_e = effective diameter,

   H_e = effective height, and

   h = the distance between the top of the speci-
   men and the top of the mold.

The distance h can be adjusted to obtain a specimen of a specific height or density. For example:

$H_e - h = 12$ inches for a 6-inch diameter specimen of aspect ratio 2.

5. To prepare a specimen of a desired density, the required weight of soil can be calculated as follows:

$$W_{req} = V_e \times \gamma_d$$

where W_{req} = required weight of the sample,

   V_e = effecive volume, and

   γ_d = desired dry density of the sample.

Usually a specimen is prepared to achieve a certain relative density (D_r). Hence, one must convert this relative density to a corresponding dry density (γ_d) and then determine the required weight of the soil. All the specimens were prepared to obtain a relative density of 30%.

6. Weigh the required amount of soil.

7. Apply a thin layer of vacuum grease to the side of the lower platen.

8. Place the membrane over the lower platen and seal it on the lower platen by an O-ring. The top surface of the platen has sharp edges. Extreme caution must be exercised so that the membrane will not be torn.

9. Place the mold over the lower platen. Pull the membrane through the mold and wrap it around the upper edge of the mold.

10. Apply vacuum to the mold so that the membrane sticks to the inner wall of the mold without any wrinkles. Seal the membrane on the top of the mold with an O-ring.

11. Place a small piece of filter paper over the center hole of the lower platen.

12. Place the "zero-raining" device in the mold. Be careful not to tear the membrane.

13. Pour the desired amount of soil in the "zero-raining" device, mix it thoroughly and then raise the device so that the soil can be uniformly deposited in the mold. Occasionally, it is necessary to tap the mold by a

plastic-head hammer while raising the device in order to achieve the desired relative density. Therefore, several trials should be performed to obtain the desired density.

14. Attach four of the locking rods to the apparatus for supporting the leveling system. Do not vibrate the sample.

15. Attach the leveling system to two of the rods and lower the lever arm so that the blade of the lever arm just touches the soil in the mold. Rotate the lever arm until the top of the specimen is completely leveled. Remove the leveling system.

16. Thinly grease the top platen and fix it in its temporary support by means of four screws.

17. Lower the temporary support with the four supporting rods slowly sliding inside its four holes until the top platen sits on top of the specimen and then carefully remove the temporary support.

18. Use a level to make sure that the top platen is properly leveled.

19. Lower the O-ring on the mold top to release the membrane, place the membrane over the top platen and seal it with the O-ring.

20. Apply a vacuum of 10 inches of mercury to the specimen and wait for 10 to 15 minutes.

21. Carefully remove the mold by removing the screws on the mold.

22. Measure the diameter of the specimen by using a "Pi-tape" as shown in Fig. 7.1. When wrapped around the specimen, "Pi-tape" directly reads the specimen diameter. Also measure the height of the specimen.

23. Back calculate the density of the specimen by using the measured values of diameter, height and weight to make sure that it is the same as the desired density.

24. Screw the nuts and washers on the bottom of the rods and place the rods on the apparatus. Tighten the nuts in order to prevent the rods from rotating and touching the bottom plate.

25. Place the plastic chamber over the specimen.

26. Connect the lead from the passive transducers to its receptacle on the lid of the apparatus. Place the lid on the apparatus and carefully hand tighten it onto the apparatus by eight nuts and washers. Then tighten each nut with a torque-wrench up to 600 lb-in as shown in Fig. 7.2.

27. Connect the pressure line to the top of the apparatus and gradually apply a confining pressure of 3 to 4 (psi) and lower the vacuum by the same magnitude.

28. Repeat the procedures until zero vacuum. Adjust the confining pressure to the desired magnitude.

29. For dry sands, the specimen will consolidate within the first 15 to 30 minutes. However, all the specimens were consolidated for one hour prior to testing and the pore pressure line was left open during consolidation and
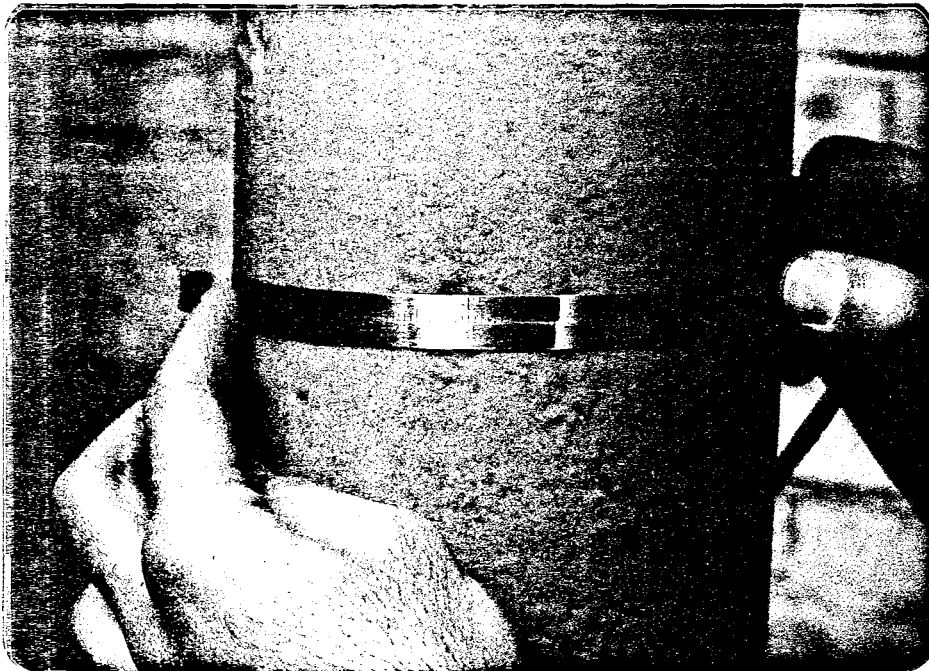
FIG. 7.1 MEASURING THE DIAMETER OF THE
SPECIMEN WITH A PI-TAPE

FIG. 7.2 TIGHTING THE NUTS WITH A TORQUE-WRENCH

testing.

7.3 Testing Procedures

Before preparing the specimen and testing, the apparatus resonant frequency should be determined in the following manner:

1. Apparatus in normal position, i.e., lower platen attached, chamber, rods, lid, and nuts in place and tightly fastened.

2. Wiring should be like the wiring diagram except that the lead from the control panel which is marked "voltmeter" must be connected to the Y-axis of the oscilloscope instead of the voltmeter. Switch B must be in the "Active" position.

3. Apply a small amount of power to the coils by gradually turning up the "Volume" knob on the amplifier.

4. Turn switch A on the control panel to "On" position.

5. Adjust the frequency until the Lissajous figure closes to a straight sloping line. The lowest frequency at which the straight line is observed is the resonant frequency of the apparatus (f_{oT}).

After the specimen is consolidated, testing can begin according to the following procedures:

1. Connect all the electrical connections according to the wiring diagram shown in Fig. 6.5.

2. Turn switch A on the control panel to the "Standby" position and switch B to the "Power" position.

3. Select a desirable wave form. Sine wave was used in

this study.

4.   Set frequency slightly above the apparatus resonant
      frequency (f_{oT}).

5.   Apply a small amount of power so that the voltmeter
      reads about 5 mv_{rms}. Record this power (torque) reading.

6.   Turn switch A on the control panel to "On" position and
      adjust the frequency until the shape of Lissajous figure
      is close to a straight sloping line. The frequency is
      the system resonant frequency (f_T). Record the
      frequency.

7.   Turn switch B on the control panel to "Passive" position
      and record the passive transducer reading with the volt-
      meter.

8.   Turn switch A on the control panel to "Off" position and
      switch B to "Power" position.

9.   Turn switch A on the control panel to "Standby" position
      and increase the power by 50% and record this power
      (torque) reading.

10.   Repeat the steps 5 to 9 until the maximum allowable
      power (50 watts) is reached.

Readings are taken at equally timed intervals (2 minutes).

7.4 Data Reduction

The procedures given in this section are for the manual calcu-
lation of shear modulus, shear strain amplitude and damping ratio.
These parameters are calculated by using the wave propagation
theory and the schematic shown in Fig. 6.1 (Drnevich, 1978).

The computer program RESCOL 7 (Drnevich and Lorenz, May 1980) was used for the calculation of shear modulus, shear strain amplitude and damping ratio.

Following are the procedures:

(Subscript T denotes torsional vibration.)

1. Record the specimen weight measured before a test.

2. The volume of the specimen should be the same as the "effective volume." Calculate the volume of the specimen from its measured diameter and height. The calculated volume should be close to the "effective volume."

3. Calculate density (γ_d):

$$\gamma_d = \frac{W}{V}$$

where   W = weight of the specimen (lb. or gr.),

         V = volume of the specimen (ft^3 or cm^3), and

         γ_d = density of the specimen (lb/ft^3 or g/cm^3).

γ_d should be the same as the "desired" density.

4. Calculate mass density (ρ):

$$\rho = \frac{\gamma_d}{g}$$

where γ_d = density (g/cm^3),

        g = 980.66 (cm/sec^2) ← gravitational acceleration, and

        ρ = mass density ($g\text{-}sec^2/cm^4$).

5. Calculate specimen rotational inertia (J):

$$J = \frac{Wd^2}{8g}$$

where   W = weight (g),

$$d = \text{diameter (cm)},$$

$$g = 980.66 \ (\text{cm/sec}^2), \text{ and}$$

$$J = \text{specimen rotational inertia } (\text{g-cm-sec}^2).$$

6. Calculate passive end inertia ratio (P_T):

$$P_T = \frac{J_p}{J}$$

where $J_p = J_{\text{top platen}} + J_{\text{top cap}} = 363.2 \ (\text{g-cm-sec}^2)$
for 6" dia. platens,

$J = $ specimen rotational inertia (g-cm-sec^2), and

$P_T = $ passive end inertia ratio.

7. Apparatus damping constant (ADC_T):

$$ADC_T = 2 \ f_{oT} \ J_A \ \delta_T$$

where $f_{oT} = $ apparatus resonant frequency (Hz),

$J_A = $ rotational inertia of the active platen
(g-cm-sec^2),

$\delta_T = $ logarithmic decrement, and

$ADC_T = $ damping constant (g-cm-sec^2-Hz).

8. Apparatus damping factor (ADF_T):

$$ADF_T = \frac{ADC_T}{2\pi f_T J}$$

where $ADC_T = $ apparatus damping constant (g-cm-sec^2-Hz),

$f_T = $ system resonant frequency (Hz),

$J = $ specimen rotational inertia (g-cm-sec^2), and

$ADF_T = $ damping factor.

ADF_T should be calculated for every value of system
resonant frequency.

9. Active end inertia factor (T):

$$T = \frac{J_A}{J} \left[1 - \left(\frac{f_{oT}}{f_T} \right)^2 \right]$$

where J_A = active end platen system rotational inertia $(g\text{-}cm\text{-}sec^2)$,

   J = rotational inertia of the specimen $(g\text{-}cm\text{-}sec^2)$,

   f_{oT} = apparatus resonant frequency (Hz),

   f_T = system resonant frequency (Hz), and

   T = active end inertia factor.

10.   Dimensionless frequency factor (F):

F is a function of system factors T, P_T, and ADF and of specimen damping ratio, D.

For cases where ADF is zero (or very small) and specimen damping ratio is less than 10%, values of F can be obtained from Figs. 7.3 and 7.4.

For cases where ADF and specimen damping ratio (D) are small and where T and P_T are both greater than 10, dimensionless frequency factor (F) may be approximated by:

$$F = \sqrt{1/T + 1/P_T}$$

where   T = active end inertia factor, and

   P_T = passive end inertia ratio.

This equation is also useful for checking results obtained from Figs. 7.3 and 7.4. F should be determined for every corresponding pair of values of T and P_T. But in most cases values of T for different resonant
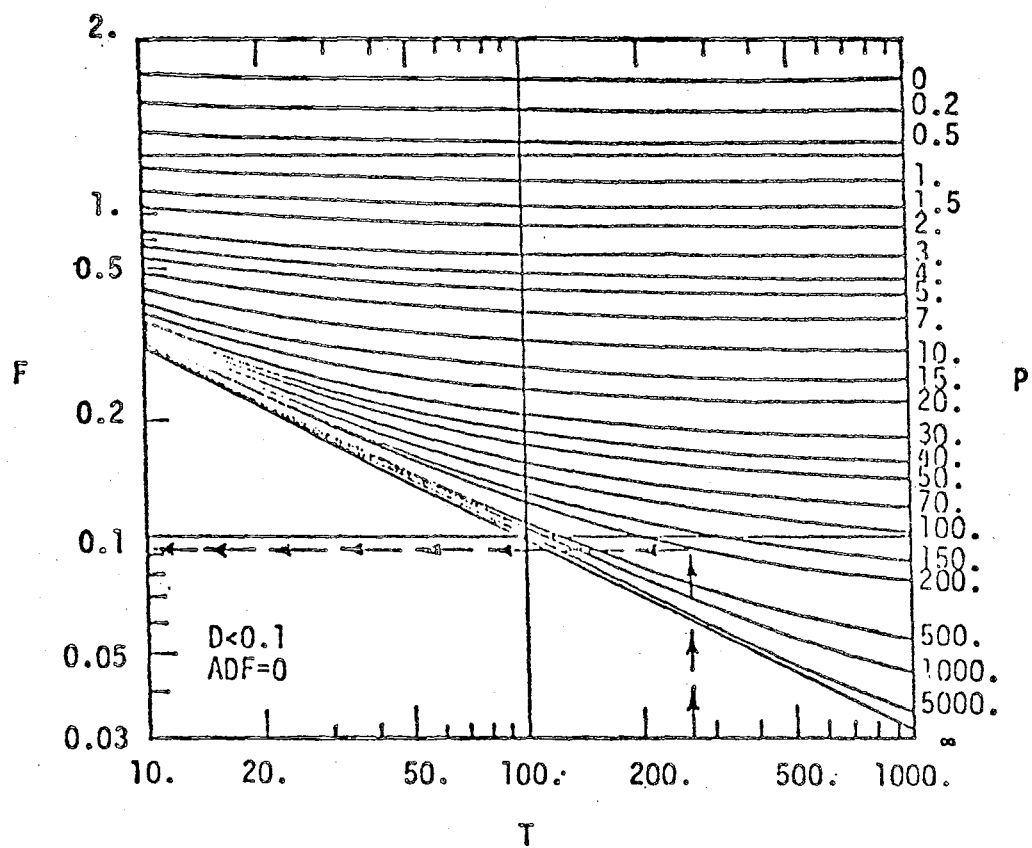
FIG. 7.3   DIMENSIONLESS FREQUENCY FACTOR
(AFTER DRNEVICH)
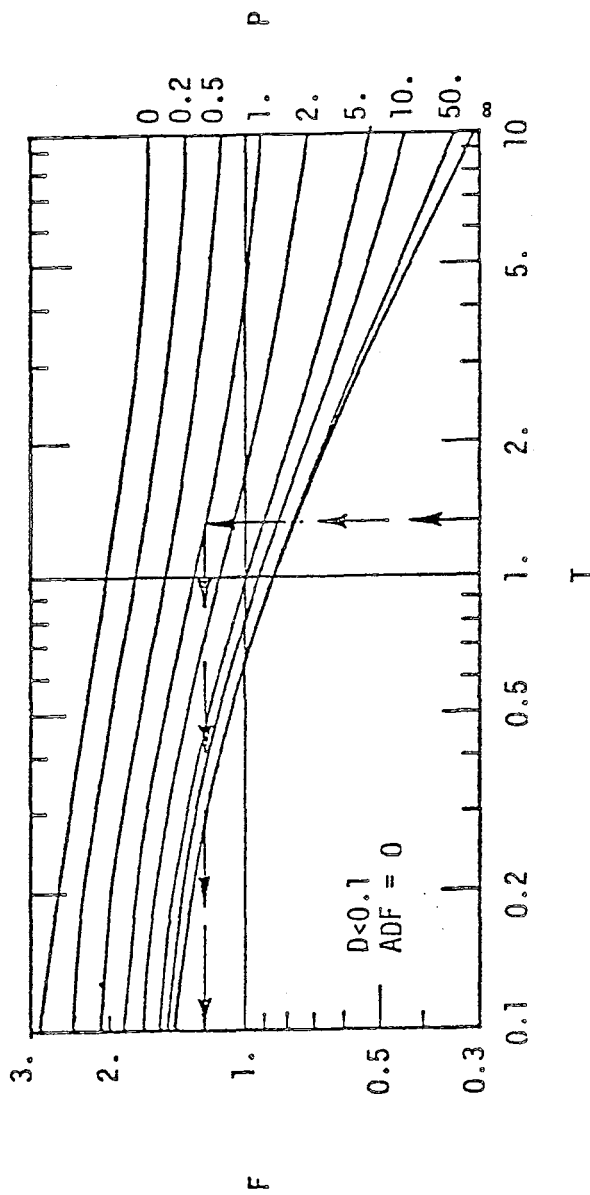
FIG. 7.4 DIMENSIONLESS FREQUENCY FACTOR
(AFTER DRNEVICH)

frequencies are close to each other and it is suffi-

cient to use one value of F.

11. Shear modulus (G):

$$G = \rho \ (2\pi L)^2 \left[\frac{f_T}{F}\right]^2$$

where ρ = mass density $(g\text{-}sec^2/cm^4)$,

L = length of specimen (cm),

f_T = system resonant frequency (Hz) or (cycle/sec),

F = dimensionless frequency factor, and

G = shear modulus (g/cm^2).

G should be calculated for each value of system resonant

frequency (f_T).

12. Shear strain amplitude (γ):

$$\gamma = (RCF)_p (RTO)_p (SF)[\frac{d}{3L}] \times 100\%$$

where
  $(RCF)p$ = rotation calibration factor for passive

transducer $\frac{PK.rad}{mv_{rms}}$,

$(RTO)_p$ = rotational passive transducer output (mv_{rms}),

SF = strain factor,

d = diameter of specimen (cm),

L = length of specimen (cm), and

γ = shear strain amplitude (%).

$$(RCF)_p = \frac{8.42 \times 10^{-5}}{f_T} \ \frac{Pk.rad}{mv_{rms}}$$

where f_T = system resonant frequency (Hz).

$(RCF)_p$ should be calculated for every f_T. $(RTO)_p$ is recorded on the data sheet. SF is a function of T and P_T and can be determined from Fig. 7.5.

13. Magnification factor (MMF_T):

$$MMF_T = [(RCF)_p (RTO)_p / (TCF)(CR_T)] J (2\pi f_T)^2$$

where

$(RCF)_p = \dfrac{8.42 \times 10^{-5}}{f_T} \dfrac{Pk.rad}{mv_{rms}}$ - rotation calibration

factor for passive tranducer,

$(RTO)_p$ = rotational passive transducer output (mv_{rms}) recorded during the test,

(TCF) = Torque/current constant $\dfrac{(g-cm)(Pk.rad^3)}{mv_{rms}}$,

(CR_T) = Current reading to torsional excitation system = torque reading (mv_{rms}) which is voltage drop across a fixed 5Ω resistor,

J = specimen rotational inertia $(g-cm-sec^2)$, and

f_T = system resonant frequency (cycle/sec).

14. Amplification coefficient (A):

This coefficient may be obtained from Fig. 7.6

For cases where ADF is close to zero and D is less than 10%. For other values of ADF, the value of A is only an approximation.

For cases where values of both T and P_T are greater than 10, the following equation may be used to approximate A.

$$A = 2(T + P_T)$$
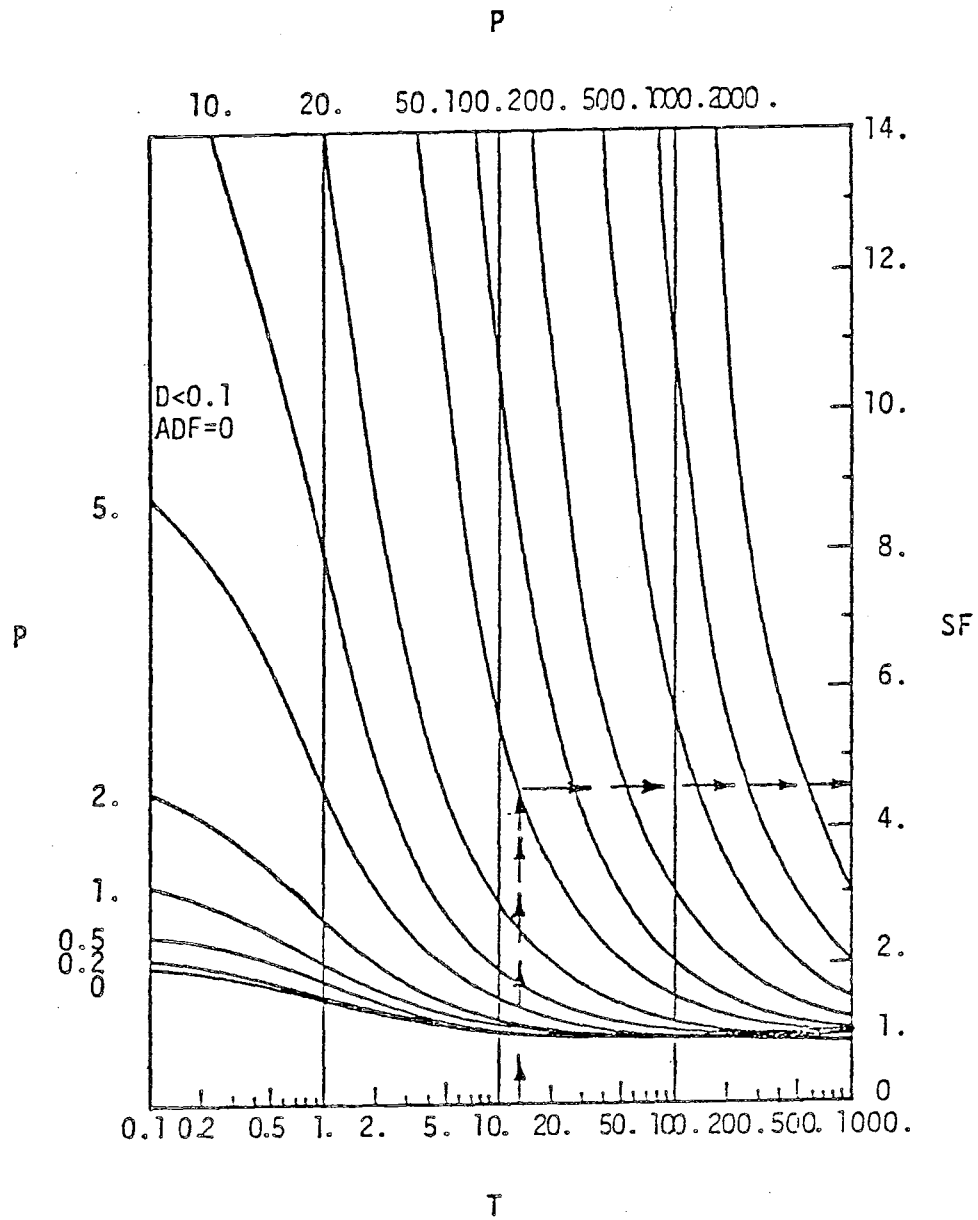
FIG. 7. 5   STRAIN FACTOR FOR RESONANCE DETERMINED BY
PHASE MEASUREMENT BETWEEN INPUT FORCE AND
MOTION AT THE PASSIVE END (AFTER DRNEVICH)
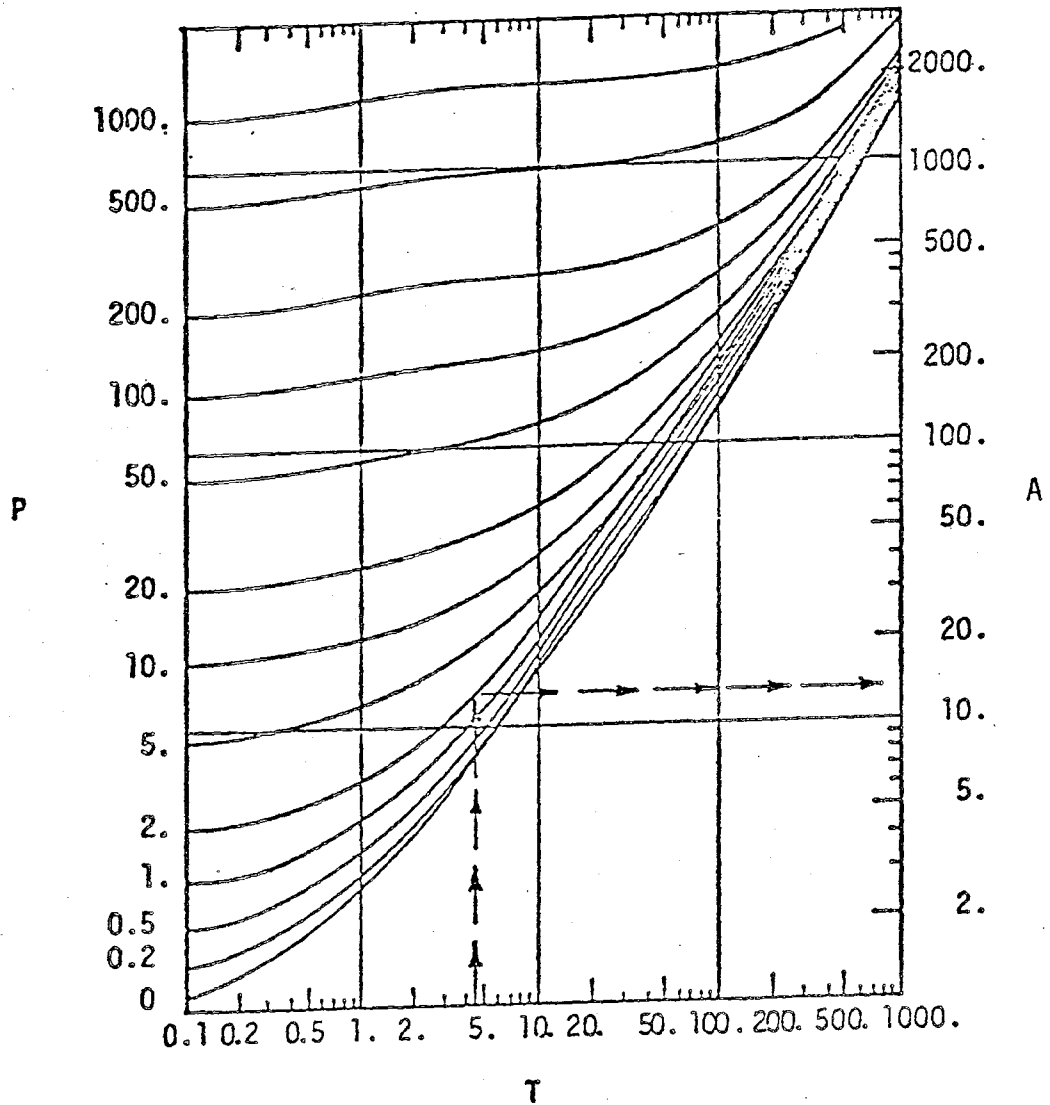
FIG. 7.6 COEFFICIENT FOR MANUAL CALCULATION OF DAMPING
RATIO FOR RESONANCE DETERMINED BY PHASE MEASURE-
MENT BETWEEN INPUT FORCE AND MOTION AT THE
PASSIVE END (AFTER DRNEVICH)

15. Damping ratio (D):

A. Steady State Vibration:

$$D = 100/[A(MMF)]$$

where A = amplification coefficient,

      MMF = magnification factor, and

      D = specimen damping ratio (%).

B. Free Vibration:

This procedure is theoretically exact for apparatus where the passive end can be assumed to be rigidly fixed. For other cases this method is approximate. The passive transducer must be used to obtain the amplitude decay curve (Fig. 7.7). Values of T and P should both be greater than 10 when amplitude decay is used.

(1) System energy ratio (S)

$$S = \frac{J_A}{J} \left[\frac{f_{oT}\, F}{f_T} \right]^2$$

where J_A = active end platen system rotational inertia (g-cm-sec^2),

      J = specimen rotational inertia (g-cm-sec^2),

      f_{oT} = apparatus resonant frequency (Hz),

      F = dimensionless frequency factor,

      f_T = system resonant frequency (Hz), and

      S = system energy ratio.

S should be calculated for each value of f_T.
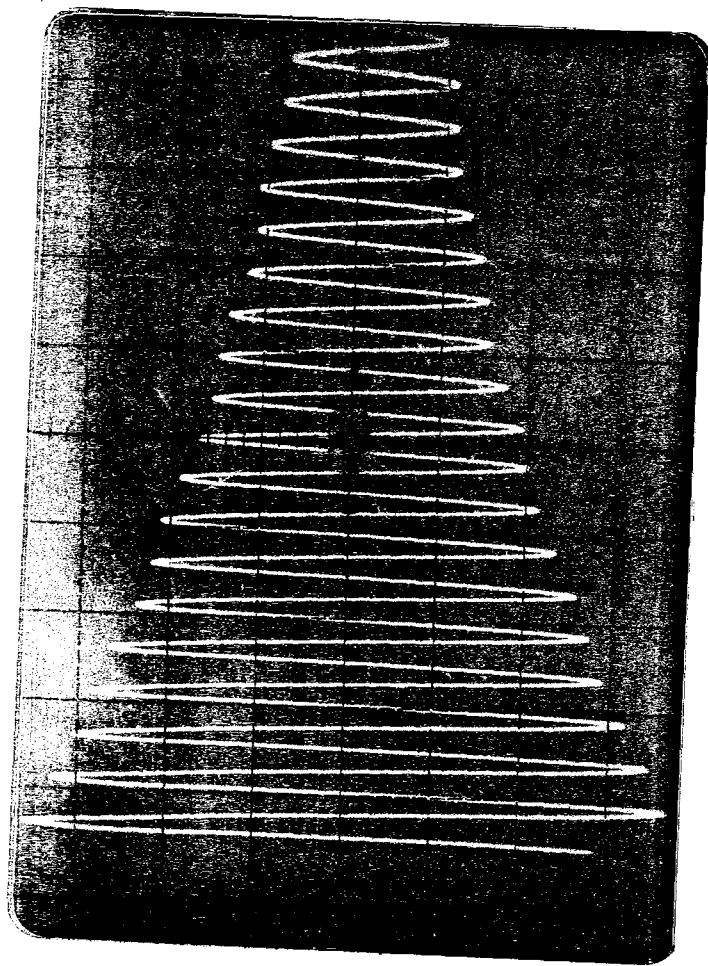
FIG. 7.7 AMPLITUDE DECAY CURVE

(2) System logarithmic decrement from the free vibration (δ_S):

$$\delta_S = (\frac{1}{n}) \log \frac{A_1}{A_{n+1}}$$

where A_1 = amplitude of vibration for first cycle after power is cut off,

A_{n+1} = amplitude of vibration for (n+1)th cycle of free vibration,

n = number of free vibration cycles which must be 10 or less, and

δ_S = system logarithmic decrement.

(3) Damping ratio (D):

$$D = [\delta_S(1+S) - S\delta_T] \times 100\%/(2\pi)$$

where δ_S = system logarithmic decrement,

S = system energy ratio,

δ_T = apparatus logarithmic decrement, and

D = damping ratio (%).

CHAPTER 8

TESTING PROGRAM AND RESULTS

8.1 <u>Testing Program</u>

The Drnevich free-free torsional resonant column device
was used to determine shear moduli (G) and damping ratio (D)
of Denver sand and Monterey No. 0 sand from California.

Twenty-four Denver sand specimens with different grain size
distribution characteristics were tested under 30 (psi) confining
pressure. All the specimens were prepared to have an initial
relative density of 30%. In addition to the above specimens,
specimen DM-d$_2$ was also tested at the Water and Power Resources
Service. The apparatus used in testing specimen DM-d$_2$ was also
a Drnevich free-free resonant column device. However, it was
not the same model as the one used for testing the other twenty-
four specimens. The purpose of this additional test was to
compare the test results from the two different models of free-
free torsional resonant column devices.

Three Monterey No. 0 sand specimens with different relative
densities were also tested. Two of the specimens were tested
under 30 (psi) confining pressure and the third one was tested
under 15, 30 and 45 (psi) confining pressures.

The specifications and index properties for all the specimens

are given in Table 7.1. It should be noted that the values of relative density (D_r) and void ratio (e) given in Table 7.1 are the initial values (prior to consolidation). After applying confining pressure and during the test, the relative density of the specimens changes by around 2%.

8.2 Test Results

Test results for Monterey No. 0 sand are shown in Figs. 8.1 to 8.5. Fig. 8.1 shows the shear modulus (G) versus shear strain (γ) curves for three specimens with three different relative densities (D_r = 12, 45, 73%). All specimens were tested under 30 (psi) confining pressure. Their damping ratio (D) versus shear strain (γ) relationships are shown in Fig. 8.2. Figs. 8.3 and 8.4 show the effect of confining pressure on shear modulus and damping ratio, respectively. In this test specimen M-3 was subjected to three different confining pressures. First, it was consolidated under 15 (psi) and tested up to strains of about 10^{-5} (M-3-1), then the test was stopped and confining pressure was raised to 30 (psi). After consolidation at 30 (psi), the specimen was tested again and strain amplitude was kept below 10^{-5} (M-3-2). Finally, the specimen was tested again under 45 (psi) and this time the strain amplitudes were as high as 6×10^{-5} (M-3-3). The reason for testing the specimen at strain levels below 10^{-5} was to prevent it from becoming disturbed so that it may be tested at different confining pressures. Fig. 8.5 illustrates the effect of confining pressure on maximum shear modulus for the specimen M-3.
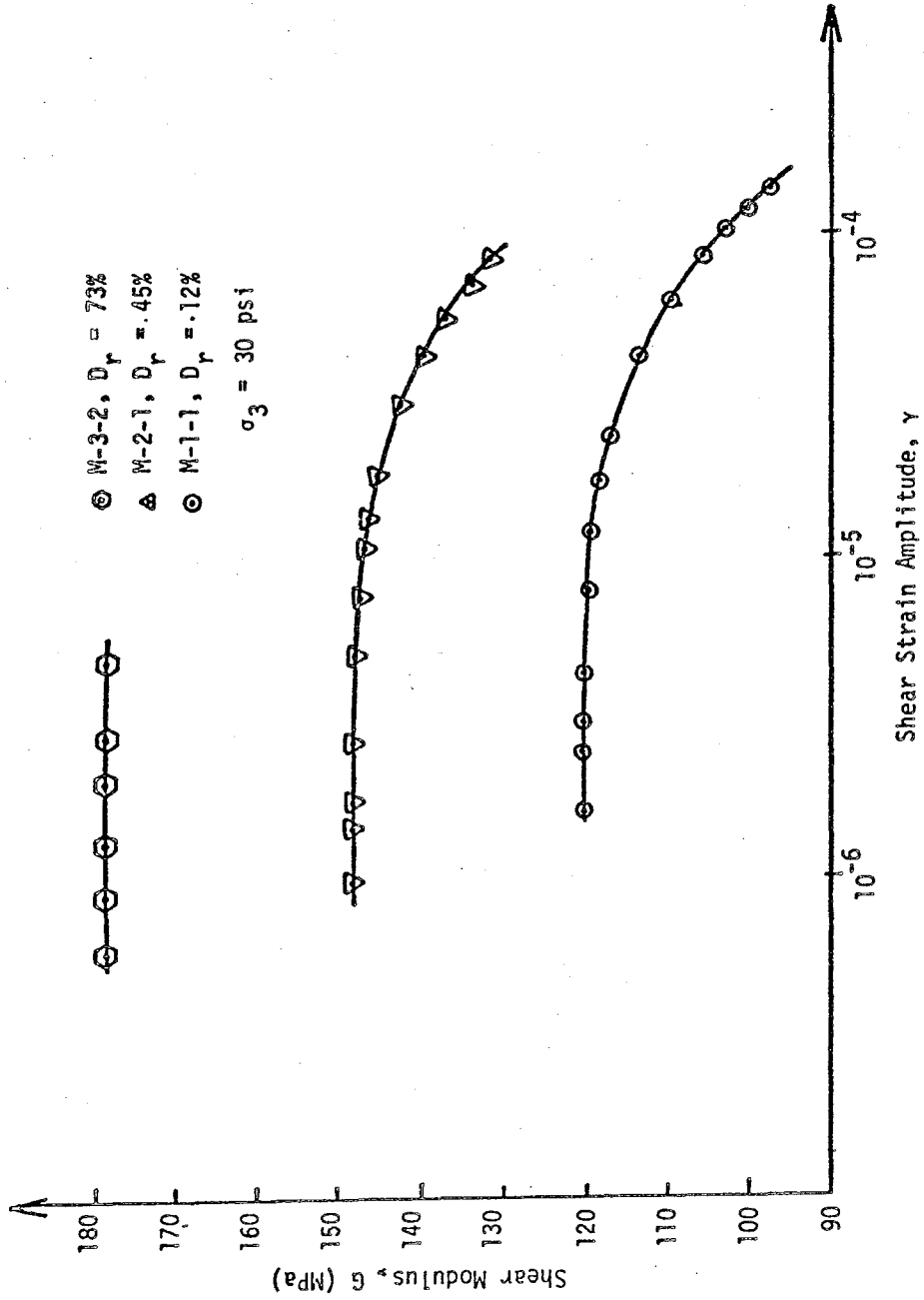
FIG. 8.1 SHEAR MODULUS VERSUS SHEAR STRAIN
(MONTEREY NO. 0 SAND)
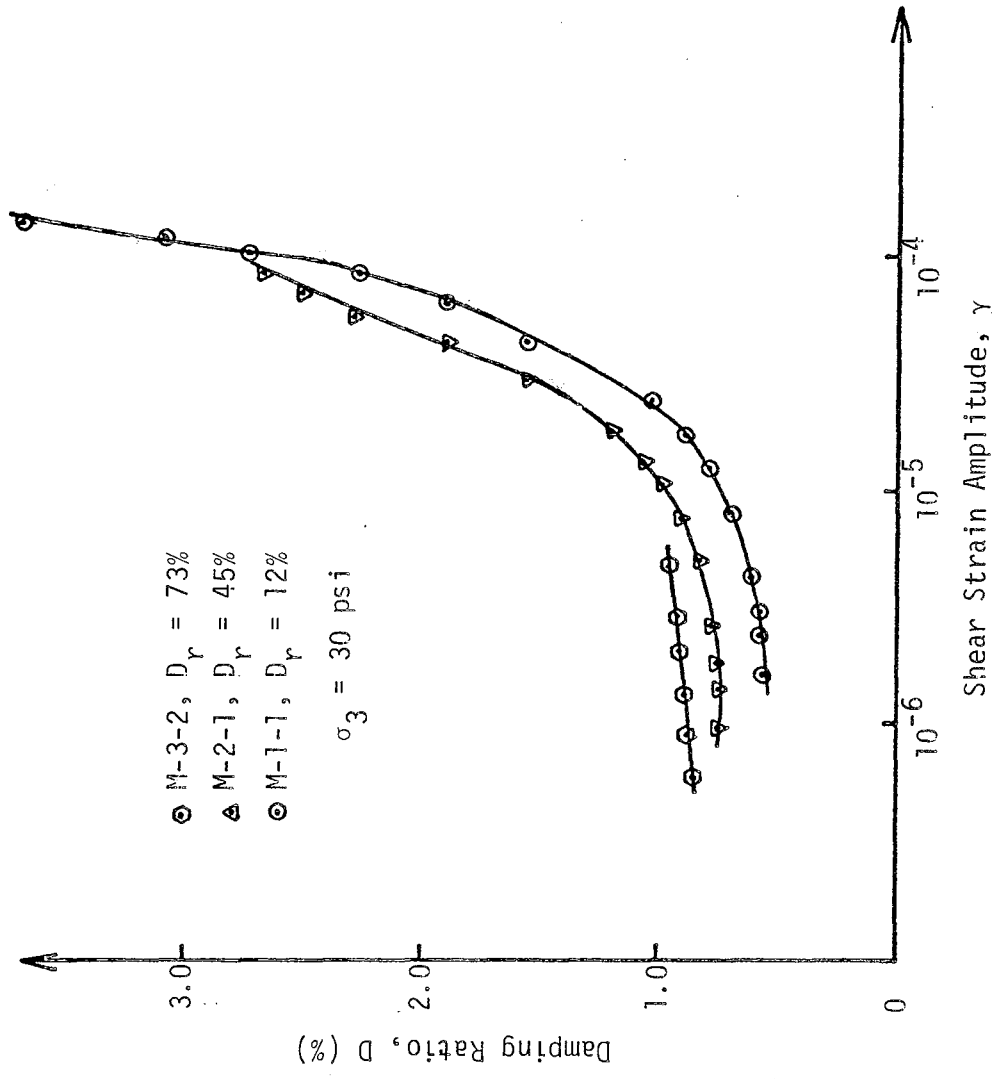
Shear Strain Amplitude, γ

FIG. 8.2   DAMPING RATIO VERSUS SHEAR STRAIN
(MONTEREY NO. O SAND)

M-3-2, D_r = 73%
M-2-1, D_r = 45%
M-1-1, D_r = 12%

σ_3 = 30 psi

Damping Ratio, D (%)

·FIG. 8.3 SHEAR MODULUS VERSUS SHEAR STRAIN
(MONTEREY NO. 0 SAND)

Shear Strain Amplitude, γ

▲ M-3-3, σ_3 = 45 (psi)

⊙ M-3-2, σ_3 = 30 (psi)

◼ M-3-1, σ_3 = 15 (psi)
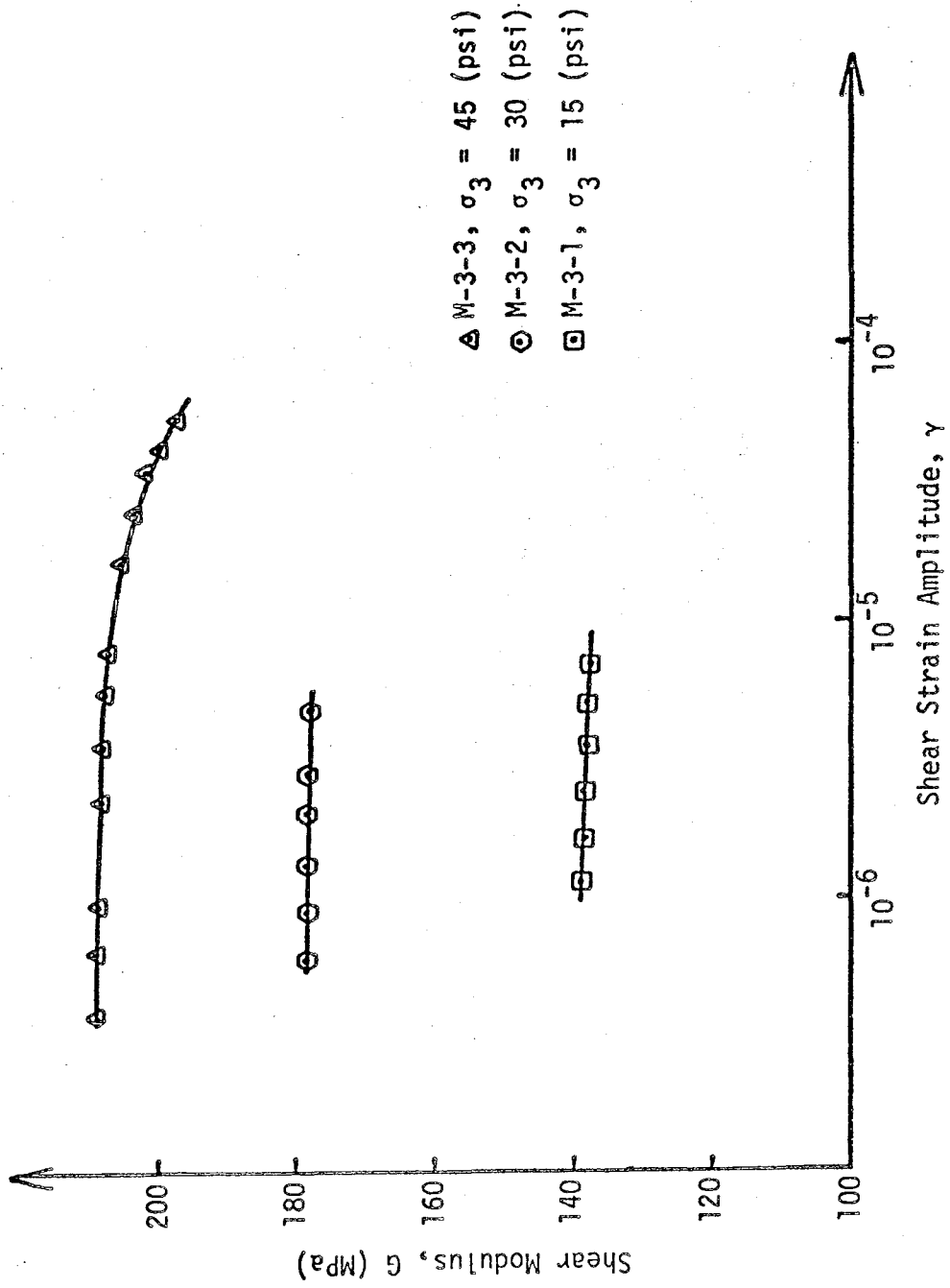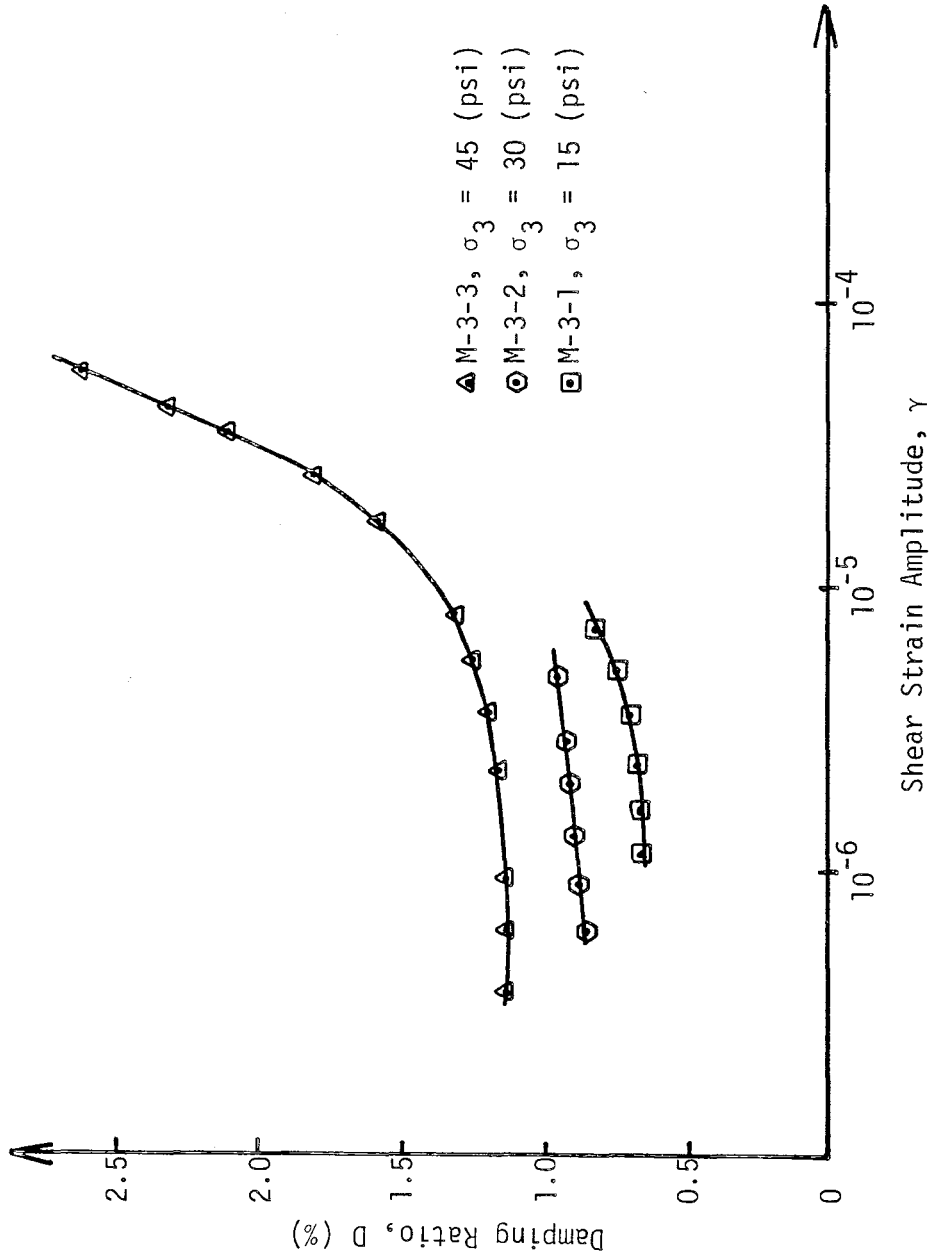
Damping Ratio, D (%)

FIG. 8.4 DAMPING RATIO VERSUS SHEAR STRAIN
(MONTEREY NO. O SAND)
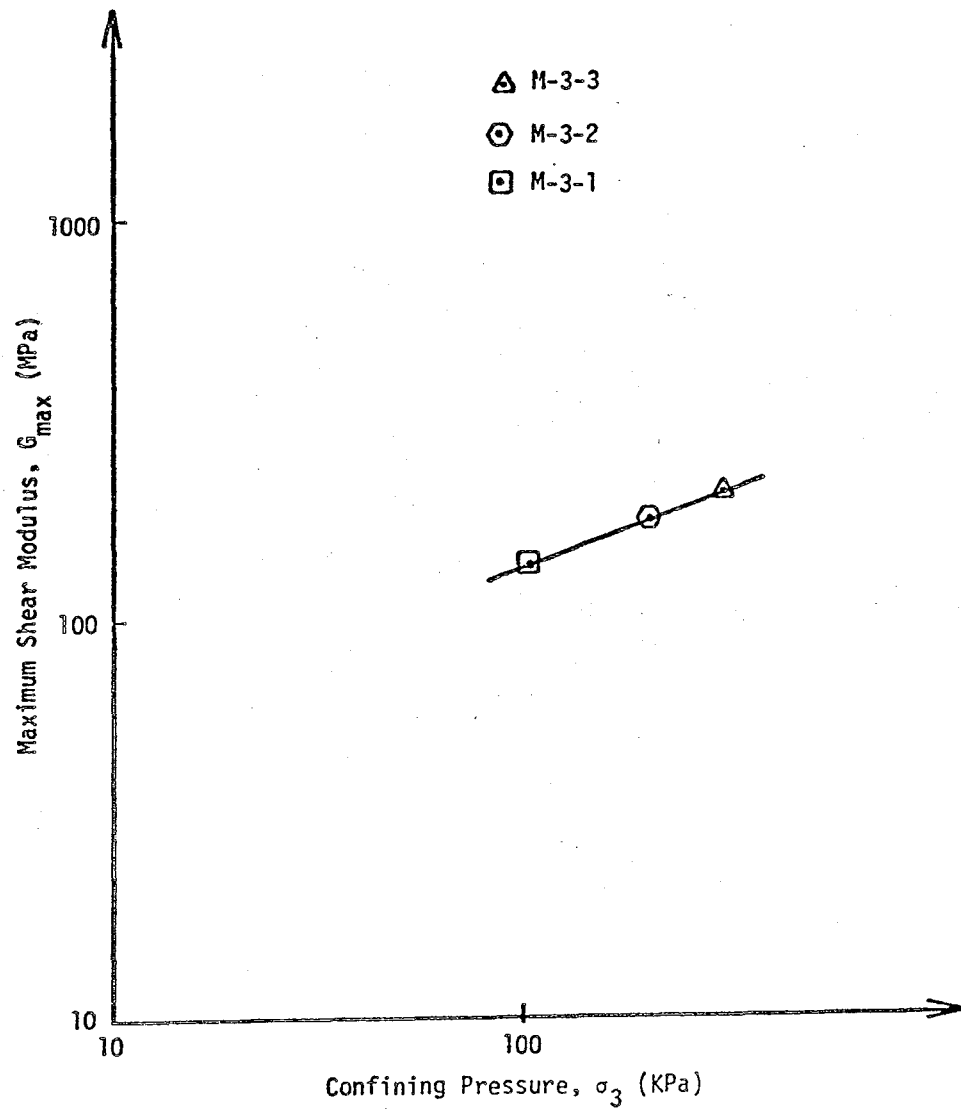
FIG. 8.5 THE EFFECT OF CONFINING PRESSURE
ON MAXIMUM SHEAR MODULUS
(MONTEREY NO. 0 SAND)

The results of the tests on Monterey No. O sand indicated that the shear modulus (G) increases with increasing relative density (or decreasing void ratio) and also increases with confining pressure. The damping ratio (D) demonstrated a trend similar to shear modulus. However, damping ratio should have decreased instead with increasing relative density (D_r) and increasing confining pressure (σ_3).

Shear modulus versus shear strain curves and damping ratio versus shear strain curves of Denver sand specimens are presented in Figs. 8.6 to 8.17. All of the specimens were consolidated at 30 (psi) confining pressure and their initial relative densities were about 30%. Figs. 8.6 and 8.7 illustrate the shear modulus (G) and the damping ratio (D) for specimens $DC-a_2$, $DC-a_4$, $DC-a_6$ and $DC-a_8$. These specimens have the same mean grain size a $(D_{50} = 1.68$ mm). Shear modulus and damping ratio curves for specimens $DC-b_4$, $DC-b_6$, $DC-b_8$, $DC-b_{10}$ and $DC-b_{15}$ with the same median grain size are shown in Figs. 8.8 and 8.9, respectively. Similarly, Figs. 8.10 to 8.17 show the shear modulus and the damping ratio curves for the rest of the specimens.

The results indicated that, in general, the shear modulus and the damping ratio of specimens increases with increasing uniformity coefficient (C_u) for the same median grain size (D_{50}) and same relative density and confining pressure.

8.3 Discussion

The results of tests on Monterey No. O sand show the effects of relative density, void ratio and confining pressure on shear
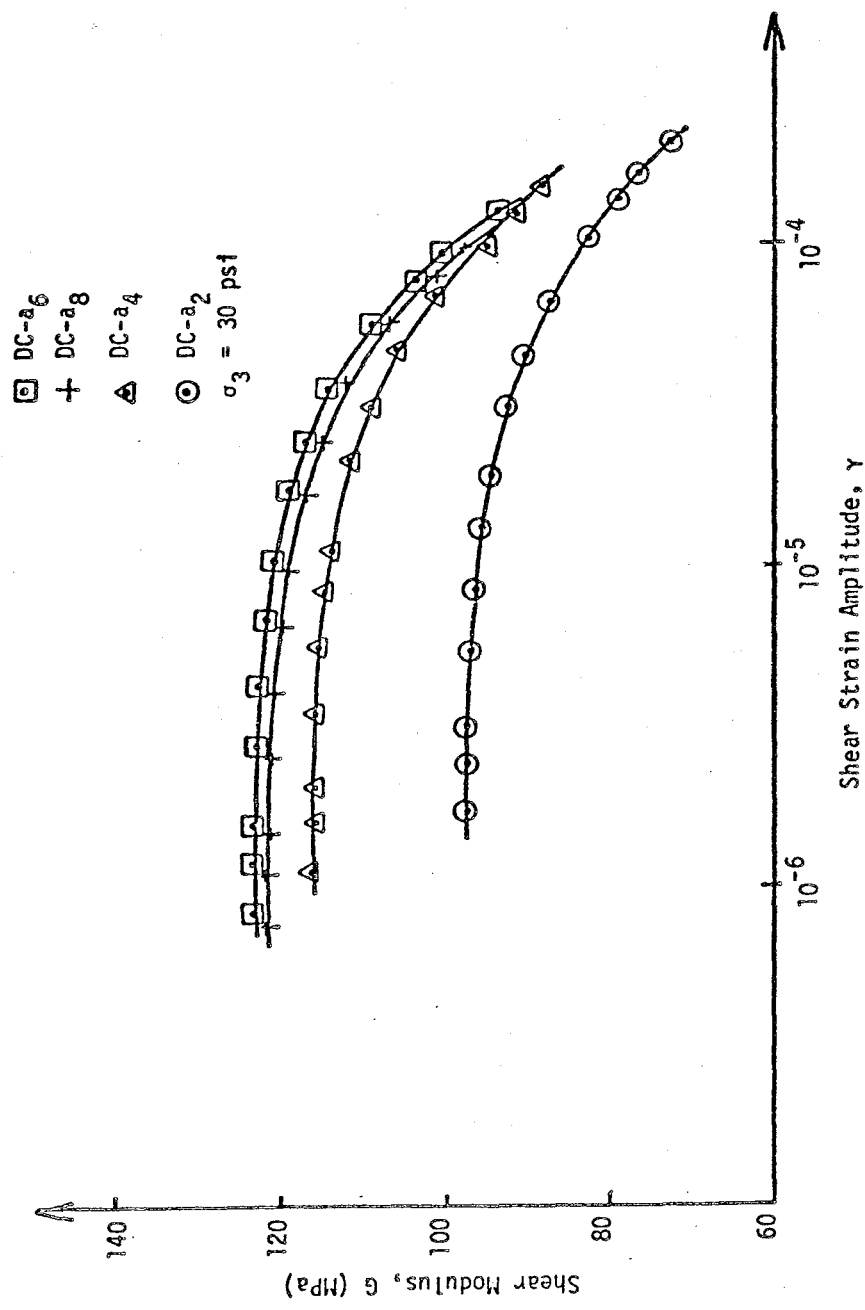
FIG. 8.6 SHEAR MODULUS VERSUS SHEAR STRAIN
(DENVER SAND, DC-a)
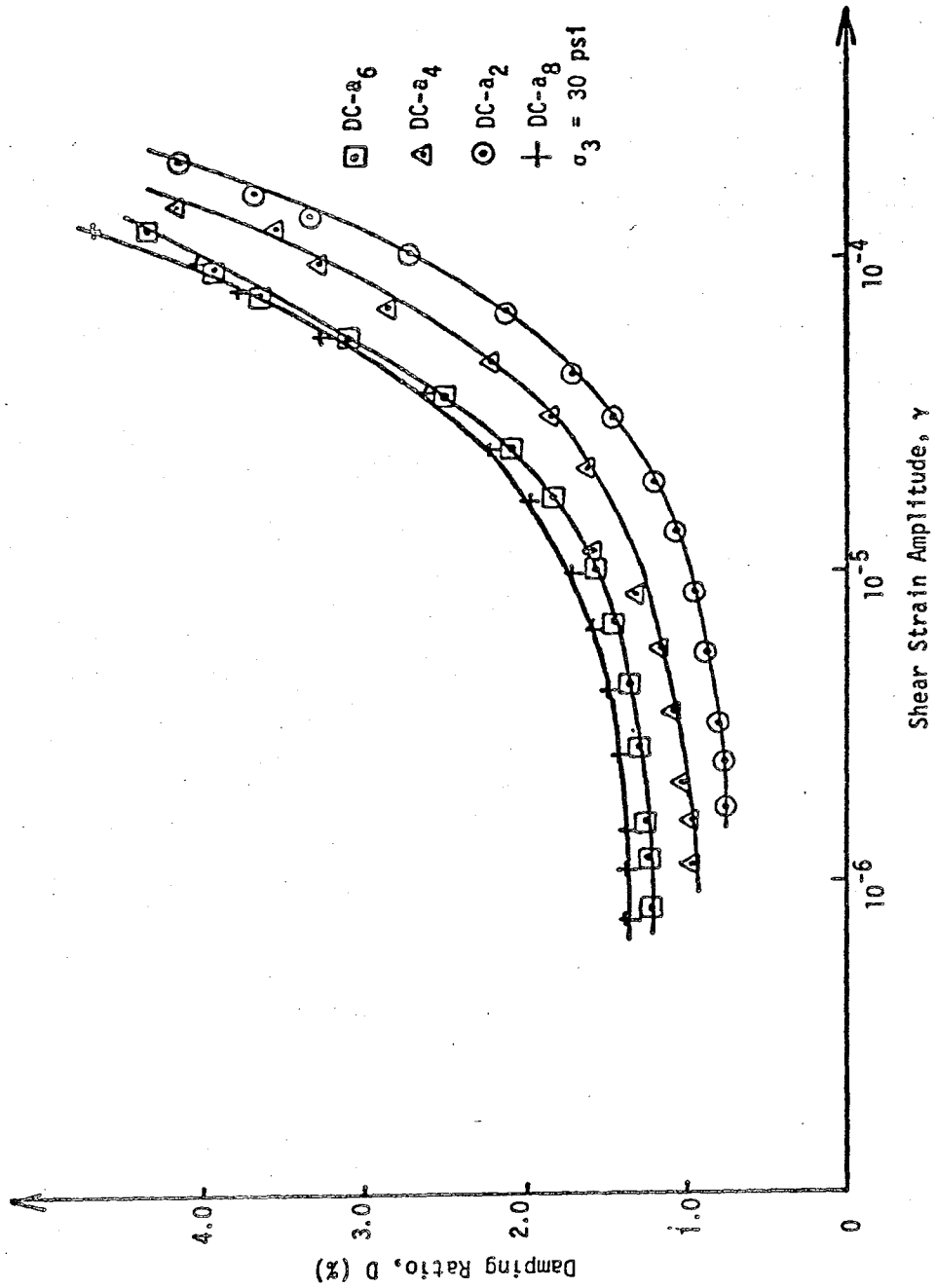
FIG. 8.7 DAMPING RATIO VERSUS SHEAR STRAIN
(DENVER SAND, DC-a)
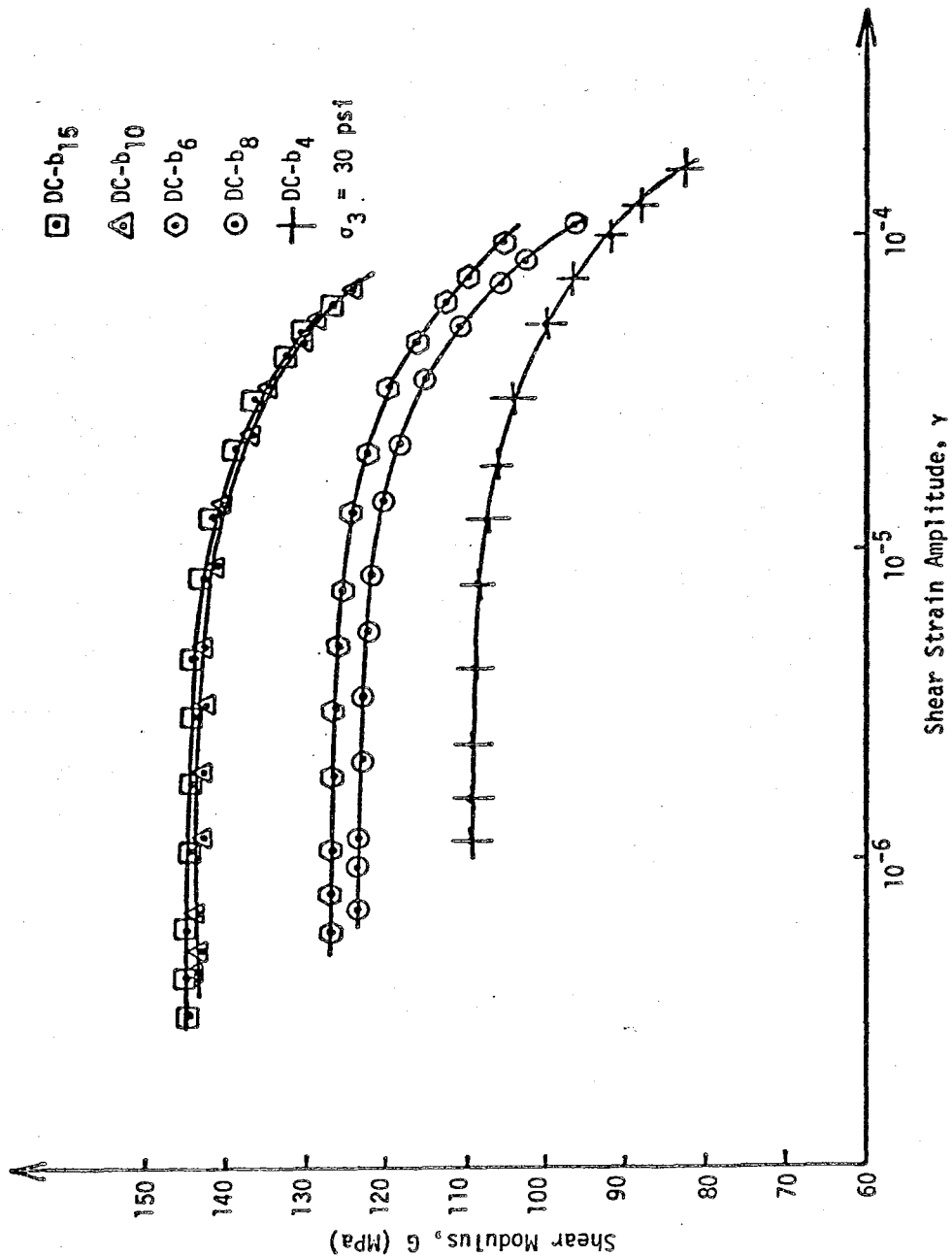
FIG. 8.8 SHEAR MODULUS VERSUS SHEAR STRAIN
(DENVER SAND, DC-b)

FIG. 8.9 DAMPING RATIO VERSUS SHEAR STRAIN
(DENVER SAND, DC-b)

Shear Strain Amplitude, γ

Shear Modulus, G (MPa)

DM-c$_{15}$
DM-c$_{10}$
DM-c$_8$
DM-c$_4$
DM-c$_2$

σ$_3$ = psi
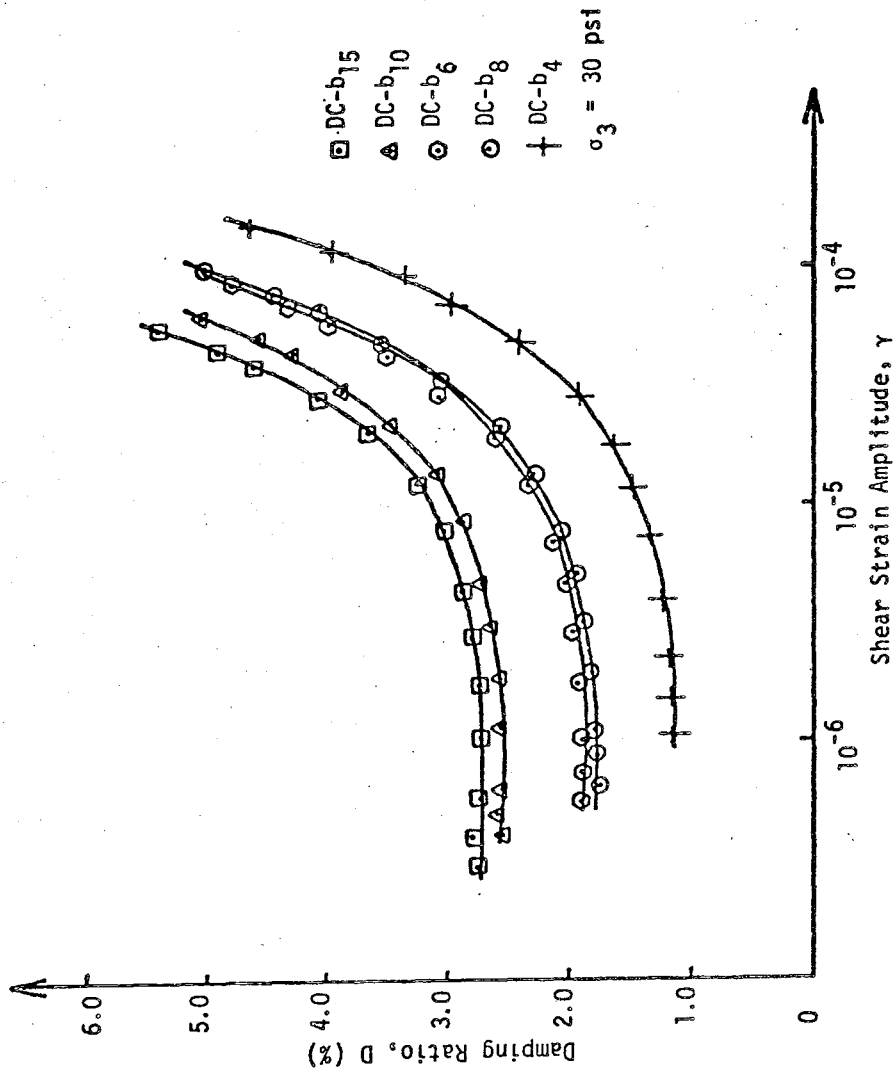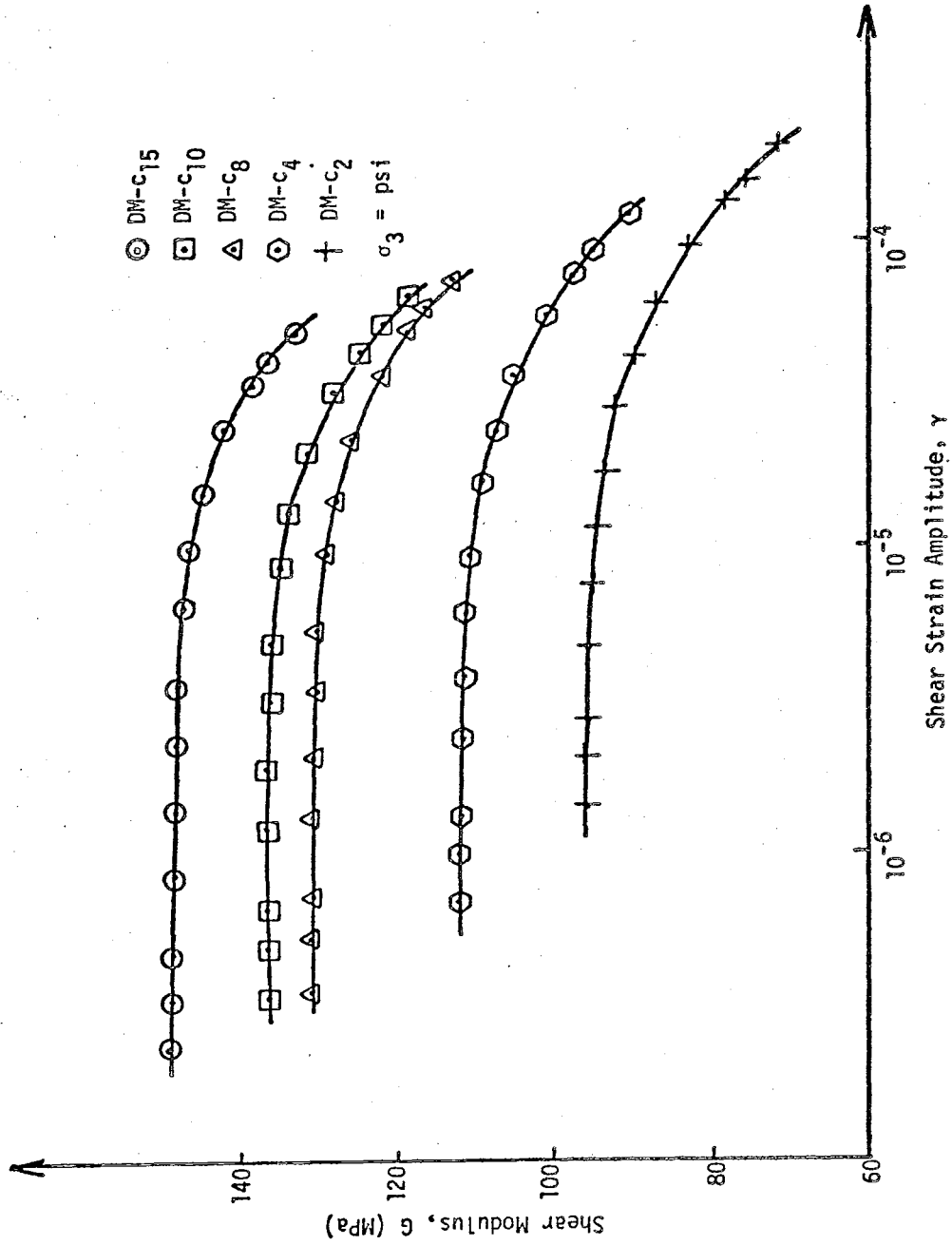
FIG. 8.10 SHEAR MODULUS VERSUS SHEAR STRAIN
(DENVER SAND, DM-c)
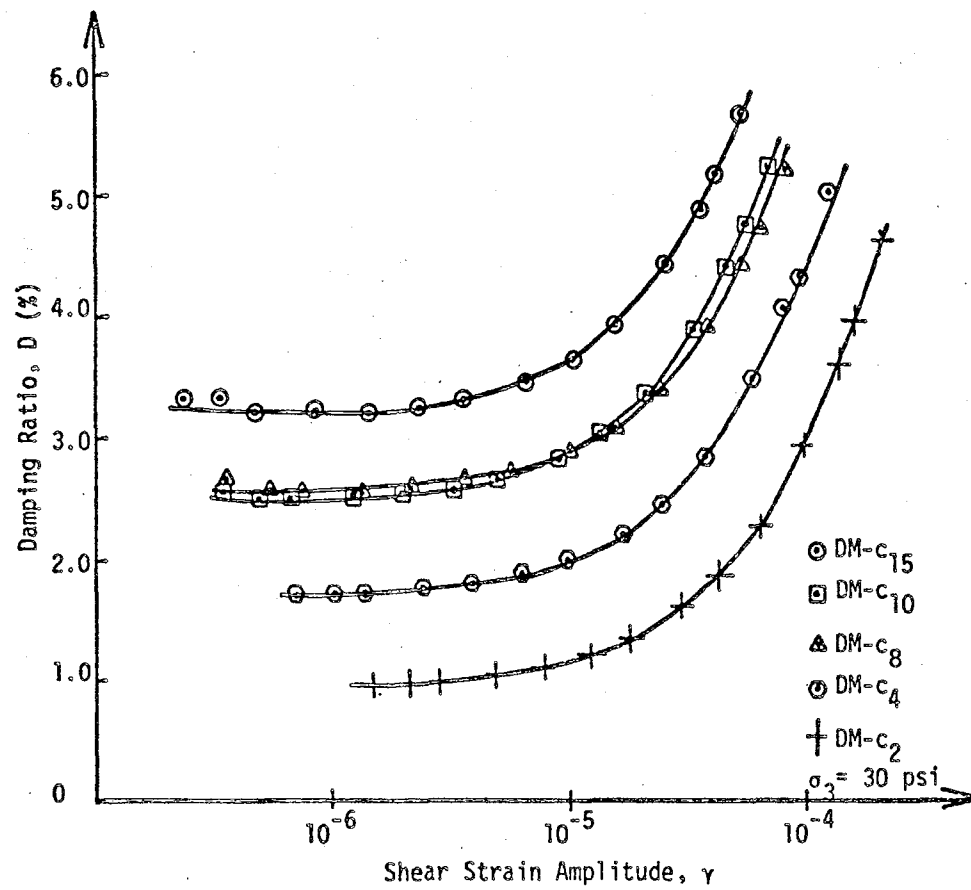
FIG. 8.11 DAMPING RATIO VERSUS SHEAR STRAIN
(DENVER SAND, DM-c)
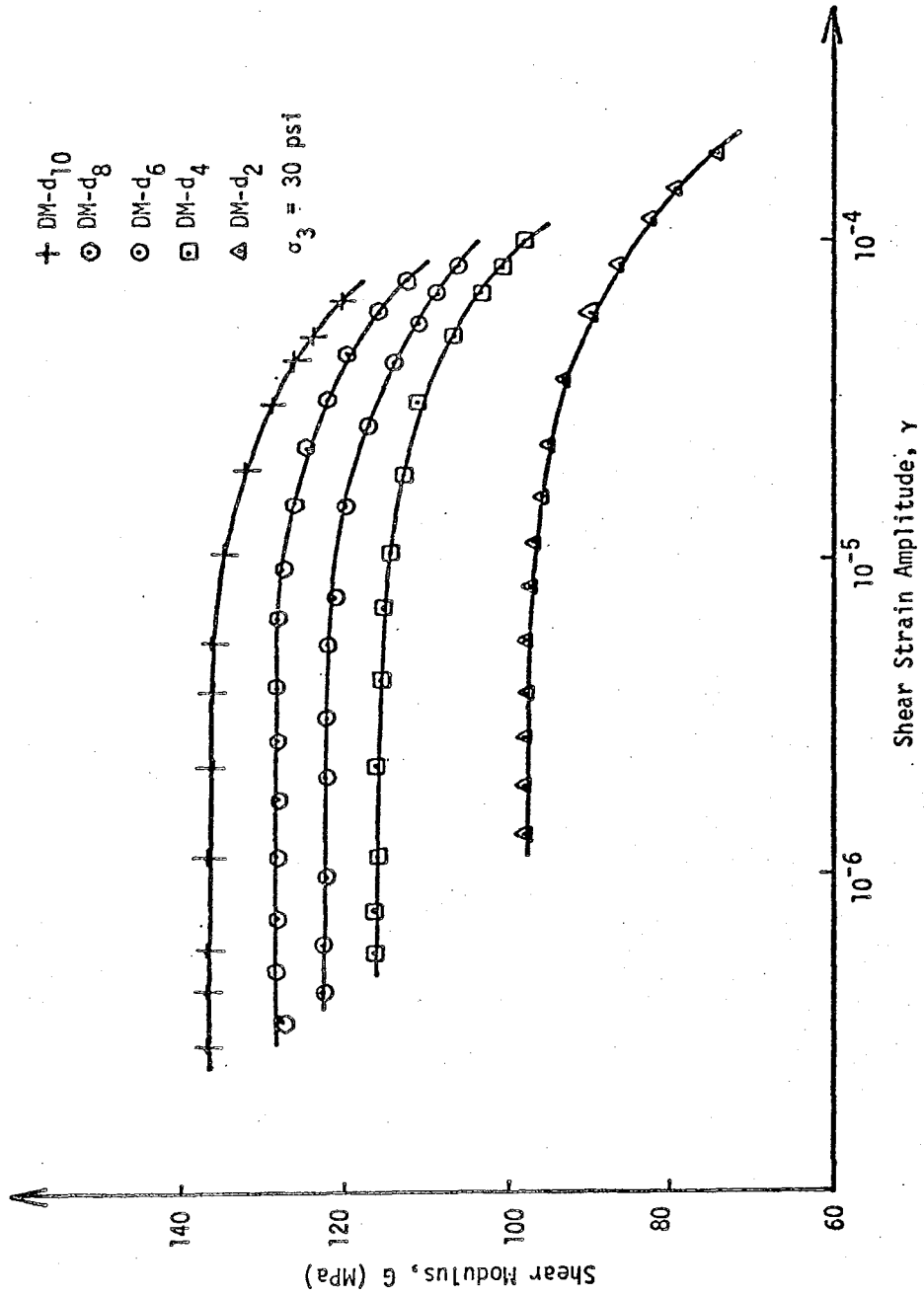
FIG. 8.12 SHEAR MODULUS VERSUS SHEAR STRAIN
(DENVER SAND, DM-d)
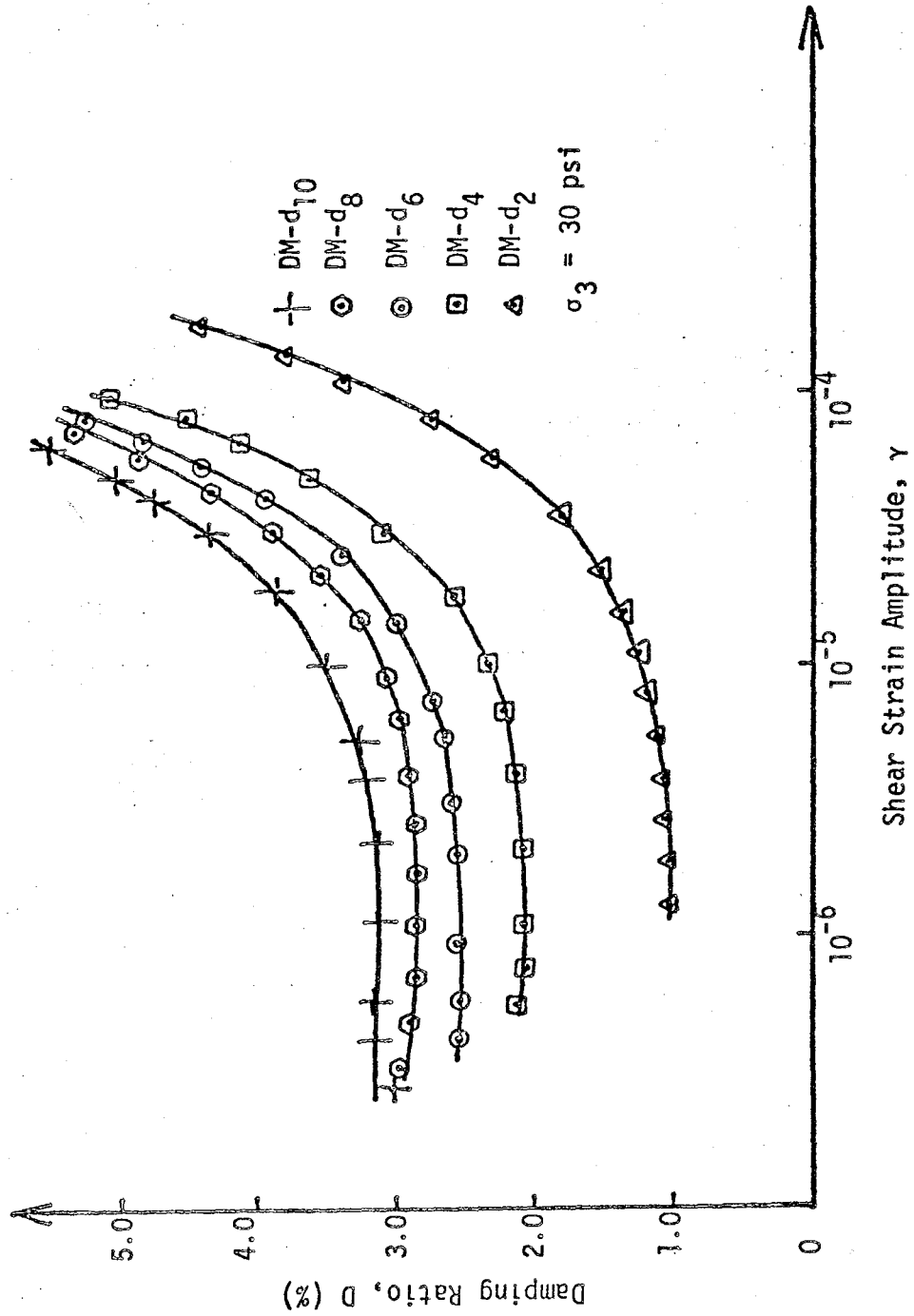
FIG. 8.13 DAMPING RATIO VERSUS SHEAR STRAIN
(DENVER SAND, DM-d)
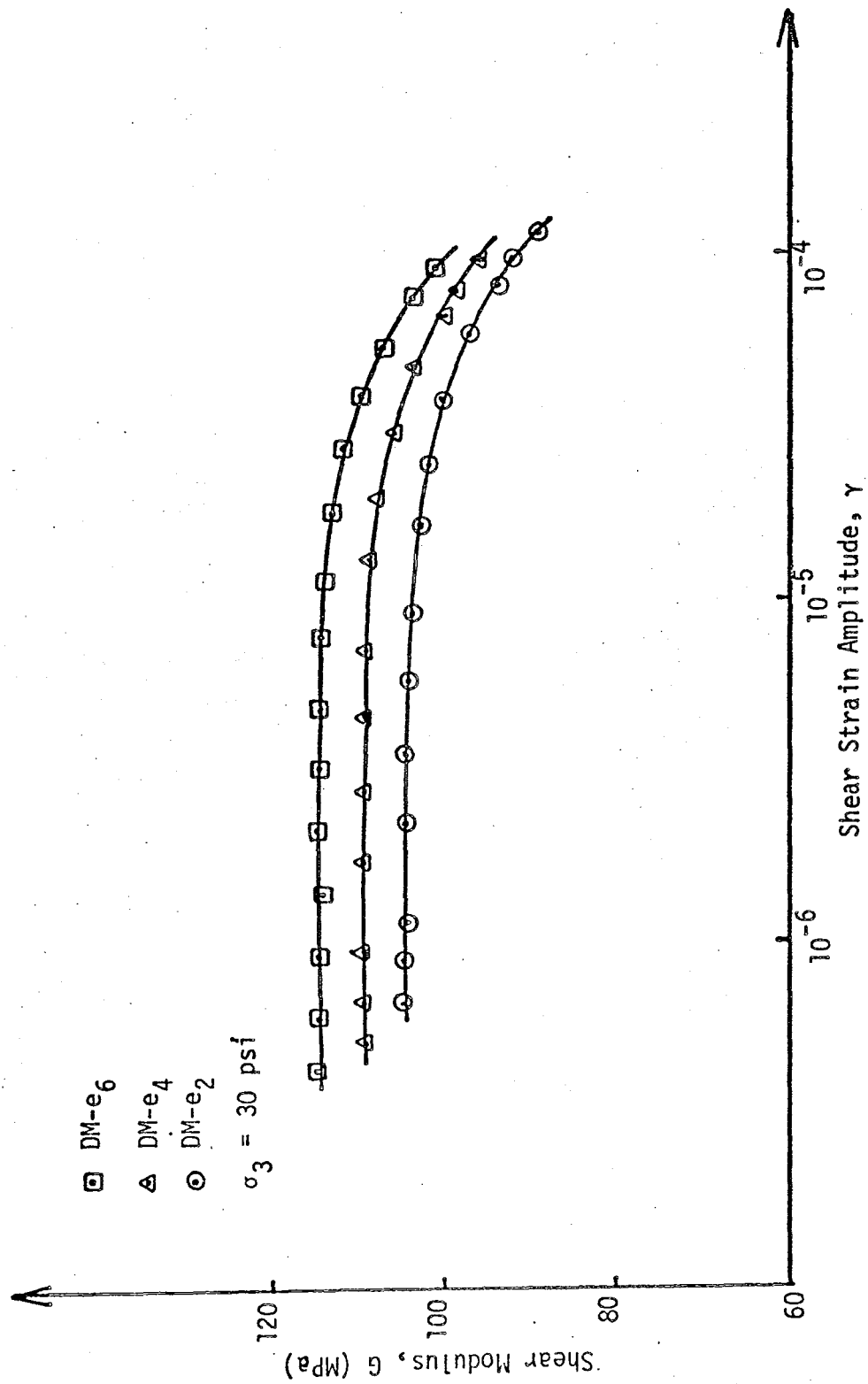
FIG. 8.14 SHEAR MODULUS VERSUS SHEAR STRAIN
(DENVER SAND, DM-e)
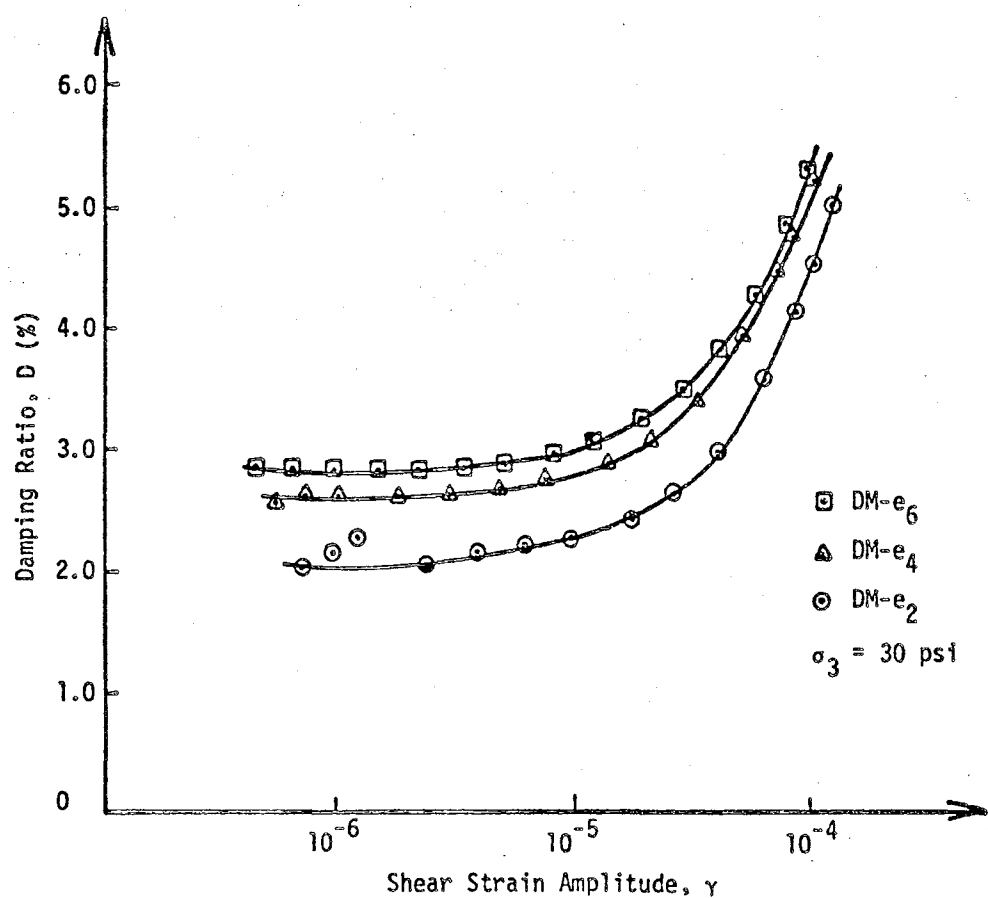
FIG. 8.15 DAMPING RATIO VERSUS SHEAR STRAIN
(DENVER SAND, DM-e)
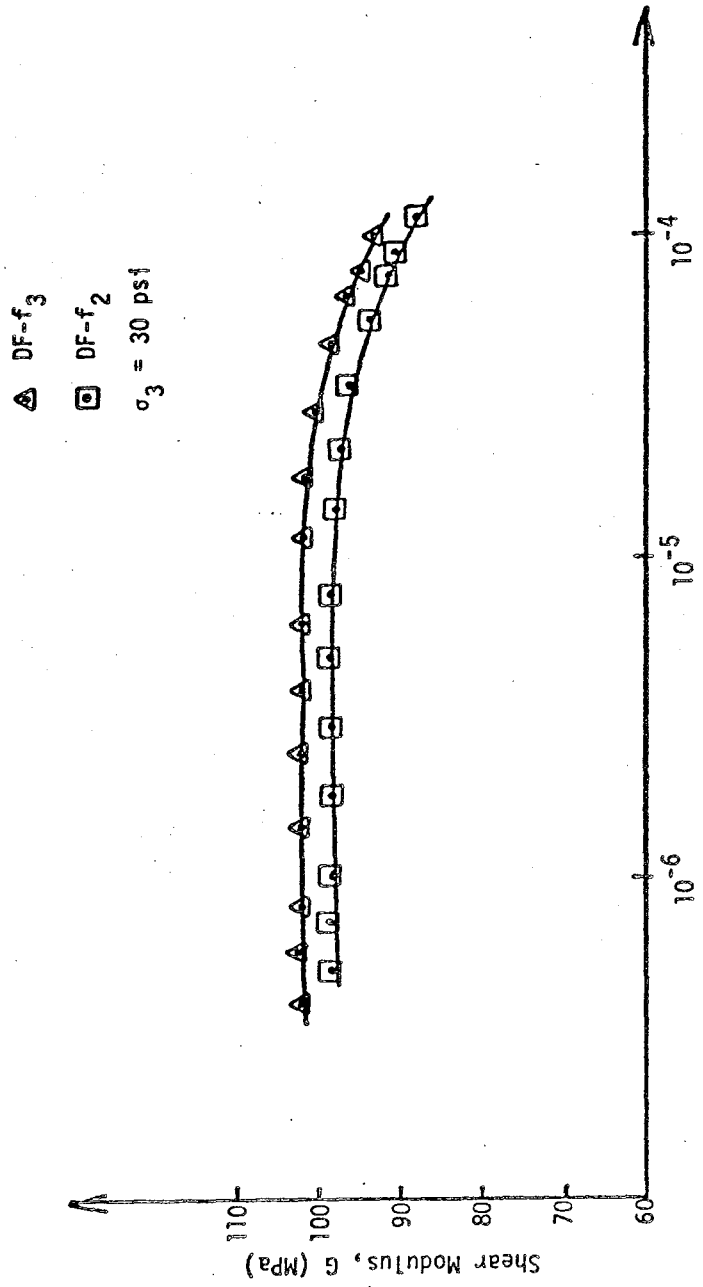
FIG. 8.16 SHEAR MODULUS VERSUS SHEAR STRAIN
(DENVER SAND, DF-f)
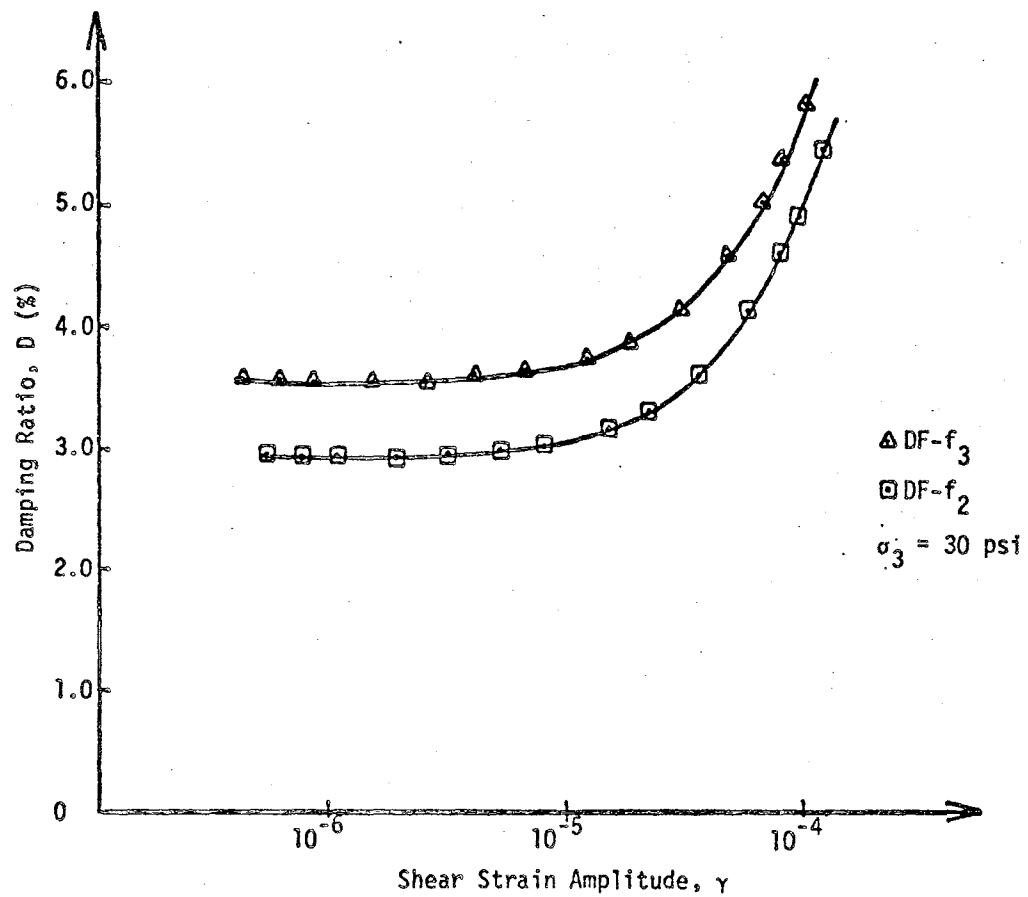
FIG. 8.17   DAMPING RATIO VERSUS SHEAR STRAIN
(DENVER SAND, DF-f)

modulus (G) and damping ratio (D). The effects of these factors on G are in general agreement with previous studies. However, the behavior of damping ratio shown in Figs. 8.2 and 8.4 is contrary to the expected trend.

Test results from Denver sand indicated that shear modulus of the specimens is affected by the uniformity coefficient (C_u) and increases with increasing C_u for the same mean grain size (D_{50}) and the same relative density (D_r) and confining pressure (σ_3). However, the results also showed that damping ratio (D) is affected in the same manner. This behavior is contrary to the expected result. In general, the values of damping ratio for all of the tests were larger than expected values. In particular, the initial values of damping ratio (at strain levels below 10^{-6}) for some of the specimens were very large (3.5% for $DF-f_3$ at $\gamma = 4 \times 10^{-7}$). In general, the specimens with larger uniformity coefficients (C_u) and small mean grain sizes (D_{50}) had larger initial damping ratios. A careful inspection of the apparatus showed that during testing some of the vibration which is generated by the driving coils is transferred to the base of the apparatus and the surrounding area. Therefore, all of the vibration generated by the coils is not applied to the specimen. The vibration at the base also causes some rocking motion and the specimen will no longer be under pure torsion. These effects reduce the passive transducers output and hence the values for damping ratio will be large. For finer and more well-graded specimens the vibration at the base was larger and therefore

the values for damping ratio were great.

Figs. 8.18 and 8.19 show a comparison between the test results of the two models of Drnevich free-free resonant column devices. As shown in Fig. 8.18 the values of shear modulus obtained from the device at the Water and Power Resources Service (WPRS) are larger than the ones obtained from the device used in this study (UCD). The difference between the values of the maximum shear moduli is about 11%. Fig. 8.19 shows that the values of damping ratio obtained from the device at WPRS are about one-tenth of the damping ratios obtained from the UCD device at strains below 10^{-5}. At higher strain amplitudes the difference is even more. The damping ratios obtained from the WPRS device are very small and remain nearly the same for the whole range of strain amplitudes.

After reviewing all the results from all the specimens, it was decided to perform a statistical analysis and obtain a functional relationship for the shear modulus (G). This analysis and corresponding relationship are presented in Chapter 9. Because of the unusually large values of damping ratio and the unusual trend of the increase of damping with confining pressure and relative density, the damping ratios in this study were considered incorrect and it was decided not to develop a functional relationship for damping ratio.
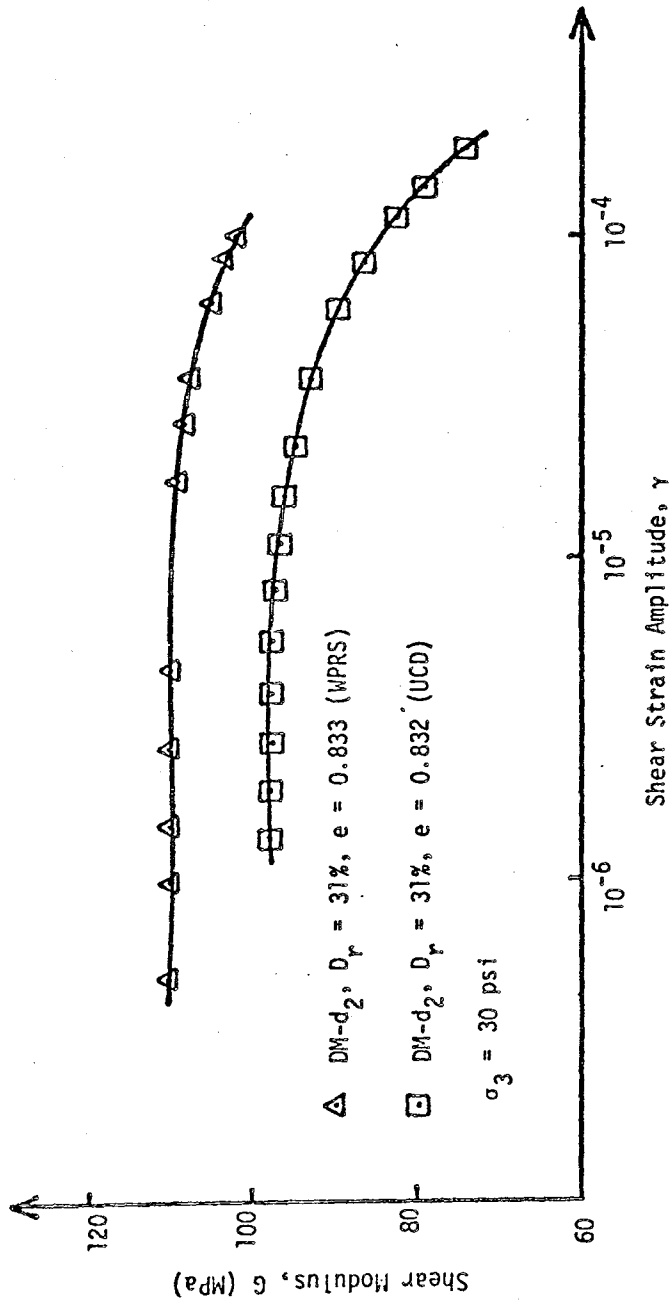
FIG. 8.18 SHEAR MODULUS VERSUS SHEAR STRAIN
$(DM-d_2)$

113
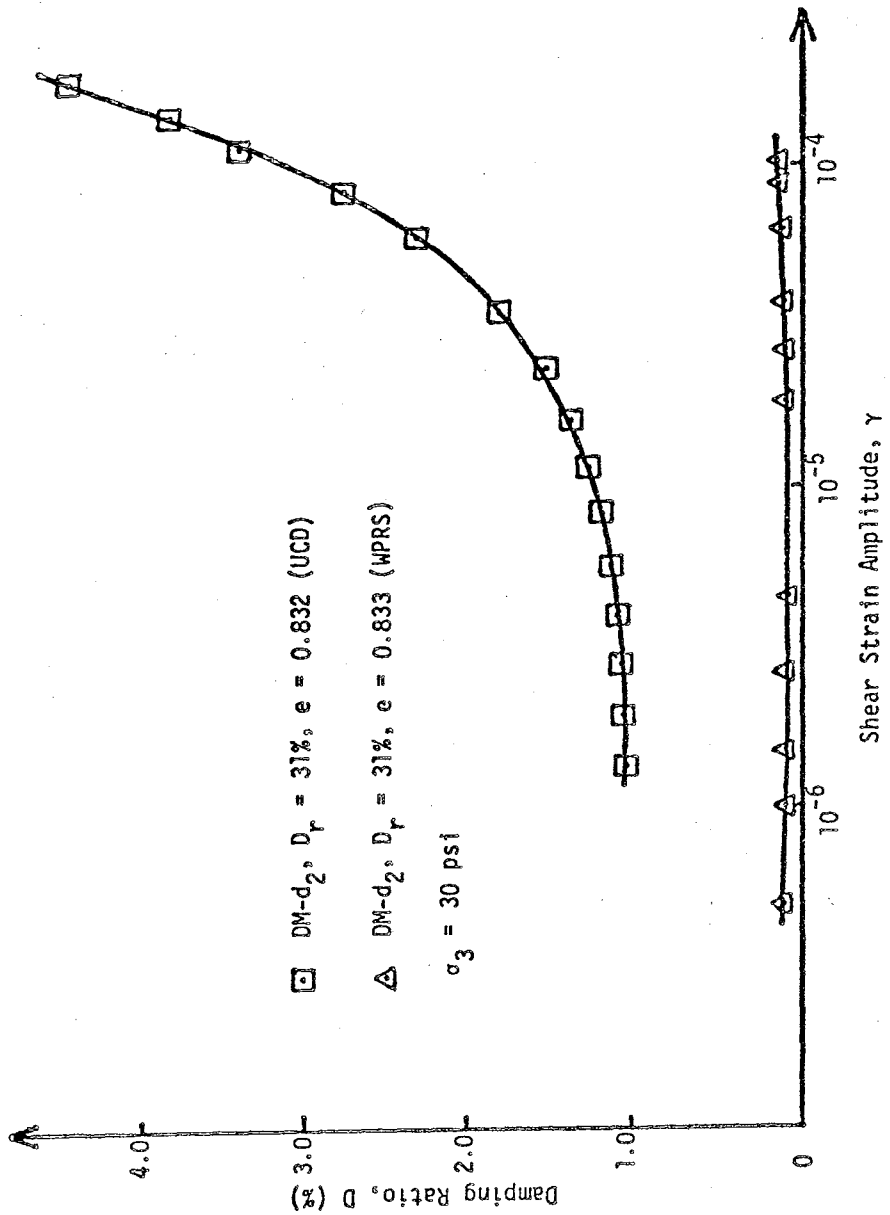
FIG. 8.19 DAMPING RATIO VERSUS SHEAR STRAIN
(DM-d$_2$)

CHAPTER 9

EVALUATION OF FUNCTIONAL RELATIONSHIP BETWEEN SHEAR MODULUS,
SHEAR STRAIN AND GRAIN-SIZE DISTRIBUTION CHARACTERISTICS

9.1 Data Selection

In conducting the statistical analyses, the results from all
of the tests on Denver sand were used. The test results indicated
that for each soil the value of shear modulus, G is approximately
constant at strains smaller than 10^{-5}. These values were desig-
nated as G_{max}, the maximum shear modulus. For each test four
points at strains greater than 10^{-5} were chosen from the shear
modulus G versus shear strain γ curve to formulate the functional
relationship between G and γ. Therefore, the result of each test
was characterized by one value of G_{max} for strains less than 10^{-5}
and four values of G for strains greater than 10^{-5}. This gives
96 pairs (24 tests x 4 points for each test) of G versus γ and
24 values of G_{max}.

In order to study the effects of gradation characteristics
on shear modulus, the data were divided into six sets. Each data
set contained the specimens with the same mean grain size, D_{50}.
Table 9.1 summarizes these six data sets.

9.2 Statistical Analyses

9.2.1 Introduction

Statistical analyses, described in Chapter 3, were performed

TABLE 9.1

DATA SETS SELECTED FOR STATISTICAL ANALYSES

Data Set No.	Specimens in the Set	D_{50} (mm)	No. of Tests
1	$DC-a_{2, 4, 6, 8}$	1.68	4
2	$DC-b_{4, 6, 8, 10, 15}$	0.84	5
3	$DM-c_{2, 4, 8, 10, 15}$	0.59	5
4	$DM-d_{2, 4, 6, 8, 10}$	0.42	5
5	$DM-e_{2, 4, 6}$	0.25	3
6	$DF-f_{2, 3}$	0.149	2

to determine the correlation coefficient and formulate the empirical relationship between the shear modulus of the twenty-four samples tested and strain or grain size distribution characteristics. These statistical analyses were performed by using the statistical programs from the SPSS, Statistical Package for the Social Sciences (Nie, et al., 1975).

9.2.2 Scatter Diagrams

Scatter diagrams were plotted for different dependent and independent variables to assist the observation of correlation and to investigate the dispersion of data points. Figs. 9.1 to 9.5 are examples of scatter diagrams.

Fig. 9.1 shows that maximum shear modulus G_{max} and void ratio e are strongly related and a linear relationship can be found between G_{max} and e or (log e) or (log e)^2 or a combination of these terms. Fig. 9.2 shows that G_{max} is also strongly related to uniformity coefficient C_u and again a linear relationship can be found between G_{max} and different functions of C_u. Fig. 9.3 indicates that G_{max} and mean grain size D_{50} are not strongly related and there is a wide dispersion. Fig. 9.4 shows that, for specimens with the same D_{50}, strong correlation exists between G_{max} and effective grain size D_{10}. However, the correlation between G_{max} and D_{10} for all data of various D_{50} is not strong as indicated by the low value of the correlation coefficient R in the next section. Fig. 9.5 shows the scatter of data with respect to relative density D_r. As stated in the earlier
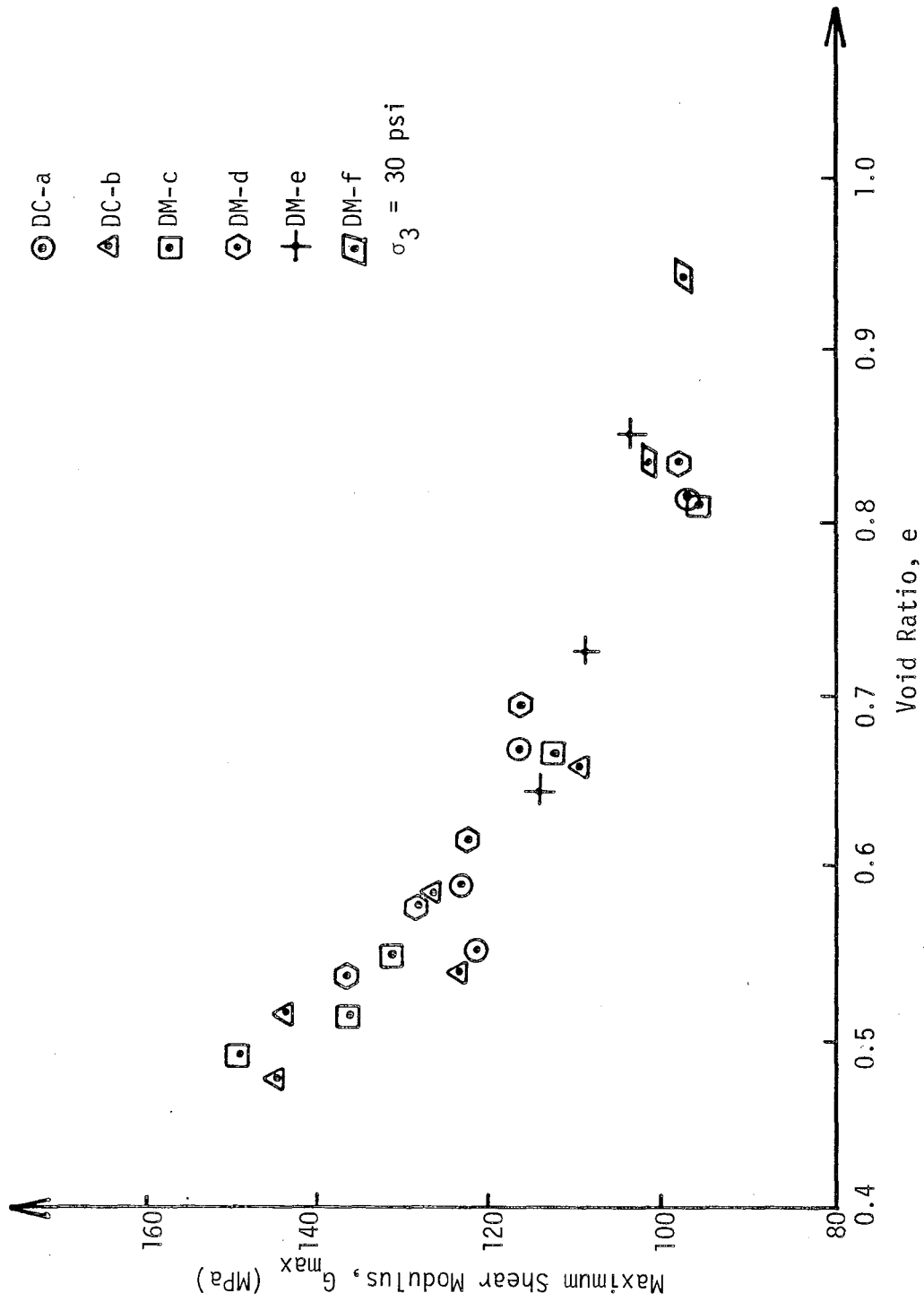
FIG. 9.1 THE EFFECT OF VOID RATIO ON MAXIMUM SHEAR MODULUS

FIG. 9.3 THE EFFECT OF MEAN GRAIN
SIZE ON MAXIMUM SHEAR
MODULUS
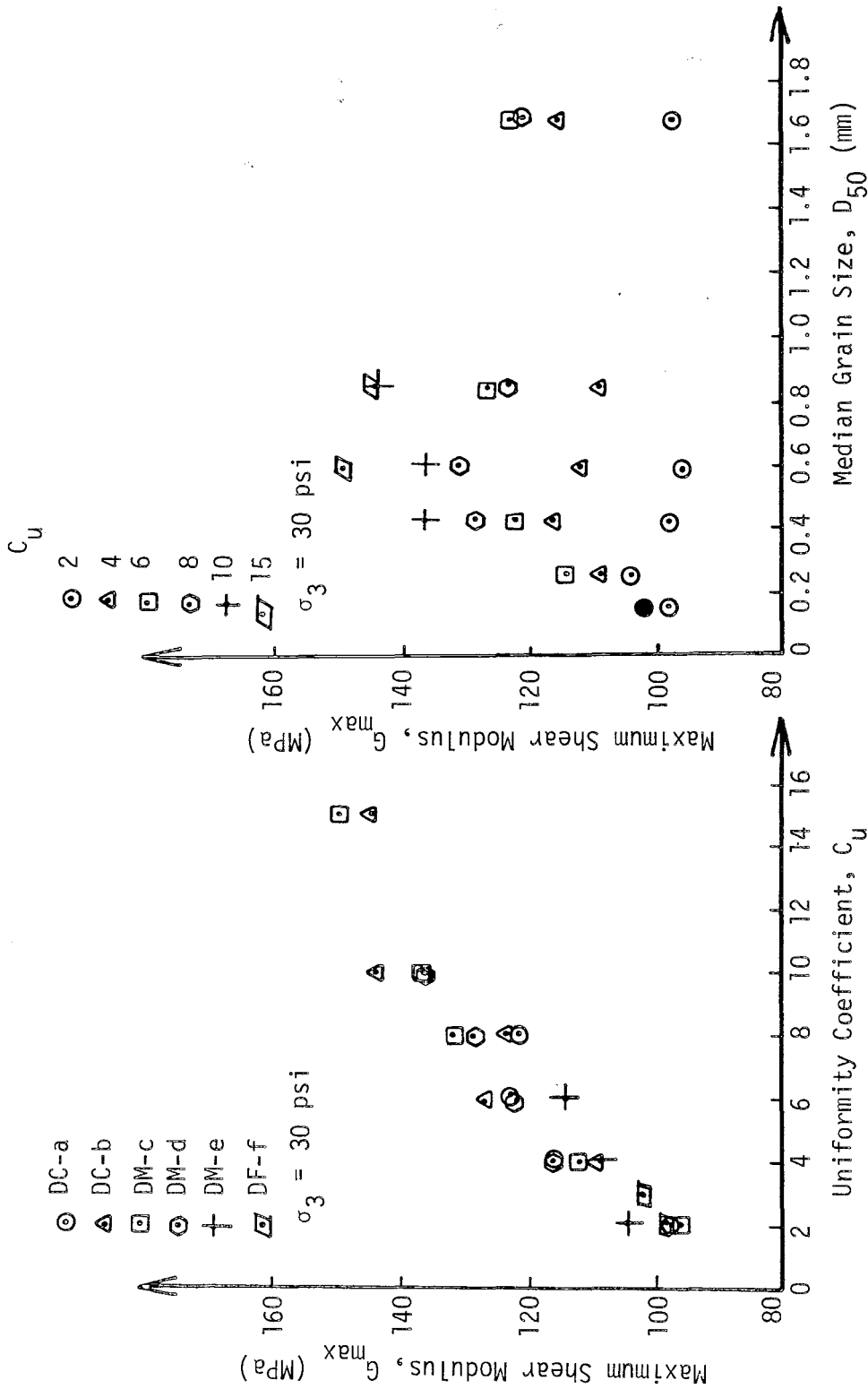
FIG. 9.2 THE EFFECT OF UNIFORMITY
COEFFICIENT ON MAXIMUM
SHEAR MODULUS
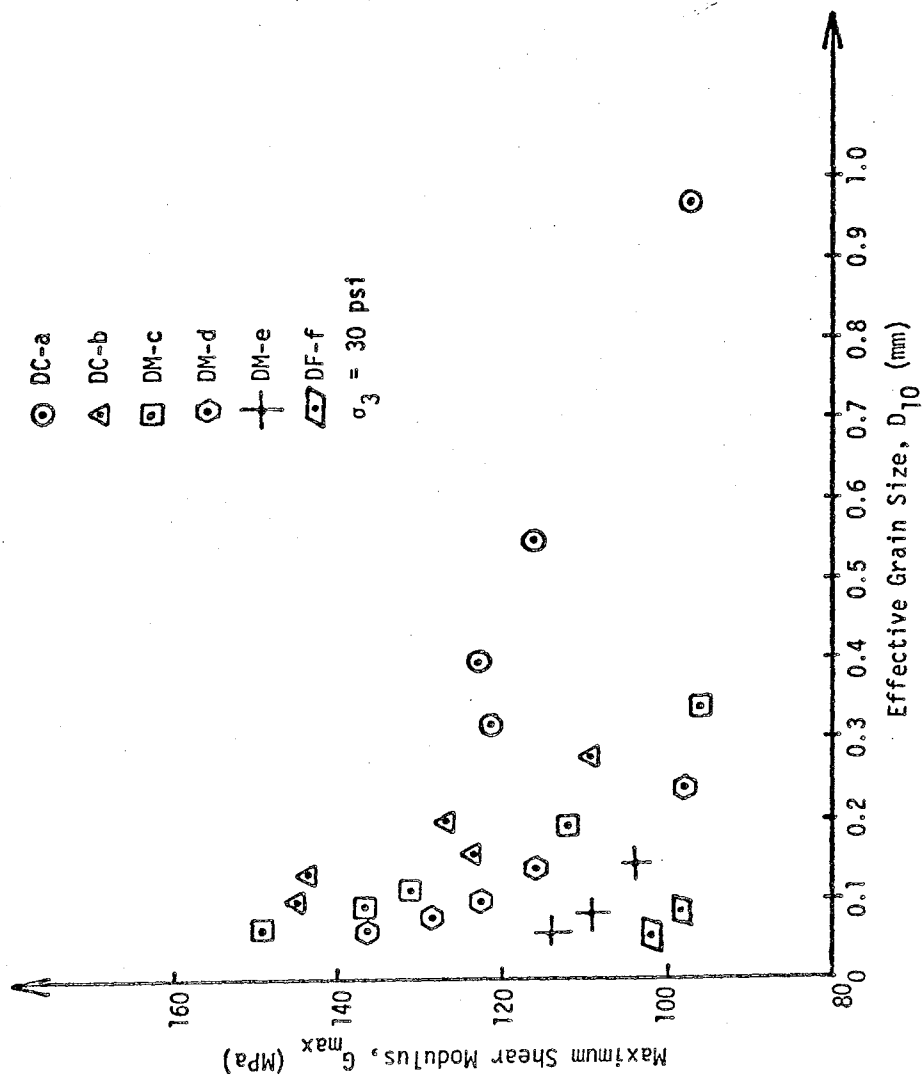
FIG. 9.4 THE EFFECT OF EFFECTIVE GRAIN SIZE
ON MAXIMUM SHEAR MODULUS
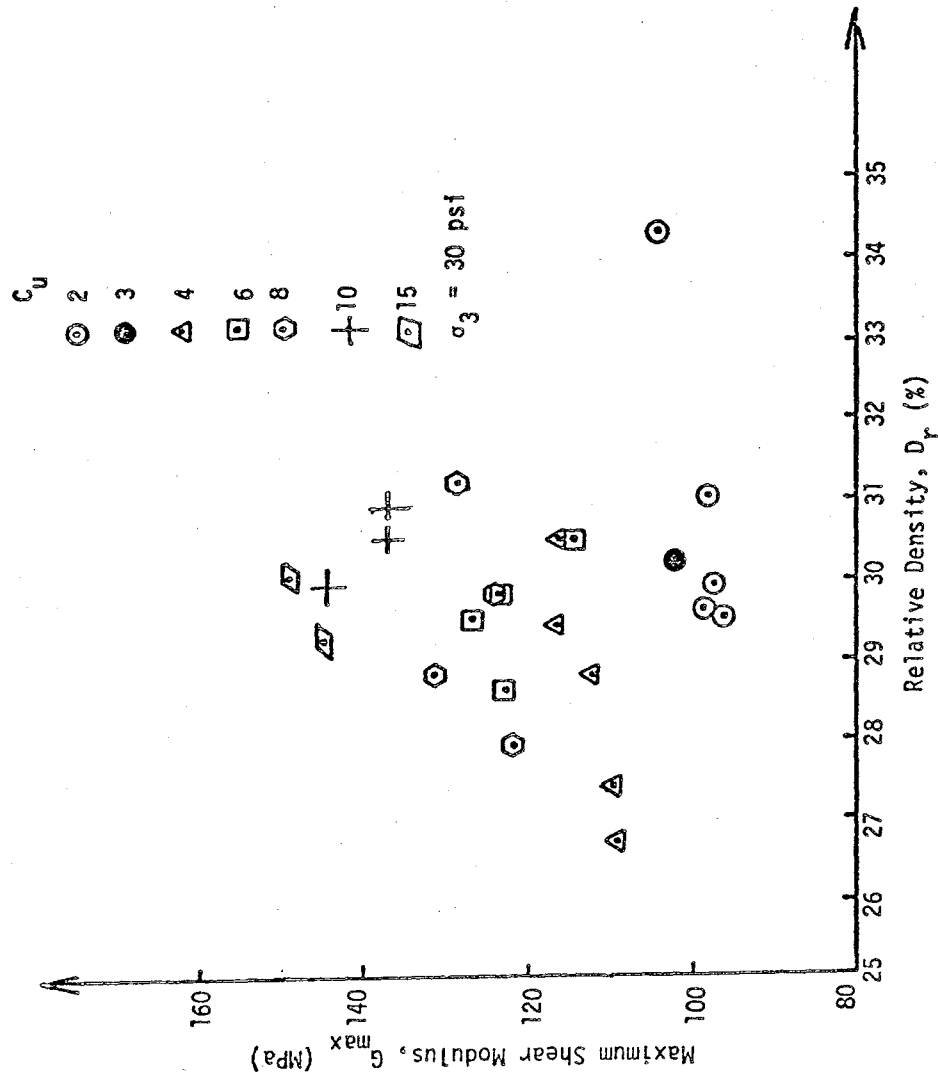
FIG. 9.5 MAXIMUM SHEAR MODULUS VERSUS
RELATIVE DENSITY

chapters the aim was to prepare the specimens with the same
relative density (D_r = 30%). However, it is difficult to prepare
identical specimens. Therefore, some of the specimens did not
have the relative density of 30% and Fig. 9.5 shows the range
of densities. Since the relative densities of most of the
specimens are close to each other and the void ratio of these
specimens is already considered as one of the variables, it was
decided to exclude D_r as a variable.

9.2.3 Statistical Correlation

After a careful study of the test results, it was decided
to perform the statistical analyses in two parts. In Part (1)
the objective was to obtain a relationship between normalized
shear modulus G/G_{max} and the shear strain amplitude γ. In
Part (2) the strength of correlation between G_{max} and various
independent variables were evaluated. Bivariate correlation
coefficients, R, between various dependent and independent vari-
ables were obtained by using the Pearson Correlation subprogram
(Nie, et al., 1975).

Part (1): G/G_{max} versus γ

In this part the correlation coefficients, R, between shear
modulus, G, maximum shear modulus, G_{max}, normalized shear modulus,
G/G_{max} and shear strain, γ, were obtained for the whole data
population. Their correlation coefficients are shown in Table
9.2. It becomes obvious that G/G_{max} and shear strain, γ have
a very strong correlation. Therefore, bivariate and multiple
regression analyses were performed to obtain a functional relation

TABLE 9.2

CORRELATION COEFFICIENT BETWEEN
SHEAR MODULUS AND SHEAR STRAIN
IN PART (1)

Variables	Correlation Coefficient R
G_{max}, γ	-0.276
G, γ	-0.657
G/G_{max}, γ	-0.949
G/G_{max}, $(\log \gamma)$	-0.891
G/G_{max}, $(\log \gamma)^2$	0.861

between G/G_{max} and γ (Section 9.2.4).

Part (2): G_{max} versus C_u, e, D_{10} and D_{50}

Table 9.3 shows all correlation coefficients obtained in Part (2). In obtaining these coefficients, all of the data points were included for each analysis. The correlation coefficients indicate that G_{max} is strongly related to uniformity coefficient, C_u, and void ratio, e. Also e and C_u show strong correlation.

9.2.4 Regression Analyses

Regression analyses were also performed in two parts. In Part (1) bivariate and multiple regressions were conducted to obtain a relationship between normalized shear modulus, G/G_{max} and shear strain, γ. In Part (2) an empirical relationship was obtained for G_{max} through the multiple regression analysis. In each part correlation coefficient, R, and coefficient of determination, R^2, between different variables were obtained and the variables which showed strong correlation (R greater than +0.7) were considered in the formulation of functional relationships.

Part (1): G/G_{max} versus γ

In order to obtain a functional relationship for G/G_{max}, first bivariate coefficients were obtained between G/G_{max} and shear strain, γ, and then multiple correlation coefficients were obtained between G/G_{max} and γ and log γ, by including all data points. Table 9.4 presents the result of these analyses. Since the two coefficients are nearly identical, it was decided to relate G/G_{max} to γ as follows:

TABLE 9.3

CORRELATION COEFFICIENT BETWEEN
VARIABLES IN PART (2)

Variables	Correlation Coefficient R
G_{max}, C_u	0.947
G_{max}, $(C_u)^2$	0.859
G_{max}, $\log C_u$	0.963
G_{max}, $(\log C_u)^2$	0.965
G_{max}, e	-0.922
G_{max}, $\log e$	-0.943
G_{max}, $(\log e)^2$	0.962
G_{max}, D_{50}	0.104
G_{max}, $(D_{50})^2$	-0.020
G_{max}, $\log D_{50}$	0.290
G_{max}, $(\log D_{50})^2$	-0.487
G_{max}, D_{10}	-0.388
G_{max}, $\log D_{10}$	-0.389

TABLE 9.3 (Continued)

CORRELATION COEFFICIENT BETWEEN
VARIABLES IN PART (2)

Variables	Correlation Coefficient R
e, C_u	-0.873
$e, \log C_u$	-0.958
$\log e, \log C_u$	0.972
$e, \log D_{10}$	0.203
$e, (\log D_{50})^2$	0.670
$C_u, \log D_{10}$	-0.419
$C_u, (\log D_{50})^2$	-0.427

$$G/G_{max} = a\gamma + b \qquad (9.3)$$

where a and b are the regression coefficients and G and G_{max} are
in MPa.

TABLE 9.4

CORRELATION COEFFICIENTS BETWEEN G/G_{max} AND γ

Dependent Variable	Independent Variable	Correlation Coefficient R
G/G_{max}	γ	0.949
G/G_{max}	γ, log γ	0.954

The next step was to obtain a relationship similar to
equation (9.3) for each of the data sets in Table 9.1. Therefore,
regression was performed for each set and Table 9.5 gives the
resulting regression coefficients.

Since the correlation coefficients for all data sets are
very strong, it was decided to perform one regression analysis
for all data. The following equation was obtained:

$$G/G_{max} = -1417 \gamma + 0.996 \qquad (9.4)$$

where G and G_{max} are in MPa. The correlation coefficient, R, for
this equation is 0.949 and the coefficient of determination, R^2,
is 0.901. Hence, the equation represents the sound functional
relationship between G/G_{max} and γ. The results of the regression
analysis for the entire data set are also shown in Table 9.5.

In order for equation (9.4) to satisfy the condition of
$G/G_{max} = 1$ at $\gamma = 0$ the constant term in the equation was changed
to 1 instead of 0.996. Therefore, the following equation was

TABLE 9.5

REGRESSION COEFFICIENTS BETWEEN G/G_{max}
AND γ FOR EACH DATA SET

Data Set No.	No. of Data Points in Set*	a	b	R	R^2
1	16	-1450	0.986	0.949	0.901
2	20	-1764	0.996	0.983	0.966
3	20	-1338	0.989	0.975	0.951
4	20	-1390	0.997	0.986	0.972
5	12	-1303	1.006	0.999	0.998
6	8	-963	1.006	0.999	0.998
All Data	96	-1417	0.996	0.949	0.901

where a and b are regression coefficients,

R is the correlation coefficient, and

R^2 is the coefficient of determination.

* These numbers all apply to similar tables to be presented later.

chosen to represent the relationship between G/G_{max} and γ for all data.

$$G/G_{max} = -1417 \gamma + 1.00, \quad R = 0.949 \qquad (9.5)$$

It should be noted that equation (9.5) was obtained from the data with strains less than 2×10^{-4}.

Part (2): G_{max} versus C_u, e, D_{10} and D_{50}

In this part an empirical relationship was obtained for G_{max} in terms of the other variables, void ratio, e, effective grain size, D_{10}, uniformity coefficient, C_u and mean grain size, D_{50}. As in Part (1), the multiple correlation coefficient, R and the coefficient of multiple determination, R^2, were obtained. Table 9.6 gives these coefficients for all data.

After studying the coefficients, for simplicity, it was decided to use the following regression equation:

$$G_{max} = a \log C_u + b \qquad (9.6)$$

where G_{max} is in MPa, C_u is the uniformity coefficient and a and b are the regression coefficients. Although a combination of functions of C_u like $\log C_u$ and $(\log C_u)^2$ gives a slightly larger correlation coefficient, but for all practical purposes the simpler form (Eq. 9.6) is adequate.

After selecting the type of the equation for G_{max}, regression was performed for the six data sets as shown in Table 9.1. Table 9.7 presents the regression coefficients for each set.

Another regression analysis was performed to obtain a relationship between G_{max} and C_u by including all data as follows:

$$G_{max} = 54.71 \log C_u + 80.46, \quad R = 0.963 \qquad (9.7)$$

TABLE 9.6

CORRELATION COEFFICIENTS BETWEEN G_{max}
AND OTHER VARIABLES

Dependent Variable	Independent Variable	R	R^2
G_{max}	$\log C_u$	0.963	0.927
G_{max}	$(\log C_u)^2$	0.965	0.931
G_{max}	$\log C_u, (\log C_u)^2$	0.968	0.938
G_{max}	$\log e$	-0.943	0.889
G_{max}	$(\log e)^2$	0.962	0.925
G_{max}	$\log e, (\log e)^2$	0.962	0.925
e	$\log C_u$	0.958	0.918
$\log e$	$\log C_u$	0.972	0.944

TABLE 9.7

REGRESSION COEFFICIENTS FOR G_{max}
FOR EACH DATA SET

Data Set No.	a	b	R	R^2
1	43.1	87.0	0.945	0.893
2	63.3	73.3	0.924	0.854
3	60.6	76.9	0.999	0.998
4	52.8	82.6	0.995	0.990
5	21.5	97.5	0.985	0.970
6	21.5	91.9	1.000	1.000
All Data	54.7	80.5	0.963	0.927

where G_{max} is in MPa. $R = 0.963$ and $R^2 = 0.927$ for this equation.

In order to study the effects of void ratio, e, effective grain size, D_{10} and mean grain size, D_{50} on G_{max}, the constants a's and b's shown in Table 9.7 were correlated to the above variables. Table 9.8 presents the bivariate and multiple correlation coefficients.

After reviewing the correlation coefficients, it was decided to formulate constant a as a function of $(\log D_{50})^2$, $\log D_{10}$ and $\log$ e. Equation (9.8) was obtained through the multiple regression analysis:

$$a = -103.83 \ (\log D_{50})^2 - 24.83 \ (\log D_{10})$$
$$+ 60.51 \ (\log e) + 55.79 \tag{9.8}$$

where D_{50} and D_{10} are in mm. $R = 0.898$ and $R^2 = 0.806$ for this equation.

The next step was to formulate the constant b as a function of the constant a. Therefore, regression analyses were performed between b and a by using the values of these constants in Table 9.7. Table 9.9 summarizes the correlation coefficients that were obtained.

After reviewing the correlation coefficients, equation (9.9) was chosen for constant b:

$$b = -0.006 \ a^2 + 98.26 \tag{9.9}$$

$R = 0.984$ and $R^2 = 0.968$ for this equation.

9.3 Summary of Results

Empirical relationships for G/G_{max} and G_{max} were obtained

TABLE 9.8

CORRELATION COEFFICIENTS FOR CONSTANTS a AND b

Dependent Variable	Independent Variables	R
a	$(\log D_{50})^2$	0.849
a	$(\log D_{50})^2$, $\log D_{10}$	0.884
a	e, $\log D_{10}$	0.704
a	$\log e$, $\log D_{10}$	0.711
a	$(\log e)^2$, $\log D_{10}$	0.708
a	$(\log D_{50})^2$, $\log D_{10}$, $\log e$	0.898
b	$(\log D_{50})^2$	0.740
b	$(\log D_{50})^2$, $\log D_{10}$	0.783
b	$(\log e)^2$, $(\log D_{10})^2$	0.704
b	$(\log D_{50})^2$, $\log D_{10}$, $\log e$	0.789

TABLE 9.9

CORRELATION COEFFICIENTS BETWEEN a AND b

Dependent Variable	Independent Variable	R	R^2
b	a	0.969	0.939
b	a^2	0.984	0.968
b	a, a^2	0.985	0.970

through statistical correlation and regression analyses. The following equations are the result of these analyses.

$$G/G_{max} = -1417 \, \gamma + 1.00 \qquad (9.10)$$

$$G_{max} = a \, \log C_u + b \qquad (9.11)$$

where $\quad a = -103.83 \, (\log D_{50})^2 - 24.83 \, (\log D_{10})$

$$+ \, 60.51 \, (\log e) + 55.79 \qquad (9.11a)$$

$$b = 0.006 \, a^2 + 98.26 \qquad (9.11b)$$

In all of the above equations, G and G_{max} are in MPa and D_{50} and D_{10} are in mm.

These are empirical equations based on the results of resonant column tests on twenty-four different gradations of Denver sand. The strain for these tests is less than 2×10^{-4}. Table 9.10 presents the range of variables, their mean, $\overline{X}$, and standard deviation, S, that were used in obtaining the above equations.

9.4 Discussion

The equations developed in the previous section were used

TABLE 9.10

STATISTICS OF VARIABLES USED IN THE DEVELOPMENT OF THE
FUNCTIONAL RELATIONSHIPS

Variable	Range of Values	Mean ($\overline{X}$)	Standard Deviation (S)
G	71.36 - 147.82 (MPa)	110.42 (MPa)	17.20
G_{max}	96.04 - 149.20 (MPa)	119.37 (MPa)	15.65
G/G_{max}	0.743 - 0.998	0.924	0.069
γ	5.54×10^{-6} - 2.1×10^{-4}	5×10^{-5}	0.005
C_u	2.0 - 15.0	6.21	3.75
D_{50}	0.149 - 1.68 (mm)	0.709 (mm)	0.494
D_{10}	0.060 - 0.97 (mm)	0.208 (mm)	0.205
e	0.475 - 0.946	0.652	0.134
a	21.47 - 63.30	48.45	15.72
b	73.34 - 97.46	82.84	8.09

to calculate the values of shear modulus at different strain levels. Fig. 9.6 shows that the measured values of shear modulus are nearly equal to the computed values. The regression line has a coefficient of determination, R^2, equal to 0.95.

Several researchers have proposed relationships for shear modulus of sands at small strains. Fig. 9.7 shows a comparison between the relationships for maximum shear modulus G_{max}. Hardin and Richart (1963) developed an empirical relationship for G_{max} for angular-grained soils such as crushed quartz sand as follows:

$$G_{max} = 1230 \frac{(2.973-e)^2}{1+e} (\bar{\sigma}_0)^{1/2} \qquad (9.12)$$

where G_{max} is the maximum shear modulus in Psi, e is the void ratio and $\bar{\sigma}_0$ is the effective mean principal stress in Psi. Iwasaki and Tatsuoka (1977) suggested an empirical relationship for G_{max} based on tests on uniform and well-graded sands as follows:

$$G_{max} = 900 \frac{(2.17-e)^2}{1+e} (\bar{\sigma}_0)^{0.40} B \qquad . \qquad (9.13)$$

where G_{max} and $\bar{\sigma}_0$ are in KSC and B is a parameter dependent on the uniformity coefficient and the content of fine particles in the soil sample.

Equations (9.12) and (9.13) were used to calculate the maximum shear modulus, G_{max}, for the Denver sand samples. G_{max} for these samples were also computed by using the relationships obtained in this study (Section 9.3). Then, the measured values of G_{max} from the test on Denver sand samples were plotted against the computed values obtained from the equations suggested by
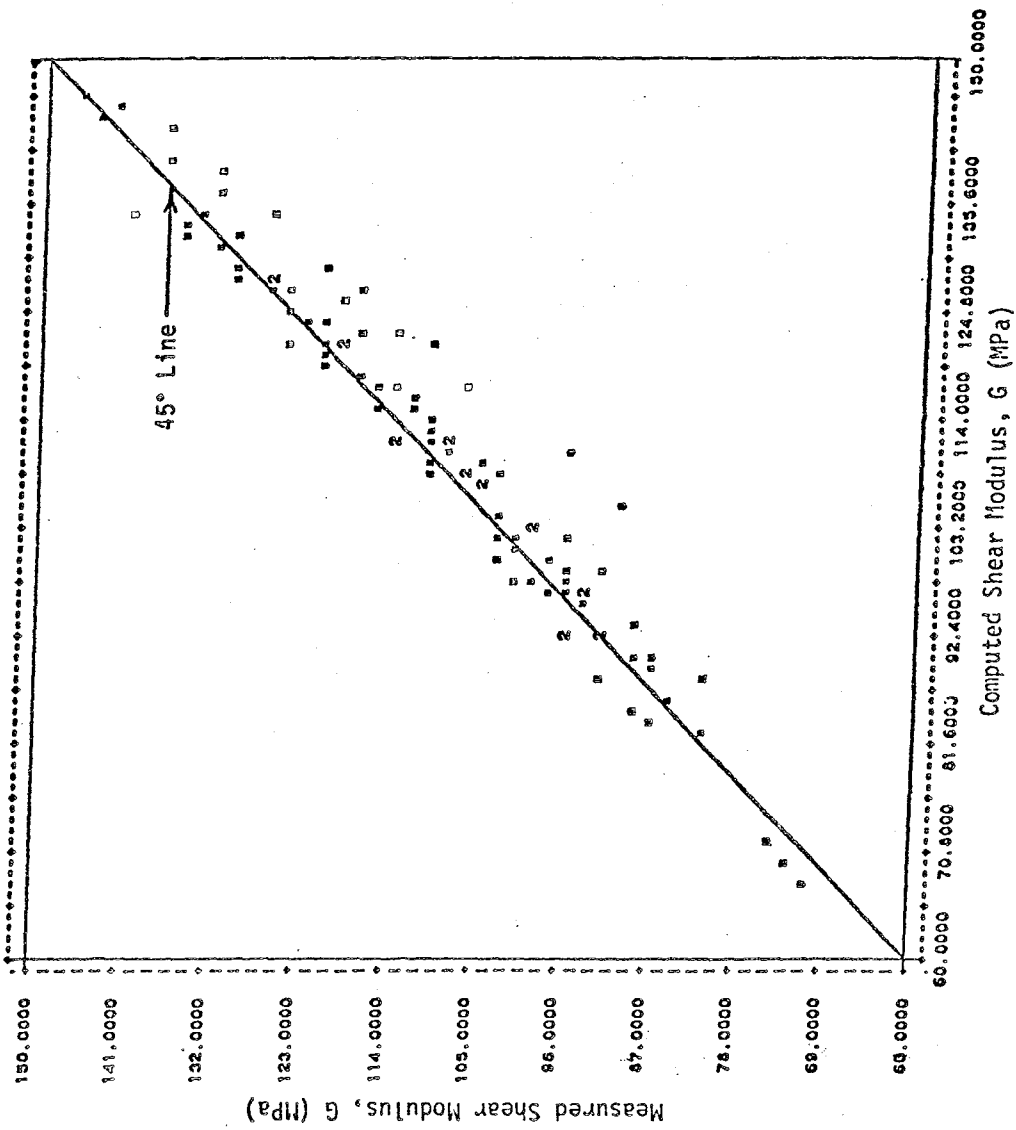
FIG. 9.6 COMPARISON OF MEASURED AND COMPUTED
VALUES OF SHEAR MODULUS
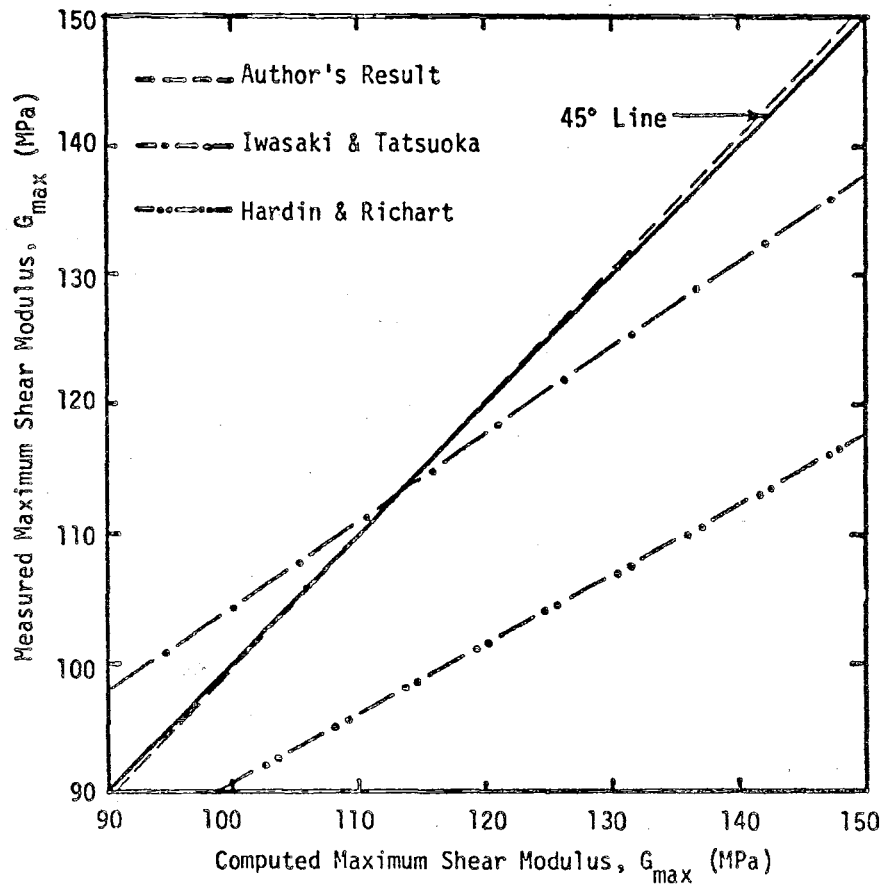
FIG. 9.7   COMPARISON OF RELATIONSHIPS
FOR MAXIMUM SHEAR MODULUS

Hardin and Richart, Iwasaki and Tatsuoka and the one derived
in this study. Fig. 9.7 shows the comparison between the three
relationships. The values of G_{max} obtained from the Hardin and
Richart equation are generally larger than the measured values,
the difference being less for uniform samples. The values obtained
from the Iwasaki and Tatsuoka equation are closer to the measured
values than the ones obtained by the Hardin and Richart equation.
Computed values of G_{max} from the equation derived in this study
are nearly the same as the measured values as shown in Fig. 9.7.
Therefore, the empirical relationship obtained in this study
estimates the values of maximum shear modulus for Denver sand
better than the other relationships proposed by Hardin and
Richart and Iwasaki and Tatsuoka.

CHAPTER 10

CONCLUSIONS AND RECOMMENDATIONS

10.1 Summary and Conclusions

The purpose of this study was to investigate the effects of grain size distribution characteristics on the dynamic properties of granular soils at small strains. To accomplish this goal, twenty-four samples of a Denver sand were prepared. These samples had a wide range of grain size distribution characteristics and contained particles from gravels to coarse silts.

Resonant column tests were performed to obtain the shear moduli and damping ratios of the samples. The specimens were prepared at an initial relative density of 30% and were con- solidated for one hour at a confining pressure of 30 (Psi) prior to testing.

Shear moduli and damping ratios were then plotted against strain amplitudes as shown in Figs. 8.6 to 8.17. The results showed unusually large damping ratios for some specimens and the incorrect trend of the increase of damping with confining pressure and relative density. The damping ratios in this study were considered incorrect. The reason for these large initial values of damping ratio were explained in Chapter 8. The values

of shear modulus seemed reasonable and the relationship between shear modulus and factors, such as void ratio, relative density and confining pressure were correct.

Statistical analyses were performed on the results of these twenty-four tests. First, correlation coefficients were obtained between dependent variables (shear modulus) and independent variables (e, C_u, D_{10}, D_{50}, γ) to evaluate the strength of their correlation. Then, functional relations were formulated for normalized shear modulus (G/G_{max}) and maximum shear modulus (G_{max}) through bivariate and multiple regression analyses. The results show that normalized shear modulus is strongly affected by shear strain amplitude, γ, and a linear relation exists between them. Also, maximum shear modulus (G at $\gamma < 10^{-5}$) is strongly affected by uniformity coefficient, C_u, and void ratio, e, and is related to effective grain size, D_{10}, and mean grain size, D_{50}. In general, the shear modulus of the specimens increased with increasing uniformity coefficient and decreased with increasing void ratio.

It should be noted again, that the relationships given in this study are empirical relations based on the results of resonant column tests on various samples of Denver sand with diverse grain size distribution characteristics. All specimens in these tests had an initial relative density near 30% and the tests were conducted under a confining pressure of 30 (Psi). The formulated equations are for strain amplitudes less than 2×10^{-4}. The most significant achievement of this study is

the formulation of functional relationships for the shear

modulus of sands in terms of their grain size distribution

characteristics: Uniformity coefficient, C_u, mean grain size,

D_{50}, and effective grain size, D_{10}.

10.2 Recommendations

As stated in earlier chapters, damping ratios obtained in

this study are incorrect and the equipment used in this study

needs to be extensively studied to determine the exact cause of

such unusually large damping ratios. After this is accomplished

and the problems are corrected, tests should be conducted to

evaluate damping ratios of sands used in this study. Functional

relationships of the damping ratio in terms of the grain size

distribution characteristics should then be formulated.

In addition to the improvements to the testing equipment

that were described in Chapter 6 (Section 6.5), several other

modifications should be adopted to achieve better accuracy and

conduct more consistent tests. These modifications include:

(1) replacement of the aluminum rods with steel rods because of

their flexibility and (2) the apparatus should be bolted to a

large isolated foundation pad. The isolated foundation pad

would eliminate effects of floor vibration.

In order to be able to establish a general relationship

for dynamic properties of granular soils, several samples of

sands and gravels from different origins and mechanical properties

should be tested with various relative densities, void ratios

and under different confining pressures.

A new apparatus should be designed to handle dynamic tests over a wide spectrum of strain amplitudes.

BIBLIOGRAPHY

Annaki, M. and K.L. Lee. "Equivalent Uniform Cycle Concepts for Soil Dynamics." Journal of the Geotechnical Engineering Division, ASCE, Vol. 103, No. GT6 (June, 1977).

Atakol, K. and H.G. Larew. "Dynamic Shearing Resistance of Dry Ottawa Sand." Journal of the Soil Mechanics and Foundations Division, ASCE, Vol. 96, No. SM2 (March, 1970).

Beniwal, R. "The Effect of Grain Characteristics on the Shear Modulus of Gravels." Ph.D. Dissertation, University of Kentucky (1977).

Chan, C.K. and J.P. Mulilis. "Pneumatic Sinusoidal Loading System." Journal of the Geotechnical Engineering Division, ASCE, Vol. 102, No. GT3 (March, 1976).

Cuellar, V., Z.P. Bazant, R.J. Krizek and M.L. Silver. "Densification and Hysteresis of Sand Under Cyclic Shear." Journal of the Geotechnical Engineering Division, ASCE, Vol. 103, GT5 (May, 1977).

Drnevich, V.P. and F.E. Richart. "Dynamic Prestraining of Dry Sand." Journal of the Soil Mechanics and Foundations Division, ASCE, Vol. 96, No. SM2 (March, 1970).

Drnevich, V.P. "Undrained Cyclic Shear of Saturated Sand." Journal of the Soil Mechanics and Foundations Division, ASCE, Vol. 98, No. SM8 (August, 1972).

Drnevich, V.P., B.O. Hardin and D.J. Shippy. "Modulus and Damping of Soils by the Resonant Column Method." ASTM Symposium on Dynamic Soil and Rock Testing in the Field and Laboratory for Seismic Studies, Denver, Colorado (June, 1977).

Drnevich, V.P. "Resonant Column Test." Geotechnical Laboratory, U.S. Army Engineer Waterways Experiment Station, Vicksburg, Mississipi, Paper S-78-6, Final Report (July, 1978).

Edil, T.B. and G.F. Luh. "Dynamic Modulus and Damping Relationships for Sands." ASCE Specialty Conference on Earthquake Engineering and Soil Dynamics, Pasadena, California (1978).

Finn, W.D.L., D.J. Pickering and P.L. Bransby. "Sand Liquefaction in Triaxial and Simple Shear Tests." Journal of the Soil Mechanics and Foundations Division, ASCE, Vol. 97, No. SM4 (April, 1971), Proceeding Paper 8039.

Hardin, B.O. "The Nature of Damping in Sand." Journal of the Soil Mechanics and Foundations Division, ASCE, Vol. 91, No. SM1 (1965).

Hardin, B.O. and J. Music. "Apparatus for Vibration of Soil Specimens During the Triaxial Test." ASTM STP 392, American Society for Testing and Materials (1965).

Hardin, B.O. and A. Mossbarger. "The Resonant Column Technique for Vibration Testing of Soils and Asphalts." Proceedings, Instrument Society of America (October, 1966).

Hardin, B.O. "Suggested Methods of Tests for Shear Modulus and Damping of Soils by the Resonant Column." ASTM STP 479, American Society for Testing and Materials (1970).

Hardin, B.O. and V.P. Drnevich. "Shear Modulus and Damping in Soils: Measurement and Parameter Effects." Journal of the Soil Mechanics and Foundations Division, ASCE, Vol. 98, No. SM6 (June, 1972).

_____ "Shear Modulus and Damping in Soils: Design Equations and Curves." Journal of the Soil Mechanics and Foundations Division, ASCE, Vol. 98, No. SM7 (July, 1972).

Ishibashi, I. and M.A. Sherif. "Soil Liquefaction by Torsional Simple Shear Device." Journal of the Geotechnical Engineering Division, ASCE, Vol. 100, No. GT8 (August, 1974).

Iwasaki, T. and F. Tatsuoka. "Effects of Grain Size and Grading on Dynamic Shear Moduli of Sands." Technical Memorandum of the Public Works Research Institute, Ministry of Construction, Japan (1977).

Nie, N.H., C.H. Hull, J.G. Jenkins, K. Steinbrenner and D.H. Bent. Statistical Package for the Social Sciences. Second Edition, McGraw-Hill Book Company (1975).

Park, T.K. and M.L. Silver. "Dynamic Triaxial and Simple Shear Behavior of Sand." Journal of the Geotechnical Engineering Division, ASCE, Vol. 101, NO. GT6 (June, 1975).

Peacock, W.H. and H.B. Seed. "Sand Liquefaction Under Cyclic Loading Simple Shear Conditions." Journal of the Soil Mechanics and Foundations Division, ASCE, Vol. 94, No. SM3 (May, 1968), Proceeding Paper 5957.

Richart, F.E., J.R. Hall and R.D. woods. *Vibrations of Soils and Foundations*. Prentice-Hall (1970).

Seed, H.B. and I.M. Idriss. "Soil Moduli and Damping Factors for Dynamic Response Analyses." Report No. EERC 70-10, University of California, Earthquake Research Center, Berkeley (1970).

Sherif, M.A. and I. Ishibashi. "Dynamic Shear Moduli for Dry Sands." *Journal of the Geotechnical Engineering Division*, ASCE, Vol. 102, No. GT11 (November, 1976).

Sherif, M.A., I. Ishibashi and A.H. Gaddah. "Damping Ratio for Dry Sands." *Journal of the Geotechnical Engineering Division*, ASCE, Vol. 103, No. GT7 (July, 1977).

Silver, M.L. and H.B. Seed. "Deformation Characteristics of Sand Under Cyclic Loading." *Journal of the Soil Mechanics and Foundations Division*, ASCE, Vol. 97, No. SM8 (August, 1971).

Silver, M.L. and T.K. Park. "Testing Procedure Effects on Dynamic Soil Behavior." *Journal of the Geotechnical Engineering Division*, ASCE, Vol. 101, No. GT10 (October, 1975).

Skoglund, G.R., W.F. Marcuson and R.W. Cunny. "Evaluation of Resonant Column Test Devices." *Journal of the Geotechnical Engineering Division*, ASCE, Vol. 102, No. GT11 (November, 1976).

Wu, T.H. *Soil Dynamics*. Allyn and Bacon, Inc. (1975).

Youd, T.L. "Densification and Shear of Sand During Vibration." *Journal of the Soil Mechanics and Foundations Division*, ASCE, Vol. 96, No. SM3 (1970).

Part III

LIQUEFACTION POTENTIAL

ABSTRACT

Catastrophic earthquake-induced ground failures may result
in either partial or total destruction of earth-embankment dams,
mine-tailings dams, slopes, and other super-structures. These
ground failures may also cause great loss of both lives and
properties. Earthquake-induced ground liquefaction is most
detrimental to any super or substructures. The research on the
quake-induced liquefaction has been greatly accelerated after
the considerable damage caused by the Alaska and Niigata earth-
quakes of 1964.

The liquefaction potential of granular soils was found to
be strongly dependent on the relative density, void ratio, mean
effective stress, and cyclic deviatoric-stress amplitude. The
effect of grain-size distribution on liquefaction potential,
while known to be significant, has not been systematically
studied over a broad spectrum of grain size.

The parameters which characterize the grain-size distribution
of soils are: Uniformity coefficient (Cu), mean diameter (D_{50})
and effective diameter (D_{10}). The effect of these parameters
on the liquefaction potential of a granular soil was investigated.
A series of isotropically consolidated undrained cyclic triaxial
tests were conducted to evaluate the liquefaction potential of
samples prepared from Denver Sand. Twenty-four samples with

different grain-size distribution characteristics were tested. The samples have the following gradation characteristics: (a) grain size: 0.038 mm to 9.53 mm; (b) mean grain size: 0.14 mm to 1.50 mm; and (c) uniformity coefficient: 1.89 to 16. The particle shape of the sand is subangular.

The result of this investigation indicated that the liquefaction potential is strongly dependent on the mean diameter of Denver sand. Thus, the functional relationship between the liquefaction potential and the mean diameter was formulated by the use of regression analysis.

CHAPTER 11

INTRODUCTION

11.1 General

The quake-induced liquefaction of cohesionless soils, because
of its disastrous damages of extensive nature has earned the
attention of worldwide researchers in the field of dynamic behav-
iors and properties of soils, since the catastrophic earthquakes
of Alaska and Niigata of 1964. The liquefaction induced in these
earthquakes resulted in massive flow slides, serious ground subsi-
dence, large differential settlement and/or bearing capacity
failures of super structures (earth and non-earth), waterfront
structures, and bridge abutments and piers, etc. To mitigate
these hazards caused by the quake-induced liquefaction requires
a clear understanding of the dynamic behaviors of saturated
cohesionless soils and the factors affecting them.

11.2 Purpose

Research studies have shown that cohesionless soil grains
when loose and subjected to cyclic stresses tend to compact and
reorient. This causes the generation of pore pressure if drainage
is restricted. This transfer of load from soil grains to pore
water results in the reduction of the effective stress. When
a cohesionless soil is subjected to a sufficient number of stress

cycles, the pore water pressure may become equal to the initial confining pressure on the soil. At this time the soil, if of low relative density, may undergo large deformations with minimal resistance and is said to have liquefied.

The liquefaction potential of a granular soil is strongly dependent on its relative density, void ratio, mean effective stress, and cyclic deviatoric-stress amplitude. All these factors have been extensively investigated, but the effect of grain-size distribution on liquefaction potential, while known to be significant, has not been systematically studied.

The purpose of this study is to investigate the effects of grain-size distribution (gradation) characteristics on the liquefaction potential of cohesionless soils. Gradation of soils can be characterized by indices, such as the uniformity coefficient, C_u, median diameter, D_{50}, and effective grain size, D_{10}, etc. Functional relationships were formulated between the liquefaction potential and gradation characteristics.

11.3 Scope

To investigate the effect of grain-size distribution on the liquefaction potential of granular soils, undrained cyclic triaxial tests were performed. Granular soil samples prepared from a Denver sand were tested. These samples were graded to have different uniformity coefficients at six selected mean grain sizes. The test sand has grain particle sizes ranging from silt to small gravels.

After completion of the laboratory work, all cyclic triaxial

test results were systematically studied and statistically analyzed. The analysis included statistical correlation and regression analysis. The liquefaction potential of granular soils was formulated as functions of gradation indices with the strong correlation. It is hoped that the result of this research will assist in the assessment of the safety of earth structures containing saturated granular soils and the foundation system on them was founded during potentially damaging earthquakes.

An extensive literature review is presented in Chapter 12. The review includes: 1) Behaviors of saturated granular soils under static and cyclic loads; 2) case histories of liquefaction induced ground failures; 3) methods for evaluating liquefaction potential of soils; 4) experimental methods for evaluating liquefaction potential; 5) factors affecting liquefaction potential; and 6) factors affecting cyclic triaxial test results. Test equipment, sample preparation and experimental procedures are detailed in Chapter 13. The test results were analyzed and discussed in Chapter 14. Summary and conclusions are presented in Chapter 15.

CHAPTER 12

REVIEW OF LITERATURE

12.1 Behaviors of Saturated Granular Soils under Static and Dynamic Loads

12.1.1 Behaviors of Saturated Sands under Static Loads

The shear deformation of sand is accompanied by volume changes (Reynolds, 1885). The volume decrease of a loose sand and the volume increase of a dense sand during shearing would tend to produce the same "critical void ratio" or "critical density" at which a cohesionless soil can undergo any amount of deformation without volume change (Casagrande, 1936). The critical void ratio (or density) is not constant for a soil. As shown in Fig. 12.1, the critical density increases with the increase of confining pressure (Seed and Lee, 1967). The critical void ratio is also a function of the type of test used to determine it (Perloff and Baron, 1976).

The critical void ratio can be reached from either a loose or dense state. Fig. 12.2 shows typical (qualitative) behavior of soils sheared under drained triaxial compression condition, i.e., the curves marked "1" represent the behavior of a dense sand, while the curves marked "2" represent that of a loose sand. If a saturated sand is not allowed to change its volume, then the tendency to change its volume will result in the change in porewater pressure.
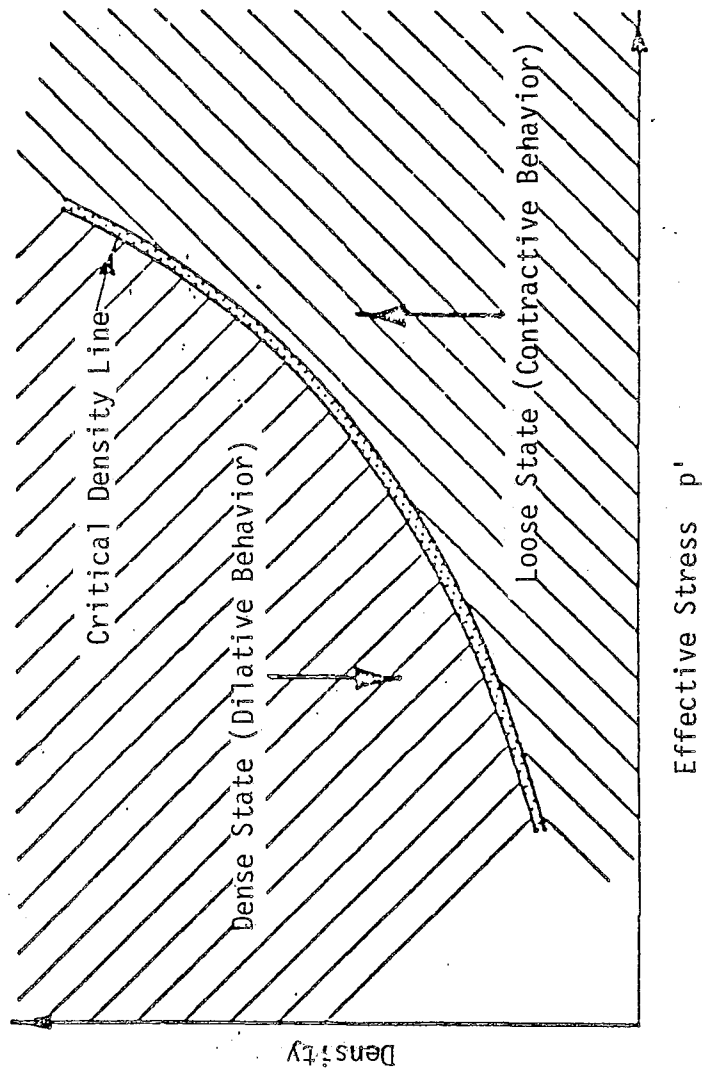
FIG. 12.1 CRITICAL DENSITY LINE
(From Baladi and Rohani, 1978)
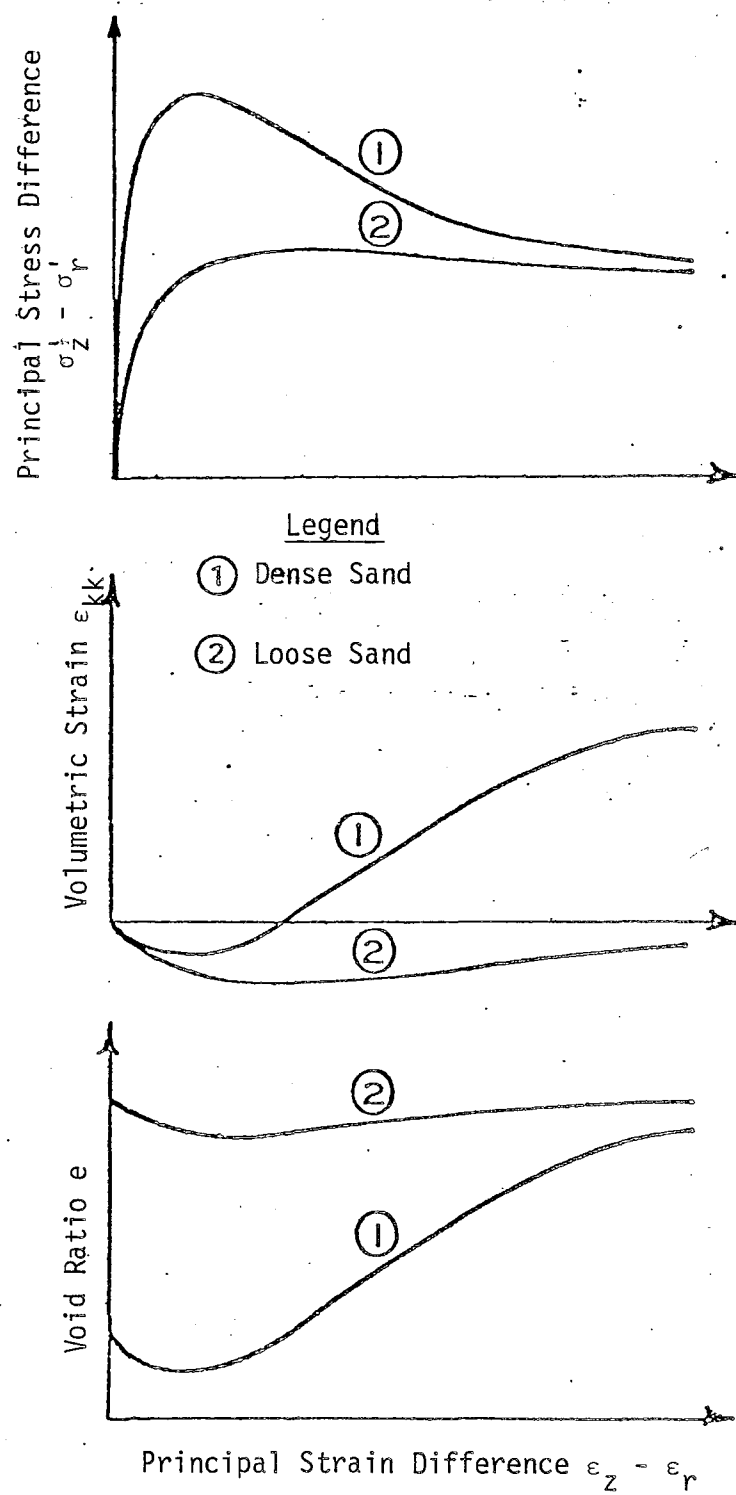
FIG. 12.2 TYPICAL BEHAVIOR OF SATURATED SOILS TESTED
UNDER DRAINED TRIAXIAL TEST CONDITIONS

Thus a sand in a looser state than that of the critical void ratio
will experience an increase in pore-water pressure, and a corre-
sponding decrease in shearing resistance. On the other hand,
a sand in a denser state than that of the critical void ratio will
experience a decrease in pore-water pressure and a corresponding
increase in shearing resistance. Fig. 12.3 shows a typical
variety of stress-strain-pore-water pressure response curves mani-
fested by a saturated soil tested in undrained shear in a triaxial
compression device. The three specimens were first isotropically
consolidated to the same effective mean normal stress level (point
2), then subjected to undrained shearing. The curves marked "2→3"
show the typical response of a very loose sand to undrained shearing.
The curves marked "2→5" show typical behaviors of a very dense sand.
Between the extreme responses of these very loose and dense soils,
there exist a gradual change in response exemplified herein by the
curves marked "2→4". The actual response depends on the state of
compactness of the material. It is clear from this figure that
only the effective stress will affect the shear strength of soil.

Theoretically speaking, the critical void ratio does exist for
a sand, however, within the usual effective stress range in labora-
tory testing (say <150 psi), sand samples on the critical state
line will be extremely loose. They are often looser than the
loosest state that can be achieved by any laboratory sample prepara-
tion method. Very often an extremely loose state for a sand can
only be reached through dilation during shear (Atkinson and Bransby,
1978; K.H. Roscoe, 1970). In other words, the behavior shown by

———————— Effective Stress Path
—·——·——·— Total Stress Path
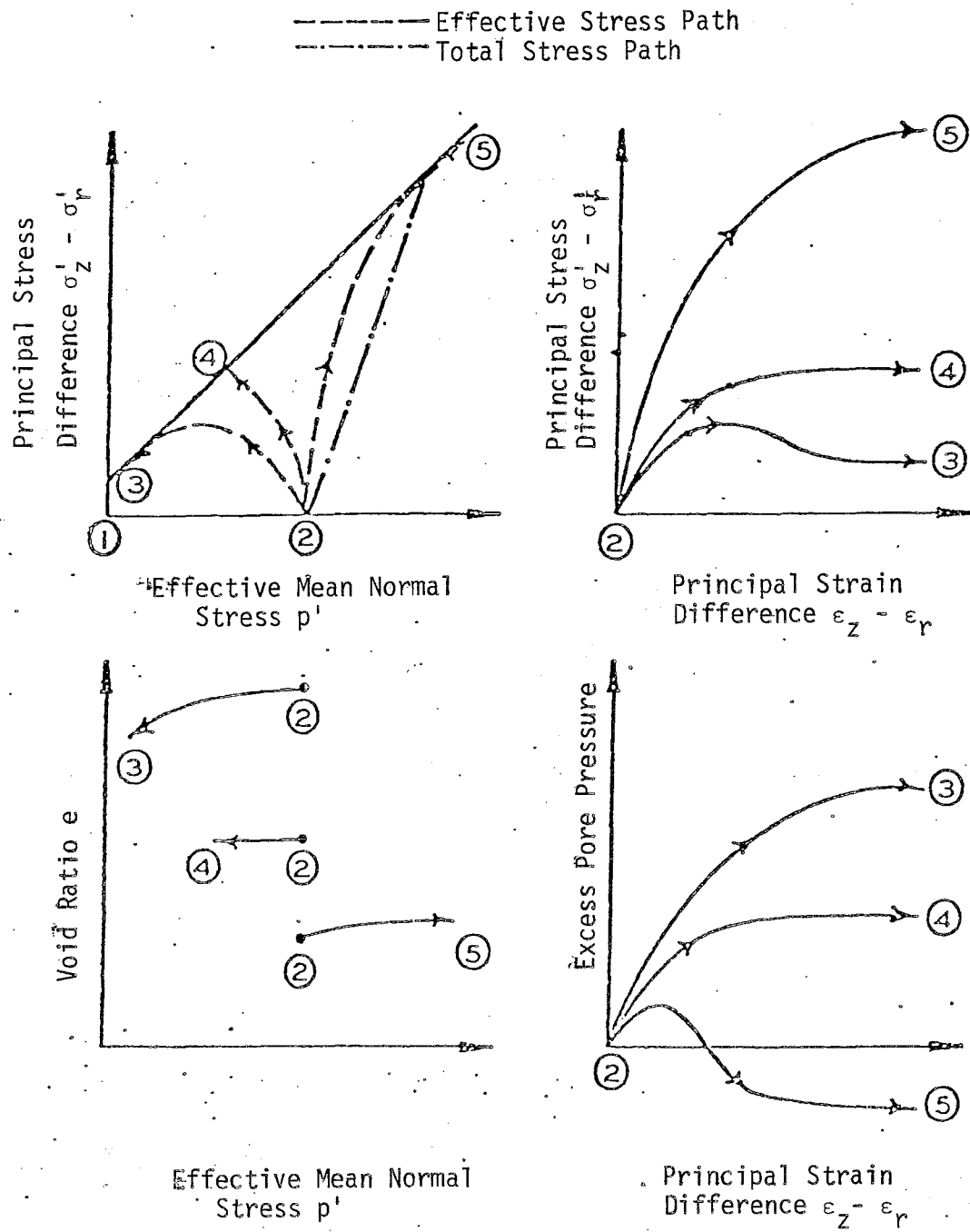
FIG. 12.3 TYPICAL BEHAVIOR OF SATURATED SOIL TESTED
UNDER UNDRAINED TRIAXIAL TEST CONDITIONS
(From Baladi and Rohani, 1978)

a loose sand in Figs. 12.2 and 12.3 were seleom observed in the laboratory. For Monterey No. 0 sand, the critical confining pressure versus the relative density of samples is shown in Fig. 12.4 (Lee and Vernese, 1978). The critical confining pressure is 8 KSC (kg/cm^2) for relative density of 60 percent and 13 KSC for relative density of 80 percent. Lade's test results (1972) indicated that the Monterey No. 0 sand shows a strong tendency of dilation under shear even for very loose sample relative density = 21%. In the literature, little work was done on the behavior of a saturated sand under a triaxial extension test in which the axial load is reduced while the radial stress is kept constant. According to the study by Castro (1975), the sample tested in triaxial extension yields considerably and eventually fails by necking under a considerably smaller deviatoric stress than that tested in triaxial compression. Fig. 12.5 shows the comparison of axial compression and extension consolidated-undrained triaxial tests of a dense clean fine to medium sand. It is imperative to know the behavior of sand under extension loads if one were to predict its behavior under a cyclic load with stress reversal.

12.1.2 Behavior of Saturated Sands under Cyclic Loads

The most important and critical phenomenon of saturated sands under cyclic loads is liquefaction. If a saturated sand is subjected to cyclic loads, it has a tendency to compact and decrease in volume. If the drainage line is closed, then the tendency to decrease in volume results in an increase in pore-water pressure. If the pore-water pressure equalizes the overburden (or the confining)
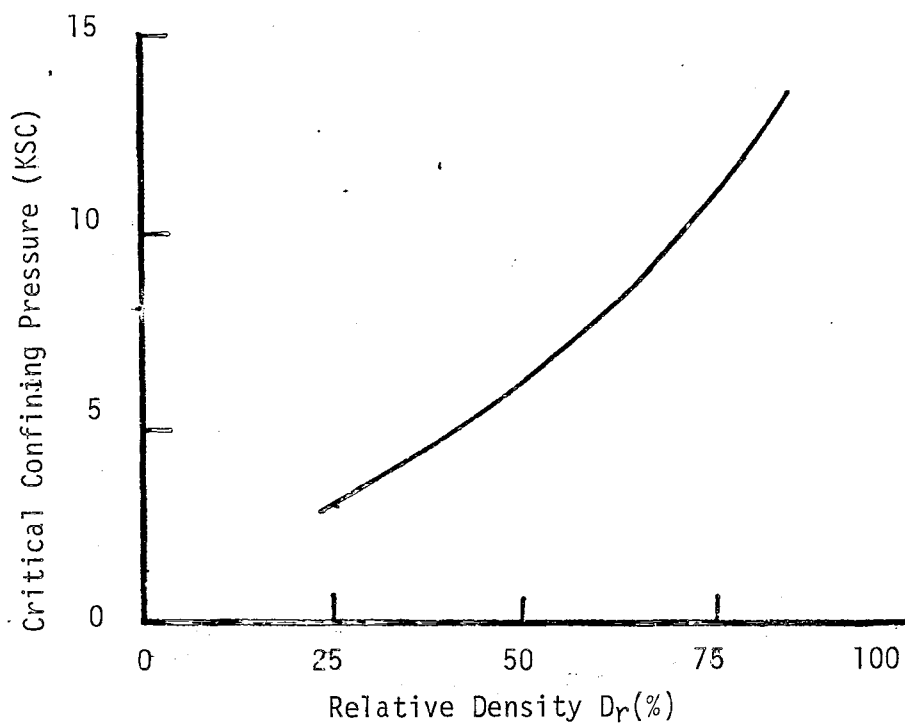
FIG. 12.4 CRITICAL CONFINING PRESSURE VERSUS RELATIVE DENSITY
OF MONTEREY NO. 0 SAND (From Lee and Vernese, 1978)
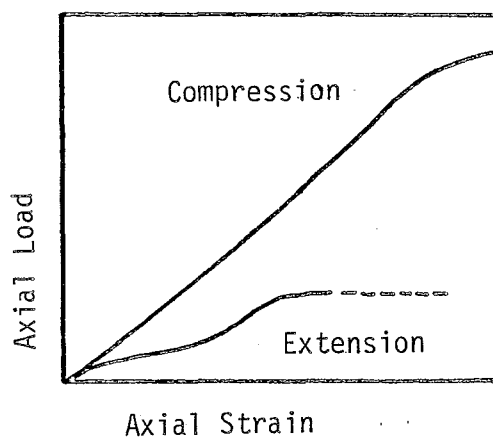
FIG. 12.5 COMPARISON OF AXIAL COMPRESSION AND EXTENSION
CONSOLIDATED-UNDRAINED TRIAXIAL TESTS (Castro, 1975)

pressure and the effective confining stress becomes zero, the sand loses its strength completely, and is in a liquefied state (Casagrande, 1936).

A quantitative approach to the prediction of the onset of liquefaction was presented by Seed and Lee (1966). In this approach the liquefaction potential was evaluated by results of cyclic triaxial tests. The main conclusion derived from this approach is that the larger the cyclic stress ratio and the looser the samples, the smaller the number of cycles of the cyclic stress are required to cause liquefaction. Test results by Seed and Lee (1966) showed that the liquefaction can be produced by cyclic loading also in dense sand and is not limited to loose sands. This behavior contradicts the sand behavior implied by the critical void ratio (or critical state) concept, which states that dense sands will only dilate under shearing. Seed and Lee (1966) concluded the critical state approach which can explain the behavior of sand under static compression loads very well cannot be used to explain the behavior of a sand under cyclic loads.

Further studies conducted by Casagrande (1975), Castro (1975), and Castro and Poulons (1977) introduced the following terms to describe the behavior of saturated sands under cyclic loads: (1) the "liquefaction" of a loose sand and (2) the "cyclic mobility" of a dense sand. The detail differences between these two terms were summarized by Holtz and Kovacs (1981) in Table 12.1. Fig. 12.6 also shows the difference of these two terms in describing the similar behavior of sands. In general, the liquefaction can take

TABLE 12.1

DIFFERENCE BETWEEN LIQUEFACTION AND CYCLIC MOBILITY*

	Liquefaction	Cyclic Mobility
General	Most likely in uniform, fine, clean, loose sand. Static load can cause liquefaction. Cyclic loads causing shear stresses larger than the steady-state strength also can cause liquefaction.	Any soil in any state can develop cyclic mobility in the laboratory if the cyclic stresses are large enough.
Effect of σ'_{3c} at constant void ratio for $\sigma'_{1c}/\sigma'_{3c}$	Increased σ'_{3c} means larger deformations if liquefaction is induced. The magnitude and/or number of cyclic loads needed to cause liquefaction increases with σ'_{3c}. Cyclic loads smaller than the steady-state strength cannot cause liquefaction but may cause cyclic mobility.	Increased σ'_{3c} means increased cyclic load to cause cyclic mobility. But the cyclic mobility ratio[†] usually decreases with increasing σ'_{3c}.
Effect of $\sigma'_{1c}/\sigma'_{3c}$ at constant void ratio and σ'_{3c}	Smaller additional loads are needed to cause liquefaction as $\sigma'_{1c}/\sigma'_{3c}$ increases. When $\sigma'_{1c}/\sigma'_{3c}$ is large, a soil is more unstable and may, in the extreme, be susceptible to "spontaneous liquefaction."	In soils that have low permeability, increased $\sigma'_{1c}/\sigma'_{3c}$ seems to result in somewhat smaller cyclic mobility stresses, which is a reasonable trend. In clean sands, cyclic mobility stress increases with $\sigma'_{1c}/\sigma'_{3c}$. This unusual result for clean sands is postulated to be due to the substantial test error due to redistribution of void ratio in the laboratory specimens.

→*After Castro and Poulos (1977).

[†]$\dfrac{(\sigma_1 - \sigma_3)/2}{\sigma'_{3c}}$, where $(\sigma_1 - \sigma_3)$ is the dynamic principal stress difference, or the cyclic mobility stress.

(After Holtz and Kovacs, 1981)
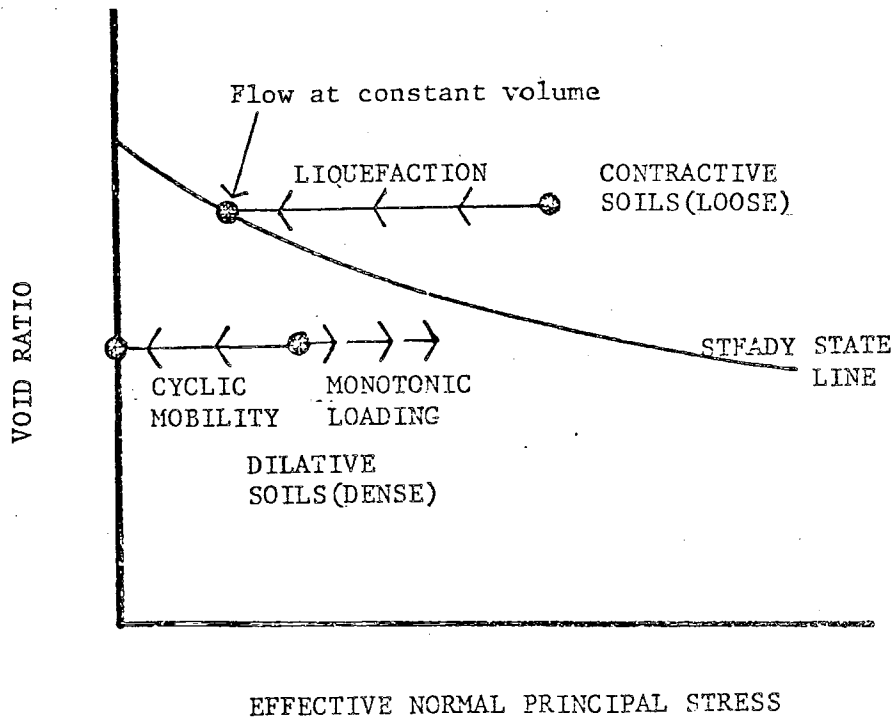
FIG. 12.6   LIQUEFACTION AND CYCLIC MOBILITY
(Castro and Polous, 1977)

place in a sand looser than its critical state either under a static or a cyclic load. The liquefaction of a loose sand still can be explained by the critical state concept. The cyclic mobility of a dense sand (denser than its critical state) cannot use the critical state concept to explain it. Liquefaction consists of a loss in shear strength and cyclic mobility consists of gradually increasing cyclic strains but does not entail a loss in shear strength.

Casagrande (1975) concluded that (1) the cyclic mobility in test specimens is caused by redistribution of water content which is generated by the mechanism that normally are absent in-situ, and (2) the cyclic mobility normally cannot develop in a dense sand in-situ. Because it is unlikely that laboratory tests can be devised to eliminate the severe stress gradients in test specimens and to reproduce the uniform stresses that exist in a typical element in-situ (Casagrande, 1975). Since the cyclic triaxial tests cannot simulate the in-situ loading condition (Casagrande, 1975; Finn, Pickering and Bransby, 1971), correction factors are necessary to be established for cyclic triaxial test results so that it can be more representative of the in-situ condition (Pedro, Seed and Chan, 1976).

Typical test results of an isotropically consolidated stress controlled cyclic triaxial strength test are shown in Fig. 12.7. The important feature of the behavior depicted in Fig. 12.7 is that the accumulated strain during cyclic loads prior to liquefaction is small compared with the strain after liquefaction, whereas the

ISOTROPIC CONSOLIDATION
MONTEREY NO.0 SAND
RELATIVE DENSITY= 60%

|————— 10 SECONDS —————|

COMPRESSION
2000
1000
0
EXTENSION
1000
2000

AXIAL   STRESS-PSF

COMPRESSION
20
15
10
5
0
5
EXTENSION
10
15
20

AXIAL   STRAIN-%

0
500
1000
1500
2000
2500

CONFINING PRESSURE ————→
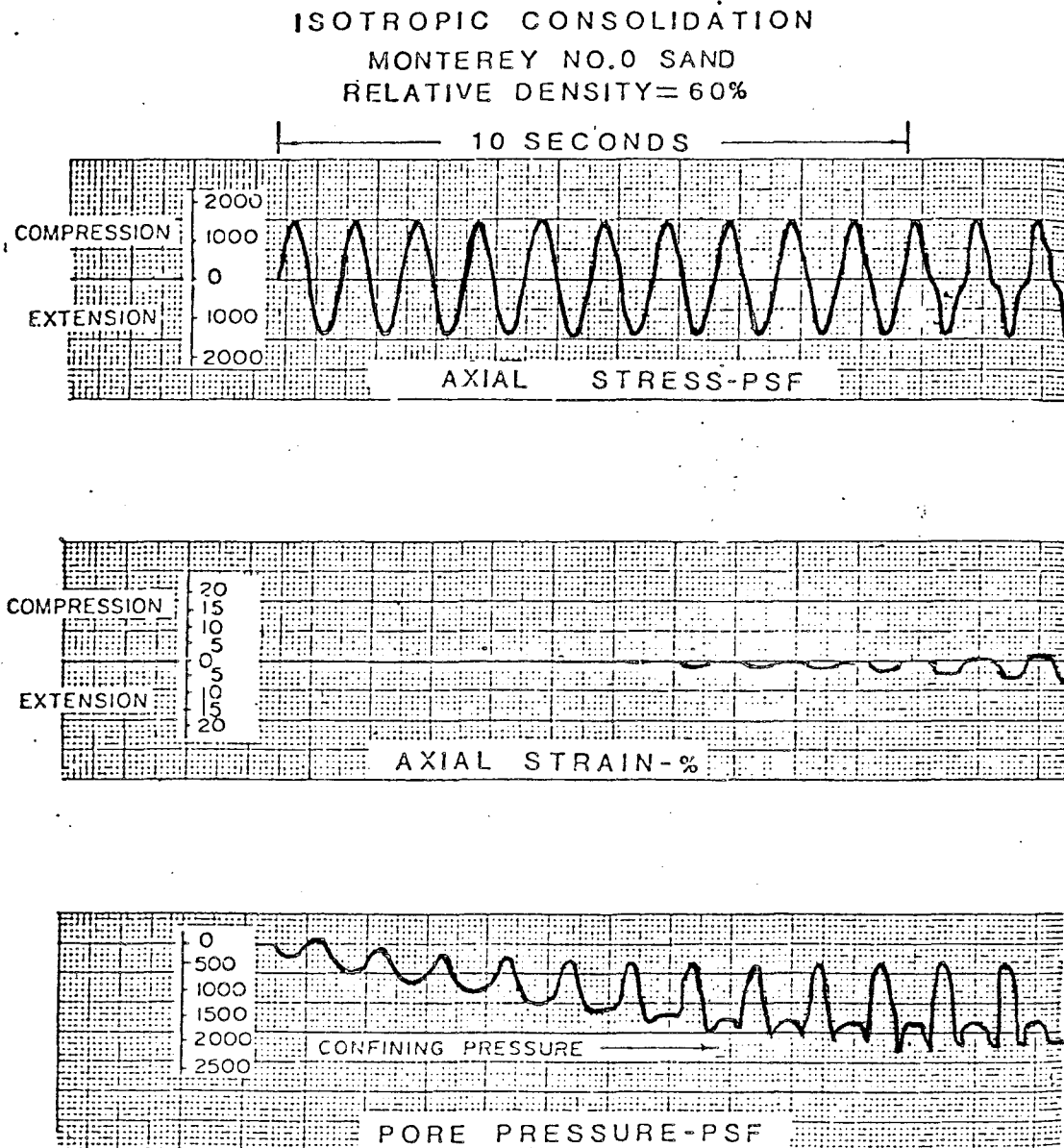
PORE PRESSURE-PSF

FIG. 12.7 TYPICAL RESULT OF AN ISOTROPICALLY CONSOLIDATED
STRESS-CONTROLLED CYCLIC TRIAXIAL TEST

pore pressure increases rapidly prior to liquefaction. The other important behavior is that the liquefaction takes place suddenly during the test (Seed and Lee, 1966).

The sudden initiation of liquefaction has been studied by many researchers and different conclusions have been drawn. According to the study by Ishihara, Tatsuoka and Yasuda (1975), liquefaction will be initiated when the effective stress touches the "phase transformation line" which is defined as the loci of the points at which the effective stress paths undergo abrupt changes in curvature and direction. Fig. 12.8 shows the phase transformation line for liquefying sands. Some other studies concluded that the liquefaction is initiated when the excess pore-water pressure reaches the magnitude of 60% of the confining pressure (Singh, Donovan and Park, 1980; Finn, 1981). Another conclusion offered by Baladi and Rohani (1978) indicates that the liquefaction is initiated when the effective stress path touches the failure envelope of a soil.

The results of cyclic triaxial tests (Seed and Lee, 1966) indicated that the liquefaction takes place when the deviatoric stress is equal to zero. The same conclusion was also reached about the state of liquefaction by Wang (1981) from this theoretical analysis.

12.2 Case Histories of Liquefaction Induced Failures

12.2.1 Introduction

Although experience has shown that the greatest damage to civil engineering structures due to liquefaction occurs as a
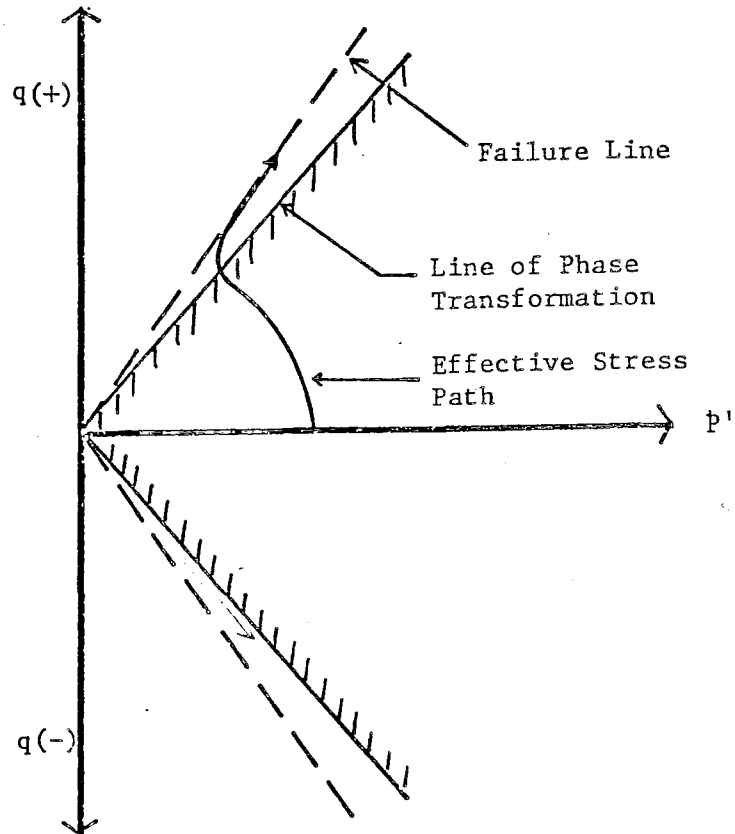
FIG. 12.8 PHASE TRANSFORMATION LINES FOR LIQUEFYING SAND

result of earthquakes, cases of failures triggered by other mechanisms will also be discussed. This chapter presents case histories of liquefaction failures grouped according to the triggering mechanism.

12.2.2 Liquefaction Induced by Monotonically Changing Stresses

12.2.2.1 Zeeland Slides

The Dutch province of Zeeland consists of a large group of islands separated by wide estuaries. On the shores of the islands in that province, numerous flow slides have occurred. From 1881 to 1946, 229 such slides were reported to involve 32.7 million cubic yards of soil and an area loss of 660 acres. The soils involved in these slides were sands deposited in shallow water by the rivers Rhine, Meuse, and Scheldt. Grain-size curves reported by Koppejan, Van Wamelen and Weinberg (1943) showed these sands to be mostly fine and uniform, with a typical D_{10} of 0.08 mm and uniformity coefficients, typically, of less than 2.

Erosion and seepage pressures resulting from tidal fluctuations of up to 4.6 m were believed to have triggered the slides. According to the description by Koppejan, these slides progressed inland as a succession of small slides starting when the toe of a slope was scoured away by tidal current, releasing lateral support in the slope. Under reduced lateral stress, the soil tended to expand, generating negative pore water pressure which caused inward seepage. Water seeping into the soil relieved

the negative pore pressure, which became positive as shear strains
occurred and finally became large enough to cause liquefaction
flow in that portion of the slope. After a certain amount of
material had flowed away in one small slide, the process would
begin again and continue in this manner until denser, more stable
material was reached at which time the flow process would stop.
Fig. 12.9 taken from Hvorslev's paper (1956) clearly illustrates
the above process. According to Koppejan, the slides progressed
inland at a rate of about 50 m per hour.

12.2.2.2 Mississippi River Flow Slides

Numerous flow slides have occurred along the banks of the
Mississippi River (Hvorslev, 1956). The materials involved in
these slides were uniform fine sands with rounded to subrounded
particles and uniformity coefficients from 1.5 to 1.8. Those
slides occurring in revetted point bar deposits have been carefully
studied, but slides have occurred in unrevetted reaches of the
river as well. The slides have damaged revetments and levees
built for flood protection. On March 24, 1949 a slide involving
the loss of a portion of a levee occurred at Free Nigger Point
near Baton Rouge, Louisiana. This single slide involved the
volume displacement of 4.4 million cubic yards of material and
occurred in less than 12 hours. The slides occurring on the
river are described by M.J. Hvorslev (1956) to be similar to
those occurring in Zeeland, Holland, in regard to form, dimen-
sions, slopes, duration, material, and groundwater conditions.
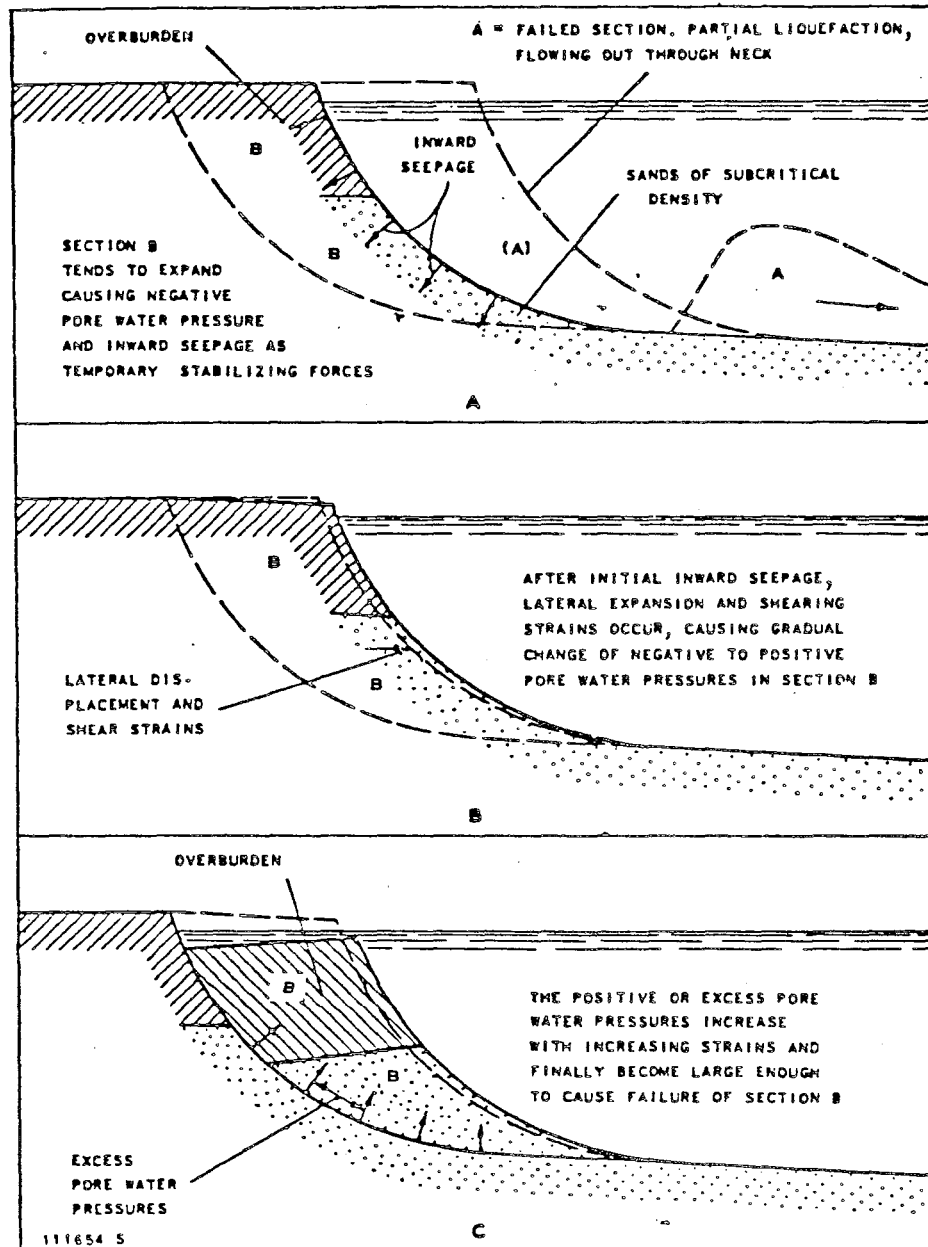
FIG. 12.9 DUTCH HYPOTHESIS FOR PROGRESSIVE FLOW FAILURES
(From Hvorslev, 1956)

12.2.2.3 Partial Failure at Fort Peck Dam

A granular shell of a dam constructed by the hydraulic fill method is likely to be deposited in a loose condition, and therefore susceptible to liquefaction failure. The Fort Peck Dam in Montana is an embankment with shells of this type. On September 22, 1938, a partial failure occurred involving a 1700-foot-long section of the upstream shell, portions of which moved some 1500 feet in a period of about 4 minutes.

The dam was constructed of river sands and finer grained alluvial soils on a foundation of alluvial sands, gravels, and clays with a total thickness of up to 130 feet. Beneath the river alluvium Bearpaw shale was present which contained layers of bentonite. In a discussion of a paper by Middlebrooks (1942), Gilboy expressed the opinion, which was shared by Casagrande, that liquefaction was the predominant failure mechanism which was triggered by shear strains in the foundation shale. This failure involved the movement of about 10 million cubic yards of material.

12.2.2.4 Flow Slide at Aberfan Village in Wales

Aberfan is a mining village, situated at the foot of a low mountain, the side of which had been used to deposit waste materials from coal mining operations. The waste materials were deposited in hillocks which were locally called "tips." From 1915 to October 1966, seven tips had been formed, and on October 21, 1966, the most recently constructed tip failed by liquefaction

sending about 200,000 cubic yards of material flowing down the mountainside and into the village. In this catastrophe, 146 children lost their lives in an elementary school in the flow path. The tip that failed had been deposited over natural springs issuing from outcrops of the underlying sandstone. At the time of failure, material was still being deposited on the tip. Heavy rainfall, common to this area in October may have eroded the base of the tip, reducing lateral stress and causing internal shear strains. This condition, coupled with the natural groundwater conditions of the mountainside and the continued loading of the tip, was believed to have triggered the liquefaction failure (Hutchinson, 1967).

Hutchinson (1967) described the material involved in the flow slide as consisting chiefly of shale fragments and mudstones ranging from clay size particles to large boulders as much as 3 feet in diameter. For the grain sizes small enough to be sieved, the average D_{10} size was between 0.1 and 0.8 mm and the coefficient of uniformity was approximately 18. Hutchinson pointed out that the Aberfan material was neither grained nor poorly graded. He described tailing materials from other sites which failed in a similar manner as having high uniformity coefficients and questions the uniformity of soils as a criterion for liquefaction susceptibility.

12.2.3 Liquefaction Induced by Cyclic Vibrations

12.2.3.1 Liquefaction of Railway Embankment Near Weesp, Holland

Koppejan (1943) described a flow slide in the approach to a railway bridge over the Merwede Canal near Weesp, Holland, in 1918. The embankment which failed had been formed by dumping moist sand. The sand had consequently "bulked," forming a very loose and unstable structure. After the water level in the canal rose and saturated the sand, the embankment was subjected to vibrations from a passing train and collapsed with the train causing heavy casualties.

It is probable that capillary forces present in the moist sand served to give the embankment initial stability. As saturation occurred, the capillary forces disappeared and the stability of the embankment decreased to the extent that vibrations from the passing train were sufficient to cause liquefaction. The coefficient of uniformity of the sand involved in the slide was about 2 and the D_{10} size was about 0.14 mm. According to Koppejan (1943) liquefaction triggered by vibrations occurs much more rapidly than liquefaction by monotonic stress changes because the entire mass subjected to vibrations liquefies almost simultaneously. This railway accident was so serious that as a result, the formal practice of soil mechanics was begun immediately in the Netherlands.

12.2.3.2 Vibrations Induced by Pile Driving

In an effort to develop a field test to evaluate earthquake potential, Ishihara and Mitsui (1972) drove piles into a sand

foundation and measured the induced pore pressure in the vicinity of the pile. According to Ishihara, this approach is superior to blasting tests since vibrations caused by blasts are very short in duration compared to the duration of an earthquake, and blasting cannot be performed in congested urban areas.

The site selected for the investigation was near Tokyo. The foundation material was a hydraulically placed, fine uniform sand about 8 meters in thickness. The uniformity coefficient of the material was between 2 and 5 and the D_{10} size between 0.05 and 0.20 mm. The standard penetration resistance blow count was approximately $N = 5$.

To measure the induced pore pressure and acceleration, piezometers and accelerometers were installed 4 or 8 meters deep in the foundation in a circular configuration about the point at which the pile would be driven. The pile was driven at the pre-selected spot by a vibratory generator capable of producing a variable oscillating force up to 35 tons at a frequency of 17 Hz. The oscillating driving force was adjusted to produce a penetration rate of 1-2 meters per minute. The pile was a closed-end steel pipe with an outside diameter of 40 centimeters. Measurements during the driving of the pile indicated that during some tests, the pore pressure became temporarily equal to the overburden pressure, but quickly dissipated. Acceleration was measured only in the vertical direction. Measurements showed that there was a unique relationship between sand denisty and acceleration level which produced a given pore pressure near the pile. The test results show a significant reduction of the strength of the

foundation soils resulted from the slow dissipation of excess pore water pressure and the remolding of soils during pile driving. Such a strength reduction, even if not sufficient to cause lique-faction, could result in large settlements or even bearing capacity failures in adjacent structures.

12.2.4 Flow Failures Induced by Earthquakes, Blasts, and Wave Action

Liquefaction induced by shock waves and the resulting random vibrations in potentially a more serious threat to civil engineering structures than that induced by other disturbing causes. Shock waves from earthquakes and blast loads or explosive charges are included in this general category. Earthquakes present probably the most serious liquefaction threat because the tremen-dous amount of energy released during an earthquake can disturb very large areas almost simultaneously. Consequently, structures built on or with cohesionless soils in seismically active areas must be designed considering the probability of earthquake shaking.

12.2.4.1 One of the Earliest Recorded Landslides Resulting from Liquefaction

The destruction of Helice, Greece described by Marinatos (1960) may possible record the earliest known case of a major land-slide resulting from soil liquefaction induced by an earthquake.

> "In the year 373 B.C., during a disastrous winter night, a strange thing happened in central Greece. Helice, a great and prosperous town on the north coast of the Pelopon-nesus, was engulfed by the waves after being levelled by a great earthquake. Not a single soul survived.... The next day two thousand men hastened to the spot to bury the dead,

but they found none, for the people of Helice had been buried under the ruins and subsequently carried to the bottom of the sea, where they now lie."

Helice was located on deltaic deposits of alluvial sand between the mouths of the Selinus and Cerynites rivers and about a mile and a half from the coast. Marinatos indicated that the city is now completely covered and no trace of it exists, neither on the ground surface nor on the bottom of the sea.

The events leading to the disappearance of Helice and its inhabitants are not immediately clear. A general subsidence of the land area during the earthquake undoubtedly occurred and this alone could have led to flooding of the city.

Marinatos (1960) who made detailed studies of the event, concluded that in addition to destruction of buildings by the ground shaking and flooding due to land subsidence, the ground slipped towards the sea possibly as much as half a mile. Marinatos noted that ordinarily it would be expected that building destruction and flooding would lead to some of the dead floating to the surface where they would have been picked up by the Achaens for burial. He concludes that only the entrapment of the inhabitants in collapsed buildings, and temporarily liquefied and flowing soils could have led to the recorded facts that no one survived and no dead were found.

Additional evidence in support of this concept is provided by the fact that

"The phenomenon was repeated, in exactly the same place though to a lesser degree, during the earthquake of December 26, 1861.... Again the soil slipped to the northeast (toward the sea) in the following way: A crack about eight miles

long and six feet wide appeared in the earth along the foot
of the mountain. A strip of plain 325 to 425 feet wide
disappeared slowly under the sea along the whole eight-mile
length, while the remaining part of the plain sank about six
feet and showed many minor cracks and small chasms."

In view of the fact that the earthquake of 373 B.C. is
estimated to have been about 10 times greater in intensity than
the 1861 earthquake, it is very likely that the disappearance of
Helice can be attributed to liquefaction of the underlying sand
foundation.

12.2.4.2 <u>Examples of Fluidation Flow Induced by Earthquakes</u>

Fluidation, i.e., flow of an essentially dry, cohesion-
less material with air as the pore fluid, can also be induced by
shock waves. One of the most dramatic series of flow slides in
recorded history occurred in the Chinese province of Kansu on
December 16, 1920. Close and McCormick (1922) described the events
in the following terms:

"Of that most remarkable series of seismic disturbances
which occurred throughout the world in November and December,
1920, the most phenomenal was undoubtedly the great Kansu
earthquake of the late evening of December 16.... Landslides
that eddied like waterfalls, crevasses that swallowed houses
and camel trains, and villages that were swept away under a
rising sea of loose earth, were a few of the subsidiary
occurrences that made the earthquake one of the most appalling
catastrophes in history."

"The area of greatest destruction, 100 miles by 300 miles
in extent, contains ten large cities besides numerous villages.
In it is the heart of the loess country...where the loose
earth cascaded down the valleys and buried every object in
its path."

"It is in the loess area that the immense slides out
of the terraced hills occurred, burying or carrying away
villages...damming stream beds and turning valleys into
lakes, and accomplishing those hardly believable freaks
which the natives name 'the footsteps of the gods.' The loss

of nearly two hundred thousand lives and the total destruc-
tion of hundreds of towns and cities calls for reconstruction
work on a staggering scale."

The authors described the scene in one valley as follows:

"Our route through this larger valley led us past three
lakes formed through the blocking of the stream by five
enormous slides.... Some of the scooped-out places left
by these slides were half a mile in width at the mouth,
extending back into the hills for a mile and furnished enough
dirt to cover several square miles of valley floor.... In
each case the earth which came down bore the appearance of
having shaken loose, clod from clod and grain from grain, and
then cascading like water forming vortices, swirls, and all
the convulsions into which a torrent might shape itself."

Fluidization of the loess material is evident from the

above description. Obviously the vibrations resulting from the

earthquake were sufficient to break down the connections between

the slightly cemented particles of loess.

Casagrande (1971) cites three examples of fluidization

probably induced by seismic motions. The first example given was

a prehistoric 400 million cubic yard slide of marble breccia

which occurred at Blackhawk Canyon in the San Bernardino Mountains

of Southern California. The slide mass was 5 miles long, 2 miles

wide, and between 30 and 50 feet thick. The second fluidization

example cited was a 40 million cubic yard slide across the Sherman

Glacier in Alaska triggered by the 1964 earthquake. The slide

formed a blanket of broken rock 2 miles wide and 10-20 feet thick.

The third example was a slide in volcanic ash in a high mountain

desert in Chile. The slide was roughly circular in shape with

an effective diameter of 1500 feet. Pore air pressure during this

slide dropped quickly enough that the slide was arrested before it

had moved very far.

12.2.4.3 Kanto Earthquake

On September 1, 1923 the Kanto region of Japan was hit
with one of the most disastrous earthquakes in Japanese history.
Kuribayashi and Tatsuoka (1975) indicated that of the 44 major
earthquakes which occurred in Japan from 1872 to 1968 the Kanto
earthquake was by far the most damaging in terms of human life.
It has been estimated that 99,331 lives were lost to this earth-
quake having a magnitude of 7.9 .

A majority of the sites which liquefied were located on
the original winding river course of the existing Tone river
located immediately to the northeast of Tokyo. Approximately
three hundred and fifty years ago, the estuary of the Tone river
was linked to the Pacific Ocean by human power. The original
Tone river had previously flowed into Tokyo Bay during which time
the river deposited very deep and soft deposits of sediment and
interwoven sand layers. These deposits retained a high potential
for liquefaction, as witnessed by liquefaction failure during
the Tone - Karyu (January 18, 1895), Nishi - Saitama (September
21, 1931), and Kanto earthquakes.

In the plains, numerous fissures and mud volcanos spurted
intermittently with water and sand; the ejection would stop and
then resume action a few seconds later, continuing long after the
earthquake.

A rather surprising event described by Ambraseys and
Sarma (1969) occurred in a paddy field near the Sagami River.
During the earthquake seven vertical wooden piles, 60 centimeters
in diameter, suddenly emerged above ground level. Successive

aftershocks caused these piles to emerge more, finally reaching

a height of 110 centimeters above ground level. It is interesting

to note that these piles were unknown to the local people before

the earthquake. Later, it was found that they belonged to a bridge

built in 1182 over the old course of the Sagami River.

12.2.4.4 Liquefaction During the Niigata Earthquake of 1964

On June 16, 1964 a violent earthquake shook Niigata,

Japan inflicting severe damage to the city. The recorded magni-

tude of this earthquake was 7.3 on the Richter scale, and the epi-

center was about 35 miles north of the city (Seed and Idriss, 1967).

Niigata is located on the west coast of Japan where the Shinano River

enters the Sea of Japan. The city is underlain by about 100 feet

of fine subangular alluvial sand with a uniformity coefficient

between 2 and 10 and a D_{10} size between 0.04 and 0.2 mm. Damage

due to the earthquake resulted primarily from liquefaction of

the loose sand deposits in low-lying areas. Buildings not imbedded

deeply in firm material sank in the resulting quicksand or tilted

toward the direction of the center of gravity. One apartment

building is reported to have tilted 80 degrees. Underground

structures such as septic tanks, storage tanks, sewage conduits,

and manholes floated upward to extend as much as 10 feet above the

ground surface. In low-lying areas, mud volcanos began ejecting

water and sand 2-3 minutes after the shaking stopped and

continued for as much as 20 minutes. Sand deposits 20-30 centi-

meters thick covered the entire city as if it had been hit

by a sand flood. Five simply supported girders of the Showa

Bridge across the Shinano River fell when pier foundation piles deflected due to the loss of lateral support.

As illustrated in other cases of liquefaction, little or no damage to buildings and engineering structures occurred as the direct result of shaking (Ambraseys and Sarma, 1969). Damage which did occur appeared to be entirely related to foundation failure. Ground movements recorded by instruments in Niigata indicated that shortly after the earthquake started ground motion had begun to subside. Once an underlying strata had liquefied it was no longer able to transfer earthquake vibrations to overlying deposits.

The greatest devastation by the quake occurred in the low-lying areas near the river. An extensive soil survey after the quake revealed that the standard penetration blow count was between N = 6 and N = 12 in the upper 30 feet in the areas suffering the greatest damage. The penetration resistance was about the same over the entire area in the upper 15 feet; but in areas where the resistance was measurable higher in the lower 15 feet, notably lighter damage occurred. The recorded peak acceleration during the quake was 0.16 g. The water table was about 5 feet below the ground surface in areas of heaviest damage and 9 feet or more in areas of lighter damage.

It was reported by Seed and Idriss (1967) that Niigata had been shaken by an earthquake of the same intensity 130 years before the event of 1964. This indicates that areas which have been shaken by an earthquake are not immune to further damage unless remedial measures are taken.

12.2.4.5 <u>Valdez Slide, 1964 Alaska Earthquake</u>

During the 1964 Alaska earthquake an extensive landslide believed to be due to liquefaction occurred in Valdez (Seed, 1968). The city is located on a deltaic deposit of silt, fine sand, and gravel, with the silt and fine sand occurring in layers within the coarse sand and gravel. The sand particles were generally subangular in shape with the uniformity coefficient greater than 10. The standard penetration resistance of the Valdez material varied between N = 7 and N = 25 . The magnitude of the earthquake was 8.3 on the Richter scale with the epicenter about 40 miles away. The landslide resulting from the quake involved approximately 98 million cubic yards of material and extended about 500 feet inland from the coastline, destroying the harbor facilities and near-shore installations. This slide was reported to have occurred so rapidly and with such violence that eye witnesses were unsure of what actually happened directly beneath their feet. The dock structure at Valdez supporting several large buildings was reported to have broken off and disappeared into the sea. The slide was responsible for the loss of 30 lives. About 40 percent of the buildings of Valdez were seriously damaged. Lateral movement toward the sea occurred as much as 3600 feet inland, causing settlement, fissuring, and ground breakage. In addition to buildings, the water and sewage systems were severely damaged by ground movement. In many instances, fissures occurring in the foundation of buildings resulted in basements being pumped full of sand and water. Open cracks spurting sand and water along the streets substantial distances inland indicated that liquefaction

was not limited to the coast. Since the year 1899 submarine

slide damage was reported to have occurred at this location on at

least five other occasions, probably caused by siesmic activity.

12.2.4.6 Turnagain Heights Slide, 1964 Alaska Earthquake

A dramatic event that occurred during the earthquake of 1964

was the large landslide along the coastline in the Turnagain Heights

area of Anchorage (Seed, 1968; Seed and Wilson, 1967). Bluffs up to

70 feet high sloping at about 1-1/2:1 down to the bay were prominent

along the coastline. The slide extended about 8500 feet from west

to east along the bluff-line and retrogressed inland a distance of

about 1200 feet at its west end and about 600 feet at its east

end. A surface area of about 130 acres was affected by the slide.

Lateral movement of the soil mass was extensive with portions

of the slide moving as much as 2000 feet out into the bay. The

ground at the west end of the slide area was undeveloped but

at the east end had been developed as a residential area. Approx-

imately 75 homes located on the east end of the slide were des-

troyed.

The Turnagain slide area was covered with a surface layer

of sand and gravel varying in thickness from 15 to 20 feet at the

east end of the slide area to about 5 to 10 feet at the west end.

A deep bed of Bootlegger Cove clay, about 100 to 150 feet in thick-

ness, underlaid the sand and gravel. Shear strength of the clay

decreased from about 1 ton/ft^2 at its surface (El. 50 approx.) to

about 0.45 ton/ft^2 at E. 0 and then increasing to about 0.6

ton/ft^2 at El. -30.

The clay deposit contained numerous lenses of silt and fine sand, particularly near the surface on which sliding occurred. These lenses varied in thickness from a fraction of an inch to several feet. Below the sliding surface the sand lenses were only occassionally encountered.

Seed (1968) performed a number of cyclic loading tests on representative samples of the sand and clay to determine, for each of these materials, the relationship between the magnitudes of the cyclic stress and the number of cycles required to cause failure of the clay or liquefaction of the sand. This analysis indicated that the sand could be expected to liquefy after about 12 stress cycles, corresponding to about 45 seconds of ground motion in the analysis, while the clay would not be expected to fail until after about 22 cycles or 1-1/2 minutes of ground shaking.

From the above information physical features on the displaced slide mass (sand boils, intermixing of sand and clay) and eye witness reports, it appears very likely that liquefaction of sand lenses was an important factor in the development of the slide.

12.2.4.7 Slides in the San Fernando Dams

On February 9, 1971 an earthquake shook southern California resulting in a major landslide in the upstream slope of the lower San Fernando Dam (Seed, et al., 1973). This earthen dam is about 140 feet high and provides 20,000 acre-feet of reservoir capacity. The water level in the reservoir was about 35 feet below the crest of the dam at the time of the event, and the resulting slides on both

the upstream and downstream slopes left about five feet of free-
board. Because of the possibility that aftershocks might cause
further sliding and possible failure of the dam, 80,000 people
living downstream were evacuated until the reservoir could be
drawn down to a safe level.

Upstream from the lower dam is the upper San Fernando
Dam which is about 80 feet high and provides a reservoir of 1850
acre-feet. During the earthquake, the crest of this dam moved
five feet downstream and settled three feet, but no water was
lost from the reservoir. Had water from the upper dam been
released, the lower dam would have been overtopped and consequently
would have failed.

This near catastrophe prompted an immediate investigation
of the safety of earth dams with respect to earthquake loading.
The event of February 9, 1971 has been assigned a Richter magnitude
of 6.6 with the epicenter located about eight and one half miles
northeast of the dams. The maximum acceleration in the vicinity
of the dams was of the order of 0.55-0.60 g .

Both the San Fernando dams were old structures, having
been constructed in the period between 1915 and 1925 by the
hydraulic-fill method. The dams were constructed directly on
alluvial soil with no stripping prior to the placement of the
embankment fill. Field investigation after the quake revealed
that penetration resistance (N values) was very low in the silt
and clay core of the hydraulic fill, but was somewhat higher in
the outer sands and gravels of the shell. The underlying alluvium
was very heterogenous, exhibiting an erratic blow count in most

of the drill holes. Laboratory investigations showed that the hydraulic-fill material was finer, more uniform, and less dense than the alluvium. The hydraulic-fill lower dam sands were coarser than the upper dam sands, D_{50} being between 0.05 and 0.8 mm for the upper dams sands and between 0.05 and 1.0 mm for the lower dams sands. The average relative density for all the hydraulic-fill material investigated was about 54 percent. The uniformity coefficients ranged from four to six for the upper dam materials and from seven to ten for the lower dam materials.

As a result of the 1971 earthquake, the upstream embankment and about 30 feet of the crest of the lower San Fernando Dam moved about 70 feet into the reservoir, the movement being due to liquefaction of the hydraulic fill near the base of the embankment. Liquefaction was evidenced by observed increases in pore pressure in the embankment, the occurrence of large horizontal displacements, and the formation of sand boils in the slide debris.

H.B. Seed, et al. (1973) concluded that a major catastrophe very nearly occurred. If any of a number of conditions had been less favorable, the lower dam could have failed resulting in the sudden release of 10,000 acre-feet of water over a heavily populated urban residential area. Laboratory tests and analytical techniques indicate that the instability of the lower dam was due to insufficient density in the water-saturated shell materials.

Other dams in the area were subjected to shaking of lesser intensity (0.2 g maximum acceleration) with no detrimental structural damage. Another hydraulic-fill dam with no water in the reservoir (unsaturated) was subjected to shaking of the same

intensity as the San Fernando dams with no detrimental damage. These observations indicate that hydraulic-fill dams are not inherently unstable but become so if the embankments are saturated and experience shaking of sufficient intensity and duration.

12.2.4.8 Ekofisk Tank in the North Sea

In June 1973 the 490,000-ton Ekofisk oil storage tank was installed in the North Sea (Lee and Focht, 1965). The structure is a reinforced concrete cylinder roughly circular in shape, about 93 meters in diameter, and 90 meters tall on a mat foundation in 70 meters of water. The tank imposes a vertical stress of about 2.72 kg/cm^2 on the foundation which is a 26-meter-thick stratum of medium-to-dense, fine, uniform sand. The sand particles were mostly angular in shape with a D_{50} of 0.11 millimeters and a uniformity coefficient of two. There was concern that the sand under the tank might liquefy due to stresses induced in the foundation by the action of storm waves against the walls of the tank.

The loading that the foundation of the tank would be subjected to was thought to be similar to earthquake loading with the following notable differences:

1. Storm waves have periods considerably longer than earthquake loadings.

2. The duration of ocean storms is much longer than that of earthquakes.

3. It is probable that a structure in the ocean would be subjected to a number of minor storms with intermittent

periods of calm before the occurrence of the design
storm.

The structure was designed for a 100-year storm producing a wave
23.8 meters from crest to trough. The design wave would exert
a lateral force of 35 million pounds on the tank.

Cyclic load triaxial tests of the type described by Seed
and Lee (1965) were performed on the foundation material and the
procedure described by Seed and Idriss (1970) used to evaluate
liquefaction potential. Because loading from wave action was of
a considerably longer period than for earthquakes, the rate of
loading was reduced from 1 Hz, typical for earthquake tests, to
1/12 Hz. The laboratory test procedures were modified to account
for the fact that during long ocean storms and during periods
between storms, pore pressure dissipation would occur in the
permeable sand. This was done by subjecting the test specimen
to several cycles of undrained cyclic loading until some desired
pore pressure response was reached, then stopping the loading and
reconsolidating the specimens. After several cycles of such
loading and reconsolidation, the test specimen was cyclically
loaded to 100 percent pore pressure response (zero effective
stress). It was found that the stability of the specimen increased
substantially after several cycles of loading and reconsolidation.
The increase in relative density due to reconsolidation was from
one to four percent and would not explain the drastic increase
in stability. Bjerrum (1973) mentioned that in addition to an
increase in density, there was a change in the packing structure
of the sand resulting from cyclic loading and reconsolidation

which may explain the disproportionate increase in stability.

This study revealed that the supporting sands of this tank could withstand a 100-year storm without liquefaction. During the ten-month period following the installation of the tank, storms approaching the design storm occurred on at least three occasions with both the storage tank and foundation performing satisfactorily.

12.2.4.9 Failure of the Swir III Dam

During the spring of 1935 construction of the Swir III Dam in the Union of Soviet Socialist Republic was completed and the reservoir filled for the first time. The Swir III Dam was a concrete dam with a sand embankment next to the concrete section. The embankment, containing a till core, was formed by dumping moist sand on both sides of the core.

With the reservoir filled, blasting operations were being performed about 600 feet upstream of the dam when the sand embankment started to liquefy and flow away. According to Terzaghi (1956) the failure started at the contact surface between the concrete section of the dam and the embankment. In less than one minute, liquefaction had spread more than 1000 feet to the outer end of the embankment. The failure reduced the embankment slope from 1V on 2H before failure to 1V on 10H after failure. The embankment sand had been deposited in a moist state and was probably in a bulked and very loose condition. The embankment became saturated as the reservoir filled, and the blasting was evidently sufficient to trigger liquefaction.

12.2.4.10 Sand Boils at Operation Snowball

On July 17, 1964, a 500-ton hemispherical TNT charge on the ground was detonated over a glacially deposited silt with underlying beds of clay, sand, and gravel (Rooke, et al., 1968). The deposit consisted of a friable silty clay to a depth of 12 feet, a brown silty clay from a depth of 12-27 feet, and interbedded stratum of coarse sand and gravel (D_{10} = 0.15 mm and C_u = 3-4) from 27-32 feet, and gray silty clay from a depth of 32-67 feet. The water table was located 23 feet below the ground surface at the time of detonation.

Postshot surveys and reconnaissance reports (Rooke, et al., 1968) showed that the detonation produced a crater immediately after the shot measuring 14 feet deep, with a radius of 140 feet. High pore pressures due to compressive stresses were indicated by water flowing both inside and outside the crater. Sand boils were also observed to occur in and around the crater. The outflow of the water, sand, and silt caused subsidence of the area and circumferential tension cracks as far as 509 feet from the center of the crater. These descriptions and the occurrence of sand boils suggest that the underlying layers of sand and silt liquefied and flowed to the surface.

12.2.5 Discussion of Case Histories

An examination of the case histories reveals that with the exception of the Aberfan and Kansu flow slides, the materials liquefied were fine, uniform sands. Typically, D_{10} sizes ranged from 0.05 to 1.0 mm and the coefficient of uniformity ranged

from less than 2 to 10. These observations are in agreement with, but broader than, the criteria of D'Appolonia (1968) and others (Seed and Idriss, 1970; Whitman, 1970; Terzaghi and Peck, 1948). D'Appolonia's criteria state that liquefaction-prone soils are cohesionless with less than ten percent fines, fine grained (D_{50} between 0.2 and 1.0 mm), and uniform (C_u between 2 and 5). In all cases the soils were loosely deposited, and in many cases they were water-saturated. However, water saturation is not absolutely necessary as soils with air as a pore fluid were reported to flow (Close and McCormick, 1922).

The case history review also shows that a variety of triggering mechanisms can cause liquefaction. These mechanisms cause collapse of the grain structure, resulting in high pore pressure and subsequent loss in strength and flow. They range from monotonically changing stresses caused by changes in externally applied loads to vibrations and shock waves caused by reciprocating machinery, earthquakes, or blast loadings. However, the most common triggering mechanisms are (1) monotonically changing stresses, such as those causing the Mississippi River and Fort Peck flow slides; and (2) earthquake-induced flow slides, such as those at Niigata and the San Fernando dams. Liquefaction flow slides induced by blasting or cyclic vibrations are less commonly observed and reported. Earthquake-induced liquefaction failures are generally more catastrophic than those induced by other mechanisms due to the tremendous energy released during an earthquake causing almost instant liquefaction over a large area. Conversely, flow slides induced by monotonically changing stresses generally are more limited in area and occur

less rapidly.

Sands which are initially loose and liquefy when subjected to earthquake shaking do not become significantly more stable against liquefaction. Ambraseys and Sarma (1969) suggested that deposits which are susceptible to liquefaction, e.g., 10-20 meters thick, have been accumulating in seismically active areas for thousands of years. It is highly improbable that such deposits have never been disturbed by shocks at some stage during their deposition. It is more probable that these deposits have been subjected to a number of earthquakes and have liquefied a number of times and are still susceptible to liquefaction. Historical records for Niigata show three occasions where liquefaction was reported in or near the city (Seed and Idriss, 1970). This would indicate that earthquakes are incapable of densifying originally loose deposits into a stable mass. This is pointed out by the fact that strong earthquake aftershocks have caused granular deposits to reliquefy after initial liquefaction during the earthquake. It seems then that the existence of deposits in seismically active areas which have been stabilized by earthquake shocks would be the exception rather than the rule. Apparently, after liquefaction occurs, the material subsides again to an unstable structure still quite susceptible to liquefaction.

Conversely, soils which are subjected to vibrations and experience an increase in pore pressure but not complete liquefaction gain stability against liquefaction far beyond what the increase in density after drainage occurs would suggest. Bjerrum (1973) suggests that the disproportionate increase in stability

stems from the fact that the structure of a sand is altered by vibrations.

12.3 Methods for Evaluating Liquefaction Potential of Soils

Newmark (1965) first proposed the basic concept and procedures for evaluating the potential deformation of an embankment dam due to earthquakes shaking. He assumed slope failure would not be developed and slip would not occur if the driving force caused by the earthquake is less than the resistance of the sliding mass. This resistance to earthquake shock motion is a function of the shearing resistance of material under an earthquake.

Newmark used this theoretical procedure to analyze three important cases of sliding which were modeled after a rock filled dam. The model tests show a fair agreement with the calculation for comparable conditions. However, the method has been proved to be useful only in cases where the yield resistance of the soil can be reliably determined (Seed, 1979). Newmark's method did not use the term "liquefaction," although it was obvious the yield resistance is affected by liquefaction potential of dam materials.

Current literature indicates that the most practical and broadly used methods for evaluating soil liquefaction potential of level grounds can be categorized into three groups: (1) Simplified procedures, (2) ground response analysis, and (3) empirical method. These will be described in the following sections.

12.3.1 Simplified Procedures

This method was developed in 1971 by Seed and Idriss (1971)

and also by Donovan (1971). The difference between these two
approaches is mainly in the manner of using the distribution of
stress cycles.

The Seed and Idriss' simplified procedure involves the com-
putation of the equivalent uniform cyclic shear stress induced by
the earthquake at any point in a soil deposit. The equivalent
uniform cycles can be related to the duration of ground shaking and
magnitude of the earthquake. On the other hand, the cyclic shear
stresses required to cause liquefaction of a given soil in a given
number of stress cycles can be determined by means of an appro-
priate test program. By comparing these two stresses, the lique-
faction potential of a soil deposit can, therefore, be evaluated.

The Donovan's simplified procedure is described by the cumula-
tive damage concept. The safety factor against liquefaction can
be obtained based on the ratio of the shear stress required to
cause liquefaction, or significant strain, to the shear stresses
induced by the earthquake for the same equivalent number of cycles.
With this method, the stress distribution developed during an earth-
quake can be scaled until a damage of unity is obtained.

12.3.2 Ground Response Analysis

Ground response analysis is based on the one-dimensional
wave propagation theory used to obtain the induced dynamic shear
stresses and their distribution and variation with time (Valera,
1977; Seed and Idriss, 1967). In this method, the potential for
liquefaction of a soil deposit can be estimated by comparing the
equivalent uniform cyclic shear stress obtained from the ground

response analysis to the laboratory test resistance.

12.3.3 Empirical Method

The empirical method involving the estimate of potential liquefaction is based on the past histories of sites where liquefaction did or did not occur during earthquakes. The standard penetration resistance of the soil is used to differentiate the liquefiable soils from non-liquefiable ones. This method was first developed in Japan after the severe structural damages caused by the Niigata earthquake in 1964.

Seed and Peacock (1971) presented the condition of various sites and their liquefaction histories and formed the most useful empirical correlation for the prediction of liquefaction potential of saturated sands. Generally speaking, this method relates the standard penetration resistance (the resistance of a soil) to the critical stress which causes the soil to liquefy in a number of cycles under an earthquake of a certain intensity. The standard penetration resistance of soils is affected by grain size and relative density (Ishihara, etc., 1978 and Tasuoka, etc., 1980).

12.4 Factors Affecting Liquefaction Potential

In the past two decades, numerous laboratory studies have been directed toward the investigation of the effect of a number of factors, such as relative density, gradation characteristics, strain history, overconsolidation, consolidation pressure, and anisotropy, etc. The effects of each individual factor are discussed in the following subsections.

12.4.1 Effect of Relative Density

Seed and Lee in 1967 first reported the significant effect of density on liquefaction. They concluded that initial liquefaction and complete liquefaction occurred almost simultaneously at relative density below approximately 50%. However, at relative denisty above approximately 70%, a considerable number of stress cycles was required after the initial liquefaction to develop a large strain amplitude. The stresses required to cause initial liquefaction increased linearly to about 60% relative density. In the simplified procedures of assessing liquefaction potentials, this linear relationship was used as a basis to evaluate the stresses causing liquefaction at the relative density below 80% (Seed and Idriss, 1971).

Fig. 12.10 clearly shows the importance of density in preventing large strains when cyclic stress loading is applied. For example, it may be noted that the cyclic stress required to cause a double amplitude of strain of 20% at a relative density of 75% (1.18 dg/cm^2) is about four times that required at a relative density of 25% (0.29 kg/cm^2). It is important to note that the most beneficial effects of densification in increasing the cyclic stress required to induce large strain amplitudes only develop above a relative density of about 70% for this sand. Thus, whereas an increase in relative density from 25% to 75% will increase the cyclic stress required to cause 20% strain amplitude in a given number of stress cycles by about 400%, an increase in relative density to 85% would increase the cyclic stresses required by
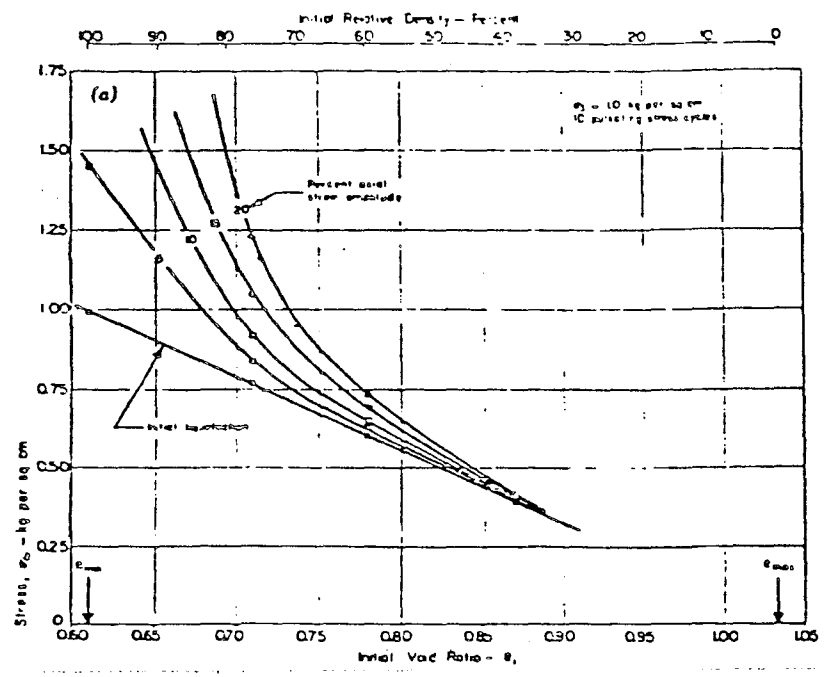
FIG. 12.10 CYCLIC STRESSES CAUSING DIFFERENT
AXIAL STRAINS, $\sigma_3 = 1$ kg/cm^2
(From Seed and Lee, 1967)

550% to 800% depending on the number of stress cycles involved. Additional densification has proportionately more beneficial effects.

Seed and Lee (1967) ran the previously discussed set of tests at higher confining pressures of 5 kg/cm^2 and 15 kg/cm^2 with results quite similar to a confining pressure of 1 kg/cm^2. One difference noted at a confining pressure of 15 kg/cm^2 was the fact that the difference between the stresses required to cause initial lique-faction and the stresses required to cause 20% strain amplitude becomes increasingly smaller. This difference in behavior may be attributed to the reduced ability of the sand to dilate and thereby stabilize itself at the higher confining pressures.

Other investigations on the effect of relative density also indicated that the stress ratio required to cause liquefaction in 10 cycles has a linear relationship with the relative density up to 60-70% (Peakcock and Seed, 1968). A comparison of the effect of relative density by using two types of testing methods is shown in Fig. 12.11.

Mulilis, et al. (1978) have presented data showing the cyclic strength of soils (Fig. 12.12). Slightly denser specimens were found to be significantly stronger. For Monterey No. 0 sand, the 12% increase in relative density can cause an increase in dynamic strength of approximately 22-30%.

12.4.2 Grain and Gradation Characteristics

Lee and Fitton (1969) performed a series of cyclic triaxial tests on alluvial sand and gravel deposits located at El Monte,
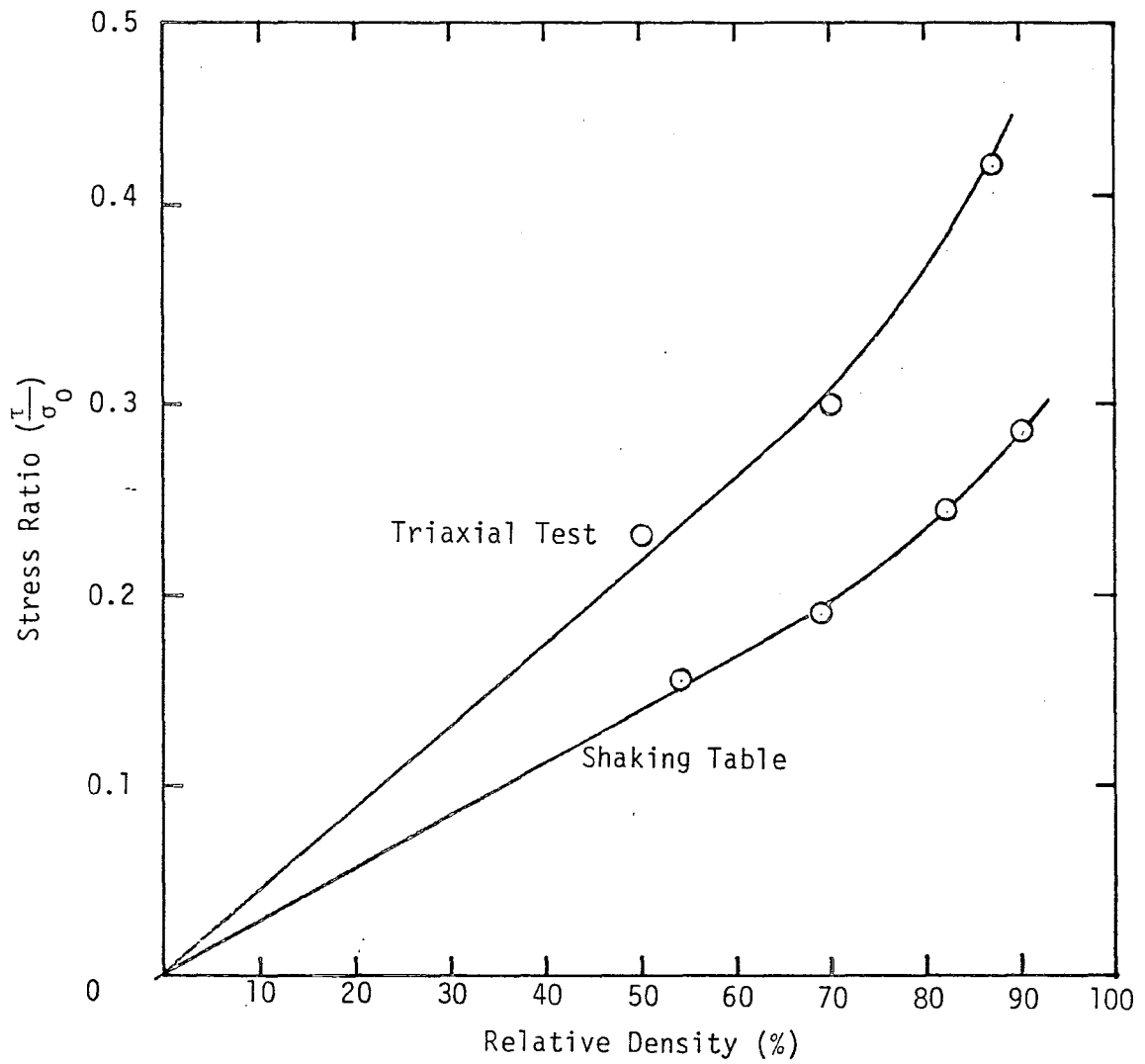
FIG. 12.11 COMPARISON OF SHAKING TABLE AND TRIAXIAL
TEST RESULT (after DeAlba, et al., 1976)
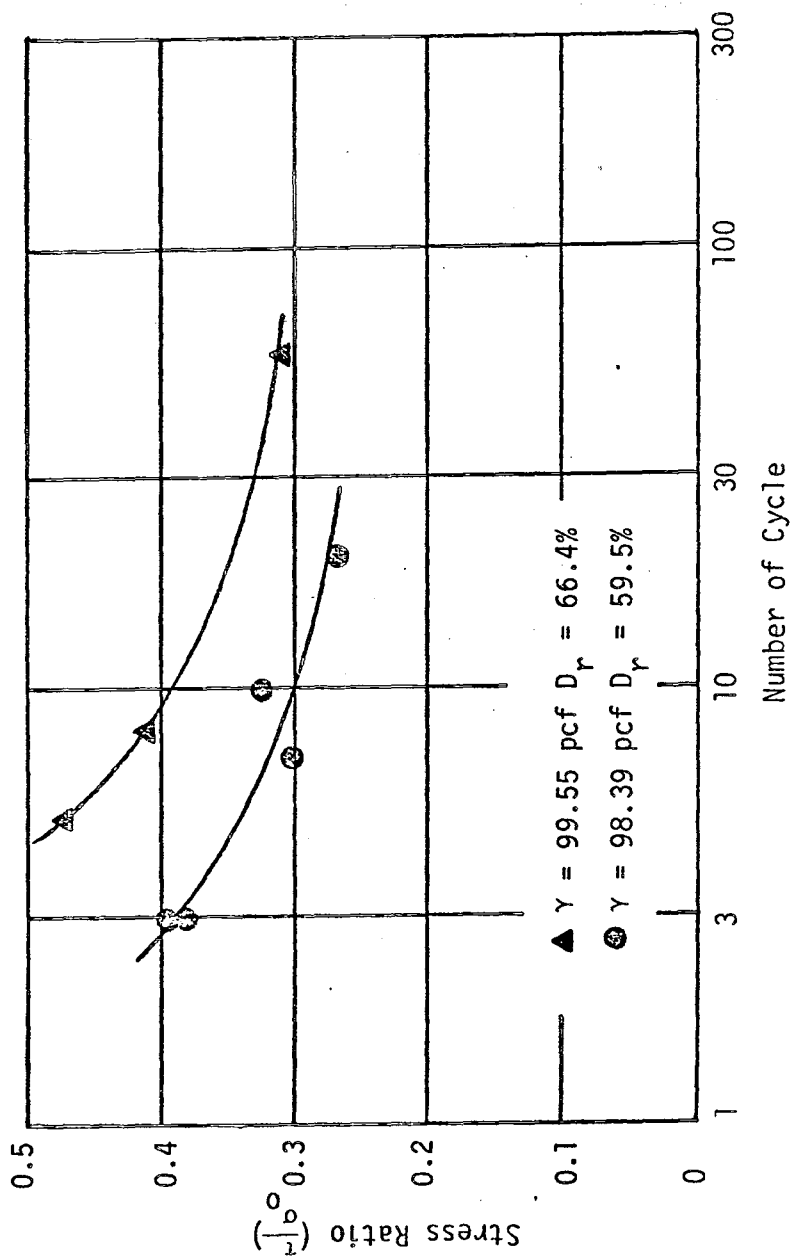
FIG. 12.12   EFFECT OF DENSITY ON NUMBER OF SQUARE WAVE LOADING CYCLE
TO CAUSE INITIAL LIQUEFACTION (after Mulilis, et al., 1978)

California. Samples were remolded and compacted to either 50 or 75 percent relative density. The granular material obtained from the deposit was sieved in six separate uniform gradations with particle sizes ranging from 3/4 to 3/8 inch-diameter down to the finest gradation containing particles between the No. 100 and No. 200 sieve. Particles of El Monte sand were angular to sub-angular. Table 12.2 shows the types of soils tested and Fig. 12.13 their gradations.

Results of the cyclic triaxial tests were presented in the form of double amplitude axial strain and peak pore water pressure versus number of cycles. Fig. 12.14 shows that the fine soil (C) had virtually no strain during the first three loading cycles but on the fourth cycle rapid straining of the sample occurred with a corresponding rapid rise in the pore water pressure. By the fifth cycle soil (C) had liquefied. Soil (B) behaves similarly to soil (C) with the exception that soil (B) does not develop a rapid increase in pore pressure and large double amplitude strains until approximately the tenth loading cycle. Soil (A) on the other hand does not build up pore pressure rapidly following a certain amount of cycles but instead has a uniform build up of pore pressure. It also should be noted that sample (A) did not reach liquefaction and following approximately 150 cycles, the sample developed severe necking. Necking of the sample created a zone of concentrated stresses dissimilar to any field loading condition thereby making results from additional loading meaningless.

Several important facts which can be gained by examination

TABLE 12.2

SOILS TESTED BY LEE AND FITTON

Code	Name and Description	Size U.S. Sieve No.	Range mm	$C_u{}^a$	$D_{50}{}^a$	LL^a	PI^a
AA	El Monte, medium gravel fraction	3/4 to 3/8	19.1 to 9.52	1.4	13.4	--	
A	El Monte, fine fraction	3/8 to 4	9.52 to 4.76	1.4	6.5	--	
B	El Monte, coarse sand fraction	4 to 10	4.76 to 2	1.5	3.0	--	
C	El Monte, medium sand fraction	20 to 30	0.84 to 0.59	1.2	0.68	--	
D	El Monte, fine sand fraction	50 to 100	0.297 to 0.149	1.4	0.22	--	
E	El Monte, very fine sand fraction	100 to 200	0.149 to 0.074	1.5	0.10	--	
F	Silt	-200	-0.074	1.9	0.018	26	3
G	Silty clay	-100	-0.149	23	0.0053	38	17
H	Silty sand, hydraulic fill from Puerto Montt, Chile	-10	-2	10	0.065	NP	
I	El Monte, pit run coarse silty sand	-4	-4.76	7.5	0.40	--	
J	Ottawa standard sand	20 to 30	0.84 to 0.59	1.2	0.68		

[a] $C_u = D_{60}/D_{10}$ The coefficient of uniformity. D_{60}, D_{50} and D_{10} are the grain sizes of the 60, 50 and 10 percent sizes respectively.

[b] LL and PI are the liquid and plastic limits respectively.
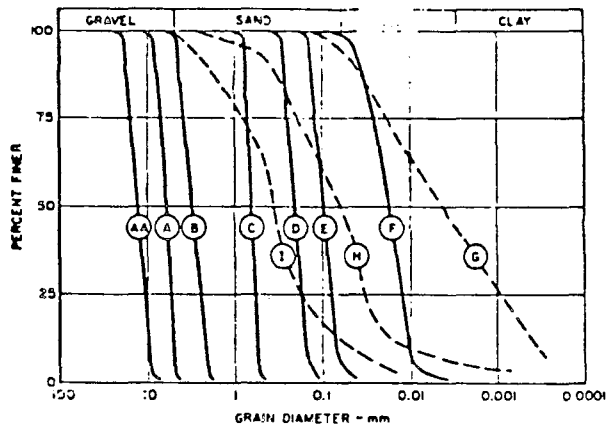
FIG. 12.13 GRADATIONS OF SOILS TESTED
BY LEE AND FITTON
(From Lee and Fitton, 1969)
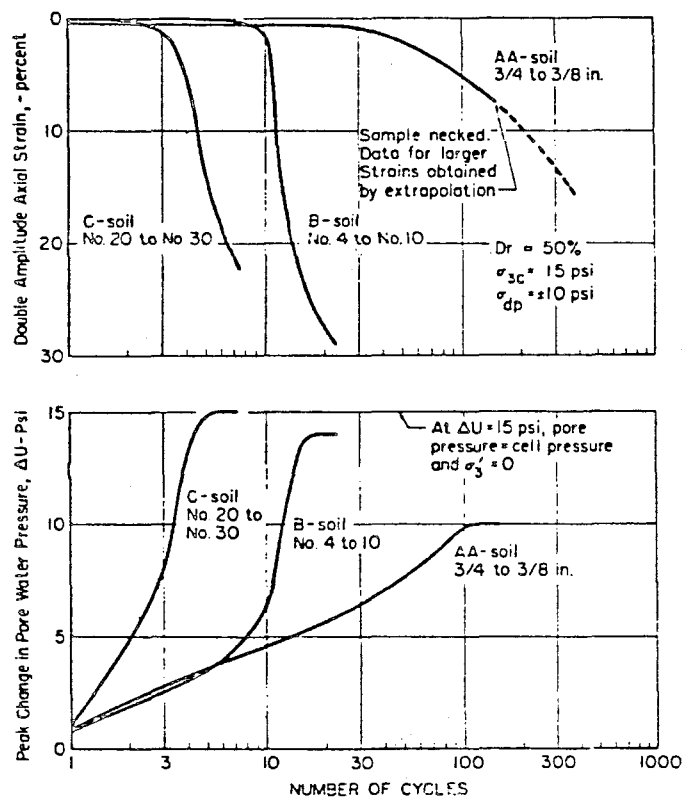
FIG. 12.14 TYPICAL LOAD-DEFLECTION AND PORE
PRESSURE CHANGE CURVES FOR
DIFFERENT GRAIN SIZES
(From Lee and Fitton, 1969)

of Fig. 12.14 are (1) medium to coarse sands reach liquefaction in far less cycles than gravels and (2) once the pore pressure starts to build up in a medium coarse sand, sudden large strains can occur within several additional loading cycles as compared to gravel soils which have a relatively slow rate of straining and generally do not reach liquefaction.

Fig. 12.15 shows the cyclic deviator stress required to cause 5 and 20 percent strain in 30 cycles. Mean (or median) grain size (D_{50}) was used as an index for comparison. It should be noted that the cyclic strength decreased with decreasing mean grain size for both relative densities until the grain size was less than the No. 200 seive. The effect of grain size distribution and grain shape was considered to be less significant than the grain size. The effect of segregation of soil particles on the liquefaction potential was also investigated (Lee and Fitton, 1969). When a well-graded soil was poured through water into the forming mold, severe segregation resulted with the larger sized particles rapidly settling through the water and finer sized particles slowly settling. As a result the segregated soil samples were approximately 10 percent stronger than the uniform sample.

Wong, et al. (1975) examined the liquefaction potential of gravelly soils. Since the grain particle for some specimens is greater than 1 in., cylindrical specimens with a diameter of 12 in. and a height of 29 in. were used. Their results showed that as the mean grain size increased from about 0.1 mm to 30 mm, the stress required to cause ±10% strain increases about 60%. However,
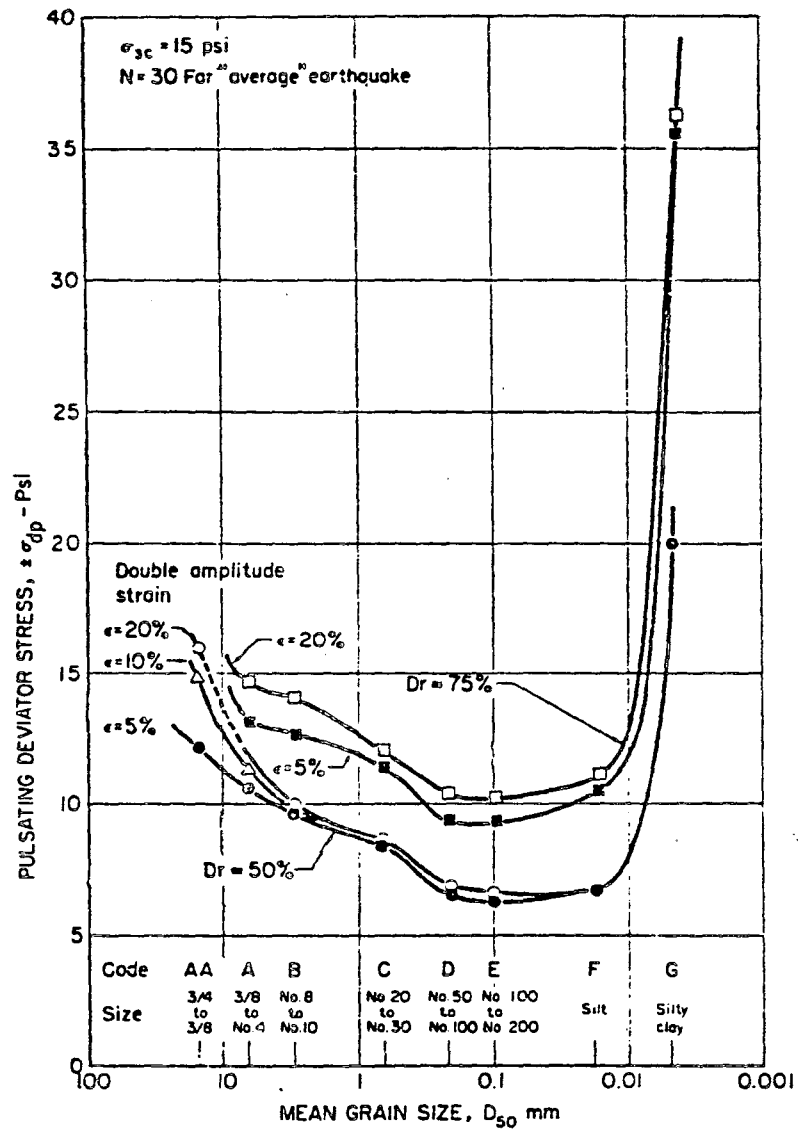
FIG. 12.15 COMPARISON OF PULSATING LOADING STRENGTHS
OF DIFFERENT GRAIN-SIZE SOILS
(From Lee and Fitton, 1969)

contrary to their expectations, the well graded material was somewhat weaker than the uniform material. These surprising results were ascribed to a greater densification tendency at the small strain in the well graded material as fine particles move into the spaces between large particles. Samples with large uniform particles have little tendency to densify under small strain amplitudes. In addition, the greater effect of membrane compliance in the tests on uniformly graded gravels is also a contributing factor to their higher dynamic resistance.

Ishihara, et al. (1978) also examined the effect of grain size and percentage of fines in the reconstituted and undisturbed samples. They concluded that the pore pressure does not build up fully to become equal to the initial effective confining pressure for soils containing a large percentage of fines, even though the considerable axial strain may develop during cyclic loading. The maximum pore water pressure that developed as a result of the application of an infinite number of loading cycles will decrease with decreasing mean grain size. Therefore, they suggested that the adoption of "initial liquefaction" as a failure criterion for liquefaction is not quite suitable for a soil containing some fines.

Martin, et al. (1978) re-examined the effect of grain size on liquefaction by considering membrane compliance. They found that the membrane penetration effect for given size samples is dependent on the particle size and independent on the sample density. The test results of Lee and Fitton (1969) and Wong, et al. (1975) were

corrected based on their finding. The corrected results indicated
that the relationship between the stress ratio and the number of
cycles to the initial liquefaction is almost identical for 2.8 in.
and 12 in. samples. Fig. 12.16 indicates that for the mean grain
diameters greater than 0.1 mm, the effect of grain size on lique-
faction does not seem to be significant. Tatsuoka, et al. (1980)
used this relationship to assess the liquefaction potential of two
sites located in Japan. There is, however, some deviation in their
finding. The approach which takes into consideration of the effect
of grain size produces a more reasonable solution.

12.4.3 Effect of Consolidation Pressure

In the 1964 Niigata earthquake, field observations showed
that liquefied zones are usually located at fairly shallow depths.
Only a few cases are below 50 to 60 feet. Kishida (1969) also
reported that in this earthquake, liquefaction did not occur
wherever the effective overburden stress exceeded 2 kg/cm^2
(27 psi).

The effect of consolidation pressure was compiled by Peacock,
et al. (1968) and Finn, et al. (1971) from the earlier studies
conducted by Lee and Seed (1966, 1967). Fig. 12.17 shows that the
shear stress required to cause liquefaction in remolded sand
specimens at relative density less than 80% varies linearly with
consolidation pressure. "Stress ratio," the ratio of the shear
stress causing liquefaction to the initial consolidation pressure,
is used to represent the liquefaction potential of a soil.

Contrary to their expectations, Mulilis (1975) and Castro
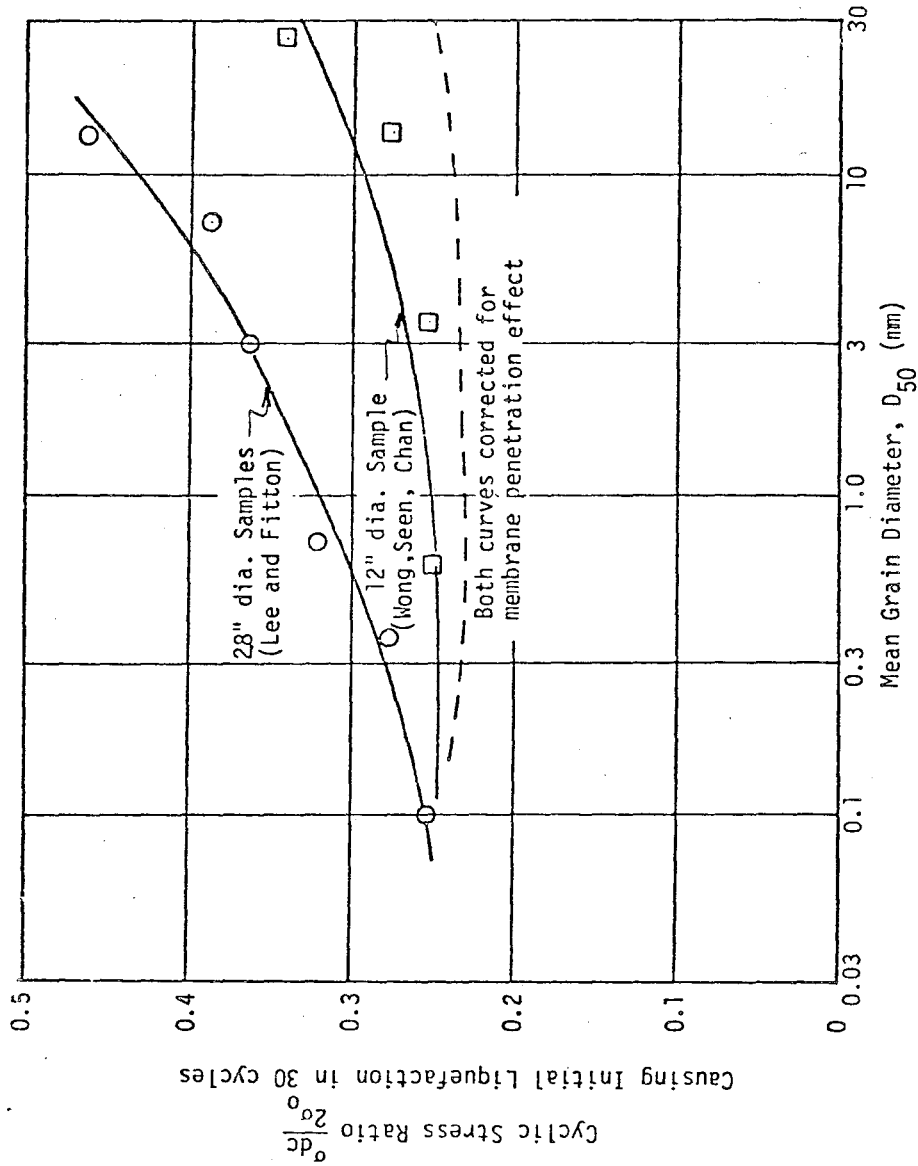
FIG. 2.3 CYCLIC TRIAXIAL TEST RESULTS SHOWING INFLUENCE OF MEMBRANE
PENETRATION EFFECTS (after Martin, et al., 1978)

FIG. 12.16 CYCLIC TRIAXIAL TEST RESULTS SHOWING INFLUENCE OF MEMBRAND
PENETRATION EFFECTS (after Martin, et al., 1978)
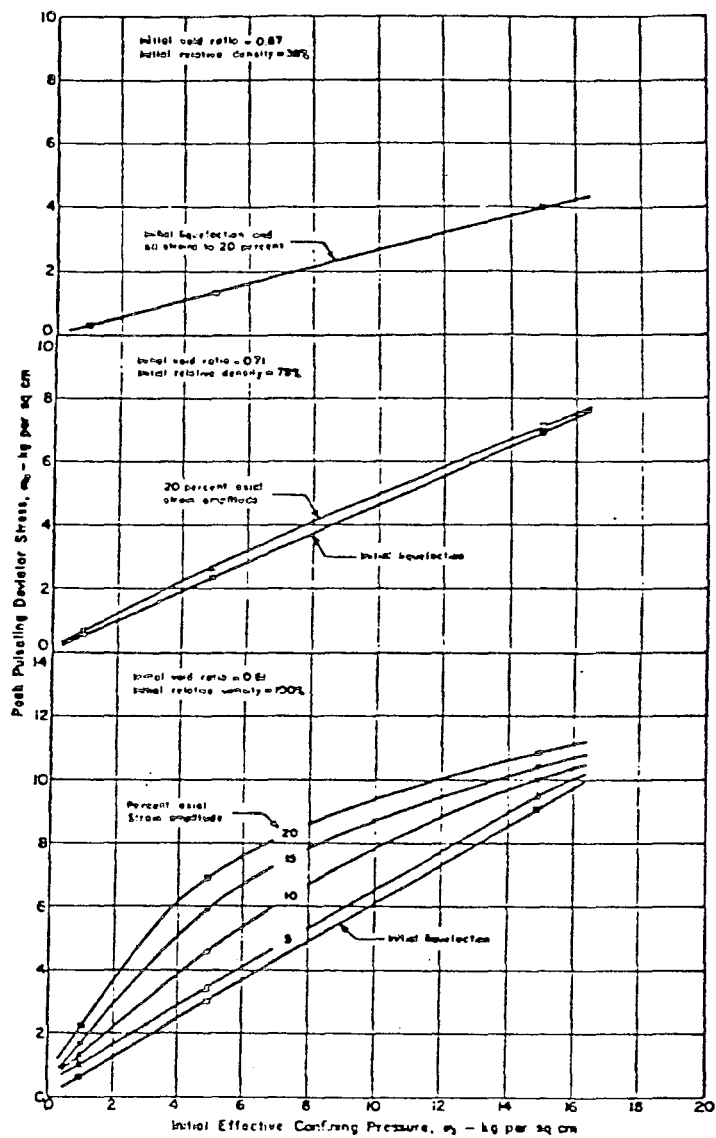
FIG. 12.17 CYCLIC STRESSES CAUSING INITIAL LIQUEFACTION
IN 100 CYCLES (From Seed and Lee, 1967)

and Poulos (1976) presented data showing that the stress ratio required to cause liquefaction decreases with increasing confining pressure. The magnitude of such decrease is dependent on the relative density, soil type and specimen preparation procedures (Castro and Poulos, 1976).

12.4.4 Effect of Anisotropy or Consolidation Ratio, K_c

Seed, et al. (1975) investigated the effect of anisotropy on the slide of the lower San Fernando Dam during the 1971 earthquake. They concluded that at a given radial pressure, the maximum deviatoric stress needed to produce a critical strain at a specified number of cycles increases with the increase of the consolidation ratio, K_c.

However, Castro and Poulos (1976) presented data showing opposite results. They found that samples consolidated under higher K_c would require a smaller increment in stresses to cause liquefaction, because at a higher K_c, the specimen is closer to failure.

12.4.5 Effect of Overconsolidation

Seed and Peacock (1971) used a simple shear test to assess the effect of K_o and overconsolidation ratio on the liquefaction potential of sands. It was found that, under the K_o condition, when the overconsolidation ratio increases from 1 to 8, the stress ratio required to cause initial liquefaction also increases.

Ishihara, et al. (1978) present the results of liquefaction tests on reconstituted and undisturbed samples of Koto Sand.

Despite the content of fines in the test samples, the resistance of soil against liquefaction was found to increase with increasing overconsolidation ratio. For a specimen with a higher percentage of fines, the increase tends to be larger.

12.4.6 Effect of Strain History

Finn, et al. (1970) used a simple shear apparatus to examine the effect of pre-strain on the dynamic strength of Ottawa Sand. A specimen that has previously liquefied is more susceptible to reliquefaction despite its potential density change. Conversely, when a specimen subjected to small strain disturbance is reconsolidated before it has liquefied, and resubjected to cyclic loading, it appears to have more resistance to liquefaction. This phenomenon can be ascribed to the densification of the specimen which results in the rearrangement of soil particles. On the other hand, the specimen of reliquefied soil loses its strength because of the destruction of the stable soil structure and soil fabric.

Seed, et al. (1977) investigated the influence of seismic history on liquefaction of sands both analytically and experimentally. They emphasized that when soil is subjected to small strains prior to liquefaction, the resistance increases even though there is no significant change in density. Mori, et al. (1977) also examined the influence of sample disturbance on the dynamic strength of soils. The conclusion was the same, but the effects of prior strain history were lost when the samples were slightly disturbed during sampling.

12.4.7 Effect of Reconstituted Versus Intact Specimens

The reconstitution of a sample can duplicate the in-situ density but not the in-situ fabric. Fabric considerations are important because research has shown that different specimen preparation procedures and resulting differences in soil fabric can significantly influence measured soil strength values both under static and dynamic loading conditions (Mulilis, et al, 1976; Lade, 1976). Thus, specimens at the same density but prepared with different specimen preparation techniques may show different strength values. Correction factors should be applied to the strength of the reconstituted samples to obtain the cyclic strength of in-situ cohesionless soils.

Marshall L. Silver (1978) performed an extensive study of the differences in strength between undisturbed and reconstituted sand samples from Niigata, Japan. Undisturbed samples were obtained from the bank of the Shinano River, an area in which severe liquefaction occurred during the 1964 earthquake. This area was reclaimed by deposition of sand into the river channel approximately five years before the 1964 earthquake. Examination of undisturbed samples obtained from this area revealed that the horizontal layering of the samples was kept intact and lenses of coarse sand, fine sand, and silt were undisturbed, clear, and sharp.

Reconstituted specimens were prepared by pluviating sand through water and tamping the sides of the mold during filling to obtain the required density. Fig. 12.18 shows that at a given relative density, undisturbed specimens were stronger than reconstituted specimens.
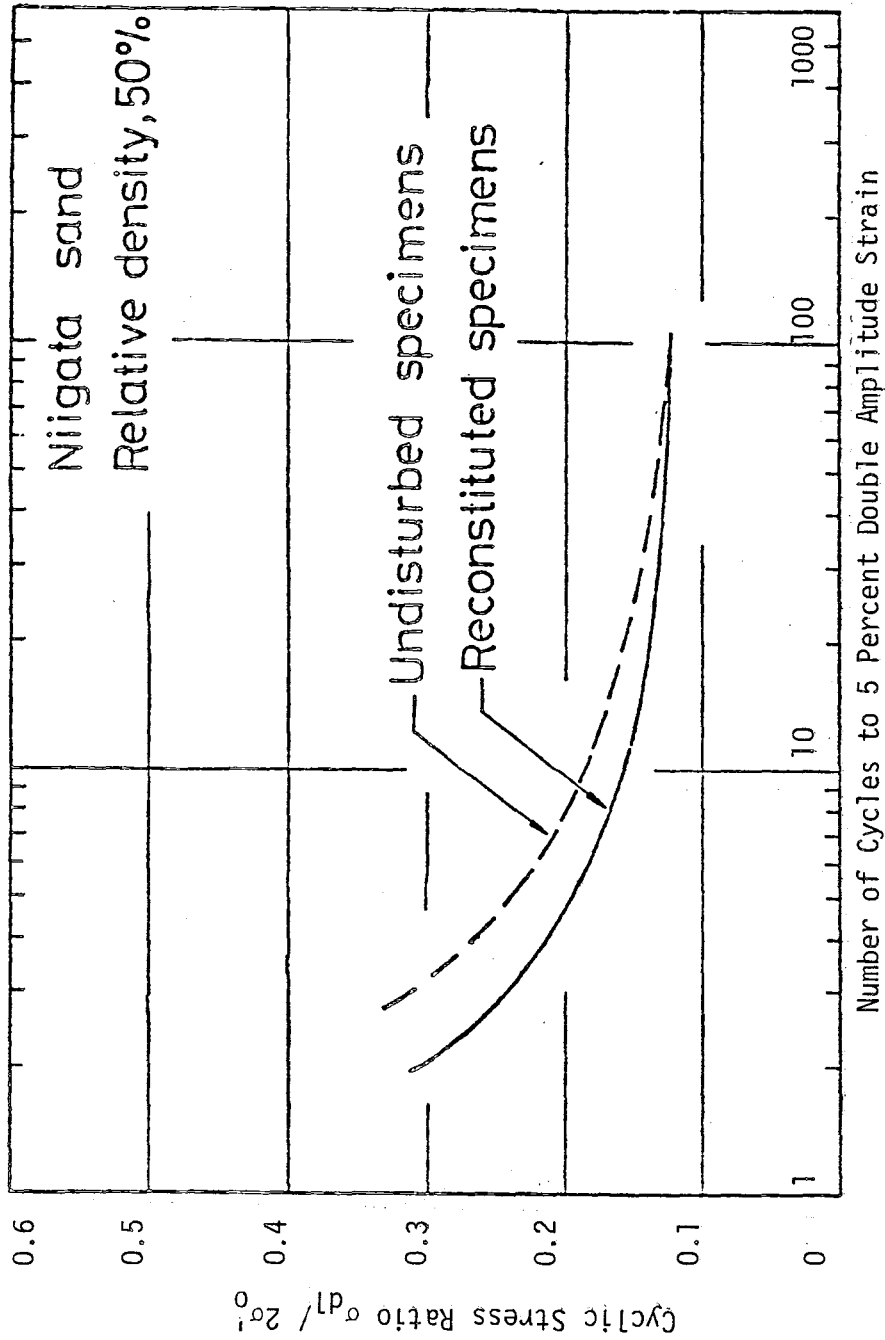
FIG. 12.18 SUMMARY CURVE COMPARING THE CYCLIC STRENGTH AT 50 PERCENT RELATIVE DENSITY OF
RECONSTITUTED AND UNDISTURBED SAND SPECIMENS FROM NIIGATA, JAPAN
(From Silver, 1978)

The U.S. Army Corps of Engineers Waterways Experiment Station following a slide failure on Fort Peck Dam obtained undisturbed samples in the vicinity of the slide and compared their cyclic triaxial strength with those of the reconstituted sample (Marcuson, et al., 1976). In place samples were obtained by using a 3-inch Hvorslev fixed-piston sampler with the aid of drilling mud.

Test results of the shell and foundation material from Fort Peck Dam indicated that reconstitution of samples changes their cyclic triaxial strengths. The results show that this effect was dependent on the sampling procedure, the remolded sample preparation procedure and the soil characteristics, i.e. cementation and stratigraphy, and grain-size distribution. Undisturbed specimens of shell material were as much as 80% stronger than reconstituted specimens. The undisturbed foundation material was approximately 70% more stable than the same material in a reconstituted state.

In summary, cyclic triaxial tests show that the "undisturbed" samples are significantly stronger than the remolded samples. The resulting difference in strength between reconstituted and "undisturbed" samples will depend on the sampling procedure, the sample preparation procedure and the soil characteristics.

12.5 Experimental Methods for Evaluating Liquefaction Potential

Where the in-situ assessment of liquefaction potential is impossible, it is necessary to simulate the field conditions under seismic shaking by a laboratory apparatus. Currently, there are four experimental devices available for such purpose:

1) Cyclic triaxial test,

2) Cyclic simple shear test,

3) Torsional shear test, and

4) Shaking table test.

12.5.1 Cyclic Triaxial Test

The use of the cyclic triaxial test to predict the resistance of a soil to liquefaction when subjected to earthquake loadings was initiated in 1966 by Seed and Lee who produced in the laboratory, liquefaction of sand by cyclic loading. Since this time the cyclic triaxial test has grown to be the predominant test in evaluating the earthquake response of various soils (Seed, 1979). Most of the factors affecting the liquefaction potential of soil, as discussed in Section 12.4, were examined by using this test.

Similar to the static triaxial test, samples are first consolidated under a confining pressure and then subjected to a cyclic deviatoric stress under an undrained condition. The factors affecting cyclic triaxial test results are discussed in detail in Section 12.6.

12.5.2 Cyclic Simple Shear Test

Due to the limitation and deficiency of the cyclic triaxial test, Peacock and Seed (1968) developed the cyclic simple shear test device. A specimen which uses a rectangular sample is consolidated under K_0 condition by a vertical stress. A cyclic horizontal shear stress is then applied to the sample with drainage prohibited.

Early simple shear devices (Peacock and Seed, 1968) all

confronted with different degrees of difficulty, such as boundary
friction, etc. These difficulties were partially removed by Seed
and Peacock (1971) and Finn, et al. (1971).

Cyclic triaxial test and cyclic simple shear results were
compared by Seed and Peacock (1979) and Park and Silver (1975)
and De Alba, et al. (1976). Generally speaking, the cyclic simple
shear strength was about 35 to 50 percent less than the comparable
cyclic triaxial strength.

Although the cyclic simple shear test can more closely simu-
late the in-situ condition, it is not readily available. Besides,
Peacock and Seed (1968) pointed out that the accurate simulation
of field stress condition by a simple shear device is also limited
by several factors. The cyclic triaxial test is more often used
to evaluate the cyclic strength under the simple shear stress
condition by reducing 35 to 50 percent from the cyclic triaxial
strength.

12.5.3 Torsional Simple Shear Test

A torsional simple shear test was introduced by Ishibashi
and Sherif (1974). A "donut-like" soil sample was used in the
test. A detailed schematic of this apparatus can be found in their
publications. From their experience, this torsional simple shear
device has the following advantages:

1) It introduces a uniform shear stress and strain through-
    out a soil sample,

2) It is possible to apply vertical and horizontal stresses
    independently,

3) Lateral strain during a test can be prevented,

4) It enables the measurement of the pore-water pressure parameter B prior to the application of the cyclic loading, and

5) It closely simulates the in-situ stress-strain conditions during an earthquake.

A comparison was also made between the conventional simple shear test and the torsional simple shear test. It was concluded that the torsional simple shear test can reduce the frictional stresses along the sides of a conventional simple shear test device. And, thus, it appears to give a lower cyclic strength than the cyclic simple shear apparatus.

De Alba, et al. (1976) also indicated that data comparable to the representative data of simple shear field condition can be obtained with a carefully conducted small-scale torsional shear test by using good quality equipment.

12.5.4 Shaking Table Test

A shaking table provides a direct method for creating lique-faction under simple shear loading. It is widely used in Japan and Europe. However, such factors as sample placement, sample confine-ment, realistic overburden and deformation characteristics of the container do complicate the procedure (Ferrito and Forrest, 1976).

A comprehensive comparison of the results of the shaking table test with the simple shear test was presented by De Alba, et al. (1976). A very good agreement was found among the results reported by Seed and Peacock (1971), Finn (1972) and Yoshimi and Oh-Oka (1973).

12.6 Factor Affecting Cyclic Triaxial Test Results

Because of its convenience and efficiency a cyclic triaxial test has been widely used, in both research and consulting, for investigating the dynamic behavior of soils. Much effort has also been devoted to the investigation of the limitation and the effects of some factors on the result of the cyclic triaxial test. Since the cyclic triaxial test was used in this study, an extensive review of the effects of various factors on the cyclic triaxial test results was conducted and reported in the following subsections.

12.6.1 Sample Preparation Methods

A number of researchers (Seed, et al., 1975; Ladd, 1974, 1976; Mulilis, et al., 1977, 1978; ect.) have investigated the effects of sample preparation methods on liquefaction potential of sand.

An extensive study was performed by H.B. Seed, J.P. Mulilis, and C.K. Chan (1977) wherein undrained stress-controlled cyclic triaxial tests were performed on saturated samples of Monterey No. 0 sand compacted to a relative density of 50% by 11 different procedures listed as follows:

1) Pluviation through the air,

2) Pluviation through water,

3) High frequency (120 Hz) vibrations applied horizontally to dry samples formed in one seven-inch layer,

4) High frequency (120 Hz) vibrations applied horizontally to dry samples formed in seven one-inch layers,

5) High frequency (120 Hz) vibrations applied vertically to dry samples formed in seven one-inch layers,

6) High frequency (120 Hz) vibrations applied horizontally to moist samples (w = 8 percent) formed in seven one-inch layers,

7) Low frequency (20 Hz) vibrations applied horizontally to dry samples formed in seven one-inch layers,

8) Low frequency (20 Hz) vibrations applied vertically to dry samples formed in seven one-inch layers,

9) Tamping moist soil (w = 8 percent) with a 1.4-inch compaction foot to form samples in seven one-inch layers,

10) Rodding moist soil (w = 8 percent) with a 3/8-inch compaction foot to form samples in seven one-inch layers, and

11) Rodding dry soil with a 3/8-inch compaction foot to form samples in seven one-inch layers.

Following its preparation, the specimen was saturated, consolidated under an effective confining pressure of 8 psi, and subjected to a sinusoidal cyclic deviatoric stress. Axial deformations, the number of cycles to reach liquefaction, and axial strains of ±2.5, ±5.0, and ±10.0 percent were recorded. The resulting curves of the cyclic stress ratios versus number of cycles to initial liquefaction are shown in Fig. 12.19.

Fig. 12.19 shows that the weakest samples were formed by pluviating the soil through air with the strongest samples being formed by vibrating the soil in a moist condition. The difference in the cyclic stress ratio causing liquefaction is approximately 110% at 10 cycles and about 61% at 100 cycles. Using the same
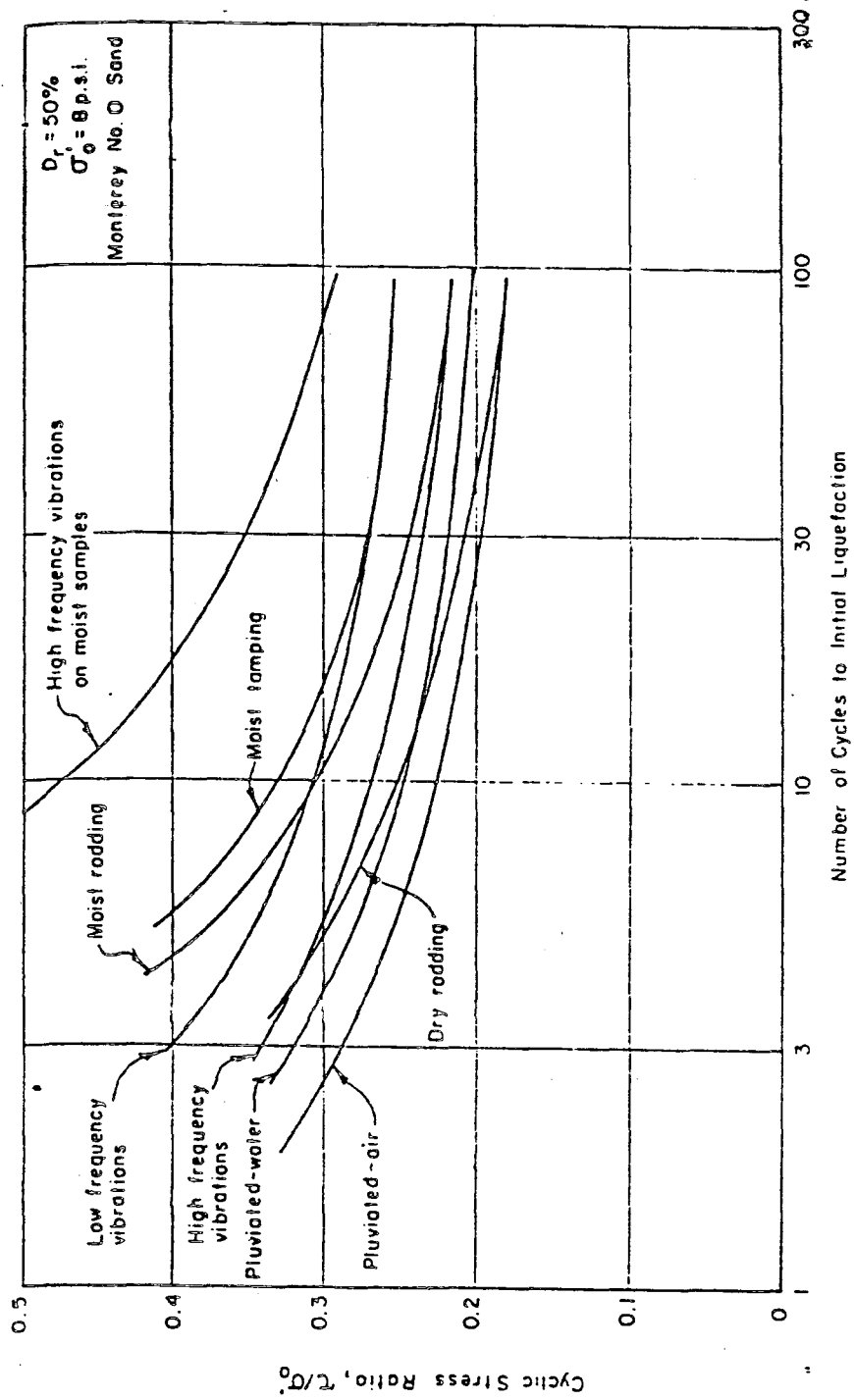
FIG. 12.19 CYCLIC STRESS RATIO VERSUS NUMBER OF CYCLES TO INITIAL
LIQUEFACTION FOR DIFFERENT COMPACTION PROCEDURES
(From Seed, 1975)

compaction methods, samples prepared in the moist condition were stronger than samples prepared in the dry condition. This is evidenced by the fact that samples formed by moist rodding were approximately 20% stronger than those formed by dry rodding at 10 and 100 cycles. Samples formed by moist vibration were between 55% and 75% stronger than those formed by dry vibration at 10 cycles.

In an attempt to investigate the reason for the effect of sample preparation methods on liquefaction potential, Mulilis, et al. (1977) also performed an investigation to determine the spatial distribution of the density within samples. Results of this study indicated that samples produced by air pluviation and low-frequency vibrations were very uniform; samples prepared in seven one-inch layers compacted by high-frequency vibrations were slightly less uniform; and samples placed in one seven-inch layer compacted by high-frequency vibrations were relatively nonuniform, and with a dense layer near the top and a loose layer at the middle of the samples. The loose layer may explain why the specimens prepared in one seven-inch layer had the lowest dynamic strength among those prepared by the three methods.

Mulilis, et al. (1978) presented the data obtained on specimens of Monterey No. 0 sand prepared by the moist-rodding and the dry-rodding methods. The result showed that the cyclic strength of the moist-rodding samples is approximately 58 percent stronger than that of the dry-rodding samples. The effect of rodding foot size was found insignificant.

Richard S. Ladd (1974) performed cyclic triaxial tests on three different sands prepared by either dry vibration or wet tamping. Results of this study shown in Fig. 12.20 also indicated that samples prepared by dry vibration were significantly weaker than those prepared by wet-tamping. At a specific number of cycles causing a peak-to-peak strain of 10%, the cyclic strength of samples prepared by dry vibration were approximately one-half that of samples prepared by wet tamping. In a similar study, Silver, et al. (1976) also reached the same conclusion.

Ladd (1977) compared the cyclic strengths of the samples prepared by moist vibration, moist tamping, dry tamping and dry vibration. The same conclusion as that of Mulilis, et al. (1977) was found.

12.6.2 Membrane Penetration

Cyclic triaxial test specimens are enclosed in thin cylindrical rubber membranes. When a confining stress is applied, the rubber membrane is forced into any interstices at the surface of the specimen as shown in Fig. 12.21. During an undrained cyclic triaxial test on a fully saturated sample, the volume of the specimen, i.e., the volume of the grain structure and the voids enclosed by the grains, is assumed to be constant. This assumption has been shown by several investigators (Manfred, et al., 1977; Lade, et al., 1977; etc.) to be violated for the following reason. At the beginning of an undrained cyclic triaxial test, when the excess pore pressure equals zero, the rubber membrane completely transmits the consolidation pressure to the grain
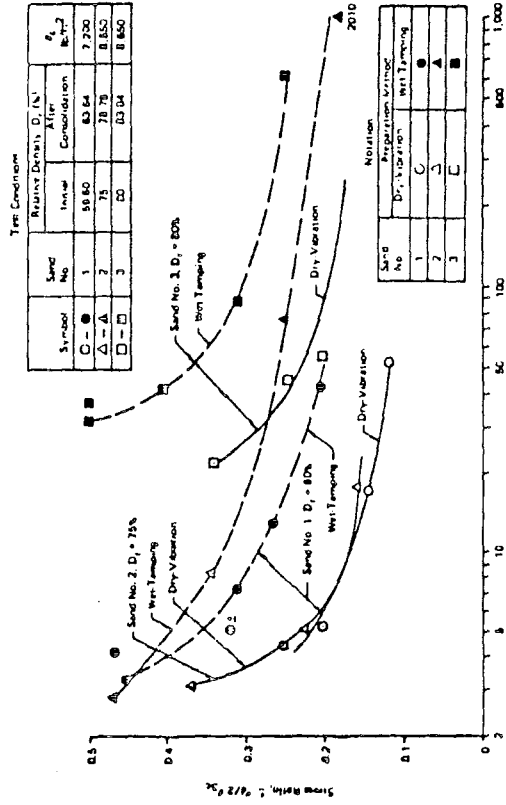
FIG. 12.20 APPLIED STRESS RATIO VERSUS NUMBER OF LOADING
CYCLES REQUIRED TO OBTAIN PEAK-TO-PEAK AXIAL
STRAIN OF 10 PERCENT (From Ladd, 1974)

$\Delta u = 0$ $\Delta u > 0$
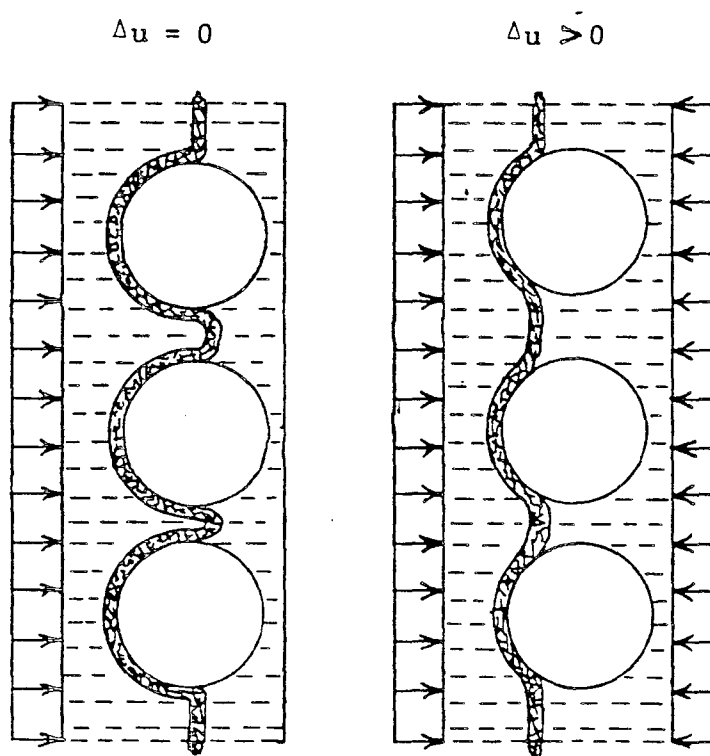
FIG. 12.21   MEMBRANE PENETRATION INTO THE INTERSTICES
OF A SAMPLE OF SAND DUE TO CHANGES OF
EXCESS PORE-WATER PRESSURE, Δu

structure as shown in Fig. 12.21. During the test, a part of the consolidation pressure is transferred to the water as excess pore-water pressure, Δu, and a change in the membrane penetration occurs. To satisfy volumetric compatibility this increased void volume along the surface of the sample due to membrane de-penetration must be accompanied by a corresponding volume decrease of the grain structure. In situ, however, the deformation of the grain structure during rapid loading may occur without volume change. Therefore the excess pore-water pressure and effective stress measured in a laboratory test where membrane penetration occurs may differ from those in situ. The volume change of the grain structure per square centimeter of membrane surface due to the membrane penetration is commonly referred to as membrane penetration.

Newland and Allely (1959) who tested samples composed of lead shot discovered the importance of the membrane effect. Assuming that the sample is isotropic, they suggested that the membrane penetration can be evaluated for the sample under an isotropic pressure as the difference between the observed volumetric strain and three times the measured axial strain. This method is questionable, however, due to possible anisotropy of sand.

Roscoe, Schofield, and Thurairajah (1963) investigated the membrane penetration by testing, under ambient pressure conditions, 1-1/2-inch diameter triaxial specimens containing central brass rods throughout the height of the sample. Rod diameters varying between 1/4 inch and 1-3/8 inch were used. The membrane penetration was obtained for each value of ambient pressure by plotting

volume change measured against rod diameter and extrapolating the resulting straight line to obtain the volume change for a 1.5-inch diameter sample.

Frydman, Zeitlen, and Alpan (1973) measured the membrane penetration in an undrained triaxial test where a membrane with a thickness of 0.2 mm was used. They found that while at a constant cell pressure of 1.0 kg/cm^2, when the excess pore-water pressure rose from zero to 0.5 kg/cm^2 the "volume of voids" along the surface of the specimen increased by $5 \times 10^{-3} cm^3/cm^2$ of membrane surface.

Wong, et al. (1975) raised the question of membrane penetration on the liquefaction potential of gravelly soils. To minimize this effect, a relatively thick membrane was used to reduce the amount of initial penetration into the irregular sample surface.

Manfred and Schuppener (1977) showed that, due to volumetric compatibility, the horizontal deformation of the grain structure of a specimen of 7.5-cm diameter will be $\varepsilon_h = 2 \times 2 \times 10^{-3}/7.5 = 5 \times 10^{-4} = 0.05\%$. If elastic behavior and a Young's modulus for sand of $E_s = 1000$ kg/cm^2 are assumed, the stresses of the grain structure corresponding to this deformation which will not be observed in situ, are $\sigma_h = \varepsilon_h \times E_s = 5 \times 10^{-4} \times 1000 = 0.5$ kg/cm^2. Therefore the error in pore pressure measurement will be in the order of 0.5 kg/cm^2.

Martin, et al. (1978) investigated the effect of system compliance on uniform sands. They concluded that the effect of membrane compliance for well graded sand samples would be less than that of uniformly graded samples. In addition, samples

containing a small proportion of gravel would produce a relatively large void on the sample surface, leading to a large increase in the apparent resistance to liquefaction.

In conclusion, in soils which contract during a cyclic loading test, test results not corrected for membrane penetration lead to an overestimation of undrained shear strength or an underestimation of the excess pore-water pressure. Also, the major factor influencing the membrane penetration for any applied cell pressure is particle size. The particle shape and distribution and the specimen density have minor effects.

12.6.3 Frictionless Caps and Bases

Vernese and Lee (1977) conducted an extensive research on the effect of "frictionless" caps and bases (ends) on the cyclic strength of Monterey No. 0 sand. The frictionless ends reduce the lateral end constraint and provide more uniform stresses throughout a sample.

"Frictionless" cap and base, as shown in Fig. 12.22, were placed on the top and bottom of a test specimen. Each "friction-less" end consisted of two layers of rubber, each 0.012-inch thick and each separated by a generous smear of high vacuum silicone grease. Long prongs, 1/8 inch in diameter and 0.5-inch long, were fixed in the center of the cap and base to keep the sample from sliding off the ends. The prongs were found to have no effect on the cyclic strength of Monterey No. 0 sand.

Samples of Monterey No. 0 sand placed at a relative density of 60 percent when tested using "frictionless" ends were
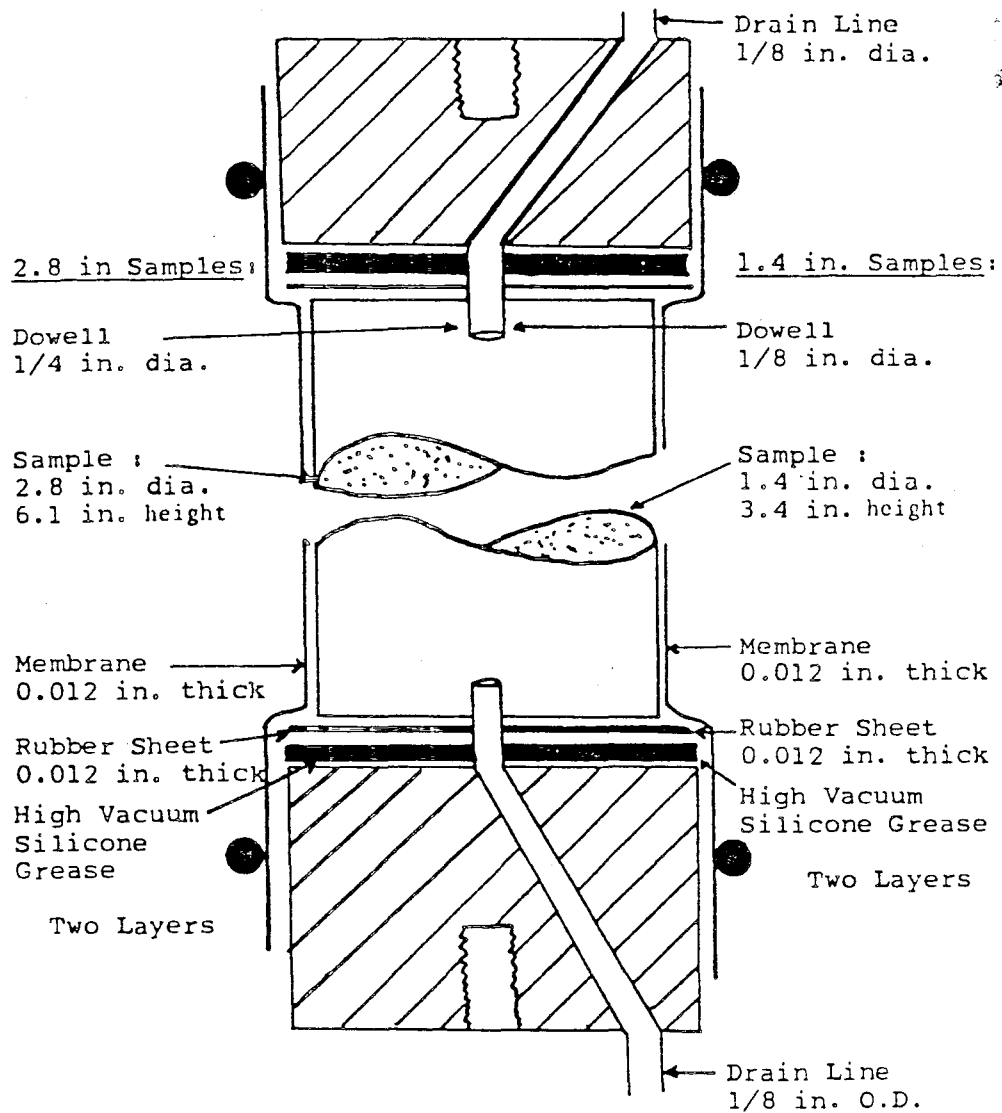
FIG. 12.22 FRICTIONLESS CAPS AND BASES USED IN UCLA STUDY
(From Vernese, 1977)

approximately 10 to 20 percent stronger than those tested using regular ends as shown in Fig. 12.23. Fig. 12.24 shows that samples of Monterey No. 0 sand prepared to a relative density of 80 percent were 30 to 35 percent stronger when tested with "frictionless" ends as compared to regular ends. This is probably due to the fact that the samples with "frictionless" ends had more of a tendency to dilate because of the reduced lateral constraint.

Silver (1977) pointed out the fact that "frictionless" top and bottom platens constitute a special test condition and, therefore, recommended that "frictionless" top and bottom platens not be used in professional practice.

Vernese (1977) also suggested that there appeared to be no advantage in adopting the "frictionless" ends when performing tests to solve routine engineering design problems. In special research, however, Vernese suggested that it might be desirable to use "frictionless" ends.

12.6.4 Effect of Sample Size

The cap and base friction of a triaxial specimen might be different for samples of different diameters. Bishop and Green (1965) recommended a height-to-diameter ratio of 2. However, for samples with large-size particles, it is also necessary to use a large-size specimen. A sample diameter of six times the maximum particle size is recommended to avoid possible effects of sample geometry (Wong, Seed and Chan, 1975).

Lee and Fitton (1969) studied the difference in the cyclic
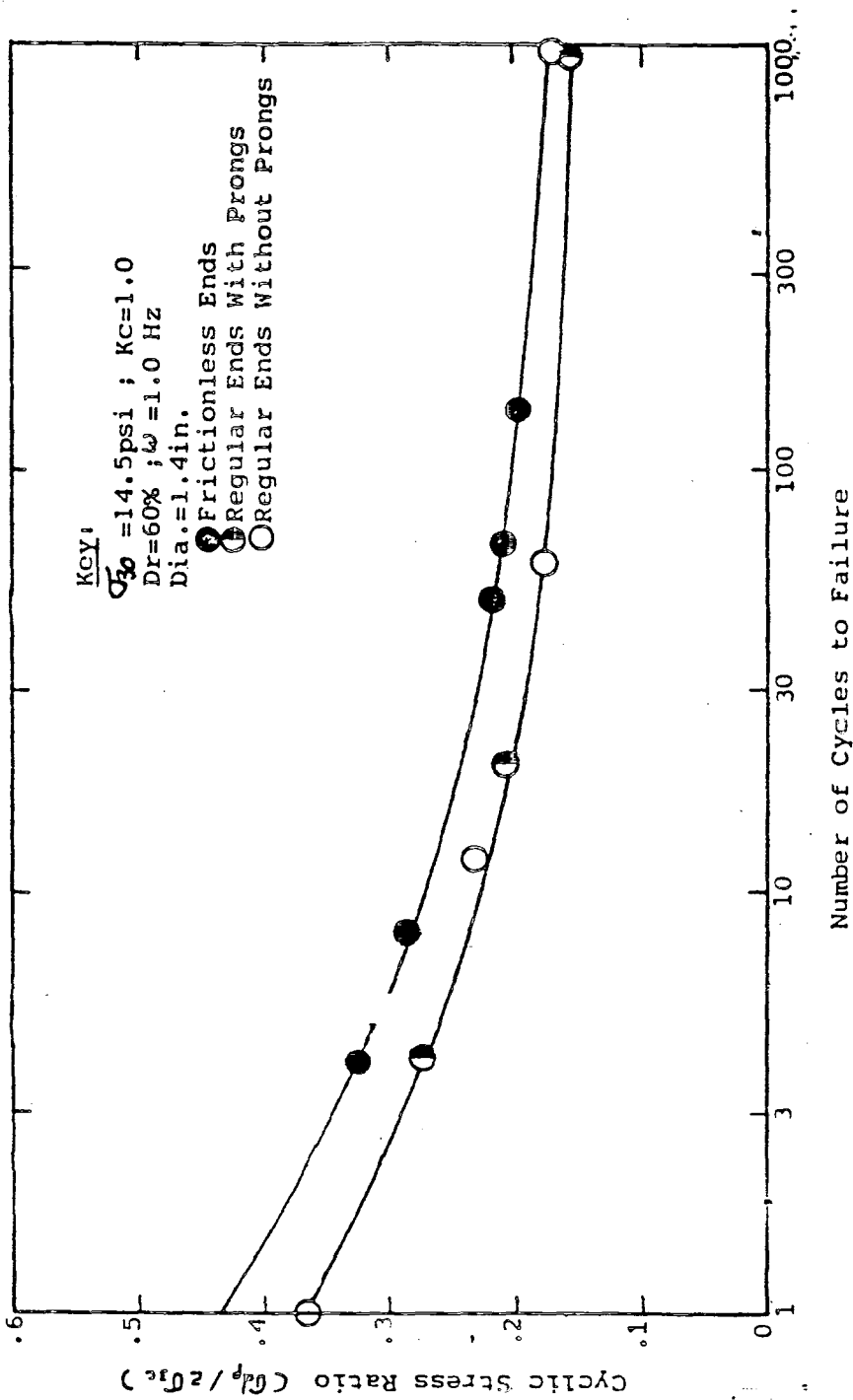
FIG. 12.23 COMPARISON OF CYCLIC STRENGTHS OF LOOSE MONTEREY SAND USING FRICTIONLESS AND REGULAR ENDS (From Vernese, 1977)

229
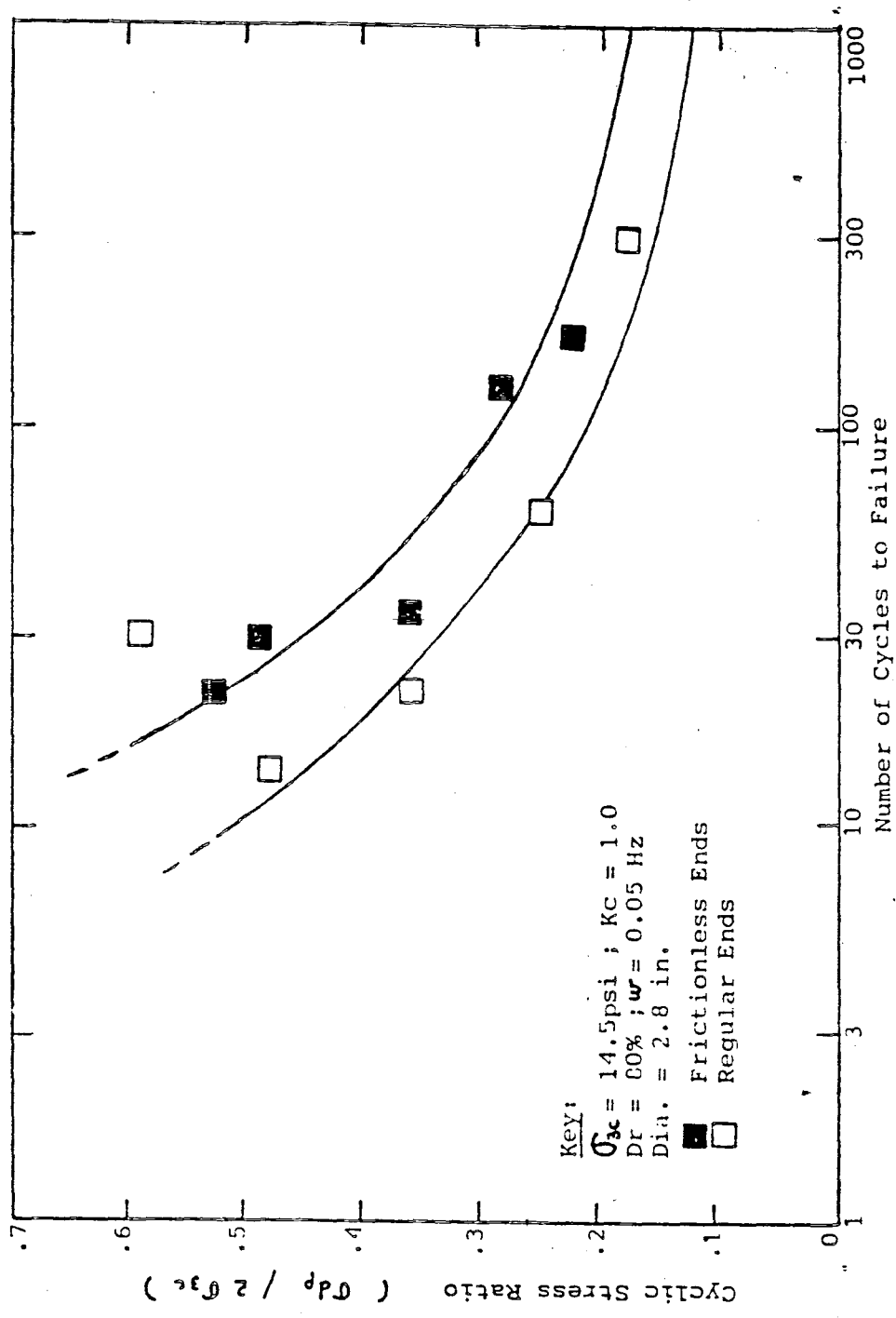
FIG. 12.24 COMPARISON OF CYCLIC STRENGTHS OF DENSE MONTEREY SAND USING FRICTIONLESS AND REGULAR ENDS (From Vernese, 1977)

strength of 1.4-inch and 2.8-inch diameter specimens of a coarse sand (No. 4 to No. 10 sieve size) and a fine sand (No. 50 to No. 100 sieve size). They concluded that the difference is insignificant with the 2.8-inch diameter samples being somewhat weaker. Vernese and Lee (1977) performed a series of tests on Monterey Sand specimens having diameters of 1.4 and 2.8 inches. Results shown in Fig. 12.25 also indicated that there was no appreciable difference between the cyclic strengths of 1.4 and 2.8-inch diameter specimens.

Wong, Seed, and Chan (1975) performed a series of tests on Monterey Sand samples of 2.8- and 12-inch diameters to determine the effect of variations in sample size on the cyclic strength of sand.

Wong, Seed and Chan pointed out two things which might change the cyclic strength of sand as the specimen diameter is varied. First, the concentration of stress near the cap and base of a triaxial cell might vary with differing specimen diameters. This effect can be minimized by using a constant height/diameter ratio and the specimen diameter of at least six times the maximum particle size. Secondly, membrane penetration will vary as the diameter and thickness of the membrane changes.

Membrane penetration is caused by the small change in volume which occurs when the pore pressure within a specimen builds up. This forces the membrane to move outwards from the crevices among soil particles. This results in a decreased rate of pore pressure generation and, therefore, the sample becomes more resistant to
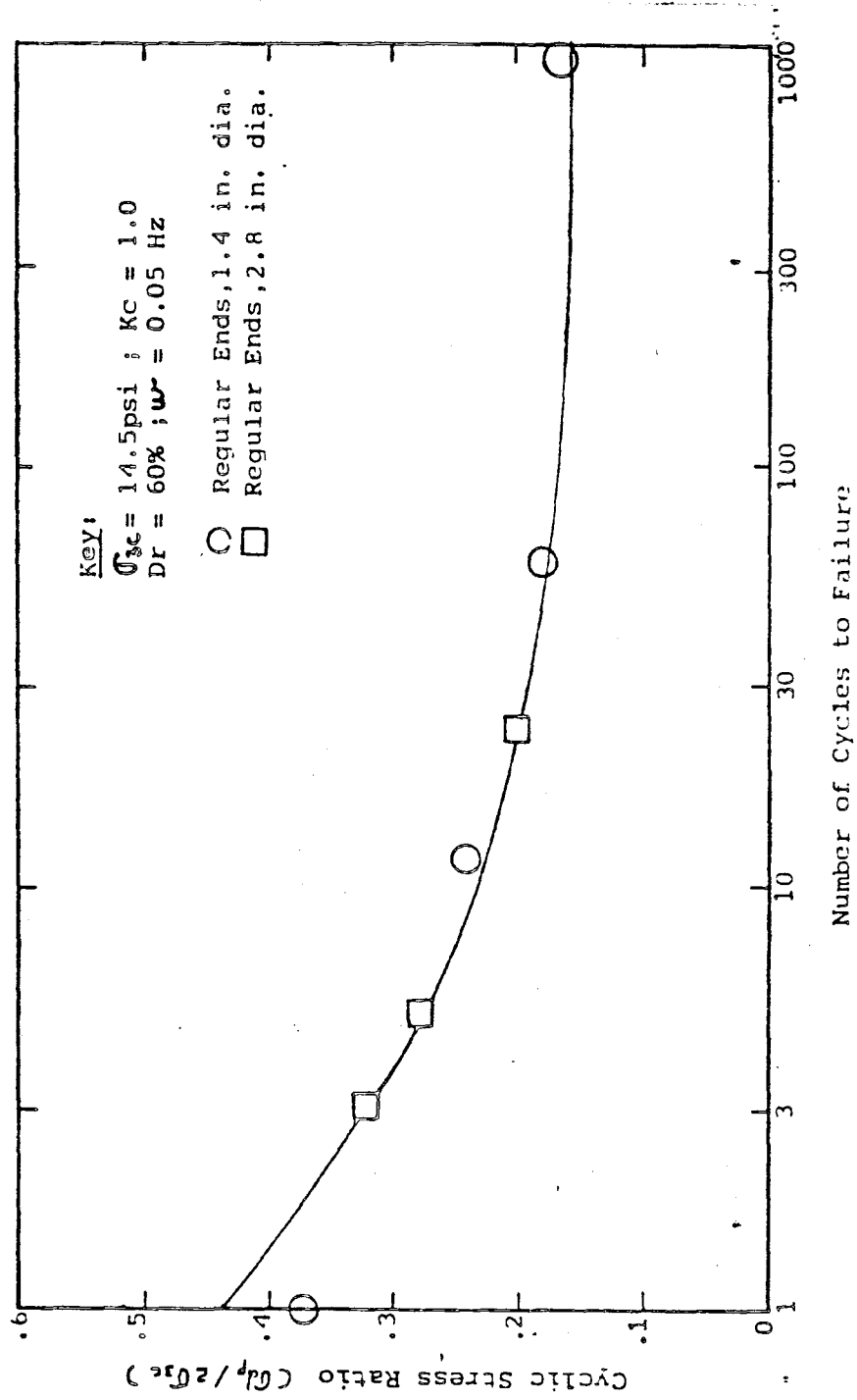
FIG. 12.25 COMPARISON OF STRENGTH DATA FROM CYCLIC TRIAXIAL TESTS
ON LOOSE MONTEREY SAND   (From Vernese, 1977)

cyclic loading. Effects of membrane penetration increase, for a given membrane thickness, as the particle size increases. Correspondingly its effect decreases, for a constant particle size and membrane thickness, as the diameter of the specimen increases. A detailed discussion of the effects of membrane compliance is found in Section 12.6.2.

Results shown in Fig. 12.26 indicated that the cyclic deviatoric stress required to cause the initial liquefaction in any given number of stress cycles were approximately ten percent less for the 12-inch diameter specimens than for the 2.8-inch diameter specimens. This difference may largely be due to the effects of membrane compliance, which, as previously discussed, would be greatest for small-diameter specimens if the particle size and membrane thickness remained constant.

12.6.5 Effect of Porewater Pressure Parameter "B"

The effect of Skempton's "B" parameter on the cyclic triaxial strength was studied by Chaney (1978). As shown in Fig. 12.27, "B" parameter ranging from 0.91 to 0.99 could significantly affect the triaxial strength. The magnitude of such difference is influenced by the density, the consolidation pressure and other soil characteristics.

Conversely, Mulilis, et al. (1978) examined the effect of the "B" parameter on the cyclic strength of Monterey No. 0 Sand. The result of testing specimens of 60-percent relative density and subjected to 14.5 psi initial confining pressure suggested that the effect was minor compared with the effect of the sample preparation
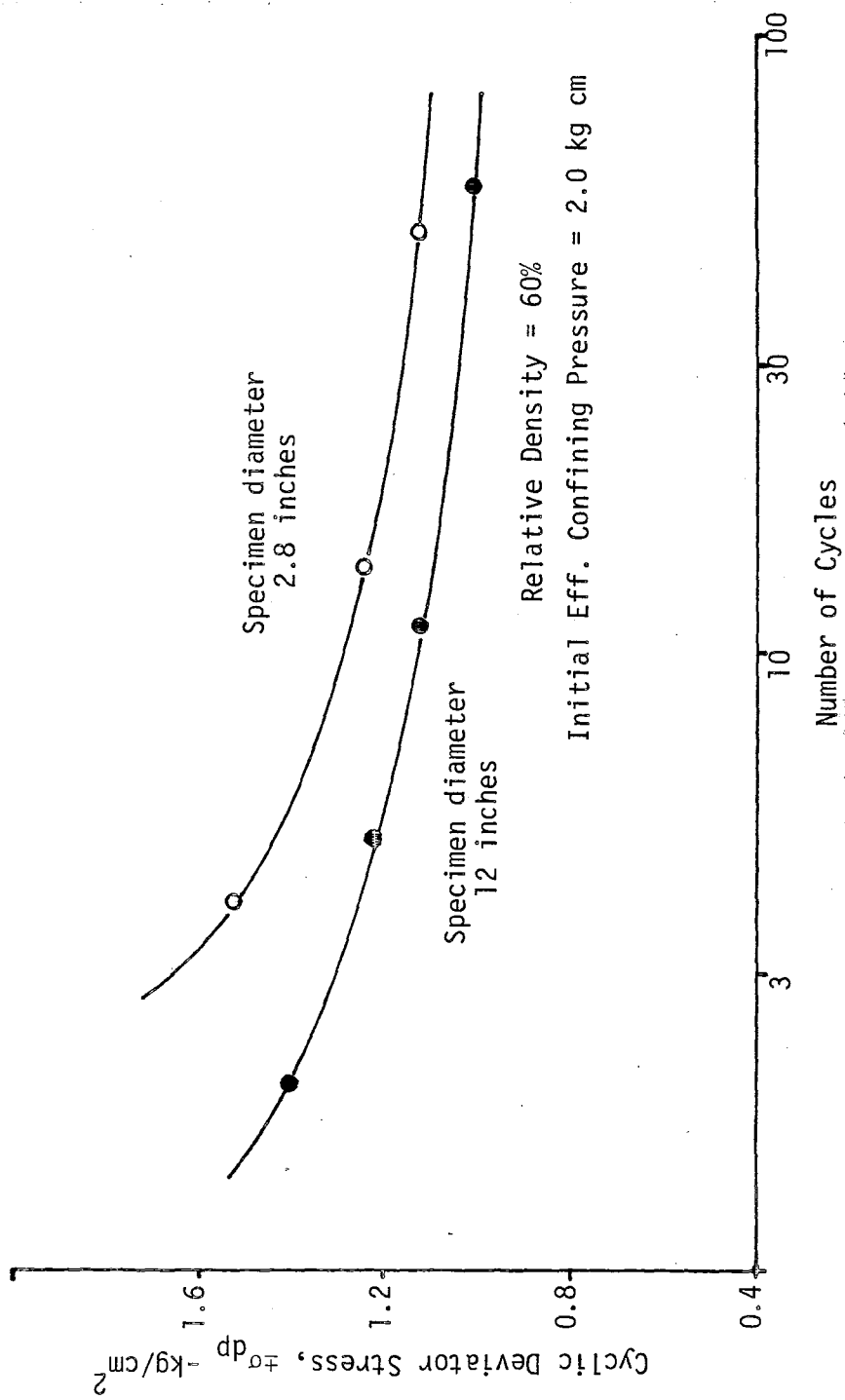
FIG. 12.26 EFFECT OF SAMPLE SIZE ON CYCLIC STRESSES CAUSING INITIAL
LIQUEFACTION ON MONTEREY SAND (From Wong, Seed and Chan, 1975)
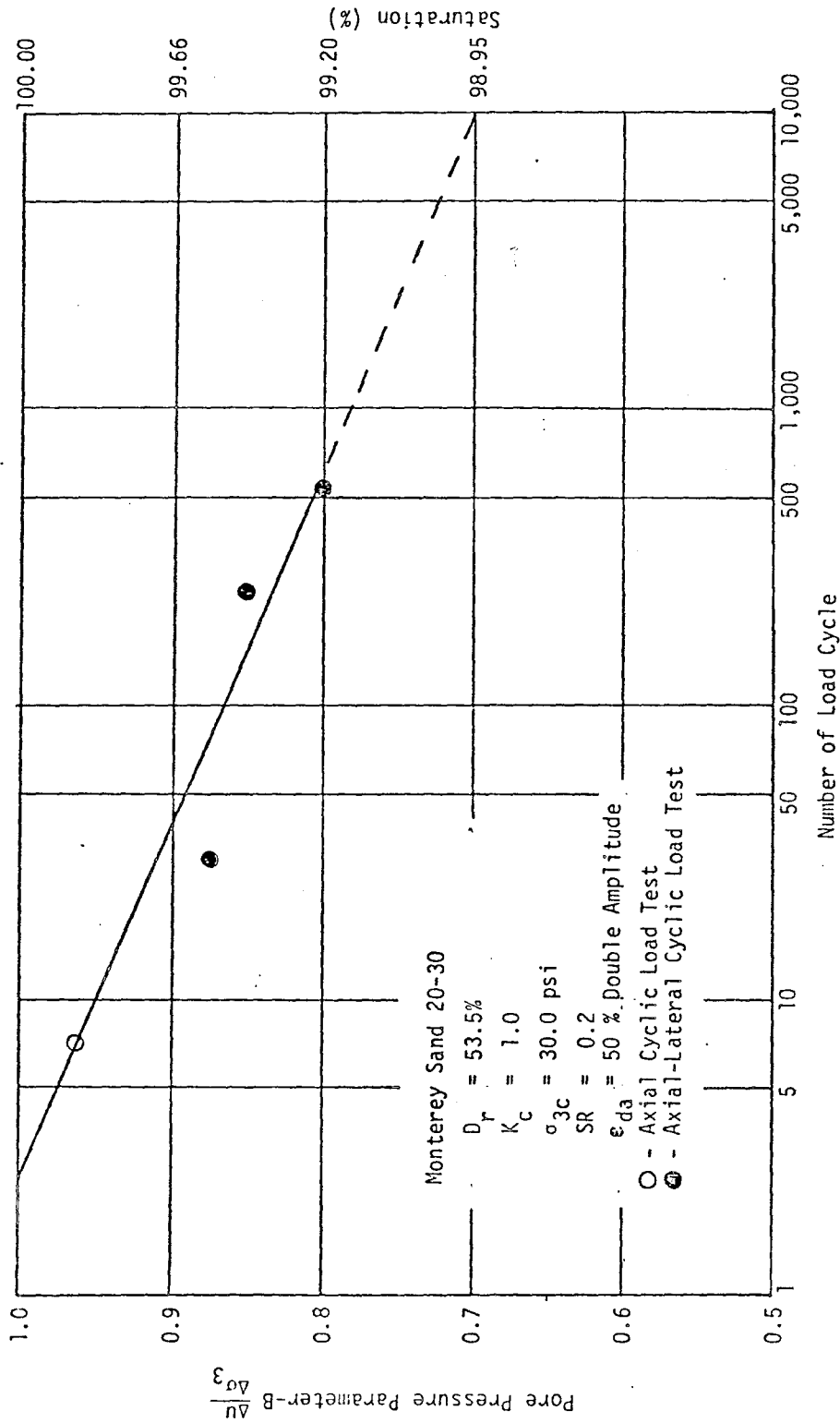
FIG. 12.27 EFFECT OF B-VALUE ON NUMBER OF LOAD CYCLES TO ACHIEVE ϵ_{da} = 5%
STRAIN FOR LOOSE SAND D_r = 53.5% (after Chaney, 1978)

procedure.

12.6.6 Loading Wave Form

Available loading wave forms for the cyclic triaxial test of
soils are: Sine, severe square, degraded square, and triangular
waves, etc. The effect of the loading wave form on the cyclic
strength of soils has been extensively studied (Lee and Fitton,
1969); Mulilis, Townsend and Horz, 1978, 1976; Silver, 1977).
Results of the study by Silver (1977) shown in Fig. 12.28 indicated
that the cyclic strength of a saturated sand is significantly
affected by the loading wave form. Specimens tested with severe
loading waves with a fast rise time showed the cyclic strength
approximately 15% less than those tested with sine or degraded
loading wave without fast rise time. The pore water pressure
recorded during the test with severe square loading waves indicated
that a stress wave was propagated through the specimen because of
the instantaneous velocity change. This stress wave reflected in the
form of pore pressure spikes. The more rapid generation of excess
pore-water pressure caused the sample to liquefy in less number of
cycles than that subjected to other loading wave forms.

Because of the rapid jump in excess pore-water pressure
associated with severe square wave loading, Silver (1977) recommended
that a sine wave loading or a degraded square wave with the rise
time approximately 10% of the loading period be used instead.

Mulilis, et al. (1978) reported that the specimens tested
using a nearly triangular loading wave and a sine loading wave
were approximately 13 and 30 percent, respectively, stronger than
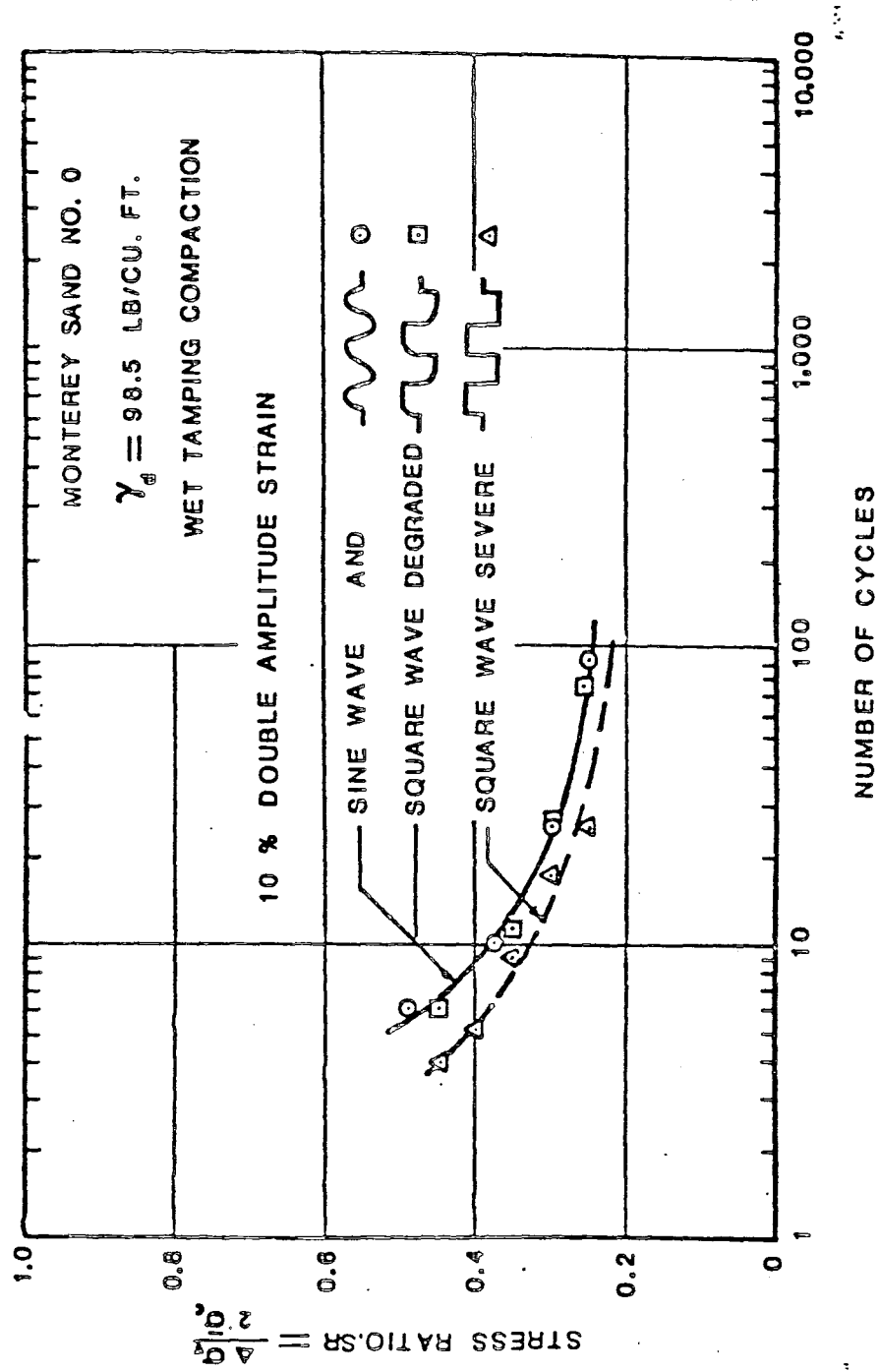
FIG. 12.28 EFFECT OF WAVE SHAPE ON THE CYCLIC TRIAXIAL
STRENGTH OF THE TEST SAND (after Silver, 1976)

specimens tested using a severe square loading wave at high stress ratios.

12.6.7 Frequency

Minor effect in the frequency ranging from 0.01 Hz to 1 Hz has been reported (Lee and Fitton, 1969; Wong, et al., 1975). Lee and Fitton (1969) pointed out that the slower loading frequency appeared to have a slightly lower strength. Conversely, Wong presented data indicating that although it has a negligible effect in the frequency range of 20 cpm to 1 cpm, the slower frequency loading does give a slightly higher strength.

To investigate the effect of frequency on the cyclic strength, Samuelson (1981) tested Monterey No. 0 Sand samples with the relative density of 30 percent and under the confining pressure of 30 psi and the cyclic stress ration R_s of 0.25. Frequencies ranging from 0.0001 Hz to 1.0 Hz were used. It was found that there was no significant effect at frequencies less than 0.01 Hz. However, the effect became increasingly significant as the frequency increases with the specimens tested with a high frequency loading waves being stronger.

CHAPTER 13

TEST EQUIPMENT, SAMPLE PREPARATION AND EXPERIMENTAL PROCEDURES

13.1 Test Equipment

13.1.1 MTS Closed-Loop Servo Electrohydraulic System

Three different types of cyclic loading systems are available:
Electrohydraulic system, pneumatic system and mechanical system.
An MTS closed-loop electrohydraulic system, Model 810 as shown in
Fig. 13.1, was used for performing stress-controlled cyclic triaxial
tests at various frequencies. The system has a hydraulic pump
with a pump capacity of 3 gpm and a loading capacity of 20,000
pounds.

This system performs very well until the onset of liquefaction
at which time an abrupt change in the specimen rigidity occurs. A
large quantity of the hydraulic fluid (oil) must be furnished at
a fast rate during liquefaction to allow the loading piston to
follow the sudden and rapid specimen deformation and maintain a
constant stress amplitude. Such a rapid rate of fluid flow might
exceed the hydraulic pump capacity. For this reason the amplitude
of the cyclic load decreases as the specimen approaches liquefac-
tion. Besides, it seems irrational to demand the machine actuator
to follow the behavior of a soil specimen which is essentially
failed.
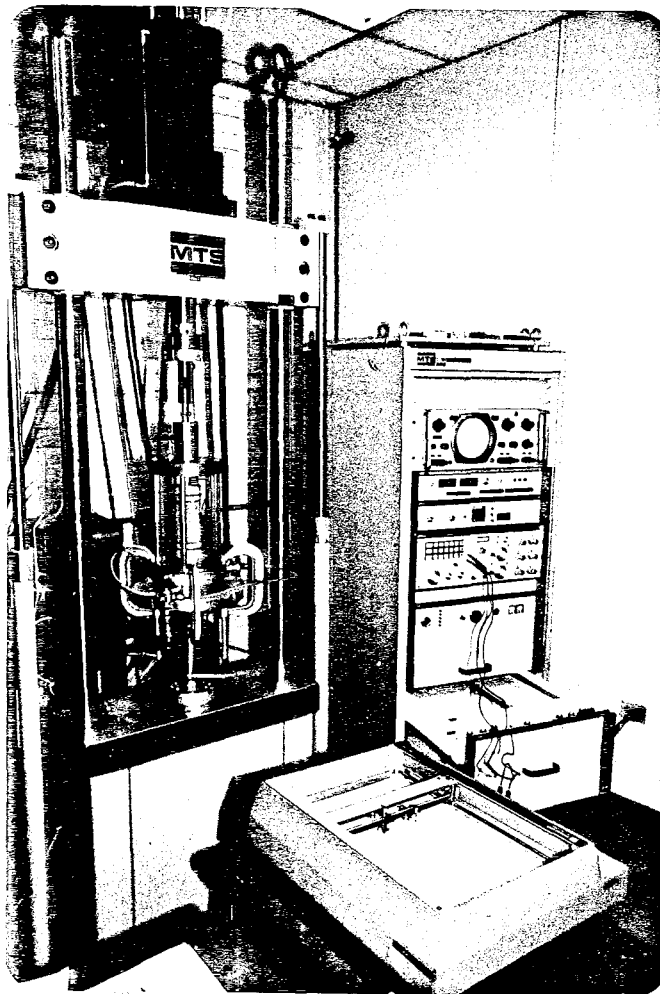
FIG. 13.1 CLOSED LOOP ELECTRO-HYDRAULIC MATERIALS
          TEST SYSTEM APPLYING A SINUSOIDAL LOADING
          TO A MONTEREY NO. 0 SAND SPECIMEN

Two levels of operation are provided: An output pressure of 300 psi for the low or bypass condition and an output pressure of 3000 psi for the high condition.

A fluid-to-water heat exchanger is used to dissipate the temperature built up in the hydraulic power supply system. A temperature-sensitive switch will prevent the hydraulic fluid temperature from exceeding a predetermined limit.

The hydraulic actuator is the force-generating and/or positioning device in the system. Movement of the loading piston is the direct result of the application of fluid pressure to one side of the piston. A load applied to some external reaction point by the piston is equal to the effective piston area times the activating pressure.

The hydraulic actuator is controlled by the opening and closing of a servovalve in response to a control signal from the valve driver or controller. The servovalve can open in either of two positions, thereby permitting high pressure fluid to enter into either side of the piston. This alternating application of hydraulic pressure to either side of the piston makes it possible to apply smooth cyclic tension and compressive loads to a test specimen. When the servovalve is opened to allow fluid to flow into one end of the cylinder, the valve on the opposite end of the cylinder is opened to provide a path for fluid to flow back to the hydraulic power supply.

The rate of fluid flow through the servovalve is in direct proportion to the magnitude of the control signal. The polarity

of the control signal determines which end of the actuator cylinder will receive additional fluid thereby determining the direction of the piston stroke.

The load cell is a force-measuring transducer that provides an output voltage directly proportional to the applied load.

The linear displacement of the loading ram is measured by a linear variable differential transformer (LVDT). The LVDT requires a-c excitation and provides an a-c output. The amplitude of the output varies in direct proportion to the amount of displacement of the LVDT core.

Transducer conditioners supply excitation voltages to their respective transducers and control the tranducer output voltages to d-c levels suitable for use in the control portion of the system. Output of each transducer conditioner is ±10 volts at 100% of the operating range which is ±20,000 pounds or ±5 inches under the stress and stroke control modes, respectively.

The servo controller compares the command and feedback inputs and provides an error signal which opens the servovalve in a direction and by an amount which causes the hydraulic actuator to correct the error. When the error signal is reduced to zero, the servovalve closes, and the system is in a state of equilibrium. Cyclic wave forms such as sine, haversine, and haversquare and various ramp functions are available. The inversion of the cyclic wave forms are also available. Frequencies range from 0.00001 to 990 Hz. The ramp functions include ramp, dual slope, triangle, saw tooth, and trapezoid. The ramp functions are adjustable from 0.001 second to 11.45 days.

Electro-mechanical counters can be programmed to stop the test after a predetermined number of these events.

The counter has a capacity of 999,999 counts at a maximum frequency of 25 Hz. A x10 and x100 multiplier can be utilized to increase the counters capacity wherein only every 10th or 100th event is counted.

13.1.2 Data Acquisition System

The axial load on the specimen, pore pressure within the specimen, and vertical deformation of the specimen were recorded during a cyclic triaxial test.

An X-Y recorder was utilized for recording the axial load versus vertical deformation relation of a specimen and the associated hysterisis loop.

The pore water pressure within the specimen and the vertical deformation of the specimen were recorded on an Esterline Angus X-Y-Y' 540 recorder as shown in Fig. 13.1. The X axis was established as the sweep axis. The rate of sweep is dependent upon the estimated amount of time required to complete a test. It should give adequate resolution to high frequency tests and be set to a slower rate of sweep during low frequency tests.

A Tektronix Power Supply and Digital Multimeter were used to supply power and measure the output voltage from the pore pressure transducer which is also manufactured by Tektronix. The Digital Multimeter in connection with the pore water pressure transducer was also used extensively to measure the cell pressure and back pressure during saturation and consolidation of a test specimen.

Fig. 13.2 shows the triaxial cell, MTS loading equipment, and data acquisition system as seen during a typical cyclic triaxial test.

13.1.3 Triaxial Testing System

The triaxial cell shown in Fig. 13.3 was used in performing all cyclic triaxial tests. A pore pressure transducer attached to a four-way valve plugged into the right side of the triaxial cell base was used to measure the cell pressure, back pressure, and pore water pressure at the top and/or the bottom of a specimen. The pore pressure transducer was attached to a four-way valve such that by changing the position of the valve the transducer could be subjected to either the cell pressure, back pressure, or pore water pressure. Fig. 13.4 shows the transducer and four-way valve disconnected from the triaxial cell.

On the left side of Fig. 13.3, four pressure lines are seen. The upper horizontal line entering the base of the triaxial cell applied the confining cell pressure, with the line passing behind the cell and over to the four-way valve used for transmitting the cell pressure to the pore pressure transducer. The middle line entering the base of the triaxial cell applied the back pressure to the specimen with the lower line used for transmitting the pore pressure from the top of the specimen to the four-way valve and pressure transducer.

The pressure control panel shown in Fig. 13.5 could be used to apply cell and back pressures simultaneously to three triaxial cells. An air compressor connected to the pressure control panel furnished a maximum air pressure of 175 psi for the pressure
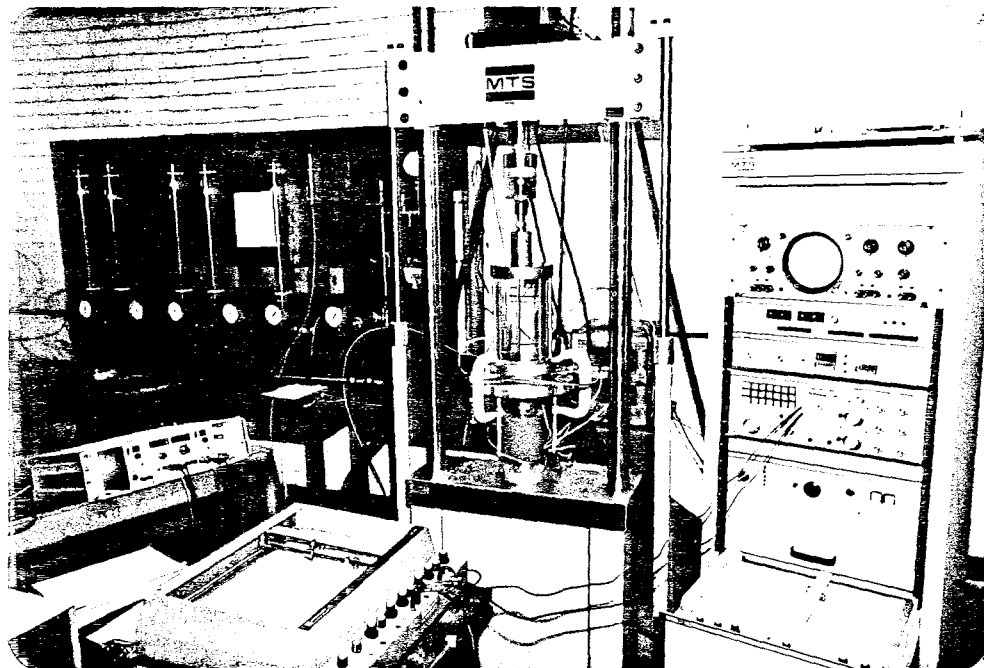
FIG. 13.2   TRIAXIAL CELL, CLOSED LOOP ELECTRO-HYDRAULIC
MATERIALS TEST SYSTEM, AND DATA ACQUISITION SYSTEM
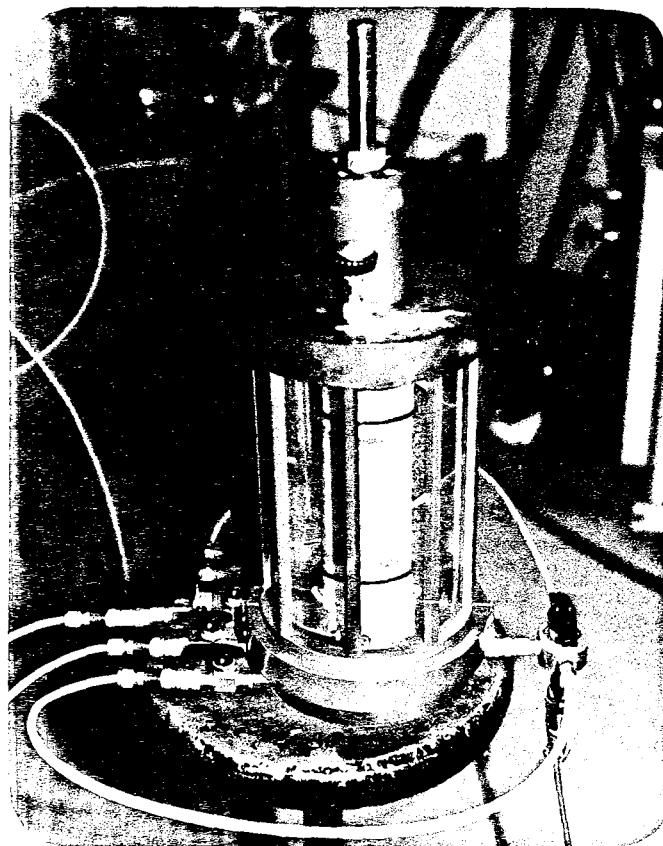
FIG 13.3   TEST SPECIMEN PLACED WITHIN THE TRIAXIAL CELL
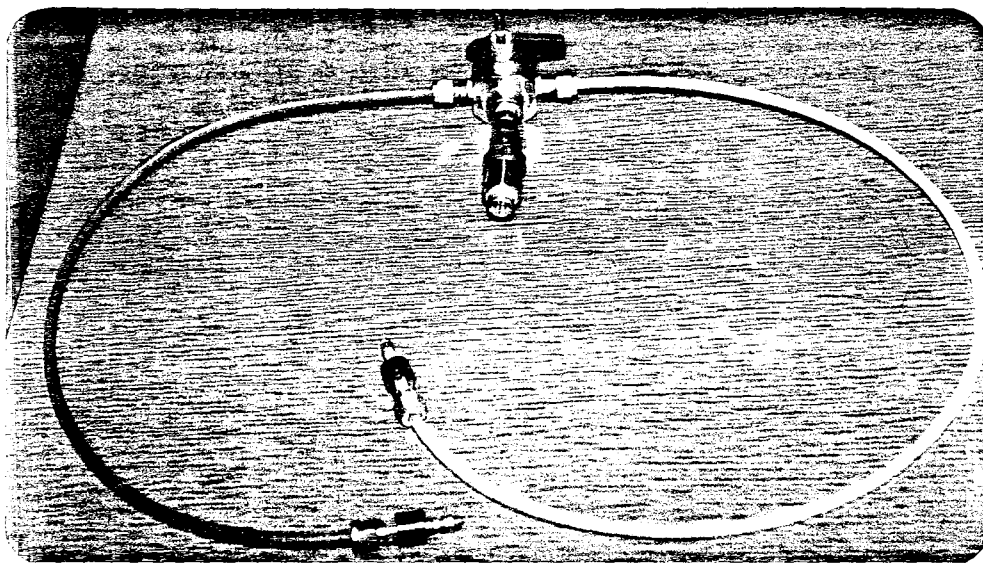
FIG. 13.4 PORE PRESSURE TRANSDUCER AND A 4-WAY VALVE
USED TO MONITOR CELL PRESSURE, BACK PRESSURE
AND SPECIMEN PORE WATER PRESSURE
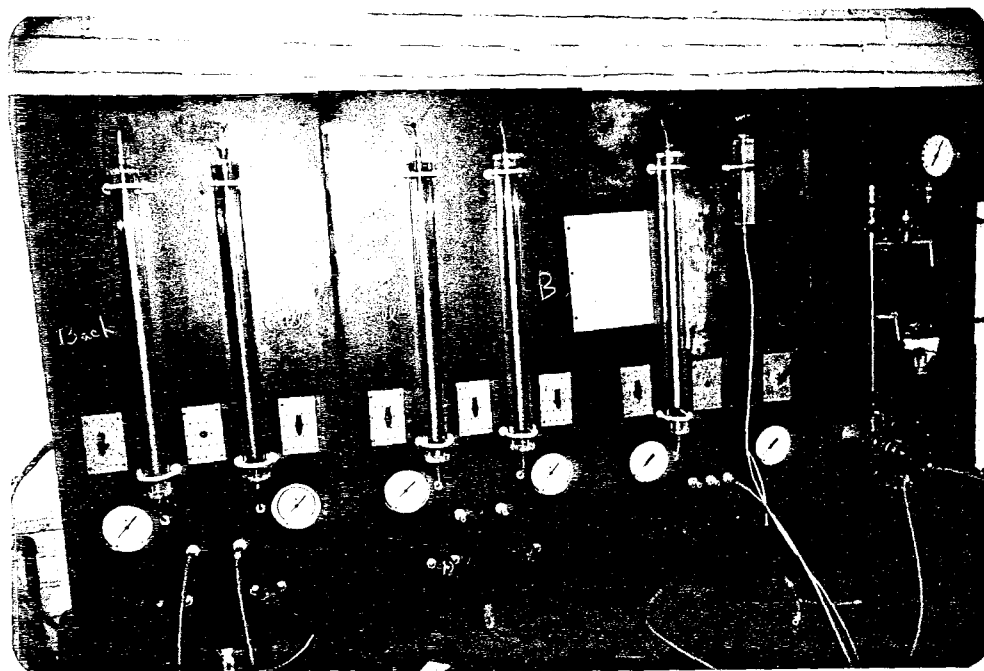
FIG. 13.5 PRESSURE CONTROL PANEL USED TO APPLY CELL AND BACK
PRESSURE TO THE TRIAXIAL CELL. GRADUATED BURETTES
WERE USED TO DETERMINE SPECIMEN VOLUME CHANGE.

control panel. When the pressure in the air tank dropped below a specified minimum value a pressure switch would turn on the compressor.

The graduated burettes (vertical standpipes) shown in Fig. 13.5 were used to measure specimen volume changes within an accuracy of 0.1 cubic centimeter. Specimen volume change measurements were made after consolidation of the test specimen and after attaching the loading ram to the specimen top cap.

13.2 Sample Preparation

Numerous researchers (Seed, 1975; Lade, 1976 and Mulilis, 1977) have shown that sand samples prepared by different sample preparation methods to the same relative density have different liquefaction potentials. Studies, including the use of qualitative x-ray analysis, indicate differences in dynamic strength of test specimens might be associated with the difference in the orientation of the sand grain contact and the uniformity of compaction received by each specimen.

13.2.1 Test Sand and Test Program

A commercially available Denver sand, a river sand, purchased from the Denver Sand and Gravel Company was selected as the test material. Both coarse and fine grains of Denver sand are subangular in shape as shown in Figs. 2.1 and 2.2. Sixteen U.S. standard sieves with opening from 3/8 in. to 38 microns (U.S. standard sieve No. 400) were used to segregate different size particles. Following the pre-selected gradation curves shown in Fig. 2.4, samples with

different mean grain diameters and/or different uniformity coefficients were prepared accordingly. To assure each sample was well mixed, a splitter was used. Samples of twenty-four different gradations were prepared. Two-inch diameter specimens were used in this study. To satisfy the rule of thumb of the maximum grain size not being greater than one-sixth of the specimen diameter, the maximum grain size is limited to 3/8". In addition, no samples contain more than 20% silt. Under these restrictions, the mean grain size of samples ranges from 0.149 mm to 1.68 mm. Their coefficients of uniformity range from 2 to 15. Each individual specimen, after completion of a cyclic test, was subjected to sieve analysis to check its grain size distribution. The index properties of the test samples were given in Table 13.1, in which the maximum and minimum densities were evaluated by following the procedure given in Earth Manual (E-12, 2nd Edition, 1974) published by the U.S. Bureau of Reclamation.

After reviewing various sample preparation methods, a zero raining device was adopted to place the sand. As shown in Table 13.2, the mesh openings of zero-raining devices increase with the increase in the maximum grain size of a specimen. It is believed that specimens prepared by using the zero raining device were uniform and without serious segregation. This is evidenced by the visual examination of each test specimen and by the repeatibility of the cyclic triaxial test results. Although the desired sample relative density after consolidation was 50%, the relative density achieved for the test specimen ranged from 49.6% to 59.3%.

TABLE 13.1

THE INDEX PROPERTIES OF TEST SAMPLES

Sample No.*	Max. Density (pcf)	Min. Density (pcf)	Specific Gravity**	D_{50}, in mm.	Uniform- ity Coef- ficient	e_{max}	e_{min}
$DC-a_2$	104.89	87.03	2.66	1.50	1.89	0.91	0.58
$DC-b_2$	104.78	88.51	2.66	0.82	2.17	0.87	0.58
$DM-c_2$	105.74	87.03	2.66	0.53	2.16	0.91	0.57
$DM-d_2$	106.08	85.05	2.66	0.38	2.20	0.95	0.56
$DM-e_2$	106.38	82.67	2.66	0.24	2.88	1.01	0.56
$DF-f_2$	102.95	79.60	2.66	0.15	2.70	1.09	0.61
$DC-a_4$	114.80	94.46	2.66	1.44	3.73	0.76	0.45
$DC-b_4$	116.00	95.45	2.66	0.68	3.71	0.74	0.43
$DM-c_4$	118.36	93.96	2.66	0.51	4.31	0.77	0.40
$DM-d_4$	115.75	91.98	2.66	0.37	4.93	0.80	0.43
$DM-e_4$	116.92	90.50	2.66	0.23	5.15	0.77	0.42
$DF-f_3$	108.87	84.06	2.66	0.14	3.40	0.97	0.52
$DC-a_6$	121.24	98.91	2.66	1.17	5.50	0.68	0.37
$DC-b_6$	121.33	99.41	2.66	0.62	5.70	0.67	0.37
$DM-c_6$	122.59	99.40	2.66	0.48	7.20	0.67	0.35
$DM-d_6$	121.78	96.93	2.66	0.40	7.00	0.71	0.36
$DM-e_6$	119.67	94.55	2.66	0.25	7.50	0.76	0.39
$DC-b_8$	123.96	102.38	2.66	0.69	9.50	0.62	0.34
$DM-c_8$	125.64	101.39	2.66	0.52	9.00	0.64	0.32
$DM-d_8$	123.35	98.91	2.66	0.37	9.70	0.68	0.35
$DC-b_{10}$	126.23	103.86	2.66	0.62	10.30	0.60	0.31
$DM-c_{10}$	127.41	103.47	2.66	0.57	11.30	0.60	0.30
$DM-d_{10}$	125.94	101.88	2.66	0.37	12.00	0.63	0.32
$DM-c_{15}$	129.21	105.35	2.66	0.35	16.00	0.58	0.28

*Sample No. provides information on the gradation characteristics. For instance, a_2 denotes sample with median grain size of "a" (1.50 mm) and a designed uniformity coefficient of 2 as shown in Figure 4.2.

**Specific gravity was assumed to be the same based on test results on c_2, c_4, c_6, c_{10}.

TABLE 13.2

MESH OPENINGS OF ZERO RAINING DEVICES

Mesh No.	Wire Diameter (in)	Opening (in)	Test Samples**
3	0.080	0.2533	*a_2, b_4, b_6, c_6, c_8, c_{10}, d_6, d_8, d_{10}
6	0.035	0.1317	b_2, c_2, c_4, d_4, e_6
10	0.028	0.0720	d_2, e_2, e_4
16	0.018	0.0445	f_2, f_3

*Sample No. provides information on its gradation characteristics. For instance, a_2 implies the sample with mean grain size of "a" (1.50 mm) and a designed uniformity coefficient of 2 as shown in Figure 2.4.

**For samples not listed in this table, zero raining device was not used.

To nicely define the curve of the stress ratio versus number of cycles to reach the initial liquefaction requires a minimum of four samples for each gradation shown in Fig. 2.4. A total of 123 cyclic triaxial test specimens were prepared and tested in this study.

13.2.2 Forming the Test Specimen

Before placing the lower porous stone and filter paper on the base of the triaxial cell shown in Fig. 13.6, the base of the triaxial cell was carefully wiped off with a clean rag to remove any standing water, particularly on the pedestal on which the lower porous stone was placed. This prevented the possibility of water from being raised up by capillary forces through the bottom porous stone and wetting the filter paper and sand placed on top of the porous stone.

The quick coupler and line in the base of the triaxial cell, which were connected to the top cap via a small diameter poly-ethylene flexible tube were also dried. This allows samples to remain dry under vacuum during the specimen preparation.

To save time, it is very important to make sure that the rubber membrane is flawless before use. To detect holes in a rubber membrane before it is placed around a specimen, the rubber membrane can be inflated with water as shown in Fig. 13.7. The triaxial cell back pressure line was connected to a water supply line and the membrane was slowly inflated with water. When the membrane had been inflated with water, the outside surface of the membrane was wiped off with a dry cloth so that newly formed drops of water passing through the membrane could be detected.
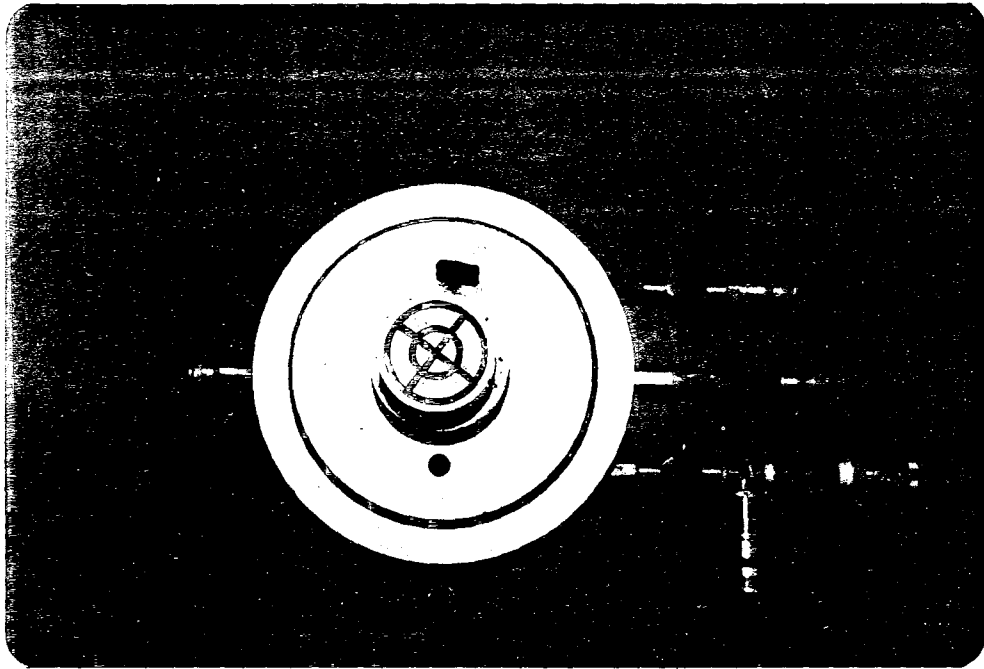
FIG. 13.6   LOOKING DOWN ON THE BASE OF THE TRIAXIAL CELL
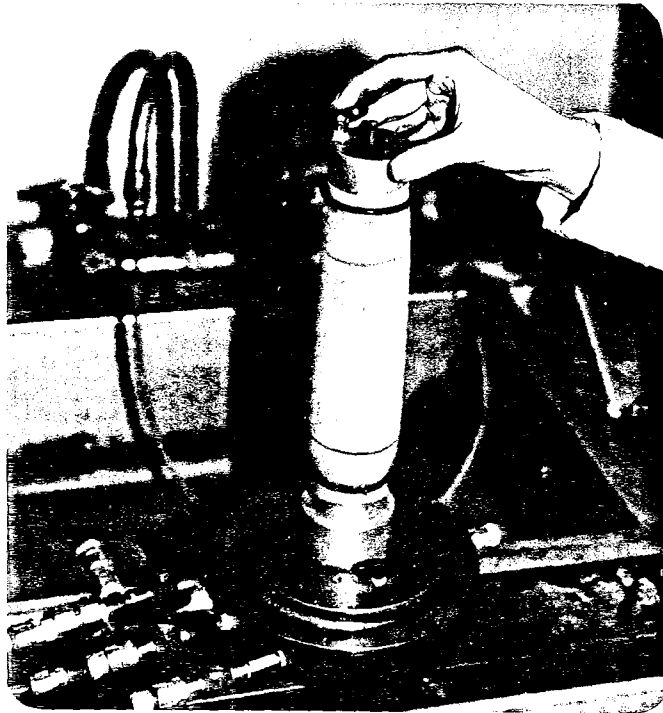
FIG. 13.7 CHECKING FOR LEAKS IN THE RUBBER MEMBRANE

After a membrane has been tested and found to contain no holes, the inside and outside surfaces of the membrane should be wiped off with a cloth. The membrane should be completely dry before the sand specimen is formed to prevent sand from adhering to the inside of the membrane.

A dry porous stone was placed on the base pedestal of the triaxial cell and a circular filter paper placed on top of the porous stone. The disc of filter paper must be cut to the right size, neither larger nor smaller than the porous stone. If the filter paper disc is larger than the porous stone, the edge of the filter paper will be lifted up by the surrounding rubber membrane resulting in a reduction in sample diameter at its contact with the porous stone. Conversely, if the paper disc is smaller in diameter than the porous stone, sand can come in direct contact with the porous stone around the perimeter of the filter paper disc.

Thickness of the rubber membrane was measured at each end of the membrane using the vernier caliper shown in Fig. 13.8. An average was taken of the thicknesses measured at both ends of the membrane. The total thickness of the top porous stone, filter paper, and top cap was also measured with the vernier caliper. This was later used in calculating the length of the specimen.

The height of the lower filter paper disc above the bottom of the triaxial cell base was measured to within 0.001 inch using the vernier caliper shown in Fig. 13.9. Measurements were taken
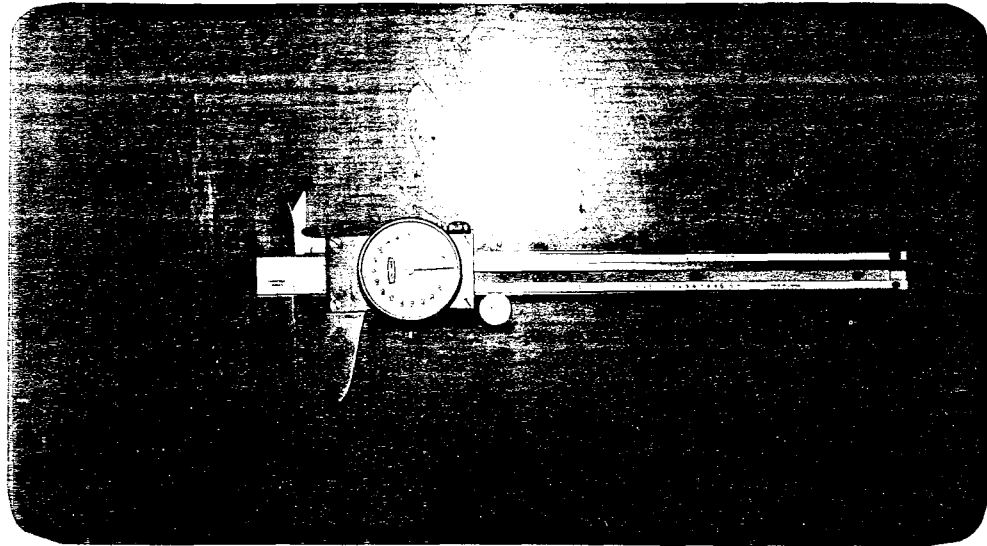
FIG. 13.8   VERNIER CALIPER USED TO MEASURE THE THICKNESS OF
THE MEMBRANE AND DIAMETER OF THE SAND SPECIMEN
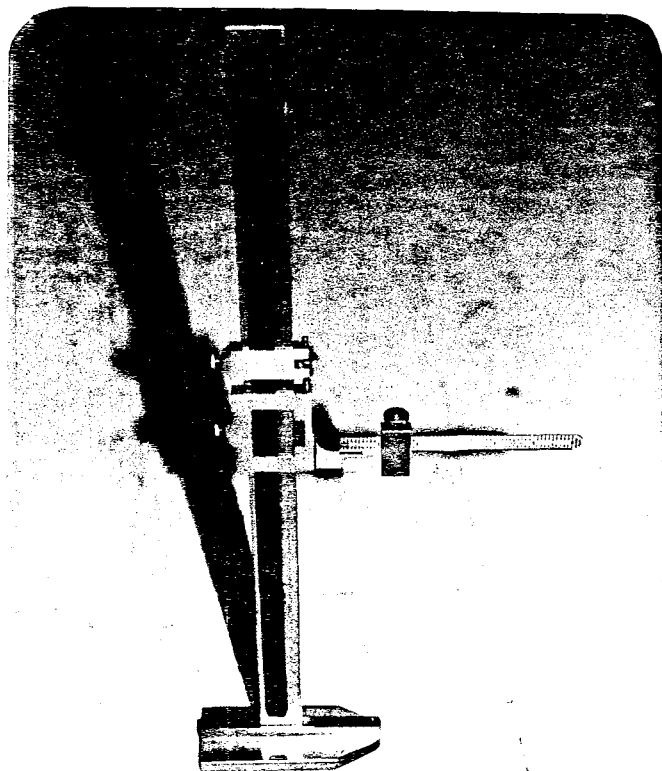
FIG. 13.9   VERNIER CALIPER TO MEASURE THE
HEIGHT OF THE TEST SPECIMEN

from three sides of the triaxial cell and their average was calculated and recorded.

The rubber membrane was carefully placed over the pedestal of the triaxial cell base as shown in Fig. 13.10 with any excess length of rubber membrane carefully folded up around the pedestal of the triaxial cell. Care was exercised such that the sides of the membrane were as vertical as possible with no unequal stretching of the membrane.

An O-ring was placed over the rubber membrane using the O-ring expander shown in Fig. 13.11. The O-ring was seated in the lower of the two grooves formed in the pedestal of the triaxial cell. This provided a water tight seal between the membrane and the pedestal of the triaxial cell.

Forming of the sand specimen was facilitated by use of the 2.020-inch diameter by 5-inch long split mold shown in Fig. 13.12. The split mold was positioned on the base of the triaxial cell with a clamp placed around the mold to hold the two halves of the mold tightly in place. A 20-inch mercury vacuum was applied to the void between the mold and the membrane. By placing four fingers within the top of the rubber membrane and equally stretching outward, the membrane was stretched over the top of the mold as shown in Fig. 13.13. With the membrane supported by the cylindrical mold a smooth inner surface of approximately 2 inches in diameter was provided.

Based on the required relative density of the specimen and the known volume of the mold, it was possible to calculate the
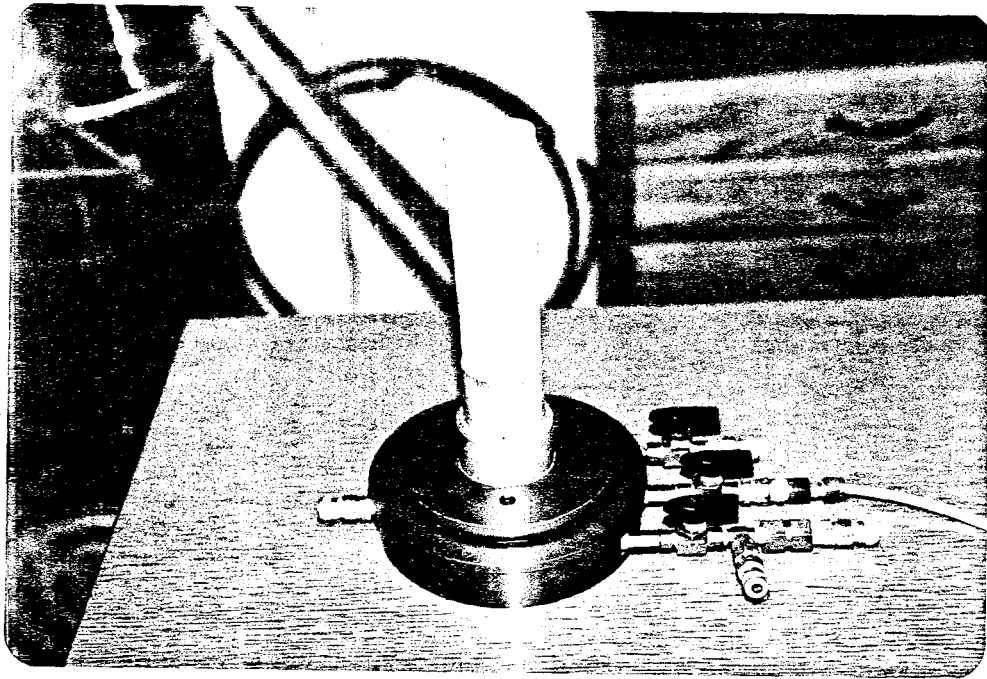
FIG. 13.10 RUBBER MEMBRANE PLACED ON THE BASE
OF THE TRIAXIAL CELL
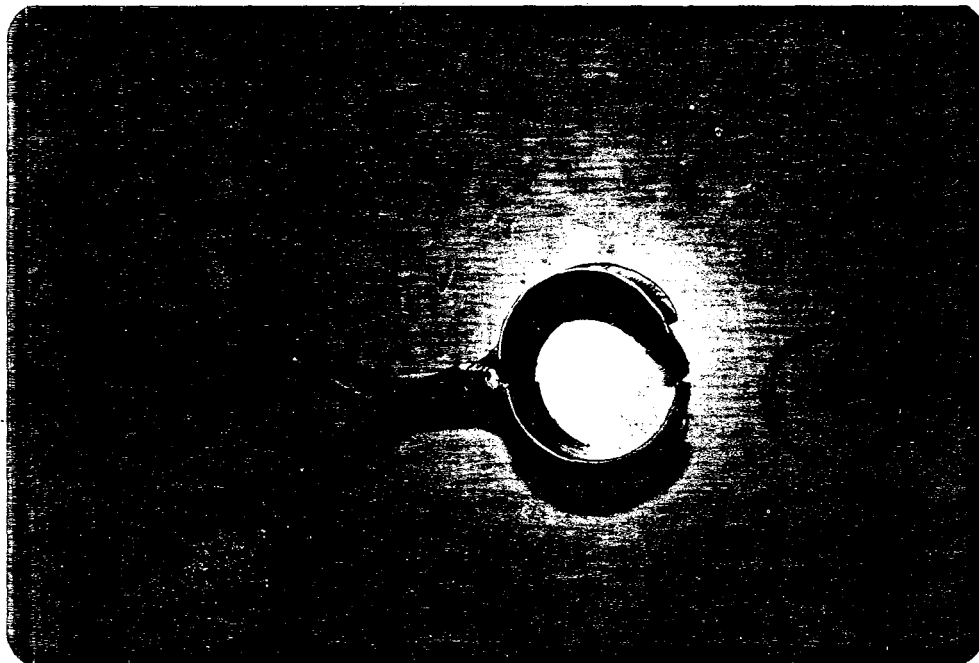
FIG. 13.11 RUBBER O-RING AND O-RING EXPANDER
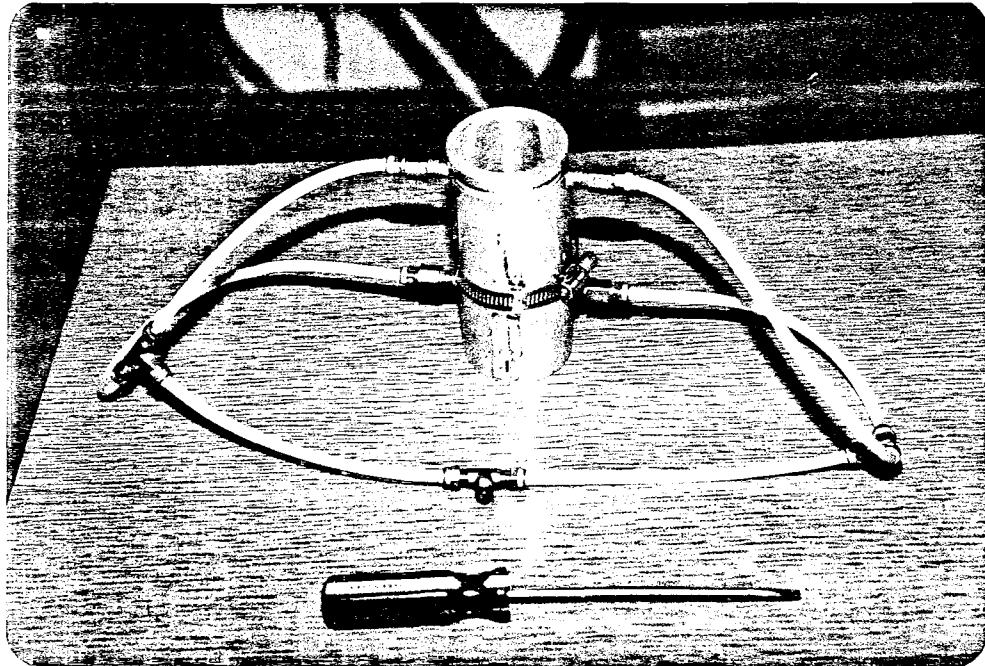
FIG. 13.12 CYLINDRICAL MOLD USED IN FORMING THE SAND SPECIMENS
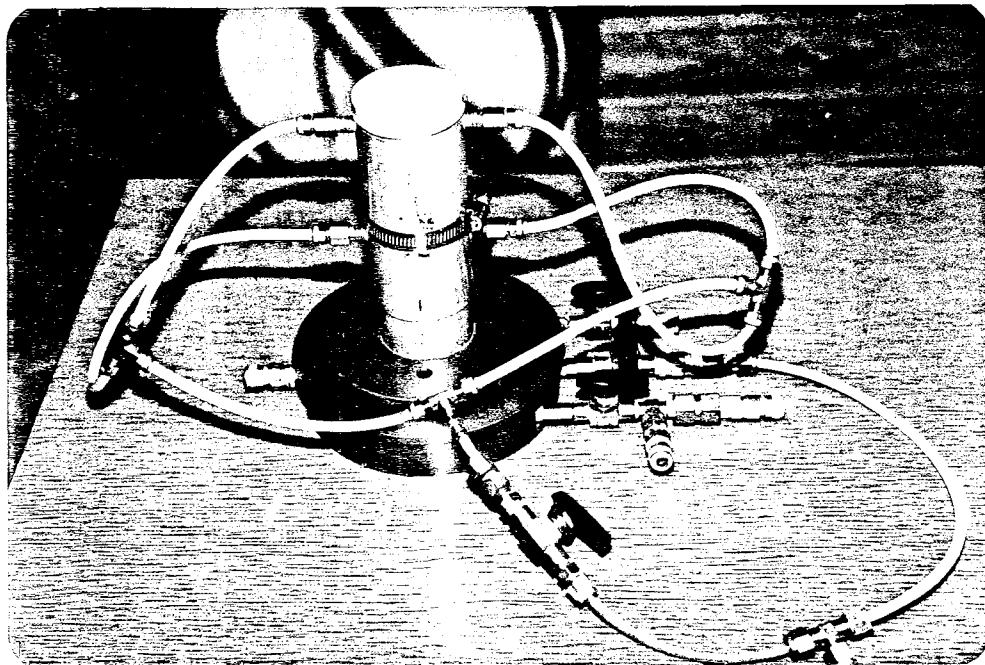
FIG. 13.13 CYLINDRICAL MOLD PLACED ON THE BASE
OF THE TRIAXIAL CELL

required weight of sand to be placed in the mold. The required

amount of sand was weighed in the Ohaus Dial a Gram Scale shown

in Fig. 13.14. This scale had a maximum capacity of 2610 grams and

and accuracy of ±0.1 gram.

A zero raining device shown in Fig. 13.15 was used in placing

the sand within the mold. The zero raining device was placed in

the mold and the sand previously weighed was poured into the zero

raining device as shown in Fig. 13.16. By slowly and smoothly

lifting up the zero raining device, the sand particles

fell through the screened opening on the end of the zero raining

device.

To ensure a direct and firm contact between the filter paper

and the bottom porous stone, a vacuum was applied to the porous

stone prior to placing any sand within the mold. After approxi-

mately 1/16-inch layer of sand was poured over the lower filter

paper disc and the edges of the filter paper disc gently tamped

with a screw driver, the filter paper disc was in all cases directly

in contact with the porous stone. The vacuum on the lower porous

stone was shut off with the remaining portion of the sand specimen

placed with the zero raining device as previously described.

Once the sand had been placed within the mold, it was necessary

to level off the top surface of the specimen so that the top porous

stone could be placed perpendicular to the longitudinal axis of

the specimen. Silver (1977) recommended that the maximum tilting

of the specimen top be limited to 0.002 times the diameter of the

specimen as shown in Fig. 13.18. Leveling of the top of the

specimen was performed by placing the top porous stone upon the
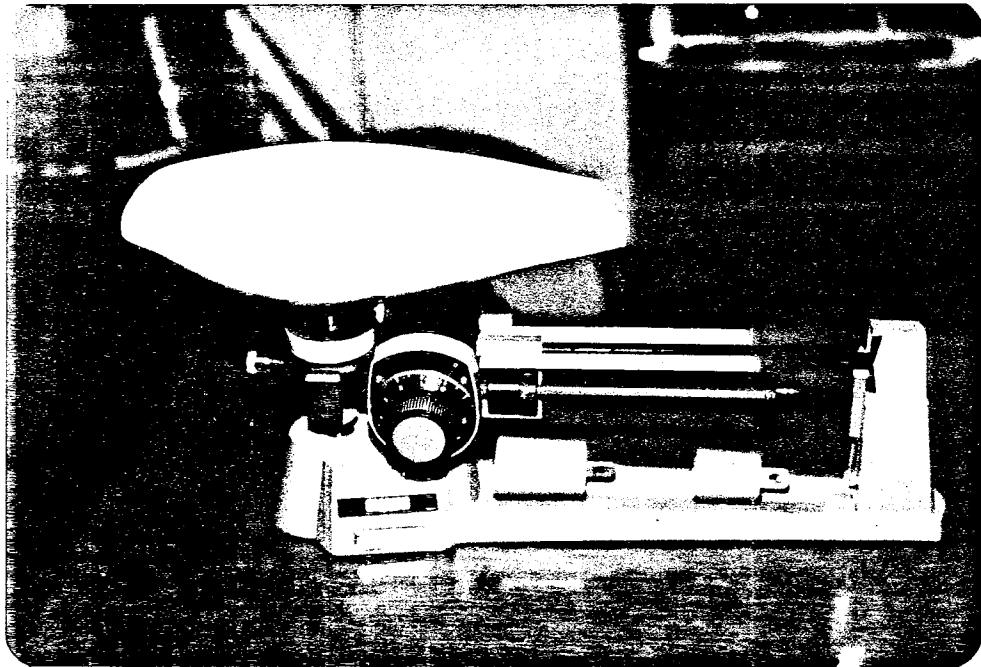
FIG. 13.14 SCALE USED TO WEIGH THE MONTEREY NO. O SAND
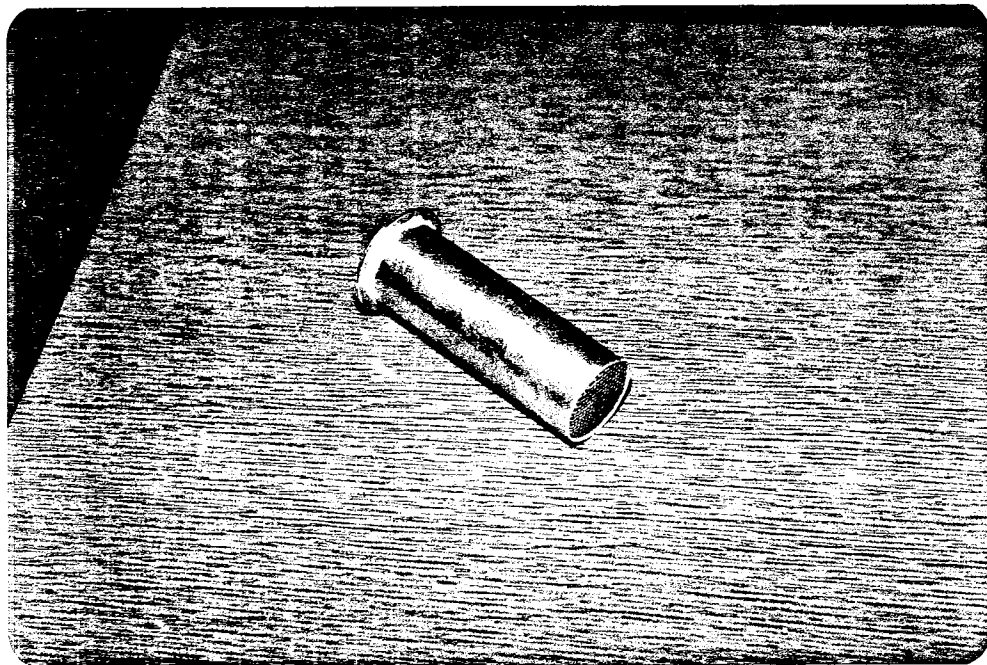
FIG. 13.15 ZERO RAINING DEVICE USED TO PLACE THE MONTEREY NO. O SAND
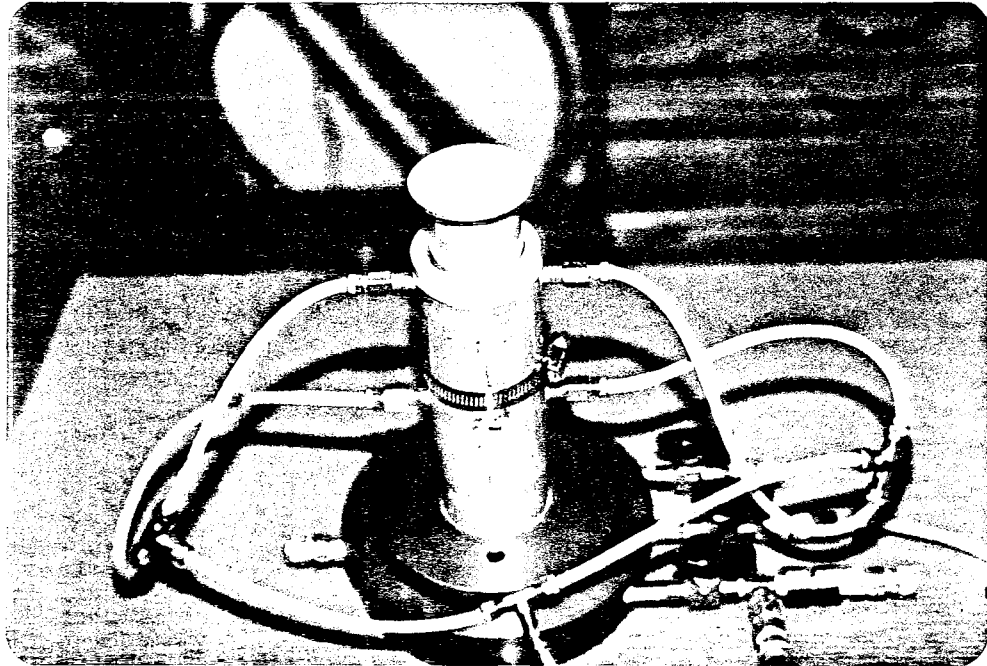
FIG. 13.16 MONTEREY NO. O SAND PLACED WITHIN THE ZERO RAINING DEVICE
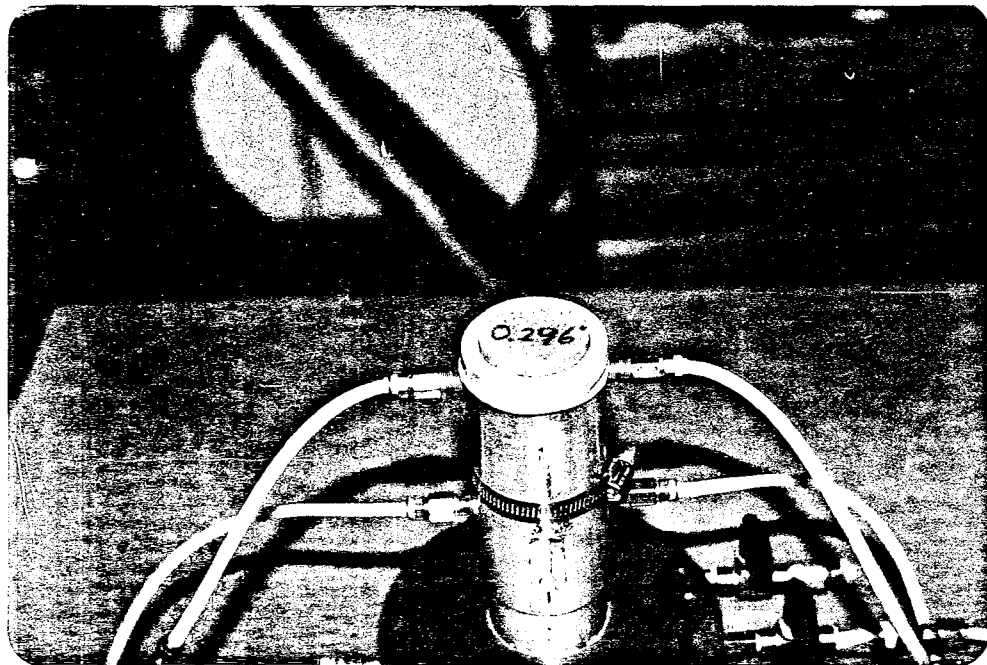
FIG. 13.17 POROUS STONE PLACED ON TOP OF THE MONTEREY NO. O SAND
            SPECIMEN

0.002D

0.002D

(B) PARALLELISM

0.002D

D

D
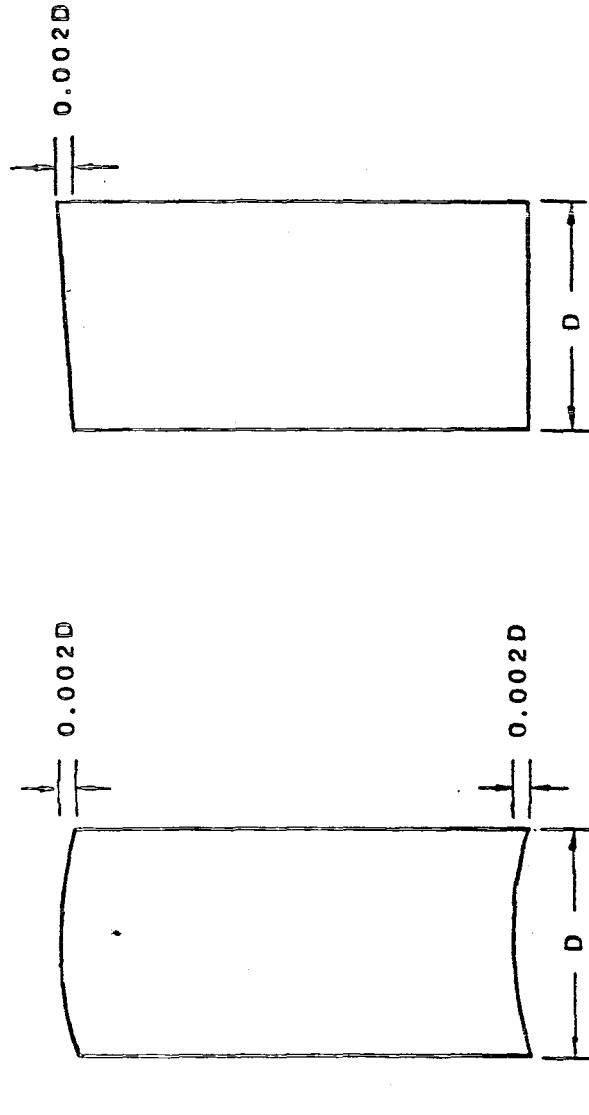
(A) FLATNESS

FIG. 13.18 REQUIREMENTS FOR FLATNESS AND PARALLELISM OF SPECIMEN ENDS (From Silver, 1977)

sand surface, and gently rotating the porous stone in a clockwise-counter clockwise direction. A filter paper disc was then placed in direct contact with the top of the sand specimen. The top porous stone was then placed on top of the filter paper disc as shown in Fig. 13.17, with a level shown in Fig. 13.19 used in positioning the porous stone parallel to the base of the triaxial cell.

Prior to placing the top cap on the specimen, the threaded stud on the top cap was lubricated with grease along with the female connection on the loading ram. Lubricating these connections facilitated the later attachment of the loading ram to the loading cap.

The top cap was positioned over the porous stone with the rubber membrane carefully pulled up around the top cap. Generally there was an excess length of rubber membrane extending above the top cap. This excess amount of membrane was folded back over itself such that there was no membrane extending above the surface of the top cap as shown in Fig. 13.20.

The top cap was checked as shown in Fig. 13.21 to assure that the top surface of the cap was parallel to the base of the triaxial cell. The plastic tubing (1/8-inch diameter) leading from the top cap was connected to the base of the triaxial cell and a 10-inch mercury vacuum (-5 psi) was applied through the back pressure line to the sand specimen. Once the vacuum had been applied to the specimen it was possible to remove the mold from around the specimen.
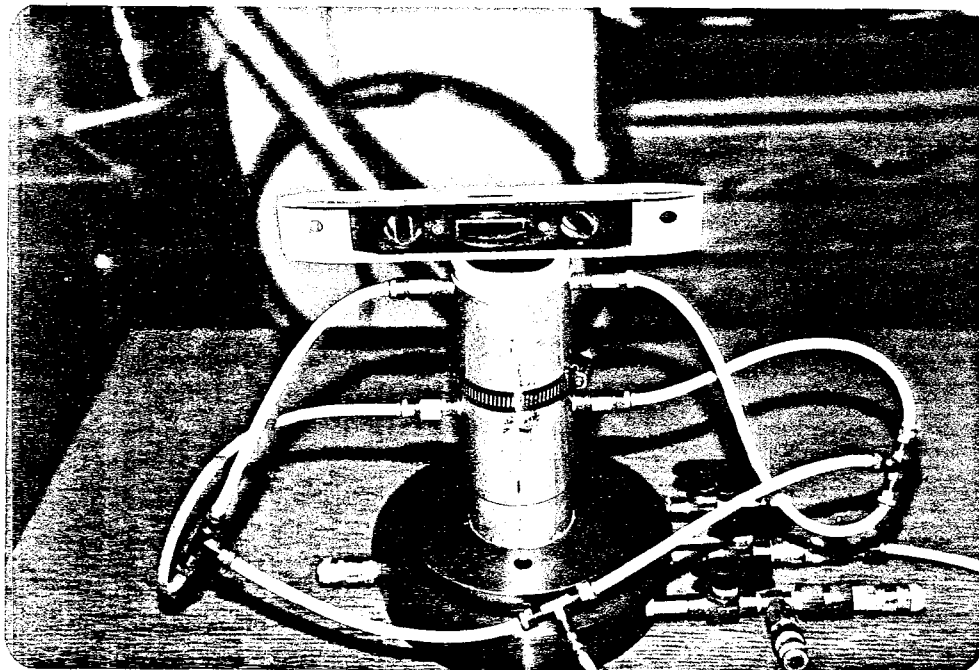
FIG. 13.19 LEVELING THE TOP POROUS STONE SO THAT THE TOP POROUS
STONE IS PARALLEL TO THE BASE OF THE TRIAXIAL CELL
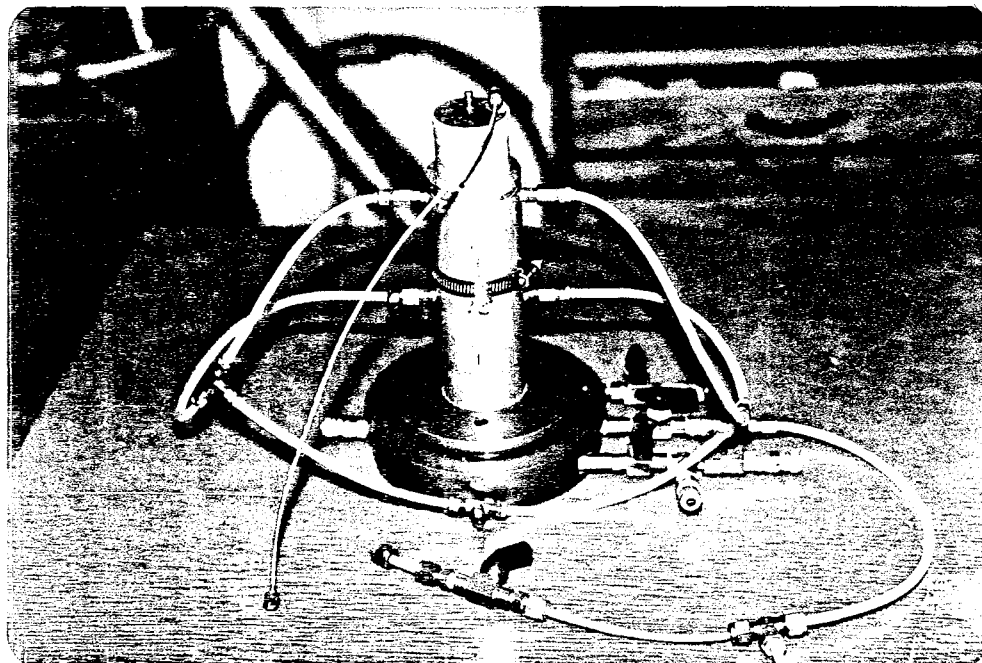
FIG. 13.20 TOP CAP PLACED ON TOP OF THE SPECIMEN WITH THE
RUBBER MEMBRANE PULLED UP AROUND THE TOP CAP

FIG. 13.21 POSITIONING OF THE TOP SURFACE OF THE LOADING CAP
PARALLEL TO THE BASE OF THE TRIAXIAL CELL
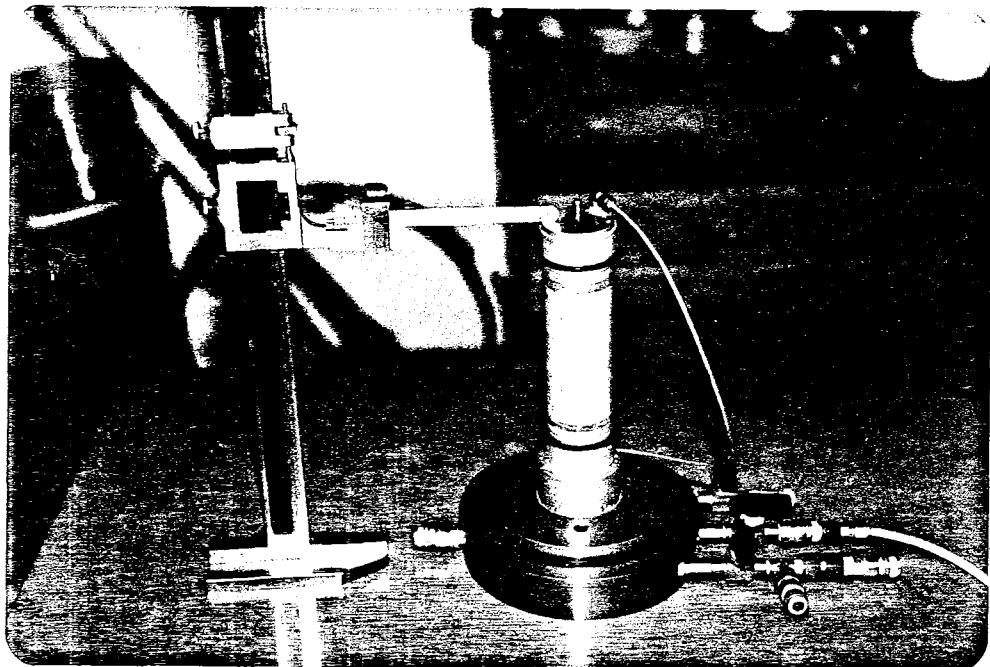
FIG. 13.22 MEASURING THE LENGTH OF THE SAMPLE USING
A VERNIER CALIPER

13.2.3 Measuring the Diameter and Length of a Specimen

The accurate measurement of the physical dimensions of the specimen is very critical as minor errors may significantly affect the calculated dry unit weight of the specimen. Extra care should be used during this step to make sure that the initial diameter and height of the specimen, D_o and H_o, respectively, are measured to an accuracy no less than ±0.001 inch.

An average diameter of the specimen must be determined following the measurement of diameters at various locations. In this research the diameter was measured twice at 90° apart between readings at the top 1/3 point, middle, and bottom 1/3 point. The average diameter was then obtained by dividing the sum of the six diameter measurements by six.

The U.S. Army Corps of Engineers (MacIver, et al., 1970) used the following equation for evaluating the average diameter:

$$D_o = \frac{D_t + 2D_c + D_b}{4}$$

where

D_o = average diameter

D_t = diameter at the top

D_c = diameter at the center

D_b = diameter at the bottom

A π-tape, a thin steel circumferential tape, was initially used to measure specimen diameters. It was found, though, that with the low specimen density, small specimen diameter, and small vacuum, the π-tape formed a groove in the specimen when it was wrapped around the specimen. Care had to be exercised so that the π-tape was placed perfectly parallel to the top cap and the

base pedestal of a triaxial cell and directly in contact with the specimen or erroneous measurements were obtained.

Due to the difficulty in obtaining accurate diameter measurements with the π-tape, a vernier caliper was used instead. While several investigators (Silver, 1977; Mulilis, 1978) have recommended against the use of a vernier caliper, our experience indicated that accurate measurements can be obtained if proper care is exercised when using a vernier caliper.

The importance of a properly measured specimen diameter on the evaluation of dry unit weight can be illustrated by the difference in dry unit weights resulting from an error in specimen diameter of only 0.01 inch. If the diameter of a 2.000-inch diameter by 4.000-inch high Monterey Number 0 sand specimen prepared to a relative density of 50% is erroneously measured as 2.01 inch an error in the dry unit weight of approximately 0.98 lb/ft^3 results. The calculated relative density of the specimen (42.9%) in this example will be approximately 7.1 percent less than the true relative density (50.0%). When this specimen is cyclically loaded it will have a greater cyclic strength than would have been estimated based on the erroneously calculated relative density.

Mulilis, et al. (1976) found that a difference in the dry unit weight of Monterey Number 0 sand of only 1.2 lb/ft^3 could result in a difference of 22-33 percent in the cyclic stress ratio required to reach initial liquefaction as shown in Fig. 13.23. It can be expected that an error in dry unit weight of 0.98 lb/ft^3 would correspondingly result in a difference of 18-27 percent in the
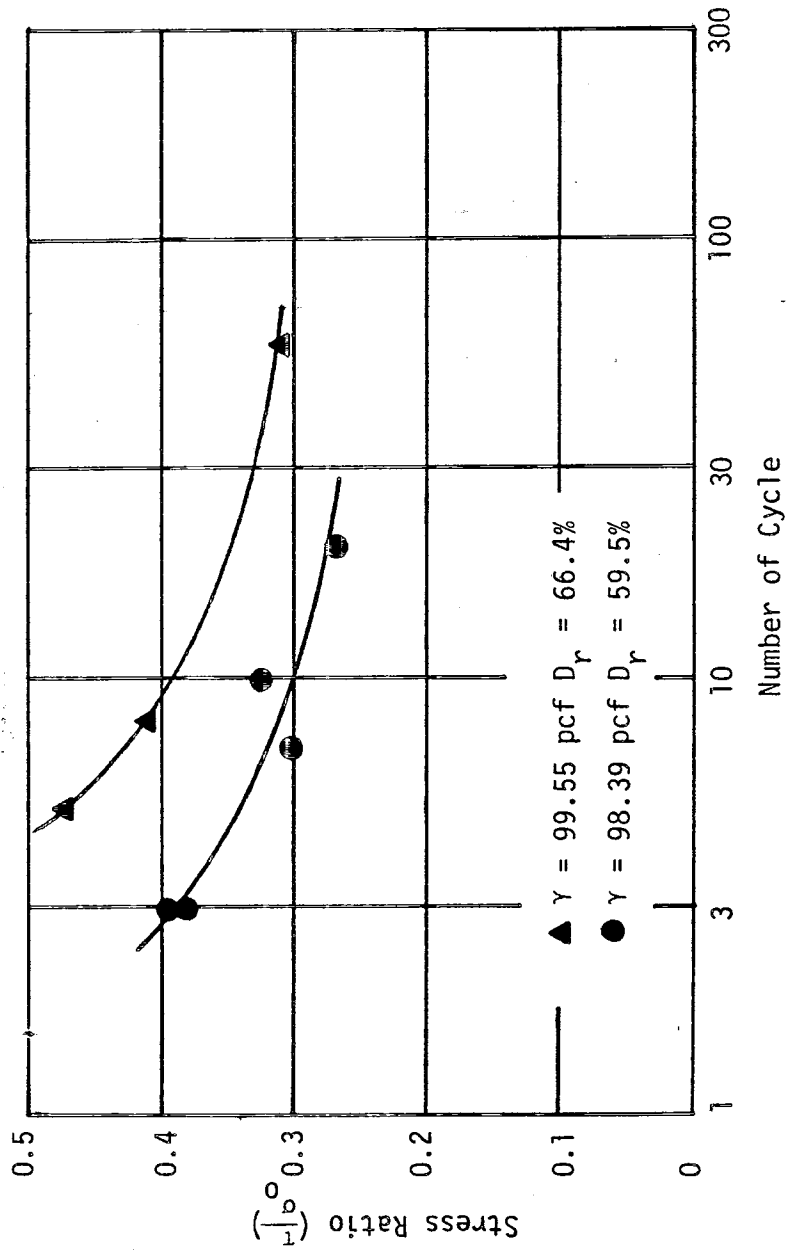
FIG. 13.23   EFFECT OF SPECIMEN DENSITY ON CYCLIC TRIAXIAL STRENGTH OF MONTEREY NO. O SAND
(From Mulilis, Horz and Townsend, 1976)

cyclic stress ratio causing initial liquefaction. Errors of this magnitude severely distort the cyclic triaxial test results and must be reduced by accurate measurements of the specimen diameter.

Careful measurements of the specimen height, H_o, should be made at four locations, 90 degrees from one another. Silver (1977) recommends that a dial gage and gage stand be used when measuring the specimen height and measurements be made to an accuracy of 0.001 inch. While a normal vernier caliper shown in Fig. 13.8 may be used to measure the specimen height, a vernier caliper with a supporting base and extension arm shown in Fig. 13.22 was used. It is believed that the measurements obtained with this instrument were of equal or greater accuracy than those obtained using a dial gage and stand.

This instrument had several advantages over the normal vernier caliper:

1. The extension arm only had to be placed in contact with the specimen cap when making a measurement as compared to a vernier caliper where both the top and bottom jaws (or arms) had to be adjusted visually.

2. Measurements had a much higher degree of accuracy as it eliminated guessing where the top and bottom edges of the porous stones were located. With the rubber membrane placed over the sample it is difficult to see through the membrane and accurately locate the porous stone edges.

3. It is very difficult to adjust each jaw of a vernier caliper such that it is lined up horizontally with the top and

bottom edges of the two porous stones. If your eyes are not looking horizontally across the jaws of the vernier caliper, an incorrect measurement will be made. In comparison with the vernier caliper shown in Fig. 13.22, alignment of the instrument is constantly maintained.

4. It is very easy to poke holes in the thin rubber membrane with the very sharp points on the jaws of the vernier caliper shown in Fig. 13.8 when measuring the specimen length. This potential is completely eliminated with the vernier caliper shown in Fig. 13.22.

Three measurements were obtained at 90° from one another with the base of the vernier caliper positioned in the same location that measurements from the top of the lower filter disc to the base of the triaxial cell were obtained as described in Section 13.2.2. By knowing the distance from the top of the lower filter paper disc to the base of the triaxial cell; thickness of top porous stone, filter disc, and top cap; and distance from the top of the top cap to the base of the triaxial cell it was possible to calculate the specimen length.

To evaluate the effect on the relative density of errors in length measurements, a calculation was made whereby the length was erroneously measured as 4.010 inch instead of the correct length of 4.000 inch. If the specimen is Monterey Number 0 sand placed at a relative density of 50%, the mistake in measuring the specimen length results in a calculated relative density of 48.2%. The error of +0.01 inch in specimen length will result in underestimating

the relative density by about 2%. It can be seen the effect is not as serious as the errorneous measurements in specimen diameter.

13.2.4 Calculation of Specimen Relative Density

The true diameter of the specimen was determined by subtracting from the average diameter of the specimen and membrane the average thickness of the membrane. Knowing the true diameter of the specimen and the measured specimen length, the specimen volume was determined. The unit weight of the specimen was determined by dividing the weight of the Denver sand placed within the mold by the specimen volume. The following equation was then used to calculate the relative density of the specimen:

$$D_r(\%) = \frac{\gamma_{d_{max}} (\gamma_d - \gamma_{d_{min}})}{\gamma_d (\gamma_{d_{max}} - \gamma_{d_{min}})} \times 100$$

where

D_r = relative density;

$\gamma_{d_{max}}, \gamma_{d_{min}}$ = maximum and minimum dry densities of the test sand; and

γ_d = dry density of the specimen.

If the relative density of the specimen was less than the required relative density, the mold was placed back around the specimen and the back pressure vacuum shut off. The side of the mold was gently tapped with the screw driver shown in Fig. 13.12 causing the sand to densify. By reapplying the vacuum, removing the mold, and remeasuring the specimen dimensions, the new relative density of the specimen could be determined. If the specimen was

still too loose, the above described procedure was repeated until
the required relative denisty was achieved. On a number of instances,
when the relative density of the specimen was greater than the
required relative density by more than 1%, the sand was poured out
of the mold and a new specimen was reformed. When the relative
density of the specimen was within ±1% of the required relative
density, no attempt was made to modify the specimen density.

13.3 Assembling the Triaxial Cell

Once the specimen had been placed to the required relative
density, the triaxial cell was assembled. The connections on the
line leading from the top cap to the base of the triaxial cell were
tightened if loose.

The base of the triaxial cell was brushed and/or wiped clean
of all sand particles. The rubber O-ring was removed from the
base and carefully wiped off with a cloth rag including the cleaning
of the portion of the triaxial cell base previously covered by the
O-ring. The O-ring was uniformly coated with a covering of high
viscosity vacuum grease and the O-ring was reseated back on the
base of the triaxial cell. It was necessary to clean and grease
the chamber and base interface. The above indicated steps on
cleaning and lubricating the triaxial cell base, chamber, and O-ring
are very important to prevent the formation of leaks between the
triaxial cell base and chamber when the cell pressure is applied.
It is equally important that the seats between the base and chamber
of the triaxial cell be cleaned of sand, to prevent sand grains from
scratching and damaging the smooth metal seal surfaces.

Before lifting the triaxial cell chamber onto the base, a check was made to make sure that the loading ram was lifted fully and secured adequately. If the loading ram is not lifted before placing the triaxial cell chamber onto the base, the loading ram could come in contact with the top loading cap and might severely disturb the specimen. Once all seals between the base and chamber of the triaxial cell had been cleaned and the loading ram lifted, the chamber of the triaxial cell was carefully placed on the triaxial cell base. The chamber was gently rocked to make sure that the chamber was tightly seated on the base and then a base clamp was placed around the base of the triaxial cell. This compression ring securely held the triaxial chamber to the base of the triaxial cell.

To help steady the top cap placed on the test specimen, the loading ram was lowered so that the ram was just in contact with the threaded stud connection on the loading cap.

13.4 Filling the Triaxial Cell with Water

Before moving the triaxial cell from the location where the specimen was formed, the back pressure valve was closed. This maintained a -5 psi effective stress on the sand specimen making it possible to disconnect the vacuum line.

A water line was plugged into the cell pressure coupling and the cell was slowly filled with water. In order for the air to escape during filling, the air vent valve at the top of the triaxial cell chamber had to be opened. Some air void was left on

top of the triaxial cell chamber when filling it with water to prevent fluctuations in the cell pressure during cyclic loading. Once the chamber was filled with water with the exception of the previously mentioned air void, the air vent valve was closed.

13.5 Specimen Saturation

A cyclic triaxial specimen should be completely saturated prior to consolidation to allow the measurement of volume changes during consolidation. Commonly the soil which liquefies is in a saturated condition below the water table. The soil specimen is saturated with water to model this field condition.

13.5.1 Flushing the Specimen with Water

A small elevated container located above the level of the sand specimen was used to saturate the sand specimen. The hydraulic gradient across the sand specimen during saturation should not exceed approximately 5 to insure that fines will not be washed out of the specimen (Silver, 1977).

Before connecting the back pressure and cell pressure lines to the triaxial cell, these lines should be free of air bubbles. This air was easily removed by connecting each line to a de-aired water supply and running de-aired water through each line expelling all air bubbles. The cell pressure line prior to entering the cell pressure valve was saturated along with the connection which was used to transmit the cell pressure to the pressure transducer.

Both the back pressure and cell pressure valves were closed when the pressure in the cell pressure line was increased to 5 psi.

Pressure in the back pressure line was 0 psi, although the effective stress in the specimen remained at 5 psi vacuum. By applying the cell and back pressures simultaneously (cell pressure valve was opened just slightly sooner than the back pressure), the cell pressure in the triaxial cell was increased to 5 psi with the back pressure in the specimen equal to 0 psi. It is desirable to minimize consolidation of the specimen during saturation; therefore, the difference between the triaxial cell pressure and back pressure did not exceed 5 psi at any time.

The back pressure line was hooked up to a small elevated water container and the back pressure valve was opened to allow de-aired water to flush through the sand specimen under a small hydraulic gradient. In order to expel the air within the specimen, a quick connection with an attached short length of tubing was plugged into the line leading to the top of the specimen. De-aired water was allowed to flush through the specimen until air bubbles were no longer observed leaving the specimen.

13.5.2 Connecting the Pore Pressure Transducer

Once the specimen had been flushed with de-aired water, it was necessary to hook up the pore pressure transducer. A four-way valve with the pressure transducer disconnected was plugged into the triaxial cell. The electrical lead on the pore pressure transducer was connected to the Tektronix Power Supply and Digital Multimeter.

Before connecting the pressure transducer to the triaxial cell, the pressure transducer output signal was zeroed. This was

accomplished by saturating the pressure transducer and then holding
the pressure transducer at the same elevation as the transducer would
be at when connected to the triaxial cell. If the output voltage
was not zero, a fine-blade screw driver was used to adjust the
Digital Multimeter until a zero reading was obtained.

All lines in the triaxial cell base had to be saturated. The
valve on the triaxial cell base controlling the line leading from
the top of the specimen was closed. By turning the four-way valve
to the back pressure position and opening the back pressure valve,
de-aired water was forced through the back pressure line in the
base of the triaxial cell. To permit full saturation of the four-
way valve, the four-way valve was rotated so that the air bubbles
flowed up through the four-way valve.

To saturate the line leading from the top of the specimen to
the four-way valve, the four-way valve was turned to this line. With
the valve in the line leading from the top of the specimen open,
de-aired water flowed through the specimen, out or the line attached
to the top cap, and through the line connected to the four-way valve
until no bubbles were observed to be coming from the sand specimen.

With all lines attached to the four-way valve fully saturated,
it was possible to connect the pressure transducer to the four-way
valve. Extreme care was required in this operation to make sure
that the transducer was not damaged. The four-way valve was opened
to the back pressure with the result that de-aired water started to
flow out of the four-way valve. The pressure transducer was
completely saturated with de-aired water flowing from the four-way

valve and then was carefully connected to the four-way valve.

Before tightening the coupling between the pressure transducer and four-way valve, a check was always made to make sure that the four-way valve was turned to the back pressure or cell pressure position. If the four-way valve is not turned to either of the previously mentioned positions, but say is turned half way between the cell pressure and back pressure position, water flow from the four-way valve when connecting the transducer may be prevented. Due to the incompressibility of water when the pressure transducer is connected to the four-way valve, the resulting high water pressure during the tightening of the transducer may rupture the diaphragm in the pore pressure transducer.

13.5.3 Raising the Cell and Back Pressure

A check was made of the water levels in the burettes connected to the cell and back pressures to make sure that the burettes were at least two-thirds full of water. When the cell pressure was raised, the air at the top of the triaxial cell chamber was compressed with the result that additional water from the cell pressure burette entered the cell. For this reason, I generally filled the cell pressure burette fully with water knowing that upon raising the cell pressure that a significant quantity of water would flow from this burette.

To assure that the specimen was not overstressed during the saturation phase, the back pressure and cell pressure were slowly increased simultaneously maintaining the cell pressure at 5 psi greater than the back pressure. It is important to slowly raise

the cell and back pressures to maintain the difference between the cell and back pressures not to exceed 5 psi. The back and cell pressures were raised to 65 and 70 psi, respectively, and the specimen was allowed to sit overnight.

13.5.4 Checking the B-Value

With the back pressure drainage lines closed, the cell pressure was increased by 9.437 psi (1 mv for the pressure transducer used). By observing the corresponding rise in the specimen's pore water pressure, Δu, it was possible to calculate the B parameter using the following equation:

$$B = \frac{\Delta u}{\Delta \sigma_3}$$

where
  B = Skempton's pore pressure parameter

  Δu = rise in pore water pressure

  $\Delta \sigma_3$ = change in cell pressure

The specimen was required to have a B parameter of greater than or equal to 0.95 before the specimen was considered satisfactorily saturated. If it turned out that the B parameter was less than 0.95, the cell and back pressures were raised while maintaining the 5 psi difference, and the B parameter rechecked after a few hours.

13.6 Consolidation of the Test Specimen

When the B parameter was greater than or equal to 0.95, the specimen was consolidated under an isotropic consolidation pressure of 30 psi. Care was used when applying the consolidation pressure

to make sure that the pore water could be gradually drained from the specimen under a slow increase in consolidation pressure as versus subjecting the specimen to a sudden jump in consolidation pressure.

The burette reading of the water table in the back pressure burette tube was noted before and a short period after application of the additional 35 psi of confining pressure.

The change in volume shown in the burette was equal to the change in volume of the saturated specimen plus the volumetric expansion of the triaxial cell, back pressure line, and pore water transducer. It was assumed that the volumetric expansion of the triaxial cell and pore water transducer was negligible.

Volumetric expansion of the back pressure line was measured by plugging the back pressure line into the pressure control panel and incrementally noting the volume change as the pressure increased. A plot of volumetric expansion versus internal pressure in the back pressure line is shown in Fig. 13.24. By subtracting the amount of volumetric expanison of the back pressure line from the measured volume change in the back pressure burette it was possible to determine the volume of the specimen after consolidation.

As can be seen from Fig. 13.24 the volumetric expansion of the polyethylene back pressure line was 0.48 cm^3 for a 30 psi increase in pressure (0.000976 in^3/psi). Volumetric expansion of this magnitude, unless corrected for, will result in significant errors in the measured volume change of the specimen during consolidation.

Silver (1977) indicated that the change in volume for all
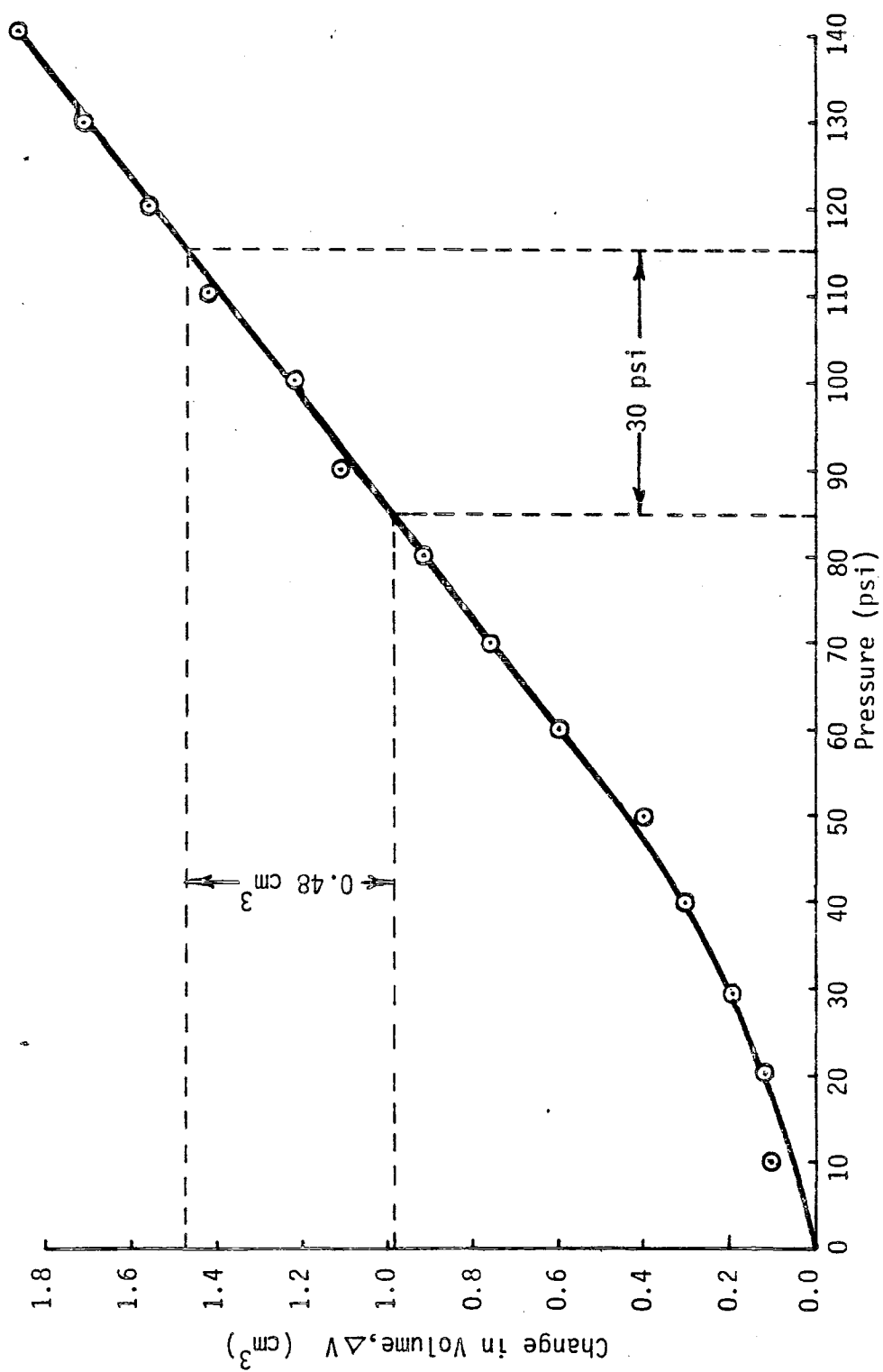
FIG. 13.24 VOLUME CHANGE MEASURED IN A 14.8 FOOT LENGTH OF 1/4 INCH DIAMETER POLYETHYLENE TUBING

assmebled components of the pore water pressure measurement system should not exceed 0.0001 in^3/psi. Short runs of stiff, small diameter metal tubing should be used to reduce volumetric expansion of the pore pressure measurement system. Rigidity of the pressure transducer and triaxial cell should also be determined.

13.7 Placing the Triaxial Cell Within the MTS Loading Frame

Following the consolidation of a test specimen, the triaxial cell was placed on the loading frame of the closed loop electro-hydraulic Materials Test System (MTS) as shown in Fig. 13.25.

The MTS machine was turned on with all reset buttons cleared. Generally this was done approximately 30 minutes before any cyclic loading was applied to the triaxial specimen, thereby permitting the MTS machine time to warm up.

Since stress controlled cyclic triaxial tests were used in this study, it is necessary to make sure that MTS was stress control tests. If the controller happened to be set on strain control and the set point control was not zeroed but instead set to apply a compressive strain, the hydraulic piston on the MTS loading frame could suddenly come down and disturb the triaxial specimen upon pressurization of the hydraulic system. For this reason, it was always necessary to make sure that the controller was on stress control and the set point control was set to lift the piston up (apply a tensile load) before starting the hydraulic pump.

"Low" pressure was initially applied to the hydraulic system for several minutes before the "High" pressure control button was
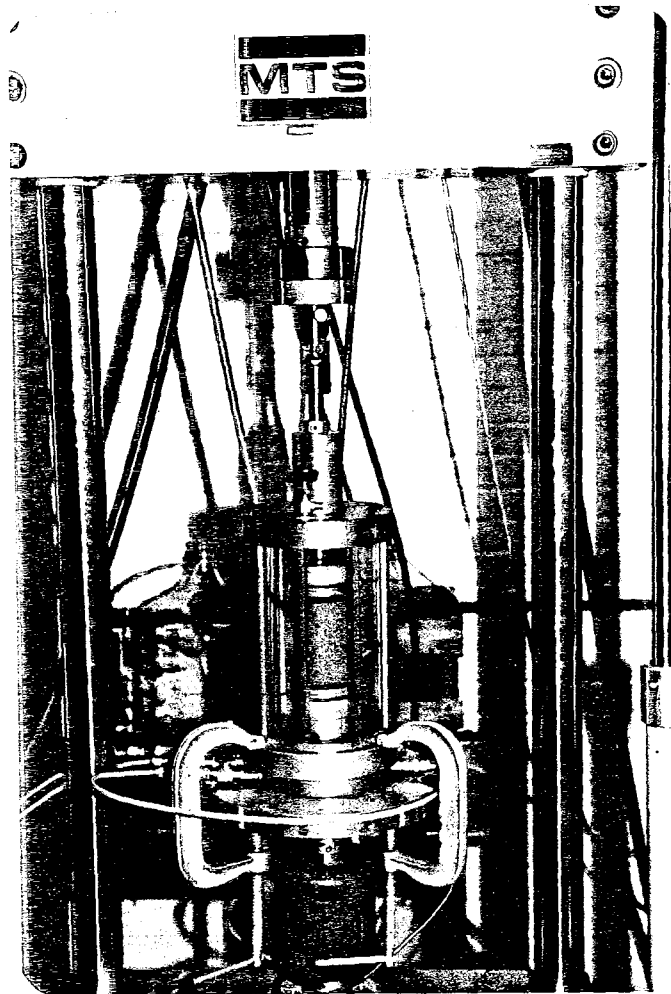
FIG. 13.25 TRIAXIAL CELL PLACED WITHIN THE
MTS LOADING FRAME

pushed to raise the hydraulic pressure from 300 to 3000 psi. By adjusting the set point control the hydraulic piston on the load frame was brought down and connected to the triaxial cell loading ram.

A universal joint was used in connecting the piston with the triaxial cell loading ram to make sure that the loading ram was not bent in case the triaxial cell was slightly off-center. By watching the ease with which the universal joint slid onto the loading ram and by close "eye-balling," it was possible to closely center the triaxial cell beneath the piston.

It was necessary to zero the SET POINT control so that the upward force on the loading ram and weight of the triaxial cell were balanced. The SET POINT control with no weight on it is zeroed at a value of 5.000. Values larger than 5.000 apply tensile loads (lift the piston up) and values less than 5.000 apply compressive loads (force the piston down). When the piston was zeroed it neither moved up nor down. To help determine if the piston was gradually moving when attempting to zero it, the X-Y recorder was utilized. Graph paper 11 x 16-1/2 inches was placed in the X-Y recorder and aligned with the recorder axes. With the POWER switch to ON and the PAPER switch to LOAD, the paper was held in contact with the recorder. Fig. 13. shows the controls on the X-Y recorder.

With the PAPER switch set on RECORD and the INPUT switch of both axes to ZERO, the pen was positioned to the desired "zero" reference point. The INPUT switches were then set to NORMAL with

PAPER
LOAD moves the carriage to the
right for paper replacement.
RECORD conditions the recorder
for normal operation.

INPUT Selects
NORMAL for external signal
ZERO for a check of pen
position without input.
SWEEP for time base signal.

CM for metric scale
IN for English scale

% OF RANGE/INCH
(1%=0.1 VOLT)
Selects one of five sensitivity
ranges for the external input.

PEN
UP lifts the pen off the paper.
DOWN lowers the pen to the paper.

SWEEP
RESET sets the sweep circuit to the
"zero" position.
START activates the sweep circuit.

RATE
Allows the selection of sweep
rate in INCHES per SECOND.

POWER
OFF removes ac power.
ON applies ac power and
illuminates switch lamp.

LOCAL/REMOTE
selects pen mode of
operation

ZERO
Adjusts no input position of pen.
Controls offset voltage for
selected portion of external
signal. Locking ring pre-
vents change of adjustment.

HIGH
LOW
GUARD
& GROUND
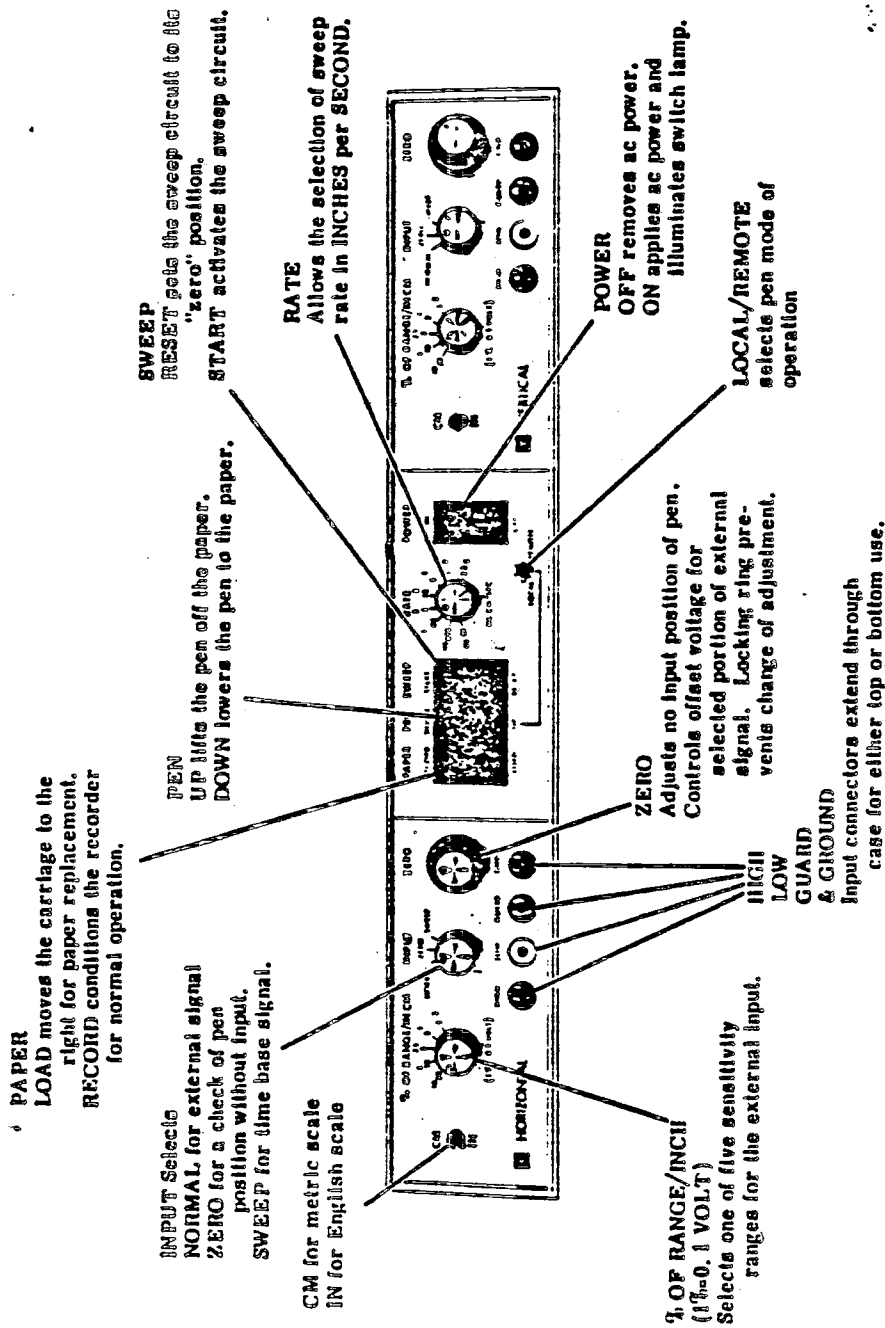Input connectors extend through
case for either top or bottom use.

FIG. 13.21   CONTROLS FOR THE X-Y RECORDER

the RANGE switches set so that the load versus deformation hysterisis could be recorded as large as possible using the 11 x 16-1/2 inch sheet of recording paper. Deformation was recorded on the X axis with load being recorded on the Y axis. By watching the horizontal movement of the pen, it was possible to determine if the hydraulic piston on the loading frame was moving.

The SET POINT control was adjusted so that the piston just started to move up and then was adjusted so that the piston just started to move down. Noting the previous two SET POINT readings and dividing the sum of the two readings by two, it was possible to determine the zero setting for the SET POINT control. With the SET POINT control set at the zero value setting, the loading ram stays at a neuturalized position and would move neither upward nor downward.

When connecting the loading ram to the triaxial specimen top cap, the back pressure valves were closed to permit the observation of the specimen pore water pressure fluctuation. By turning the SET POINT control to a value slightly less than the zero setting the loading ram was pushed down toward the loading cap. When the loading ram came in contact with the top cap, the loading ram was screwed onto the top cap until the loading ram was securely attached. An attempt was always made to limit the generated pore pressure produced while attaching the loading ram to a maximum value of 1 psi. Following attachment of the loading ram to the top cap the SET POINT control was zeroed and the piston was held in a stationary position. A pin was used to secure the universal joint to the hydraulic piston.

The back pressure valve was opened to dissipate the very small pore pressure generated during the process of engaging the loading ram and the top cap.

Three C-clamps shown in Fig. 13.25 were used to attach the triaxial cell to the pedestal of the MTS loading frame. Each of the three C-clamps were placed at 120 degrees from one another and tightened uniformly to prevent possible tilting of the triaxial cell.

13.8 Connecting X-Y and X-Y-Y' Recorders

The X-Y recorder was used for recording the load versus deformation relationship. The pen was zeroed at the center of the paper and the PEN switch was placed in the DOWN position. Vertical load was recorded on the Y axis and axial deformation recorded on the X axis. With the load control set at 10% of the range (20,000 pounds x 10% = 2,000 pounds) and the range of Y axis set at 1% of the range/ inch, the pen moved vertically one inch for each 20 pounds (1%/inch x 2,000 pounds = 20 pounds/inch). The range of X axis was set at 2% of the range/inch. With the strain controller set at 100% of the range, the pen moved horizontally one inch for each 0.100 inch of axial deformation (2% x 5 inch = 0.10 inch of axial deformation/ inch).

The specimen pore pressure with time was recorded on the X-Y-Y' recorder utilizing the X-Y' channel. Electric wires from the pore pressure transducer were connected to the X-Y-Y' recorder. Paper was placed in the recorder and the POWER switch was turned to LOAD to hold the paper in place.

By adjusting the X ZERO control, the pen was moved to the

far left of the paper with the pen lined up with the left edge of the graph paper. The X RANGE switch was set to SWEEP with the SWEEP RATE switch set based on the anticipated amount of time required to run the cyclic triaxial test.

The Y' RANGE switch was set at 1 mv/inch. Maximum change in pore water pressure to occur in the specimen during cyclic loading would be 30 psi because of the confining pressure being 30 psi. Knowing that the particular pressure transducer used has a change in output voltage of 1 mv/9.437 psi, the output voltage would change 3.18 mv for a 30 psi rise in the specimen's pore water pressure. This change in voltage of 3.18 mv would move the Y' pen vertically 3.18 inches. Knowing that the Y' pen could move a maximum of 3.18 inches vertically, the pen was zeroed four inches from the top of the paper with the four-way valve on the triaxial cell turned to the back pressure line.

A small tick mark was made to show the zero pore pressure reference line by moving the POWER switch to PEN (moves pen down) and the pen moved in the X direction by utilizing the START switch. When a short tick line had been drawn the pen was moved back to its original starting point by flipping the switch from START to RESET.

To show the vertical location of 30 psi on the Y' recorder, the four-way valve was turned from the back pressure line to the cell pressure, an increase in pressure of 30 psi. A tick mark was made on the graph paper in the same manner as described in the previous paragraph and then the four-way valve was turned back to monitor the specimen back pressure.

The X-Y-Y' recorder was used to record the vertical deforma-
tion of the specimen with time. Electrical leads plugged into the
MTS controller chassis transferred the voltage output from the
transducer conditioner connected to the LVDT to the Y-axis of the
recorder. One of these leads was plugged into the controller
chassis immediately to the right of the STROKE LOWER LIMIT light
with the second lead plugged in a ground. The lead other than the
ground was plugged into the HIGH connection on the Y axis of the
X-Y-Y' recorder with the ground lead plugged into the LOW connection.

The Y pen was zeroed over a horizontal line on the graph paper
and a tick mark was made as previously described for the Y' pen. If
the tick mark was not perfectly centered on the line a minor adjust-
ment was made in the pen and a new tick mark was drawn.

13.9 <u>Determination of Cyclic Load to be Applied to the Specimen</u>

All cyclic triaxial tests were performed at controlled stress
ratios with the stress ratio being defined in the following equation:

$$S.R. = \frac{\sigma_{dc}}{2\bar{\sigma}_3}$$

where
        S.R. = stress ratio;

        σ_{dc} = average single amplitude cyclic deviatoric

            stress = $(\sigma_1 - \sigma_3)$ cyclic; and

        $\bar{\sigma}_3$ = initial effective confining pressure.

By knowing the required stress ratio and the effective
confining pressure on the specimen (30 psi) it was possible to
calculate the required average single amplitude cyclic deviatoric

stress (15 psi). The cyclic single amplitude load was determined by multiplying the consolidated area of the specimen by the required single amplitude cyclic axial stress.

The SPAN control, located immediately to the right of the SET POINT control on the MTS control panel, was used to adjust the amplitude of the axial load command signal originating in the function generator.

The SPAN control on the MTS machine is calibrated so that the peaks of the input function drive the controlled load amplitude to 100% of the operating range, i.e., 20,000 pounds tension and 20,000 pounds compression, when the control is set at 1000. The dial setting for the SPAN control to provide a desired dynamic loading amplitude can be determined by either of the following two methods:

1. The MTS Instruction Manual gives the following equation for determining the SPAN control setting:

$$SPAN = \frac{(P_{max} - P_{min})f}{OR}$$

where

P_{max} = maximum value of the controlled variable (most positive or least negative);

P_{min} = minimum value of the controlled variable (least positive or most negative);

f = scale factor of the input funtion = 500, for functions varying between ±100% = 1000, for functions varying between zero and +100% or -100% ; and

OR = Operating Range.

The following example illustrates the use of this equation in calculating the SPAN setting:

With the consolidated area of the specimen, A_c = 3.141 in^2, S.R. = 0.25, $\overline{\sigma}_3$ = 30 psi, the load control set at 10% of the operating range, then the SPAN setting for the cyclic sinusoidal load to be applied to the specimen can be determined as follows:

σ_{dc} = S.R. x $2\overline{\sigma}_3$ = 0.25 x 2 x 30 psi = 15 psi;

P_{max} = σ_{dc} x A_c = 15 psi x 3.141 in^2 = 47 lbs;

P_{min} = $-P_{max}$ = -47 lbs.;

f = 500;

OR = 20,000 x 10% = 2,000; and

$$\text{SPAN} = \frac{[47 - (-47)]\ 500}{2000} = 23.5.$$

Therefore, the SPAN dial when set at a scale reading of 23.5 would apply a cyclic loading of ±47 pounds.

2. The second method for determining the SPAN setting is to divide the programmed operating range of the controlled variable by the number of dial divisions on the SPAN control. For example if the operating range of the controlled variable is ±2000 pounds as in the above example and the number of SPAN dial divisions is 500, each SPAN dial division equals four pounds of single amplitude cyclic load. Thus, to apply a single amplitude cyclic load of 47 pounds, the SPAN dial would be set on 11.75 divisions (47 lbs/4 lbs per division = 11.75 divisions).

Since there are only 500 divisions on the SPAN control
for the full scale reading of 1000, each scale division
is equal to a scale reading of 2. The SPAN Dial would be
set at a scale reading of 23.5 (11.75 divisions) which
is the same SPAN setting as determined by the first
method.

13.10 Data Reduction

13.10.1 Specimen Length and Diameter after Consolidation

Before the magnitude of cyclic load to be applied to each
specimen could be determined, it was necessary to determine the
consolidated diameter and length of the specimen. When calculating
the specimen consolidated diameter and length, an assumption was
made that the sand specimen was isotropic; that is the stress-strain
relations were the same regardless of the orientation of the axes
on which the stress-strain relations were measured. If this assump-
tion is accepted, it is possible to write the following two simul-
taneous equations from which the consolidated diameter and length
can be determined:

$$L_i \cdot \frac{\pi D_i^2}{4} - \Delta V = L_c \cdot \frac{\pi D_i^2}{4}$$

$$\frac{L_i}{L_c} = \frac{D_i}{D_c}$$

where

ΔV = change in volume during consolidation, $V_i - V_c$,

V_i = initial specimen volume,

V_c = specimen volume after consolidation,

L_i = initial specimen length,

L_c = length of specimen after consolidation,

D_i = initial specimen diameter, and

D_c = specimen diameter after consolidation.

Knowing the diameter after consolidation, and the selected stress ratio as defined in Section 13.9, the single amplitude for a cyclic load test can be determined. From the volume change at the completion of consolidation, the specimen volume and relative density before the commencement of the cyclic loading test can be calculated.

13.10.2 <u>Stress Ratio versus Number of Stress Cycles Causing Initial Liquefaction</u>

Each sample was subjected to the cyclic triaxial test under a selected stress ratio R_s after full consolidation and saturation. The cyclic stress versus deformation, excess pore water pressure and axial deformation versus number of stress cycles were recorded throughout a test. The records are shown in Figs. 14.4.a, b, and c. From this record, the number of stress cycles causing initial liquefaction, N_L, is determined. N_L is defined as the number of stress cycles required to cause the excess pore water pressure to be equal to the initial effective confining pressure.

As can be observed in Fig. 14.4.a, the cyclic stress amplitude decreases somewhat at the onset of liquefaction where the sample axial deformation increases. This occurred before the initial liquefaction and when the excess pore water pressure equals approximately two thirds of the initial effective confining pressure. This stress amplitude reduction necessitates an empirical adjustment of N_L to a number smaller than the number of stress cycles causing

the excess pore water pressure to equalize the initial effective confining pressure. This adjustment was based on the degree of load amplitude reduction as the sample approached the initial liquefaction.

The number of stress cycles causing initial liquefaction, N_L, as evaluated in the previous paragraph paired with the selected stress ratio, R_S, under which the cyclic triaxial test was conducted formed a data point on the R_S versus N_L space. Four data points are usually required to satisfactorily define the R_S versus N_L curve. After a minimum of four cyclic triaxial tests on samples of a certain gradation were conducted, R_S versus N_L curve was then constructed.

CHAPTER 14

ANALYSIS OF TEST RESULTS AND DISCUSSION

14.1 Correction of Relative Density

A total of 123 cyclic triaxial tests were performed using the
sample preparation and testing procedures described in Chapter 13.
From the experience of previous works, it is known that to prepare
the sample at an exact relative density was extremely difficult.
Although a relative density of 50% was targeted, the relative
density achieved for the specimen used in this study ranged from
49.6% to 59.3%. To investigate the effect of grain size distribu-
tion characteristics on liquefaction, the same base relative density
must be used. A test program was then carried out to investigate
the effect of small differences in relative density on the cyclic
strength of a saturated sand. The test results are discussed
in the following paragraphs. This resulting information was then
used to adjust the cyclic stress ratio of each specimen to the
magnitude corresponding to that of the base relative density of
50%.

The medium sand samples with the median grain size, D_{50} = 0.38 mm
and Cu = 2.2,were chosen for this correction study. This soil was
designated DM-d_2 in Table 13.2. Three groups of samples were
prepared to achieve the relative density of 50.3%, 55.7% and 60.7%,

respectively. Each group contains five samples. All samples were back pressured to achieve the Skempton pore water pressure parameter B of no less than 0.95 and consolidated under a 30 psi consolidation pressure before cyclic triaxial tests. The test results are shown in Fig. 14.1. From Fig. 14.1 the stress ratios causing the initial liquefaction in 5, 10, 20, 40 and 100 cycles were determined. The resulting stress ratios were then plotted against the relative density in Fig. 14.2. This relationship was found to be linear. However, these straight lines do not pass through the origin (zero stress ratio and zero relative density) as reported by Seed, et al. (1967). A similar conclusion was also reported by Mulilis, et al. (1978).

To correct the cyclic strength of samples with the relative density ranging from 50% to 60%, correction factors plotted with respect to the number of cycles causing initial liquefaction are shown in Fig. 14.3. These factors basically are the slopes of the straight lines in Fig. 14.2 at each stress cycle to cause initial liquefaction. It was assumed that the results obtained for soil DM-d_2 are applicable to all other samples. The cyclic stress ratio (R_s) at the relative density higher than 50% was, therefore, corrected by using the following equation:

$$(R_s)_{50\%} = R_s - (D_r - 0.5) \times R$$

where
$(R_s)_{50\%}$ = stress ratio to cause initial liquefaction at 50% relative density;

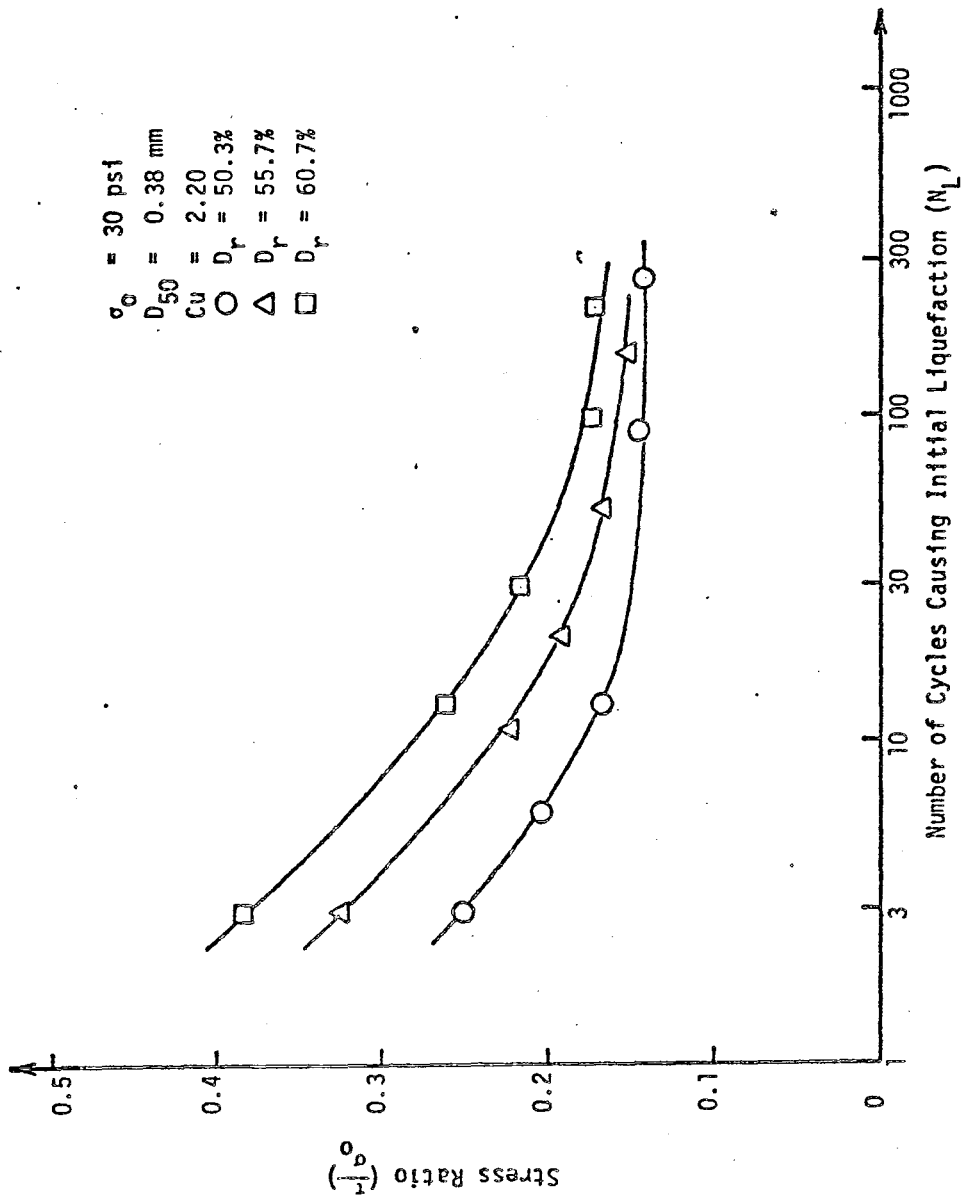R_s = stress ratio to cause initial liquefaction in the test;

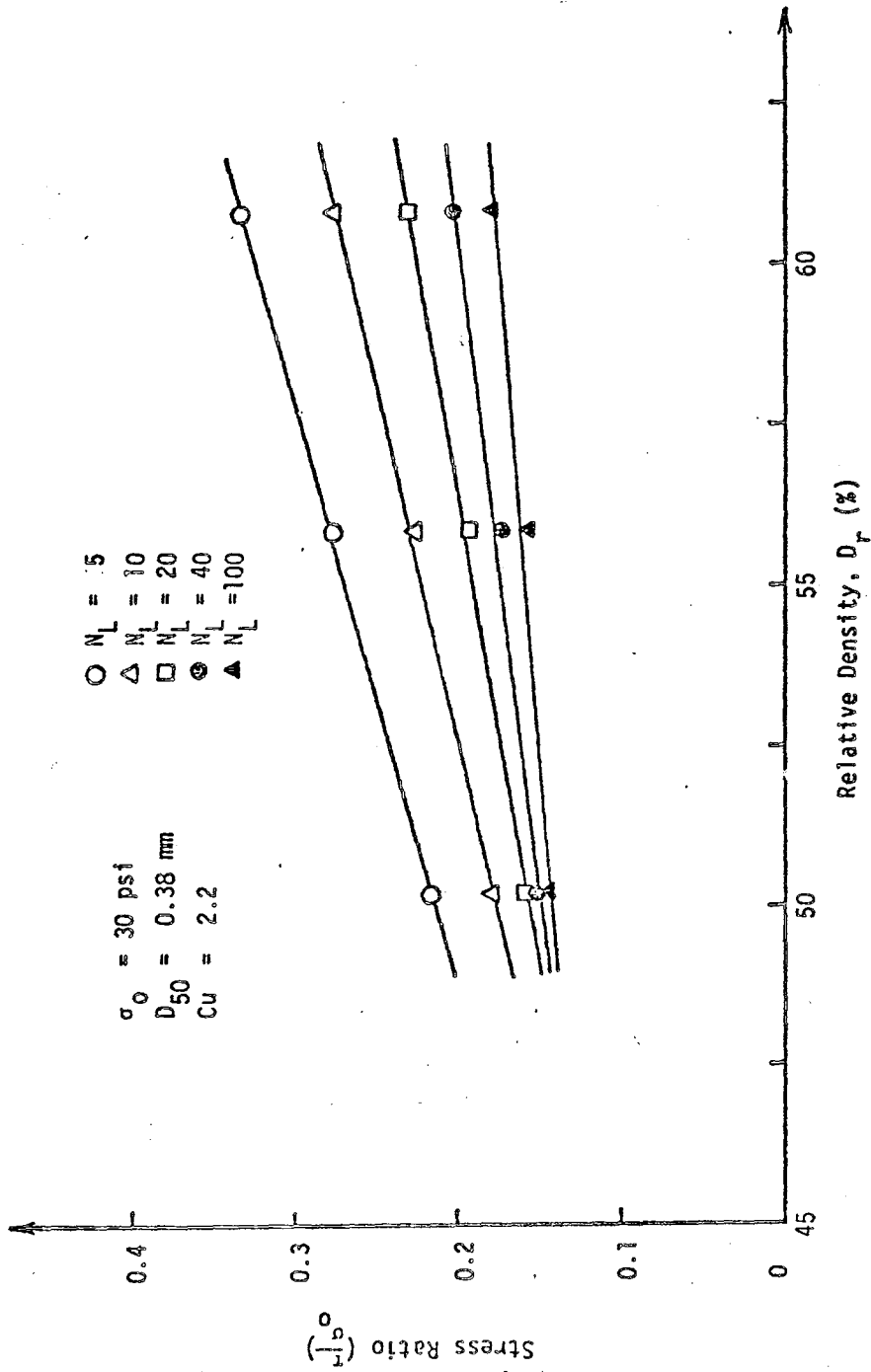FIG 14.1 EFFECT OF RELATIVE DENSITY ON DENVER SAND

FIG. 14.2 EFFECT OF RELATIVE DENSITY ON LIQUEFACTION POTENTIAL
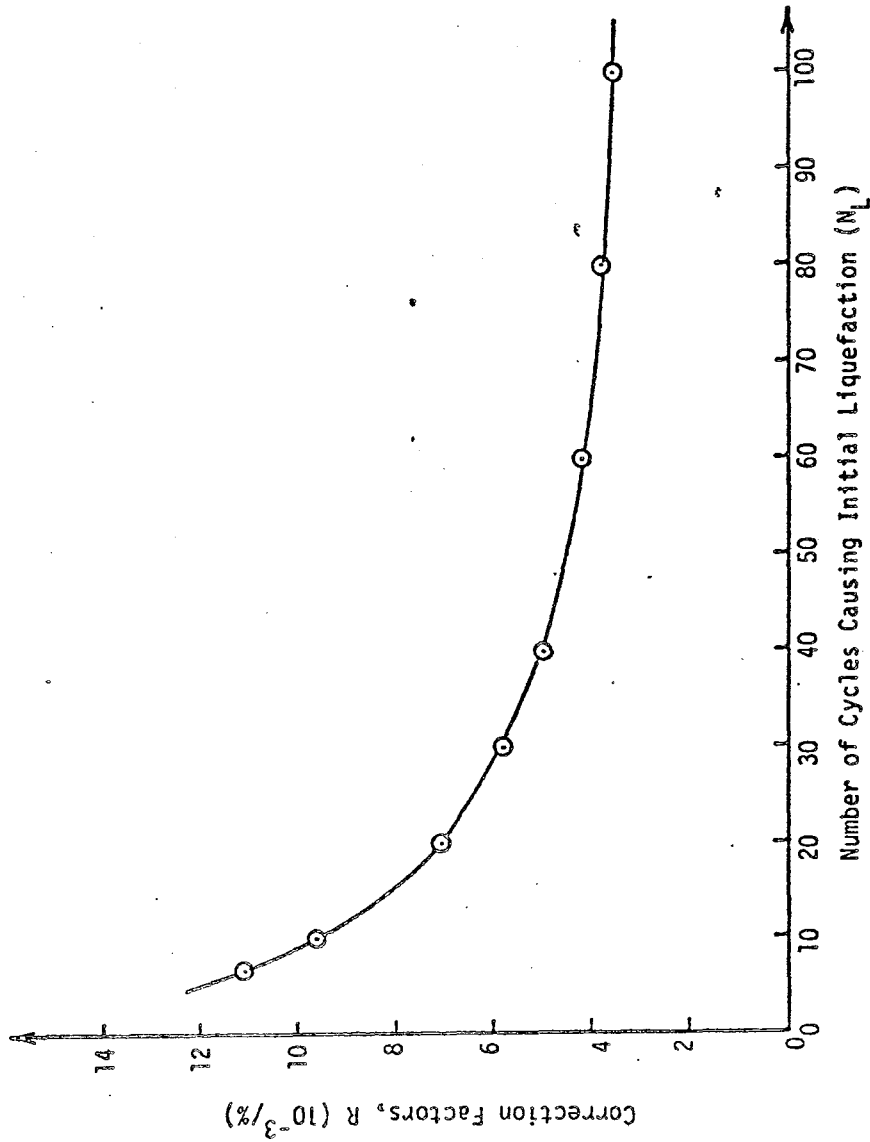OF DENVER SAND AT DIFFERENT STRESS CYCLES

296

FIG.14.3   CORRECTION FACTORS VERSUS NUMBER OF CYCLES CAUSING
          INITIAL LIQUEFACTION

$$D_r = \text{relative density, in decimal, of the sample}$$

tested; and

$$R = \text{correction factor from Fig. 14.3.}$$

14.2 General Test Results

After the completion of a cyclic triaxial test, the specimen was subjected to sieve analysis to check its grain size distribution characteristics. Compared with the designed gradation shown in Fig. 2.4, some changes in distribution characteristics were observed. The gradation curves all shifted somewhat toward fine side. This could be attributed to the washing of samples.

Records obtained from a typical cyclic triaxial test on a medium uniform sand at a low stress ratio are shown in Fig. 14.4. The same general shape of test record was observed from all cyclic triaxial tests. From the figure, it was observed that a hysteresis loop was formed for each loading cycle and that as the number of cycles of loading increased, the shear modulus decreased, the damping ratio increased, and the hysteresis loop increased in size. However, the study of the general dynamic behavior of the saturated sand with different grain size distribution characteristics is beyond the scope of this study.

The pore pressure generated during the application of cyclic load increased steadily until it reached a value of approximately two-thirds of the initial effective confining pressure. The rate of pore water pressure generation became increasingly large afterward. The sample deformation was also found to increase rapidly.
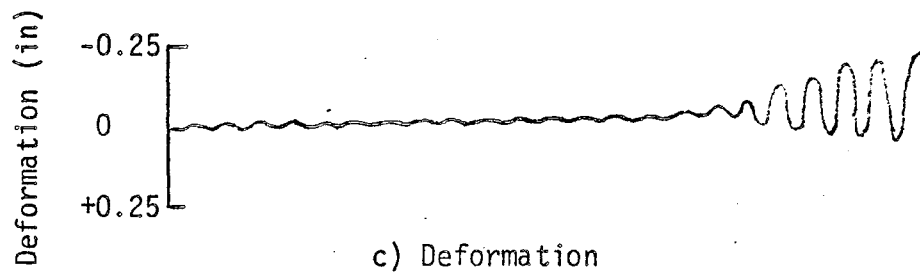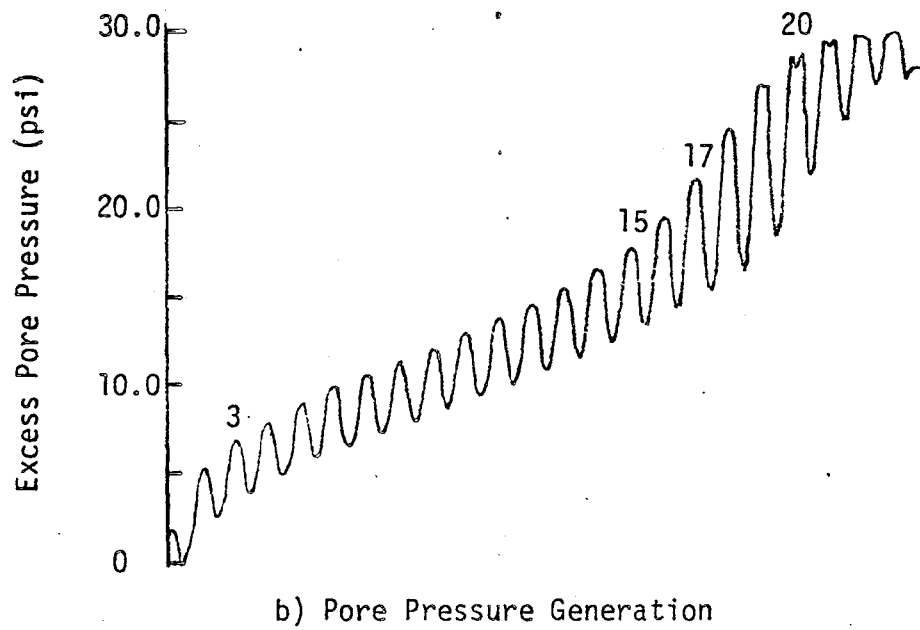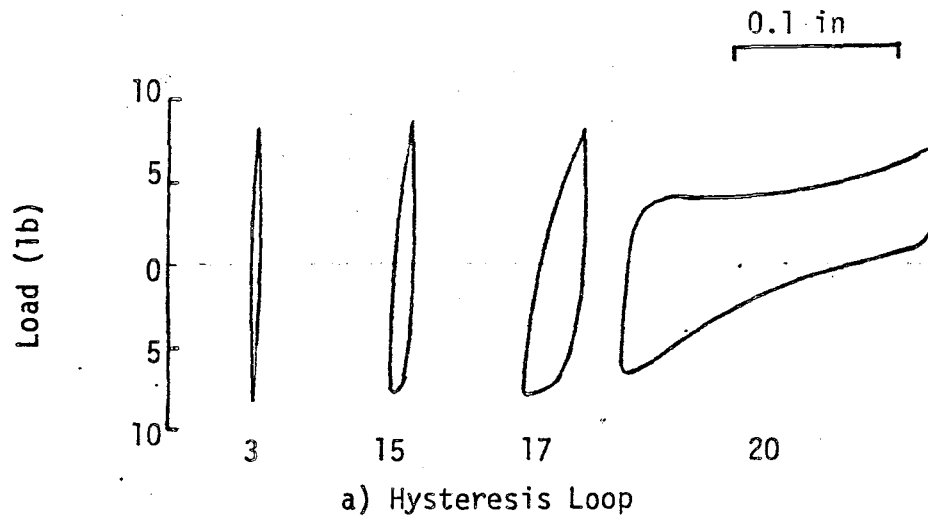
FIG. 14.4 TYPICAL RECORDED DATA

The upper bound of the pore pressure curve as shown in Fig. 14.4 is interestingly found to be similar to a creep curve in shape. A pore pressure generation similar to tertiary creep was initiated after the excess pore pressure reached a value of two-thirds of the initial effective confining pressure. Therefore, an empirical equation similar to a creep function can be formulated to evaluate excess pore pressure generation under cyclic loading.

14.3 Effect of Mean Grain Size

Results of the cyclic triaxial tests performed on the samples with different mean grain sizes and uniformity coefficients ranging from 1.9 to 16.0 are presented in Figs. 14.5 to 14.9. In each graph, the test results of samples with similar uniformity coefficients were presented. As the data indicated, if the small variation in uniformity coefficients of the samples is disregarded in each figure, the effect of mean grain size on the liquefaction potential of sands was found to be significant. The dynamic strength of the samples with large mean grain size, D_{50}, was found to be stronger than those of the samples with small D_{50}. Samples with D_{50} within the range of fine sands are the weakest among the soils investigated.

Stress ratios needed to cause the initial liquefaction at the tenth and thirtieth cycles were plotted against the logarithm of the mean grain size. As shown in Figs. 14.10 and 14.11, with the uniformity coefficient ranging from 1.9 to 16.0, the overall cyclic strength of samples containing a small amount of fine gravel size particles was found to be about two times as strong as the cyclic

FIG. 14.5 EFFECT OF MEAN GRAIN SIZE ON INITIAL LIQUEFACTION

FIG. 14.6 EFFECT OF MEAN GRAIN SIZE ON INITIAL LIQUEFACTION
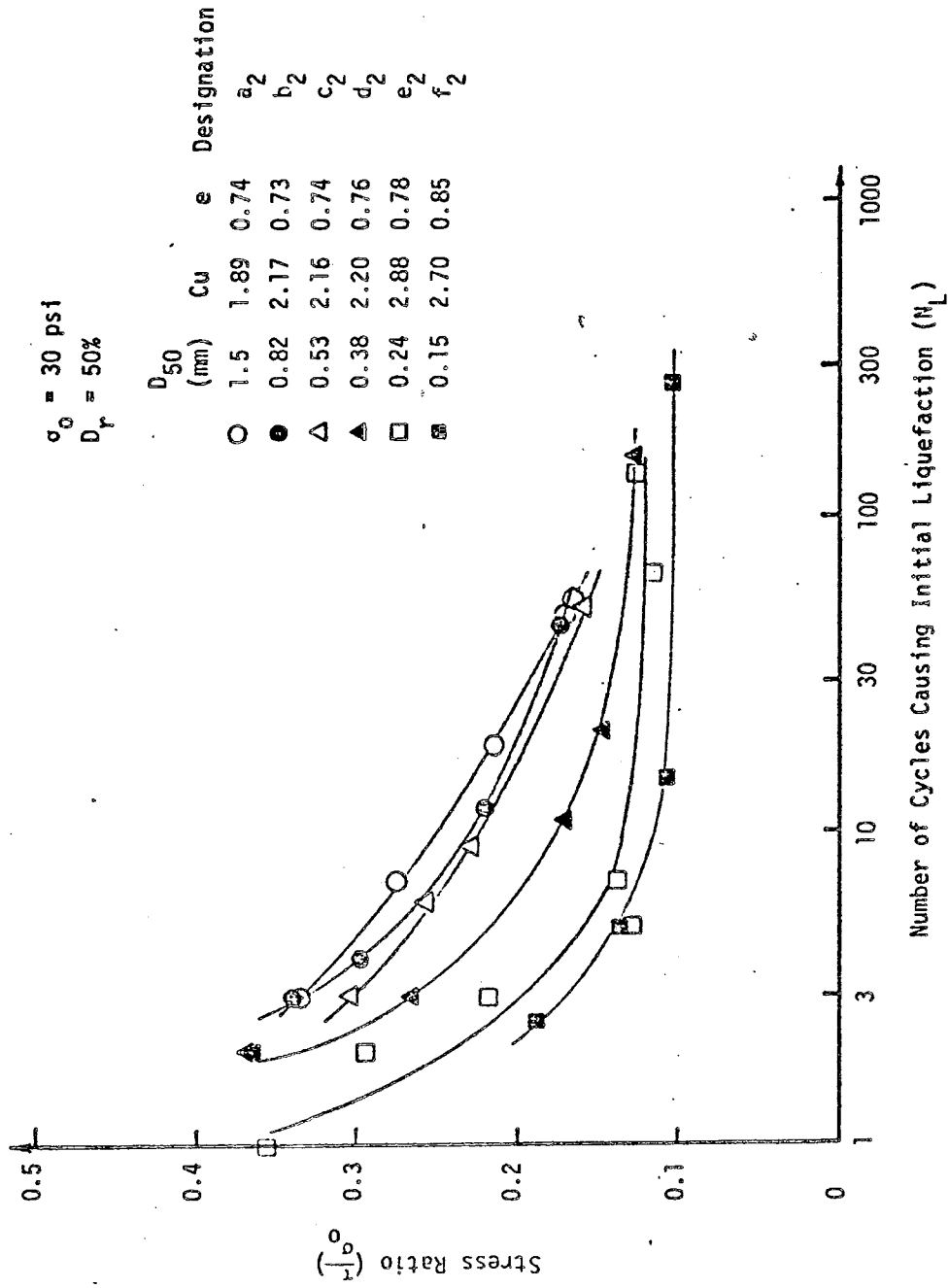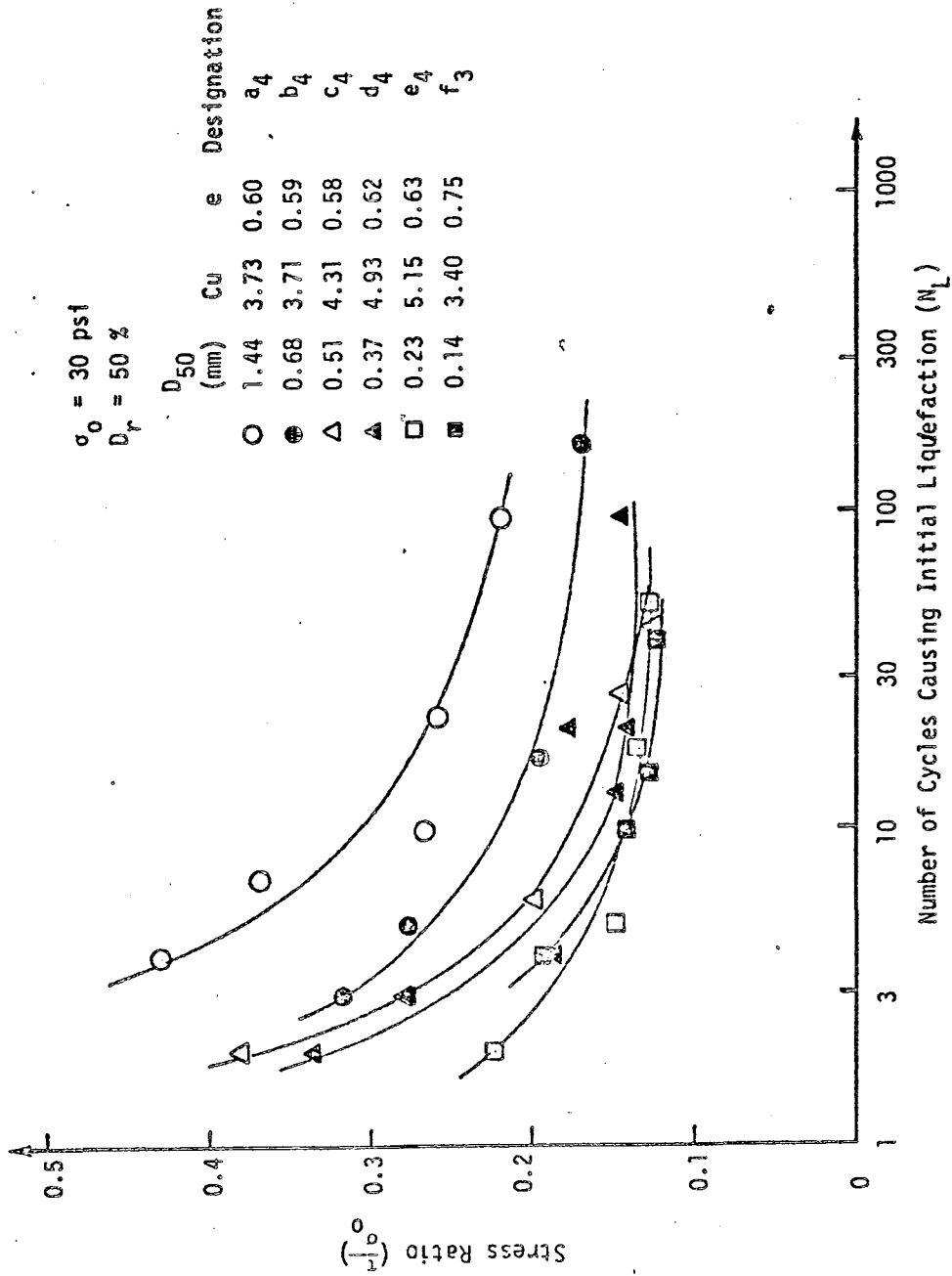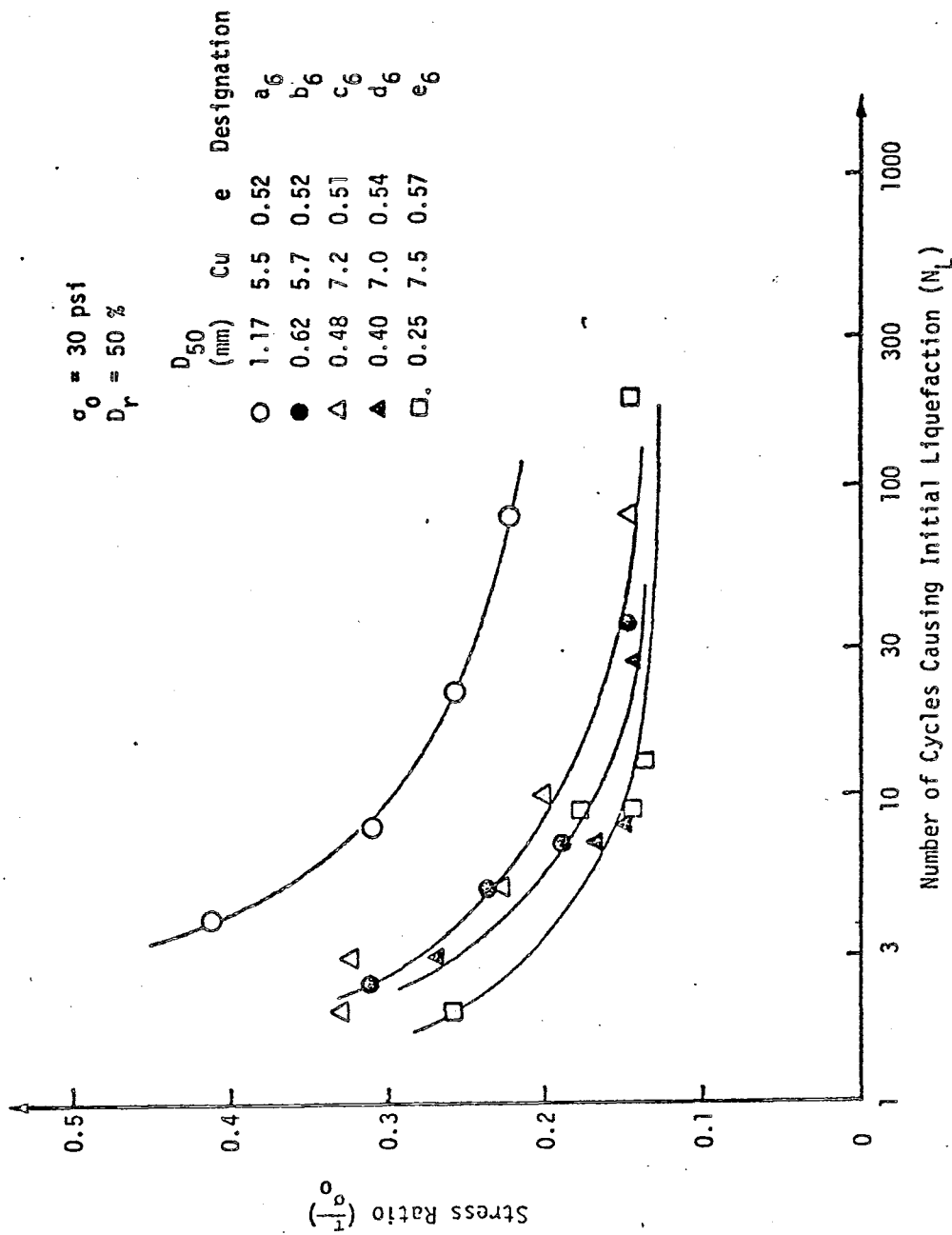
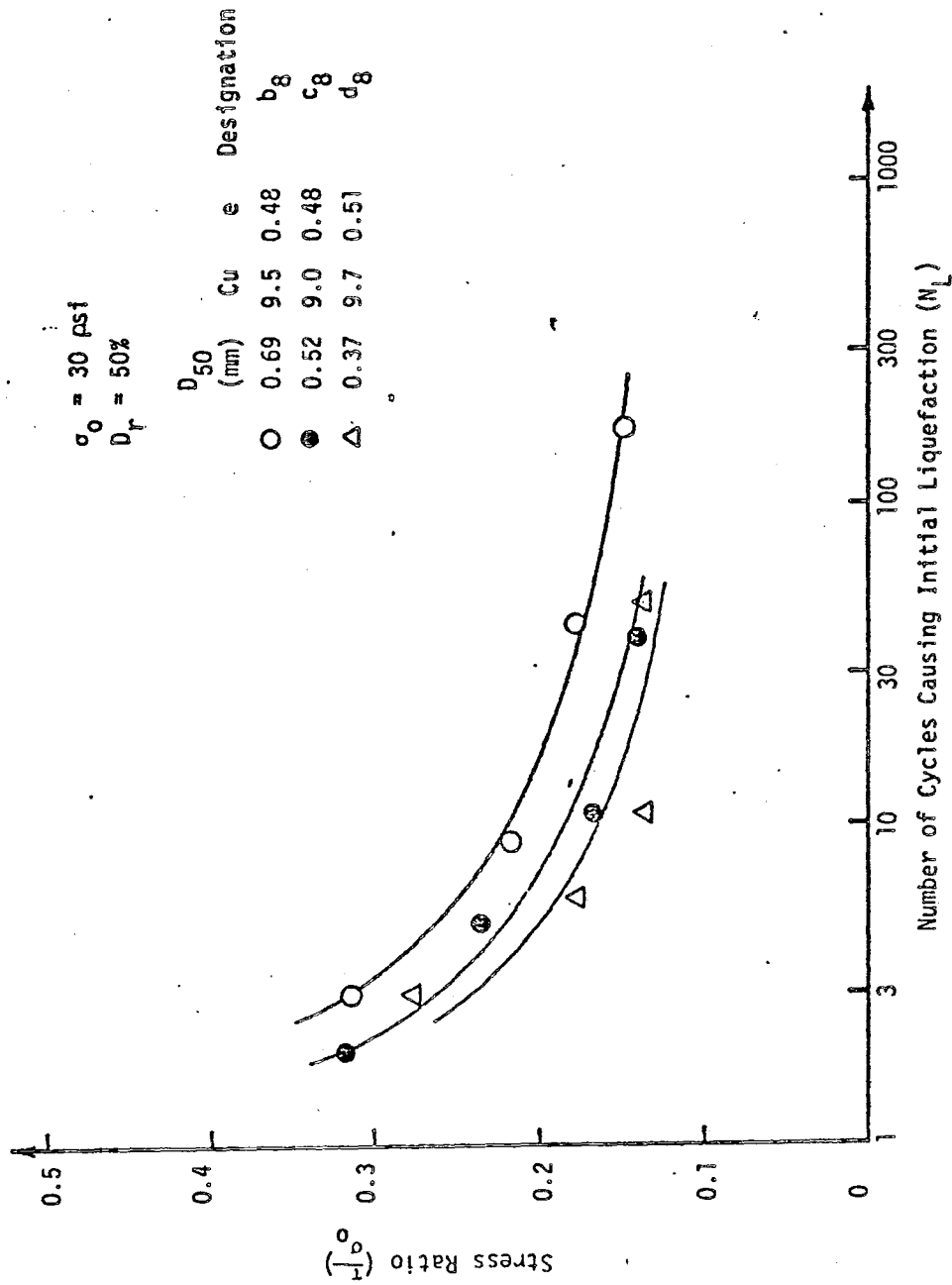FIG. 14.7 EFFECT OF MEAN GRAIN SIZE ON INITAIL LIQUEFACTION

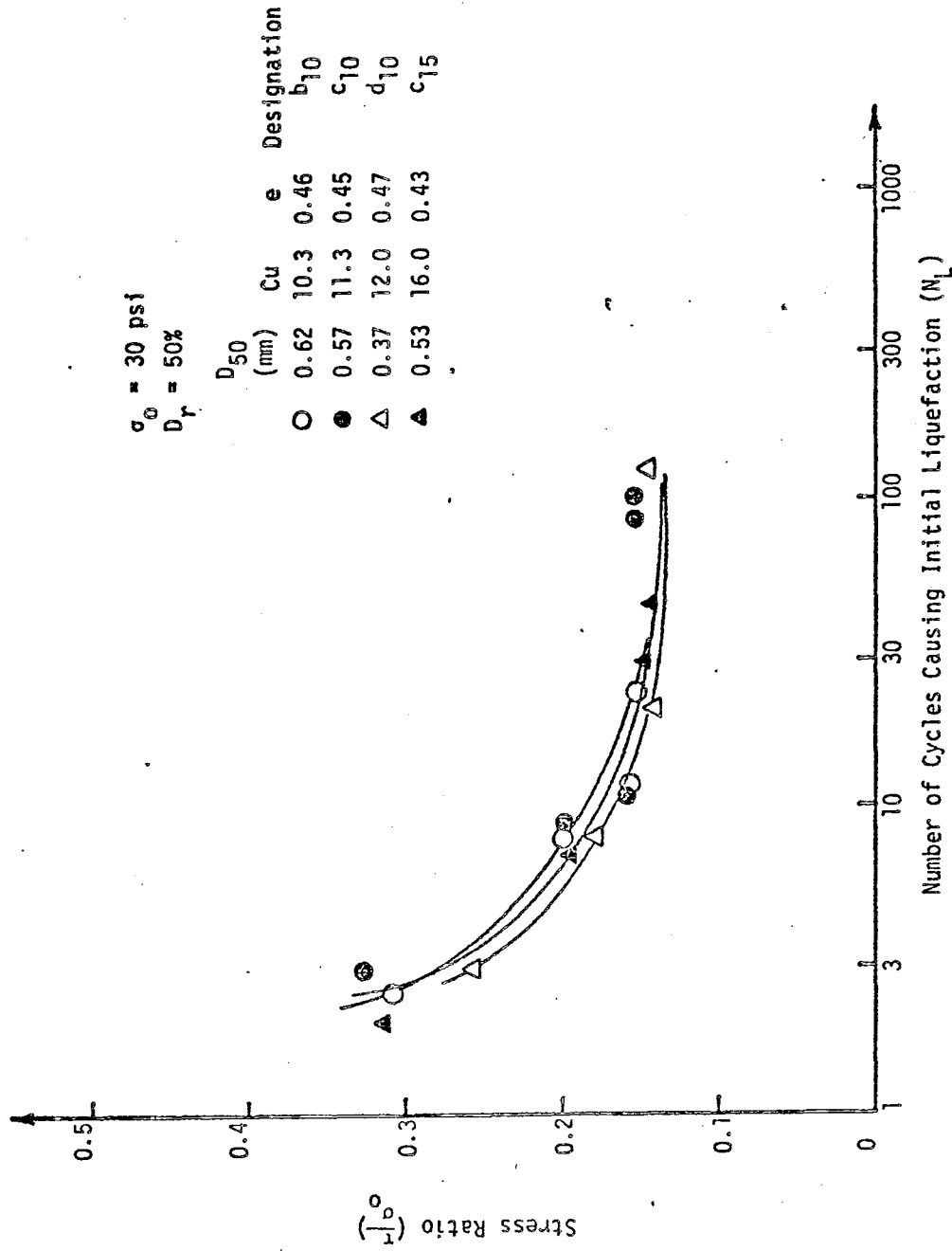FIG. 14.8 EFFECT OF MEAN GRAIN SIZE ON INITIAL LIQUEFACTION

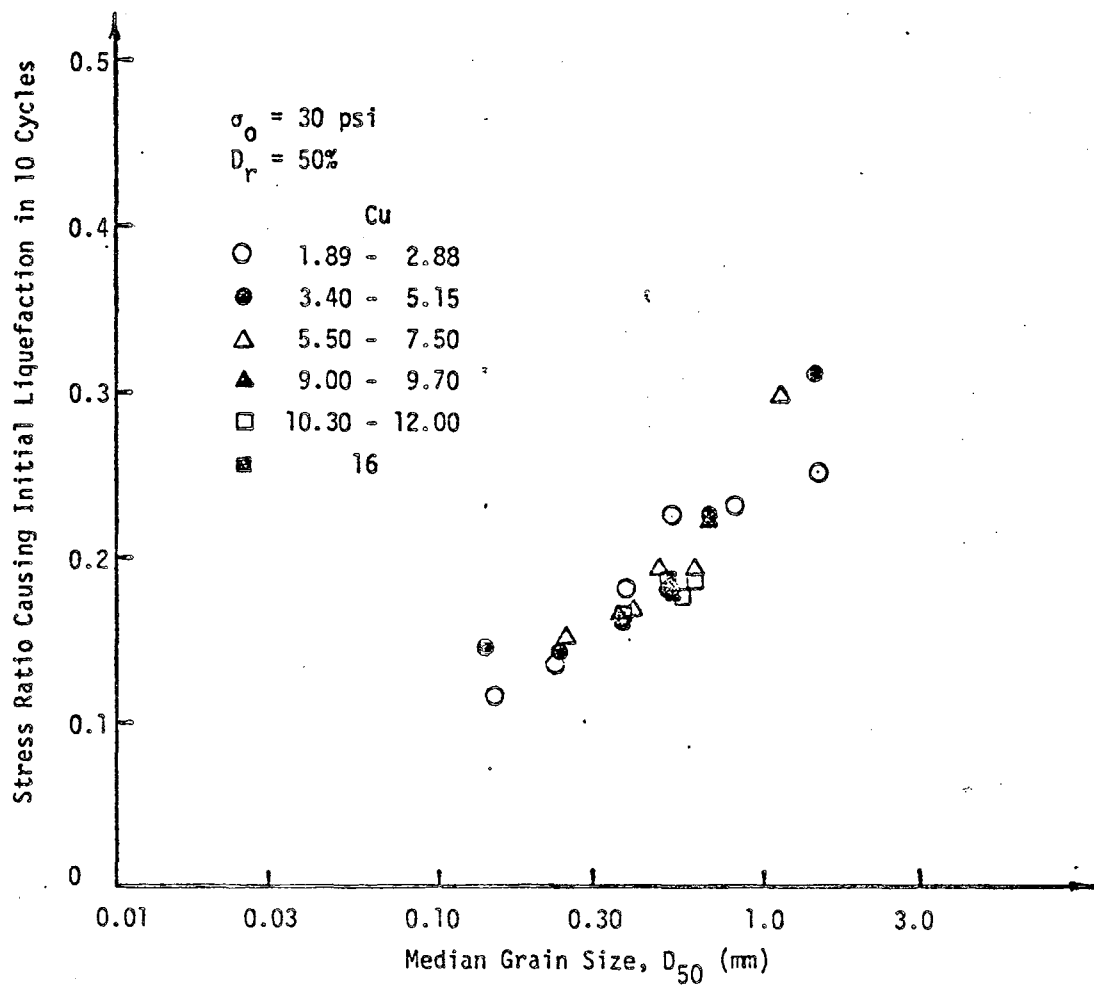FIG. 14.9 EFFECT OF MEAN GRAIN SIZE ON INITAIL LIQUEFACTION

FIG. 14.10 EFFECT OF MEAN GRAIN SIZE ON STRESS
RATIO CAUSING INITIAL LIQUEFACTION
IN 10 CYCLES
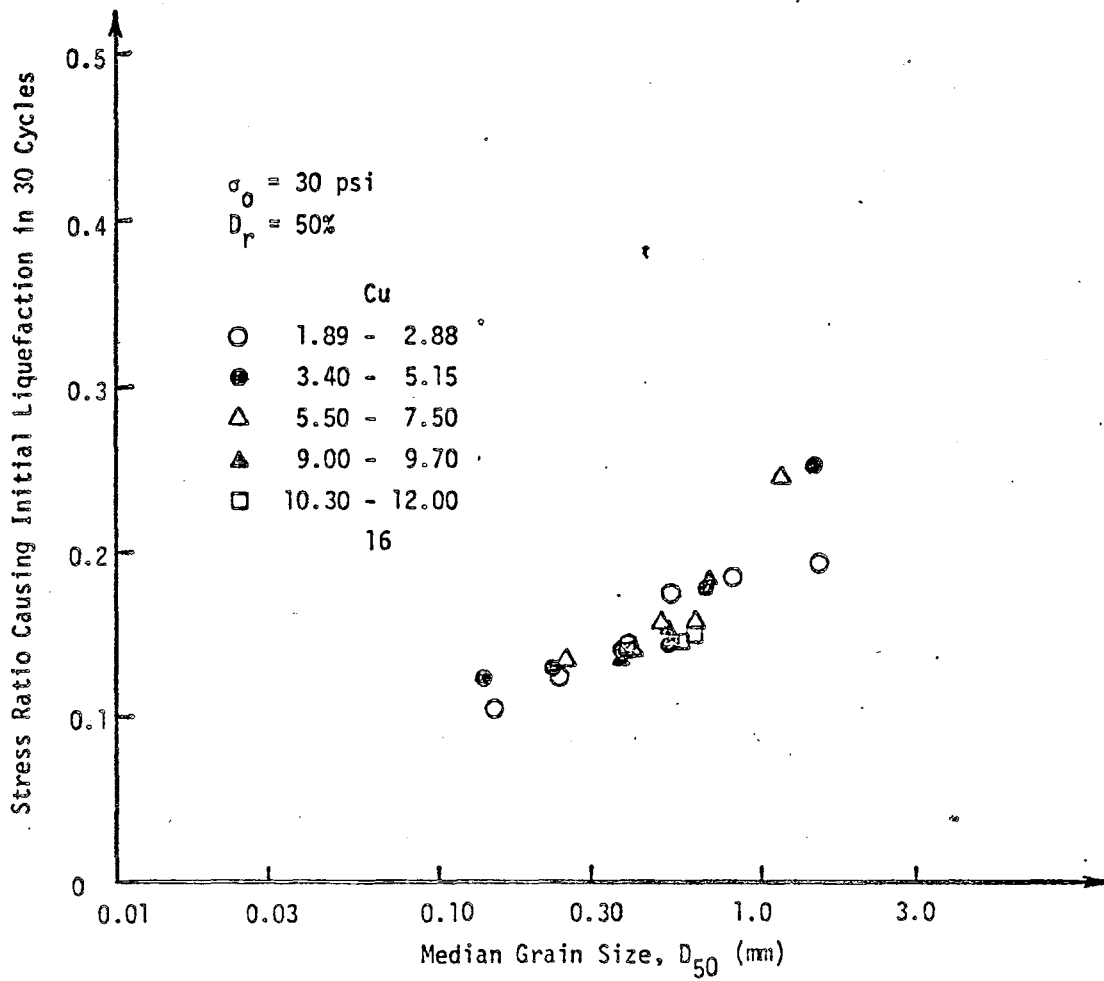
FIG. 14.11 EFFECT OF MEAN GRAIN SIZE ON STRESS RATIO
CAUSING INITIAL LIQUEFACTION IN 10 CYCLES

strength of very fine sands. This is larger than the values obtained by Lee and Fitton (1969) and Wong, et al. (1975). This can be ascribed to the differences in test sands, test sample density, and initial stress conditions.

Membrane compliance and fine particle migration during a test might also contribute to the false dynamic strength of coarse sands as discussed below.

Membrane Effect

As described by Wong, et al. (1975) and Martin, et al. (1978), the effect of membrane compliance can be significant. The following two possible effects of membrane compliance can be observed in the test:

During the consolidation phase:

The relative density of the testing sample can be exaggerated by the penetration of membrane due to application of the effective confining pressure; and

During the cyclic test phase:

The generation of excess pore pressure results in a decrease of effective confining pressure. As a result of this decrease, the membrane penetration caused by application of the initial effective confining pressure reduces. Therefore, the sample appears to show more resistance. Typical test results affected by the membrane compliance are shown in Fig. 14.12. From this figure, the rate of pore pressure generation decreases as the excess pore pressure approaches the initial confining pressure, and the number of cycles

$\sigma_o = 30$ psi
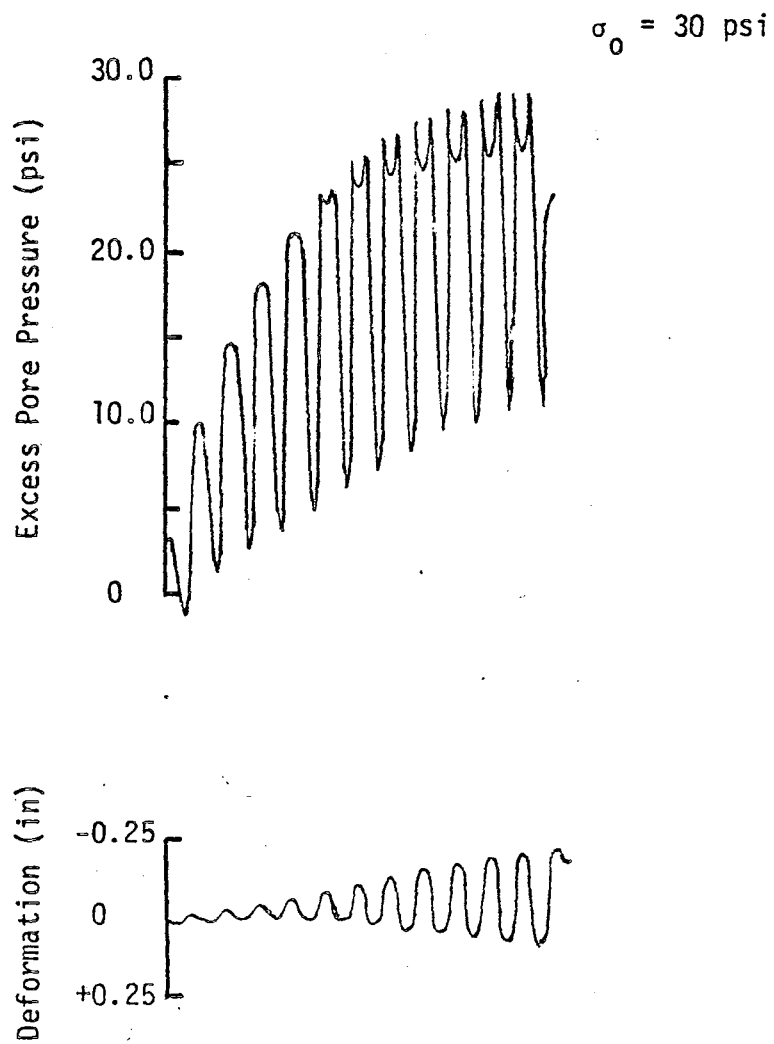
FIG. 14.12 TYPICAL RECORDED TEST DATA
FOR COARSE SAND

required to cause initial liquefaction seems to be somewhat too high.

Particle Migration

Another source of error may be caused by the segregation of fine grain soils in the specimen prior to initial liquefaction. In fact, it was visually observed that some fine particles migrated downward in the voids created by coarse particles as a result of excess porewater pressure generation during undrained cyclic tri-axial tests. As shown in Figs. 14.6 and 14.7, the cyclic strength of samples with mean grain size ranging from 1.17 mm to 1.44 mm was found to be significantly stronger than another sample. It is believed that the downward migration of fine particles might have resulted in increase in the membrane penetration effect in the upper portion of the sample and caused either or both aforementioned errors. This may result in over-estimation of the cyclic strength.

No attempt was made to correct these errors in this investigation. Despite the above inevitable errors, the test results in this study for liquefaction indicated that fine sands tend to possess less resistance to liquefaction than coarse sands.

14.4 Effect of Uniformity Coefficient

In an attempt to investigate the effect of uniformity coefficient, C_u, on the liquefaction potential of sands, the data presented in Figs. 14.5 through 14.9 were rearranged. The results of samples with similar D_{50} and different uniformity coefficient, C_u were plotted in the same figure as shown in Figs. 14.13 through 14.18. It was observed that the effect of the uniformity coefficient

FIG. 14.13 EFFECT OF UNIFORMITY COEFFICIENT ON LIQUEFACTION

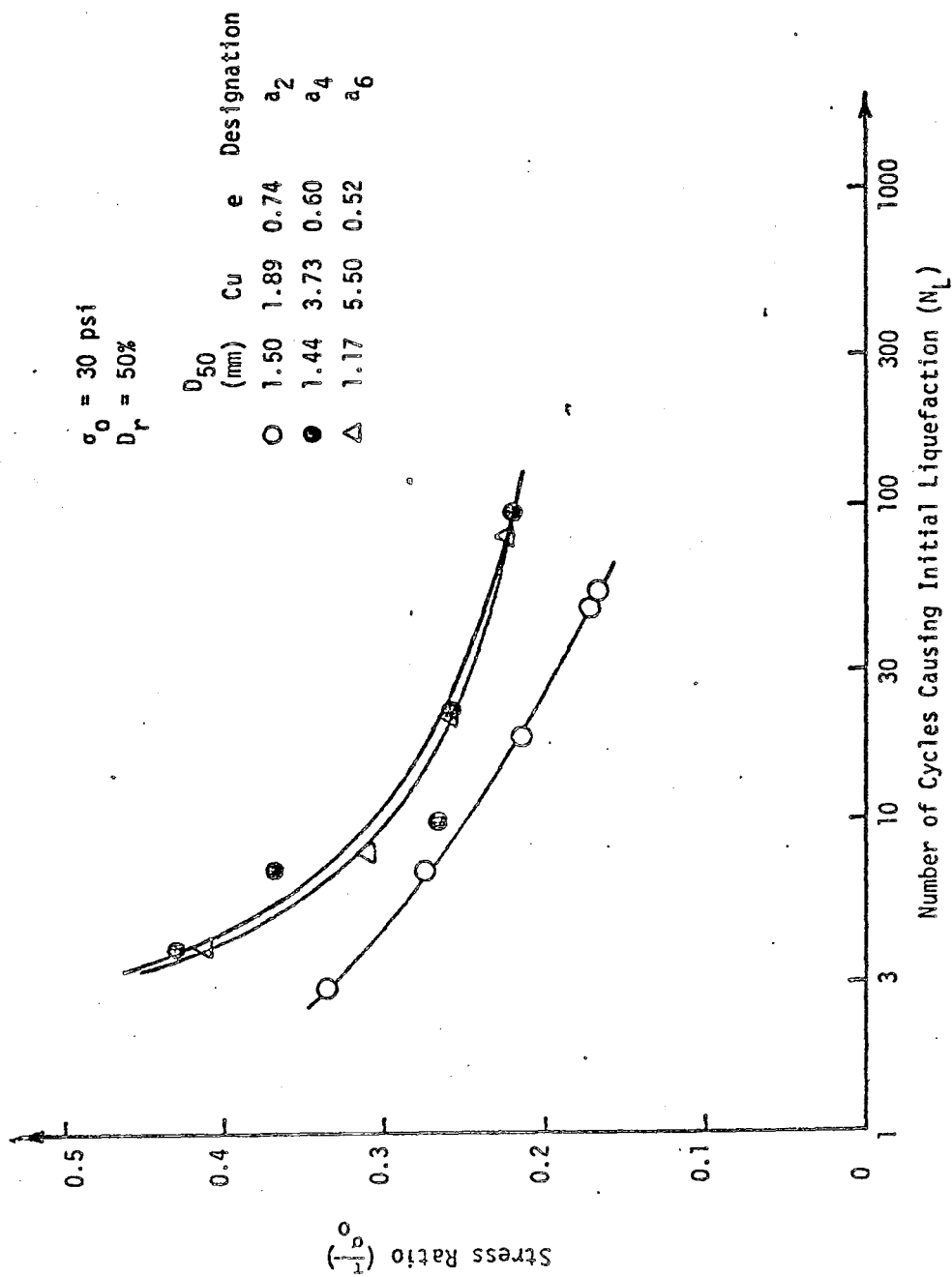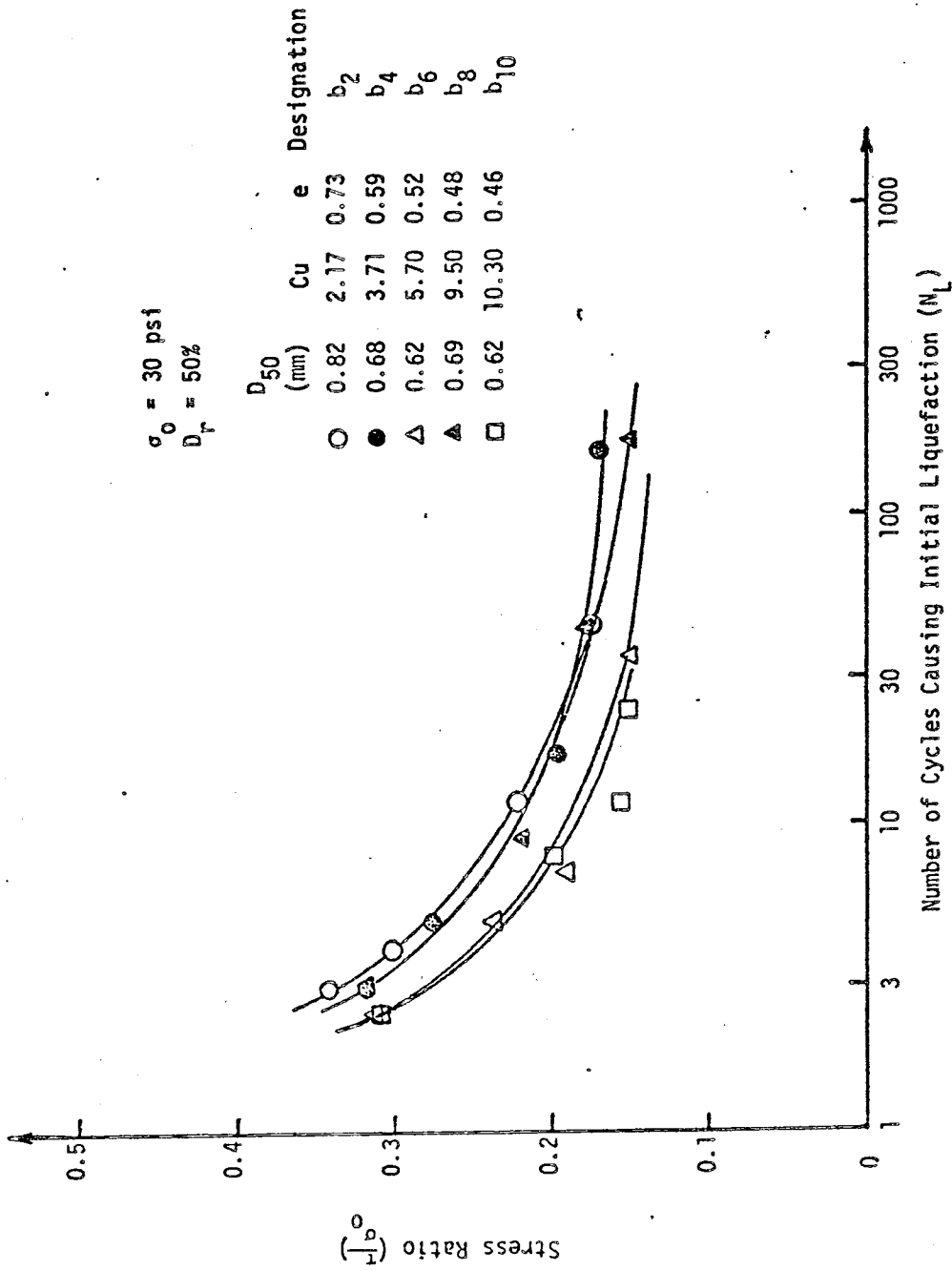FIG. 14.14 EFFECT OF UNIFORMITY COEFFICIENT ON LIQUEFACTION
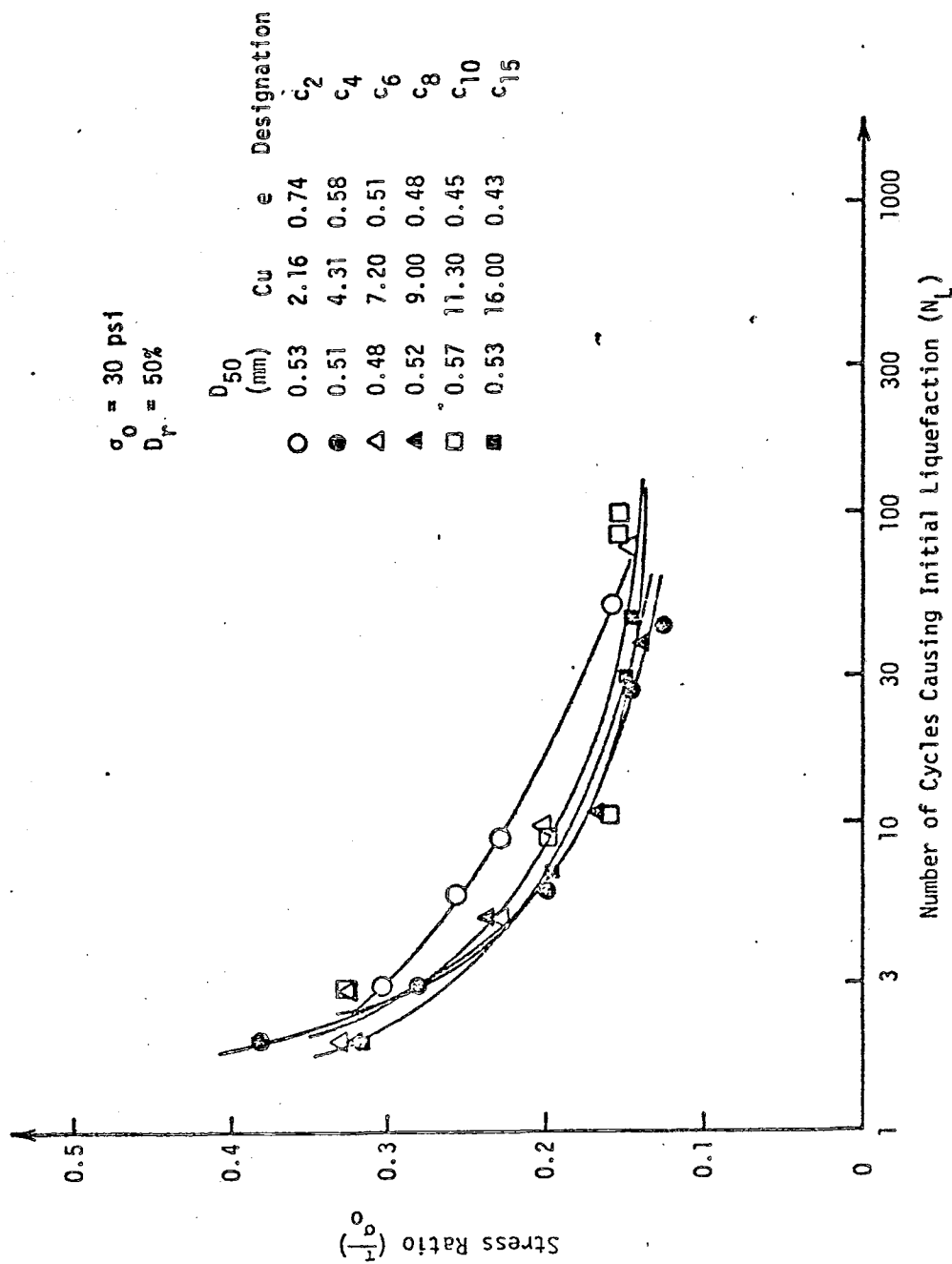
FIG. 14.15 EFFECT OF UNIFORMITY COEFFICIENT ON LIQUEFACTION
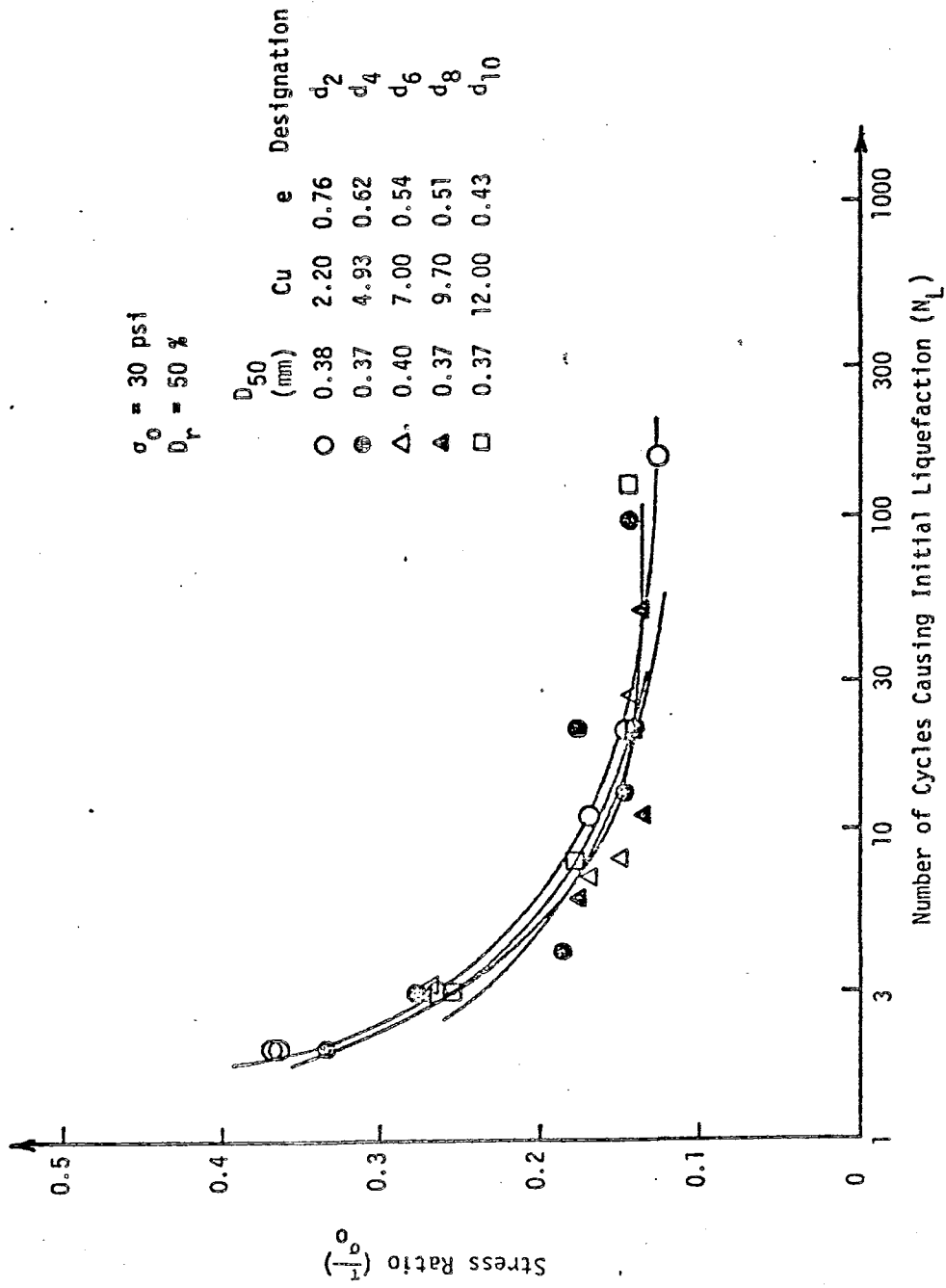
FIG. 14.16 EFFECT OF UNIFORMITY COEFFICIENT ON LIQUEFACTION
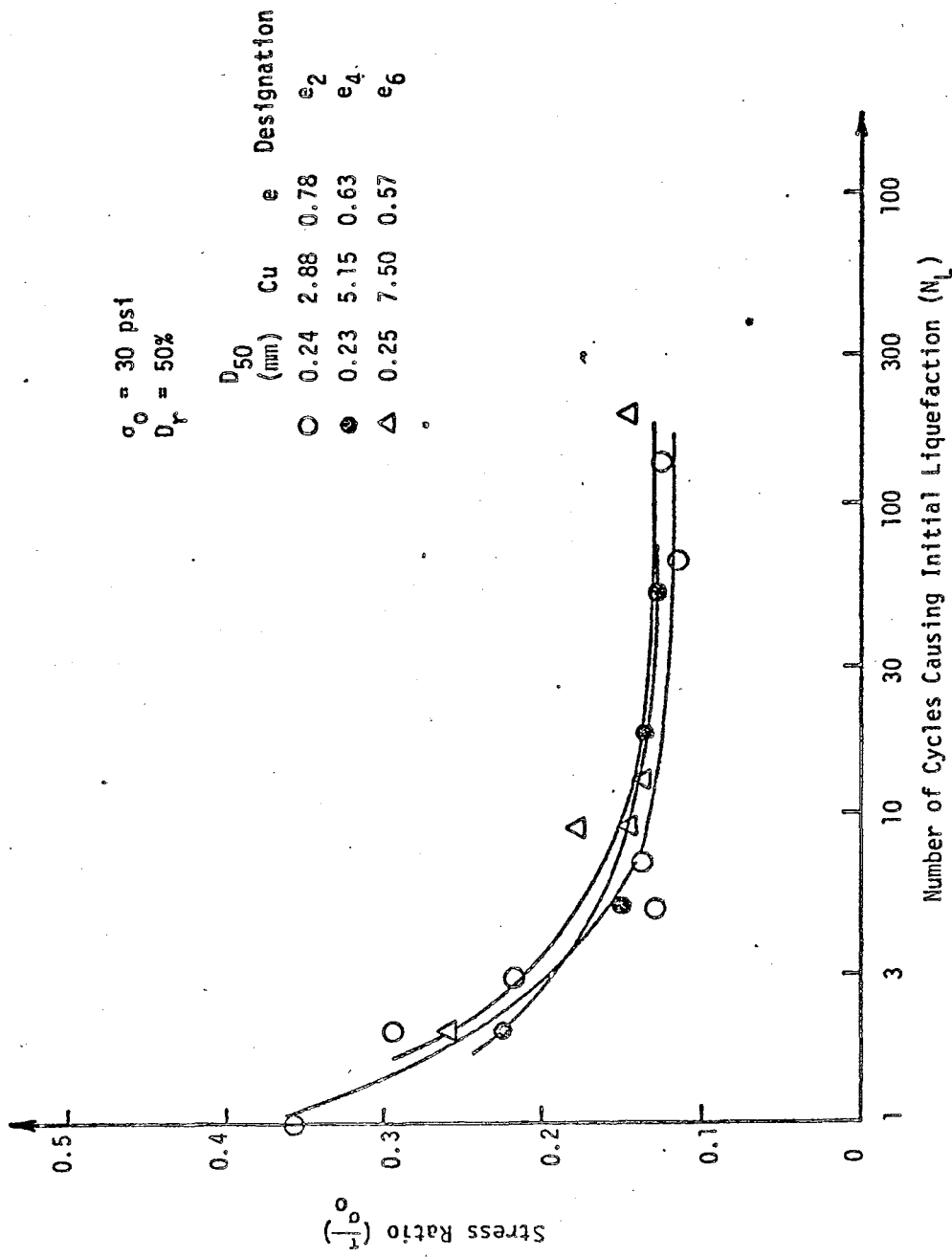
FIG. 14.17 EFFECT OF UNIFORMITY COEFFICIENT ON LIQUEFACTION

315
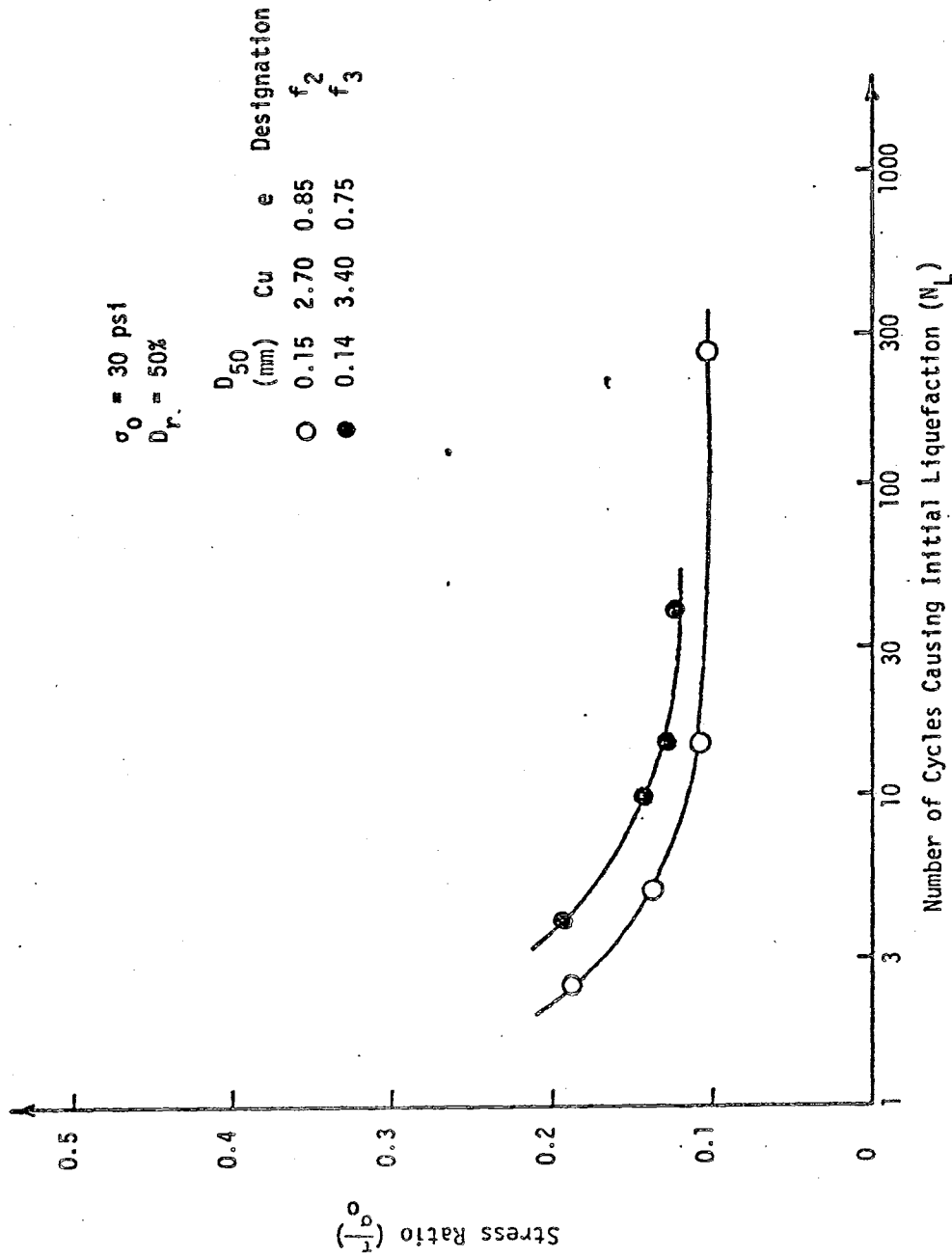
FIG. 14.18 EFFECT OF UNIFORMITY COEFFICIENT ON LIQUEFACTION

was found to be less important than that of the mean grain size.

As shown in Figs. 14.10 and 14.11, the stress ratios required to

cause initial liquefaction at the tenth and the thirtieth cycles

increase monotonically with mean grain size. However, the effect

of the uniformity coefficient on the stress ratio required to cause

initial liquefaction was found to be relatively small. One must

be cautioned that the data in each figure also contain the variation

in void ratios. Therefore, a definite conclusion cannot be drawn

on the effect of uniformity coefficient. However, the data indicates

that the effect of uniformity coefficient on the liquefaction

potential of sand in negligible.

By comparing the band width of data points in Figs. 14.13

through 14.18, it was observed that the effect of membrane penetra-

tion and uniformity coefficient seems to become smaller as the

mean grain decreases. Hence, the effect of uniformity coefficient

and membrane penetration is smaller for the fine sand than the

coarse one. At the same D_{50}, the samples with smaller C_u seem

to possess a higher cyclic strength. However, compared with the

effect of mean grain size, the effect of sample uniformity on

the cyclic strength was found to be negligible. As shown in

Figs. 14.15 to 14.17, the same conclusion can be drawn for medium

sand and fine sand. However, the cyclic strength of very fine

sands, as shown in Fig. 14.18, was found to be somewhat stronger for

the fine sand samples with higher C_u. The specimen $DF-f_3$ with

20% fines (minus 0.074 mm), coarse silt, is somewhat stronger than

the specimen without any fine. It implies that the presence of

silt might have some effect on cyclic strength of soils. This effect is currently being investigated by the authors.

Based on the summary of all test results, as shown in Figs. 14.19 and 14.20, the effect of sample uniformity on initial liquefaction at the tenth and the thirtieth cycles is negligible for samples with mean grain size smaller than 1.5mm. However, the effect of mean grain size on liquefaction is strongly affected by the uniformity of the sample. The dispersion of data points is larger for uniform soils than for well graded soils. At the same uniformity coefficient, the cyclic strength of the sample with a large mean grain size is higher than the sample with a small mean grain size. But for samples with uniformity coefficient greater than 8, the stress ratios required to cause initial liquefaction at the tenth and the thirtieth cycles are almost constant despite the difference in the mean grain size.

14.5 Development of Functional Relationship

One of the major purposes of this study is to obtain a functional relationship between the stress ratio causing initial liquefaction and the gradation characteristics of sand. The result may aid in assessing liquefaction potential of sands before laboratory cyclic tests are performed. The statistical correlation analysis was performed to assess the strength of the relationship between the dependent and independent variables. The regression analysis was then used to formulate the functional relationship between the dependent variable and the independent variable(s). The SPSS (Statistical Packages for the Social Sciences) programs
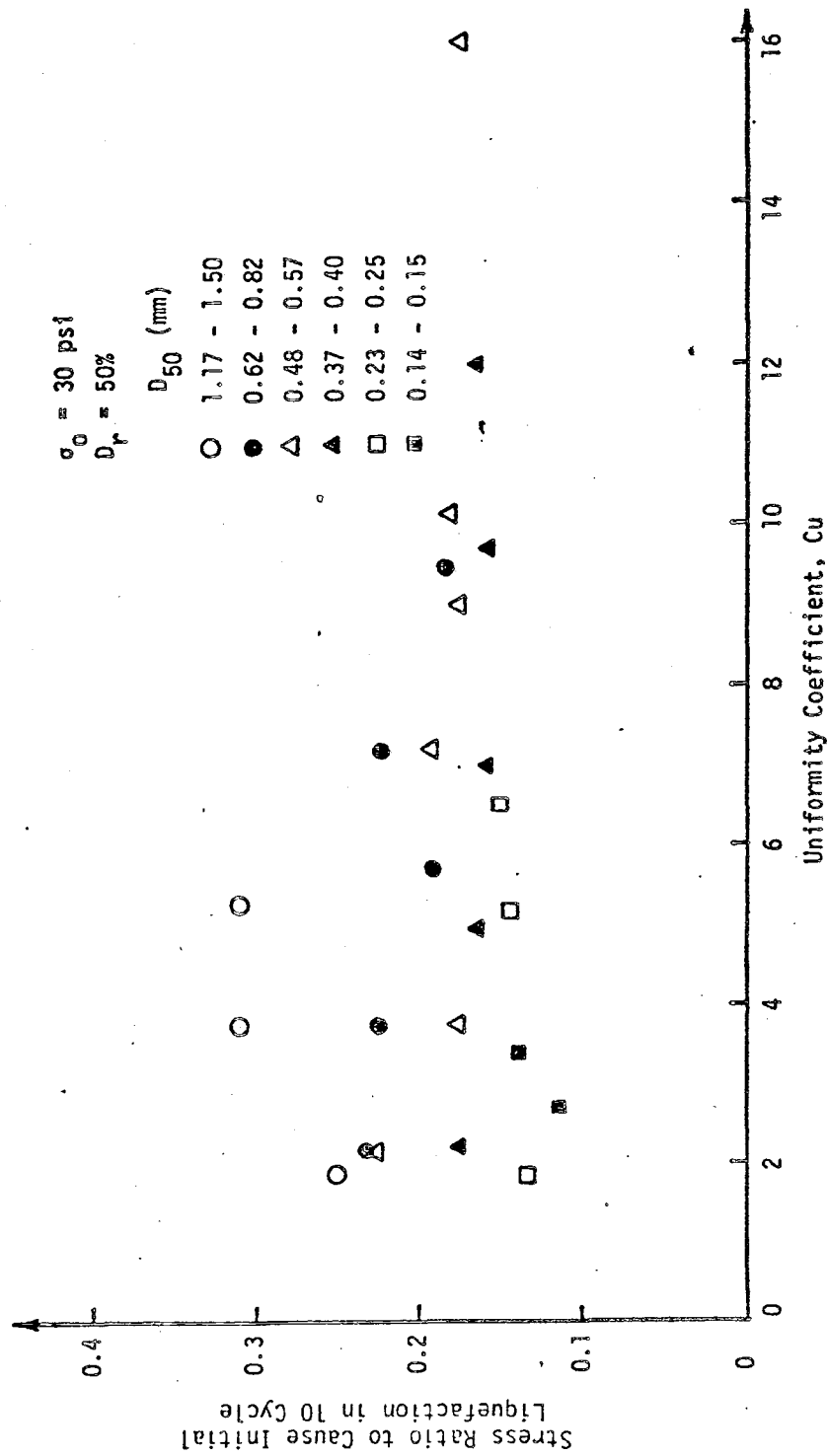
FIG. 14.19 EFFECT OF UNIFORMITY COEFFICIENT ON STRESS RATIO
CAUSING INITIAL LIQUEFACTION IN 10 CYCLES
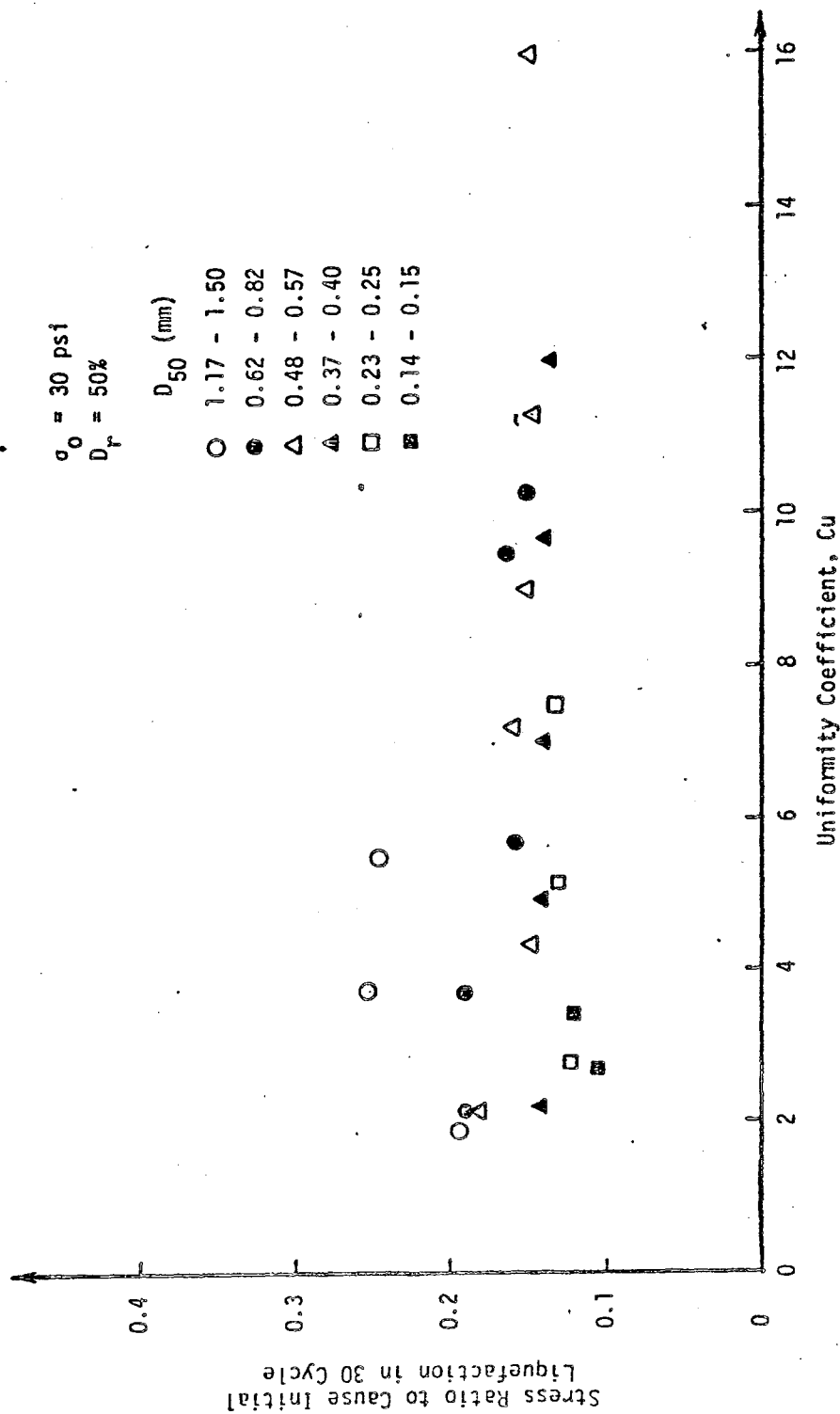
FIG. 14.20   EFFECT OF UNIFORMITY COEFFICIENT ON STRESS RATIO
             CAUSING INITIAL LIQUEFACTION IN 10 CYCLES

were used in performing these analyses.

The curves of Fig. 14.5 to Fig. 14.9 will first be formulated to relate the cyclic strength (expressed by stress ratio) to number of cycles to cause initial liquefaction. From statistical correlation and regression analyses, these curves can be fitted well by the general form of the following equation:

$$R_s = a + b \log_{10} N_L + c(\log_{10} N_L)^2$$

where

$$R_s = \frac{\sigma_{dc}}{2\sigma_3} \ (or \ \frac{\tau}{\sigma_0}\ ) = cyclic \ stress \ ratio;$$

N_L = number of cycles to cause initial lique-

faction; and

a,b,c = coefficients determined by regression

analysis and a is equal to the cyclic

stress ratio at one cycle.

The R value, the correlation coefficient between dependent and independent variables, was found to be higher than 0.97 in most of the cases. Twenty-four sets of coefficients,as shown in Table 14.1, were determined by this analysis. The variation of the coefficients is believed to be related to the grain size distribution characteristics.

By the same technique, the relationships between the coefficients and the grain size distribution characteristics were obtained as follows:

$$a = 0.5781 - 0.1383 \ D_{10} + 0.3729 \ \log_{10} D_{50}$$

(R = 0.783)

TABLE 14.1

VALUES OF COEFFICIENTS a, b AND c IN EQUATION 14.2

Sample No.*	a	b	c	R	Sample No.*	a	b	c	R
a_2	0.4995	-0.3268	0.0778	0.9985	a_6	0.6401	-0.4733	0.1339	0.9916
b_2	0.4781	-0.3496	0.1000	0.9976	b_6	0.4712	-0.4657	0.1657	0.9957
c_2	0.4041	-0.2347	0.0535	0.9999	c_6	0.4301	-0.3263	0.0928	0.9725
d_2	0.4605	-0.3950	0.1118	0.9845	d_6	0.5047	-0.6223	0.2572	0.9988
e_2	0.3657	-0.3821	0.1291	0.9761	e_6	0.3287	-0.2514	0.0752	0.9704
f_2	0.2468	-0.1817	0.0508	0.9920	b_8	0.4096	-0.2392	0.0555	0.9874
a_4	0.6912	-0.5423	0.1541	0.9581	c_8	0.4088	-0.3268	0.0986	0.9972
b_4	0.4468	-0.3067	0.0820	0.9993	d_8	0.5066	-0.5853	0.2169	0.9992
c_4	0.5199	-0.5704	0.2050	0.9887	b_{10}	0.4451	-0.4027	0.1368	0.9667
d_4	0.4051	-0.3470	0.1109	0.9264	c_{10}	0.5430	-0.5365	0.1711	0.9926
e_4	0.2621	-0.1859	0.0696	0.8173	d_{10}	0.3763	-0.2985	0.0898	0.9996
f_3	0.3367	-0.2994	0.1033	0.9999	c_{15}	0.4433	-0.3432	0.1135	0.9988

*Sample No. provides information on its gradation characteristics. For instance a_2 denotes sample with mean grain size of "a" (1.50 mm) and a designed uniformity coefficient of 2.

$$b = -0.3096 + 0.785 \log_{10} e + 0.145 \log_{10} Cu$$
$$+ 0.1307 \left(\log_{10} D_{50} \right)^2$$

$$(R = 0.422)$$

$$c = 0.306 - 0.0492 \log_{10} Cu - 0.258 e$$

$$(R = 0.364)$$

where

D_{50} = mean grain size in millimeters;

Cu = uniformity coefficient of the sand;

e = void ratio of the soil; and

D_{10} = effective grain size in millimeters.

From the discussion in Section 14.4, the effect of uniformity is negligible compared with the effect of mean diameter. If the effect of mean grain size is the only governing factor among the grain size distribution characteristics, the stress ratio required to cause initial liquefaction at the tenth cycle and the thirtieth cycle can be expressed by the following equations:

At the tenth cycle

$$R_s = 0.249 + 0.2374 \log_{10} D_{50}$$
$$+ 0.111 \left(\log_{10} D_{50} \right)^2$$

$$(R = 0.936)$$

At the thirtieth cycle

$$R_s = 0.1979 + 0.1783 \log_{10} D_{50}$$
$$+ 0.096 \left(\log_{10} D_{50} \right)^2$$

$$(R = 0.908)$$

The above equations are similar to the following equations which were obtained by Finn (1972). But the latter equations give higher

stress ratios:

At the tenth cycle

$$\frac{\tau}{\sigma_0} = 0.285 + 0.068 \ \log_{10} D_{50}$$

At the thirtieth cycle

$$\frac{\tau}{\sigma_0} = 0.259 + 0.0814 \ \log_{10} D_{50}$$

where

τ = cyclic shear stress;

σ_0 = confining pressure; and

$\frac{\tau}{\sigma_0}$ = cyclic stress ratio.

CHAPTER 15

SUMMARY AND CONCLUSIONS

15.1 Summary

The purpose of this study was to investigate the effect of grain size distribution on the liquefaction potential of granular soils. Laboratory cyclic triaxial tests were performed on samples prepared from Denver sand. The mean grain size and the uniformity coefficient of these samples range from 0.1 mm to 1.5 mm and 2 to 16, respectively. At each uniformity coefficient, samples of several different mean grain sizes were prepared.

All samples were consolidated under 30 psi initial confining pressure, and prepared to achieve the relative density of approximately 50%. Due to the difficulty of achieving exactly 50% relative density, a test program was performed to investigate the effect of the small variation in relative density on liquefaction. The result of this investigation was then used to adjust the cyclic stress ratio of samples with relative density other than 50% to the stress ratio corresponding to 50% relative density. A slow frequency of 0.05 Hz was used to reduce the effect of deficiency in the hydraulic power.

The effect of mean grain size on liquefaction potential was studied by using the test results on samples with the same uniformity

coefficient and different mean grain sizes. Although the actual uniformity of samples varied slightly, the result was found to be consistent to that of other researchers. The effect of uniformity coefficient was investigated by using the data from samples with the same mean grain size and varying uniformity coefficients.

Functional relationships between the liquefaction potential and the mean grain size were formulated by using regression analyses.

15.2 Conclusions

The liquefaction potential was found to be significantly affected by the mean grain size. However, its effect becomes less significant when the uniformity is greater than 10. Since the test results were not corrected for the membrane penetration effect, the effect might have been overestimated. Because of the strong correlation between the liquefaction potential and the grain size, the cyclic stress ratios causing initial liquefaction at the 10th and 30th cycles were formulated as the function of the mean grain size.

The uniformity coefficient has much less effect on the liquefaction potential than the mean grain size. However, its effect is more significant for the coarse-grained soil than the fine-grained one. For soils with their mean grain sizes smaller than 0.40 mm, the effect of the uniformity coefficient on the liquefaction potential was found to be insignificant.

The effect of membrane penetration on the triaxial test result has received very much less attention than it really

deserves. The effect is believed to be more significant for coarse and uniform soils.

15.3 Recommendation for Future Study

Many factors have various degrees of effect on the liquefaction potential of sands. To have a preliminary assessment without an elaborate laboratory testing program of the liquefaction potential of a sand of a given gradation, one must be equipped with the knowledge of the degree of the effect of various factors. However, no priority of importance and a definite rule for assessing the liquefaction potential were given to facilitate the preliminary assessment of the cyclic strength of sands by a geotechnical engineer. Thus, a sensitivity study on the factors affecting the liquefaction potential and cyclic strength of sands is now overdue.

It is extremely important to develop a proper mathematical model and implement it in a finite element analysis program. This program can then be used to investigate the progressive deterioration of bearing capacity of saturated sands, the interaction between saturated sands and structures, and the behavior of a saturated sand deposit under a cyclic or seismic load. The mathematical model should handle the problems involving a compression wave and a wave with the stress reversal. To be able to predict the behavior of a saturated sand subjected to the latter wave, the model should also be capable of simulating the behavior under an extension wave.

From a practical standpoint, the use of the in-situ SPT (standard penetration test) result in predicting the potential of

liquefaction of a saturated sand deposit has a great practical value. This is mainly due to the availability of the massive SPT data in both the United States and Japan and the SPT being a part of basic subsoil investigation. However, to achieve this goal requires the study on the relation between the standard penetration resistance and the standardization of SPT.

A natural sand deposit frequently is not clean but contains some fines (minus 60 mm). Thus, it is important to study the effect of fines on the cyclic strength and the liquefaction potential of sands.

In a lacustrine deposit, alluvial deposit and hydraulic fill, sands often exist as isolated lenses or layer within low permeable media, such as clay. Under a dynamic load, the sand would be essentially undrained. Therefore, the study on the undrained cyclic behavior of a saturated sand and its effect on the global behavior of the above deposits becomes worthwhile.

Finally, an extensive study on the effect of membrane penetration on the dynamic properties, the pore water generation mechanism and the liquefaction potential of sands under nonstatic loads is required to provide a necessary correction factor for cyclic triaxial test results.

REFERENCES

Ambraseys, N., and S. Sarma. "Liquefaction of Soils Induced by Earthquakes." Bulletin, Seismological Society or America, Vol. 59, No. 2 (April, 1969), pp. 651-664.

Atkinson, J.H. and P.L. Bransby. The Mechanics of Soils--An Introduction to Critical State Soil Mechanics. McGraw-Hill Book Company, 1978.

Baladi, G.Y. and B. Rohani. "Liquefaction Potential of Dam and Foundation." Research Report S-76-2, Report 5, U.S. Army Engineering, Waterways Experiment Station (August, 1978).

Bishop A.W. and D.J. Henkel. The Measurement of Soil Properties in the Triaxial Test. Edward Arnold, Ltd., London, 1976.

Bishop, A.W. and G.E. Green. "The Influence of End Restraint on the Compression Strength of a Cohesionless Soil." Geotechnique, 15:3:2 (1965).

Bjerrum, L. "Geotechnical Engineering Problems Involved in Foundations of Structures in the North Sea." Geotechnique, Vol. 23, No. 3 (1973), pp. 319-358.

Casagrande, A. "Characteristics of Cohesionless Soils Affecting the Stability of Slopes and Earth Fills." Journal of Boston Society of Civil Engineers." (June, 1936)

_____. "Liquefaction and Cyclic Deformation of Sands--A Critical Review." Harvard Soil Mechanics, Series No. 88, M.I.T., Cambridge, Massachusetts (January, 1975).

Castro, G. "Liquefaction of Sands." Harvard Soil Mechanics, Series No. 81, M.I.T., Cambridge, Massachusetts (January, 1969).

_____. "Liquefaction and Cyclic Mobility of Saturated Sands." Journal of Geotechnical Engineering Division, ASCE, Vol. 101, No. GT 6 (June, 1975), Proc. Paper 11388.

Castro, G. and S.J. Poulos. "Factors Affecting Liquefaction and Cyclic Mobility." Journal of Geotechnical Engineering Division, ASCE, Vol. 103, No. GT 6 (June, 1977), Proc. Paper 12994.

Chaney, R.C. "Saturation Effects on the Cyclic Strength of Sands." Earthquake Engineering and Soil Dynamics, Proc. of the ASCE Geotechnical Engineering Division, Special Conference, Pasadena, CA (June, 1978).

Close, U. and E. McCormick. "Where the Mountains Walked." The National Geographic Magazine, Vol. XLI, No. 5 (May, 1922).

D'Appolonia, E. "Dynamic Loadings." Paper presented at the American Society of Civil Engineers Specialty Conference on Placement and Improvement of Soil to Support Structures, M.I.T., Cambridge, Massachusetts (August, 1968).

DeAlba, P., H.B. Seed and C.K. Chan. "Sand Liquefaction in Large-Scale Simple Shear Tests." Journal of the Geotechnical Engineering Division, ASCE, Vol. 102, No. GT 9 (September, 1976)

Donovan, N.C. "A Stochastic Approach to the Seismic Liquefaction Problem." Proceedings of the First International Conference on Applications of Statistics and Probability to Soil and Structural Engineering, Hong Kong (September, 1971).

Ferritto, J.M. and J.B. Forrest. "Determination of Seismically Induced Soil Liquefaction Potential at Proposed Bridge Sites." Report No. FHWA-RD-77-127, Office of Research and Development, Federal Highway Administration, U.S. Department of Transportation (1977).

Finn, W.D.L., P.L. Bransby and D.J. Pickering. "Effect of Strain History on Liquefaction of Sand." Journal of the Soil Mechanics and Foundations Division, ASCE, Vol. 96, No. SM 6 (November, 1970).

Finn, W.D.L., D.J. Pickering and P.L. Bransby. "Sand Liquefaction in Triaxial and Simple Shear Tests." Journal of the Soil Mechanics and Foundations Engineering, ASCE, Vol. 97, No. SM 4 (April, 1971), Proc. Paper 8039.

Finn, W.D.L. "Liquefaction of Sands." Proceeding of International Conference on Microzonation for Safer Construction, Research and Applications, Seattle, Washington, Vol. 1 (1972).

Finn, W.D.L., D.J. Pickering and P.L. Bransby. "Sand Liquefaction in Triaxial and Simple Shear Tests." Journal of Geotechnical Engineering Division, ASCE, Vol. 103, No. GT 6 (June, 1977), Proc. Paper 13008.

Florin, V.A. and P.L. Ivanov. "Liquefaction of Saturated Sandy Soils." Proceedings, 5th International Conference on Soil Mechanics and Foundation Engineering, Paris, France (1961).

Frydman, S., J.G. Zeitlen and I. Alpan. "The Membrane Effect in Triaxial-Testing of Granular Soils." Journal of Testing and Evaluation, Vol. 1, No. 1 (1973), pp. 37-41.

Green, P.A. and P.A.S. Ferguson. "On Liquefaction Phenomena by Professor A. Casagrande: Report on Lecture." Geotechnique, Vol. 21, No. 3 (September, 1971), pp. 197-202.

Holtz, R.D. and W.D. Kovacs. An Introduction to Geotechnical Engineering. Prentice-Hall, Inc., 1981.

Hutchinson, J.N. "Discussion of Flow Slides." Proceedings, Geotechnical Conference on Shear Strength Properties of Natural Soils and Rocks, Oslo, Vol. 2 (1967).

Hvorslev, M.J. "A Review of Soil Studies." Potamology Report 12-5, U.S. Army Engineer Waterways Experiment Station, Vicksburg, Mississippi (June, 1956).

Ishibashi, I. and A. Sherif. "Soil Liquefaction by Torsional Simple Shear Device." Journal of the Geotechnical Engineering Division, ASCE, Vol. 100, No. GT 8 (August, 1974).

Ishihara, K. and S. Mitsui. "Field Measurements of Dynamic Pore Pressure During Pile Driving." Proceedings, International Conference on Microzonation for Safer Construction, Research and Application, University of Washington, Seattle, Washington (October-November, 1972).

Ishihara, K. F. Tatsuoka and S. Yasuda. "Undrained Deformation and Liquefaction of Sand under Cyclic Stresses." Soil and Foundations, Japanese Society of Soil Mechanics and Foundation Engineering, Vol. 15, No. 1 (March, 1975).

Ishihara, K., M. Sodekawa and Y. Tanaka. "Effect of Overconsolidation on Liquefaction Characteristics of Sands Containing Fines." Dynamic Geotechnical Testing, ASTM STP 654, American Society for Testing and Materials (1978).

Kishida, H. "Characteristics of Liquefied Sands during Mino-Owari, Tohnankai and Kikui Earthquake." Soils and Foundations, Japanese Society of Soil Mechanics and Foundation Engineering, Vol. 9, No. 1 (March, 1969).

Koppejan, A.W., B.M. Van Wamelen and L.J.H. Weinberg. "Coastal Flow Slides in the Dutch Province of Zeeland." Proceedings, Second International Conference on Soil Mechanics and Foundation Engineering, Vol. V (1943), pp. 89-96.

Kuribayashi, E. and F. Tatsuoka. "Brief Review of Liquefaction During Earthquakes in Japan." Soils and Foundations, Japanese Society of Soil Mechanics and Foundaton Engineering, Vol. 15, No. 4 (December, 1975), pp. 81-92.

Ladd, R.S. "Specimen Preparation and Liquefaction of Sands." Journal of the Geotechnical Engineering Division, ASCE, Vol. 100, No. GT 10 (October, 1974).

_____. "Specimen Preparation and Cyclic Stability of Sands." Journal of the Geotechnical Engineering Division, ASCE, Vol. 103, No. GT 6 (June, 1977).

Lade, P.V. "The Stress-Strain and Strength Characteristics of Cohesionless Soils." Ph.D. Dissertation, University of California, Berkeley, California (1972).

Lade, P.V. and S.B. Hernandez. "Membrane Penetration Effects in Undrained Tests." Journal of the Geotechnical Engineering Division, ASCE, Vol. 103, No. GT 2 (February, 1977), pp. 109-125.

Lambe, T.W. and R.V. Whitman. Soil Mechanics. John Wiley and Sons, Inc., New York, New York, 1969.

Lee, K.L. and H.B. Seed. "Cyclic Stress Conditions Causing Liquefaction of Sand." Journal of the Soil Mechanics and Foundation Division, ASCE, Vol. 93, No. SM 1 (January, 1967), Proc. Paper 5058.

Lee, K.L. and J.A. Fitton. "Factors Affecting the Cyclic Loading Strength of Soil." Vibration Effects of Earthquakes on Soils and Foundations, ASTM STP 450, American Society for Testing and Materials (1969).

Lee, K.L. and J.A. Focht, Jr. "Liquefaction Potential at Ekofisk Tank in North Sea." Journal of the Geotechnical Engineering Division, ASCE, Vol. 101, No. GT 1 (January, 1975), pp. 1-18.

Lee, K.L. and F.J. Vernese. "End Restraint Effects on Cyclic Triaxial Strength of Sand." Journal of Geotechnical Engineering Division, ASCE, No. GT 6 (June, 1978), Proc. Paper 13839.

MacIver, B.N. and G.P. Hale. "Laboratory Soils Testing." EM 1110-2-1906, U.S. Army Engineer Waterways Experiment Station, CE, Vicksburg, Mississippi (November, 1970).

Manfred, K. and B. Schuppener. "Membrane Penetration and Its Effect on Pore Pressures." Journal of the Geotechnical Engineering Division, ASCE, Vol. 103, No. GT 11 (November, 1977), pp. 1267-1279.

Marcuson, W.F. and F.C. Townsend. "Effects of Specimen Reconstitution on Cyclic Triaxial Results." Miscellaneous Paper S-76-5, U.S. Army Waterways Experiment Station, Vicksburg, Mississippi (1976).

Marinatos, S.N. "Helice Submerged Town of Classical Greece." Archeology, Vol. 13, No. 3 (Autumn, 1960).

Martin, G.R., W.D.L. Finn and H.B. Seed. "Effect of System Compliance on Liquefaction Test." Journal of the Geotechnical Engineering Division, ASCE, Vol. 104, No. GT 4 (April, 1968).

Middlebrooks, T.A. "Fort Peck Slide." Transactions, ASCE, Vol. 107, (1942), pp. 723-742.

Mori, K., H.B. Seed and C.K. Chan. "Influence of Sample Disturbance on Sand Response to Cyclic Loading." Journal of the Geotechnical Engineering Division, ASCE, Vol. 104, No. GT 3 (March, 1978).

Mulilis, J.P. "The Effects of Method of Sample Preparation on the Cyclic Stress-Strain Behavior of Sands." EERC Report 75-18, College of Engineering, University of California, Berkeley, California (July, 1975).

Mulilis, J.P., C.K. Chan, J.K. Mitchell and K. Arulanandan. "Effects of Sample Preparation on Sand Liquefaction." Journal of the Geotechnical Engineering Division, ASCE, Vol. 103, No. GT 2 (February, 1977).

Mulilis, J.P., F.C. Townsend and R.C. Horz. "Triaxial Testing Techniques and Sand Liquefaction." Dynamic Geotechnical Testing, ASTM STP 654, American Society for Testing and Materials (1978).

Newland, P.L. and B.H. Allely. "Volume Changes During Undrained Triaxial Tests on Saturated Dilatant Granular Materials." Geotechnique, London, England, Vol. 9 (1959), pp. 174-182.

Newmark, N.M. "Effects of Earthquakes on Dams and Embankment." The Fifth Rankine Lecture of the British Geotechnical Society (February, 1965).

Park, T.K. And M.L. Silver. "Dynamic Triaxial and Simple Shear Behavior of Sand." Journal of the Geotechnical Engineering Division, ASCE, Vol. 101, No. GT 6 (June, 1975).

Peacock, W.H. and H.B. Seed. "Sand Liquefaction under Cyclic Loading Simple Shear Conditions." Journal of the Soil Mechanics and Foundations Division, ASCE, Vol. 94, No. SM 3 (May, 1968), Proc. Paper 5957.

Perloff, W.H. and W. Baron. Soil Mechanics--Principles and Application." John Wiley and Sons, Inc., 1976.

Reynolds, O. "The Dilating of Media Composed of Rigid Particles in Contact." Philosophical Magazine, London, S. 5, Vol. 20, No. 127 (December, 1885), pp. 469-481.

Rooke, A.D., Jr., et al. "Operational Snowball, Project 3.1, Crater Measurements and Earth Media Determinations, The Apparent and True Craters." Miscellaneous Paper No. 1-987, U.S. Army Engineer Waterways Experiment Station, CE, Vicksburg, Mississippi (April, 1968).

Roscoe, K.H., A.N. Schofield and A. Thurairajah. "An Evaluation of Test Data for Selecting a Yield Criterion for Soils." Proceedings, Laboratory Shear Testing of Soils, American Society for Testings and Materials, Special Technical Publication No. 361 (1963), pp. 111-128.

Roscoe, K.H. "The Influence of Strains in Soil Mechanics." Geotechnique, Vol. 20, No. 2 (1970), pp. 129-170.

Samuelson, D.L. "The Effect of Frequency on the Liquefaction Potential of Monterey No. 0 Sand." Master Thesis, University of Colorado, Denver, Colorado (1981).

Seed, H.B. and K.L. Lee. "Studies of the Liquefaction of Sands under Cyclic Loading Conditions." Report No. TE-65-5, College of Engineering, University of California, Berkeley, California (December, 1965).

_____. "Liquefaction of Saturated Sands During Cyclic Loading." Journal of the Soil Mechanics and Foundations Division, ASCE, Vol. 92, No. SM 6 (November, 1966), Proc. Paper 4972.

Seed, H.B. and I.M. Idriss. "Analysis of Soil Liquefaction: Niigata Earthquake." Journal of the Soil Mechanics and Foundations Division, ASCE, Vol. 93, No. SM 3 (May, 1967), pp. 83-108.

Seed, H.B. and S.D. Wilson. "The Turnagain Heights Landslide, Anchorage, Alaska." Journal of the Soil Mechanics and Foundations Division, ASCE, Vol. 93, No. SM 4 (July, 1967), pp. 325-353.

Seed, H.B. and K.L. Lee. "Undrained Strength Characteristics of Cohesionless Soils." Journal of the Soil Mechanics and Foundations Division, ASCE, Vol. 93, No. SM 6 (November, 1967).

Seed, H.B. "Landslides During Earthquakes Due to Soil Liquefaction." Journal of the Soil Mechanics and Foundations Division, ASCE, Vol. 94, No. SM 5 (September, 1968), pp. 1055-1122.

Seed, H.B. and W.H. Peacock. "Test Procedures for Measuring Soil Liquefaction Characteristics." Journal of the Soil Mechanics and Foundation Division, ASCE, Vol. 97, No. SM 8 (August, 1971), Proc. Paper 8330.

Seed, H.B. and I.M. Idriss. "Simplified Procedure for Evaluating Soil Liquefaction Potential." Journal of the Soil Mechanics and Foundation Division, ASCE, Vol. 97, No. SM 9 (September, 1971).

Seed, H.B., K.L. Lee, I.M. Idriss and F. Makdisi. "Analysis of the Slides in the San Fernando Dams During the Earthquake of February 9, 1971." Earthquake Engineering Research Center, Report No. 73-2, University of California, Berkeley, California (June, 1973).

Seed, H.B., I.M. Idriss, K.L. Lee and F.I. Makdisi. "Dynamic Analysis of the Slide in the Lower San Fernando Dam During the Earthquake of February 9, 1971." Journal of the Geotechnical Engineering Division, ASCE, Vol. 101, No. GT 9 (September, 1975).

Seed, H.B., K. Mori and C.K. Chan. "Influence of Seismic History on Liquefaction." Journal of the Geotechnical Engineering Division, ASCE, Vol. 103, No. GT 4 (April, 1977).

Seed, H.B. "Soil Liquefaction and Cyclic Mobility Evaluation for Level Ground during Earthquakes." Journal of the Geotechnical Engineering Division, ASCE, Vol. 105, No. GT 2 (February, 1979).

Silver, M.L. "Laboratory Triaxial Testing Procedures to Determine the Cyclic Strength of Soils." Report No. NUREG-0031, U.S. Nuclear Regulatory Commission, Washington, D.C. (1976).

Silver, M.L., et al. "Cyclic Triaxial Strength of Standard Test Sand." Journal of the Geotechnical Engineering Division, ASCE, Vol. 102, No. GT 5 (May, 1976).

Silver, M.L. "Comparison Between the Strengths of Undisturbed and Reconstituted Sands from Niigata, Japan." Technical Report S-78-9, Department of Materials Engineering, University of Illinois at Chicago, Chicago, Illinois (1978).

Singh, S., N.C. Donovan and F. Park. "A Re-examination of the Effect of Prior Loading on the Liquefaction of Sands," Proceedings, 7th World Conference on Earthquake Engineering, (September, 1980).

Tatsuoka, F., T. Iwasaki, K. Tokida, S. Yosuda, M. Hirose, T. Imai and M. Kon-no. "Standard Penetration Tests and Soil Liquefaction Potential Evaluation." Soils and Foundations, Japanese Society of Soil Mechanics and Foundation Engineering, Vol. 20, No. 4 (December, 1980).

Terzaghi, K. and R.B. Peck. Soil Mechanics in Engineering Practice. John Wiley and Sons, Inc., New York, New York, 1948.

Terzaghi, K. "Varieties of Submarine Slope Failures." Proceedings, Eighth Texas Conference on Soil Mechanics and Foundation Engineering, Austin, Texas, Special Publication No. 29 (September, 1956).

Valera, J.E. and N.C. Donovan. "Soil Liquefaction Procedures--A Review." Journal of the Geotechnical Engineering Division, ASCE, Vol. 103, No. GT 6 (June, 1977).

Wang, W.S. "Mechanism of Soil Liquefaction." International Conference on Recent Advances in Geotechnical Earthquake Engineering and Soil Dynamics, St. Louis, Missouri (April, 1981).

Whitman, R.V. "Resistance of Soil to Liquefaction and Settlement." M.I.T., Cambridge, Massachusetts (1970).

Wong, R.T., H.B. Seed and C.K. Chan. "Cyclic Loading Liquefaction of Gravelly Soils." Journal of the Geotechnical Engineering Division, ASCE, Vol. 101, No, GT 6 (June, 1975).

Yoshimi, Y. and H. Oh-Oka. "Influence of Degree of Shear Stress Reversal on the Liquefaction Potential of Saturated Sand." Soils and Foundations, Japanese Society of Soil Mechanics and Foundation Engineering, Vol. 15, No. 3 (September, 1975).